

# The consolidated European synthesis of CO<sub>2</sub> emissions and removals for EU27 and UK: 1990-2020

Matthew J. McGrath<sup>1</sup>, Ana Maria Roxana Petrescu<sup>2</sup>, Philippe Peylin<sup>1</sup>, Robbie M. Andrew<sup>3</sup>, Bradley Matthews<sup>4</sup>, Frank Dentener<sup>5</sup>, Juraj Balkovič<sup>6</sup>, Vladislav Bastrikov<sup>7</sup>, Meike Becker<sup>8,9</sup>, Gregoire Broquet<sup>1</sup>, Philippe Ciais<sup>1</sup>, Audrey Fortems-Cheiney<sup>1</sup>, Raphael Ganzenmüller<sup>10</sup>, Giacomo Grassi<sup>5</sup>, Ian Harris<sup>11</sup>, Matthew Jones<sup>12</sup>, Juergen Knauer<sup>13</sup>, Matthias Kuhnert<sup>14</sup>, Guillaume Monteil<sup>15</sup>, Saqr Munassar<sup>16</sup>, Paul I. Palmer<sup>17</sup>, Glen P. Peters<sup>3</sup>, Chunjing Qiu<sup>1</sup>, Mart-Jan Schelhaas<sup>18</sup>, Oksana Tarasova<sup>19</sup>, Matteo Vizzarri<sup>5,20</sup>, Karina Winkler<sup>18,21</sup>, Gianpaolo Balsamo<sup>22</sup>, Antoine Berchet<sup>1</sup>, Peter Briggs<sup>13</sup>, Patrick Brockmann<sup>1</sup>, Frédéric Chevallier<sup>1</sup>, Giulia Conchedda<sup>23</sup>, Monica Crippa<sup>5,24</sup>, Stijn Dellaert<sup>25</sup>, Hugo A. C. Denier van der Gon<sup>25</sup>, Sara Filipek<sup>18</sup>, Pierre Friedlingstein<sup>26</sup>, Richard Fuchs<sup>20</sup>, Michael Gauss<sup>27</sup>, Christoph Gerbig<sup>16</sup>, Diego Guizzardi<sup>5</sup>, Dirk Günther<sup>28</sup>, Richard A. Houghton<sup>29</sup>, Greet Janssens-Maenhout<sup>5</sup>, Ronny Lauerwald<sup>30</sup>, Bas Lerink<sup>18</sup>, Ingrid T. Luijkx<sup>18</sup>, Géraud Moulas<sup>31</sup>, Marilena Muntean<sup>5</sup>, Gert-Jan Nabuurs<sup>18</sup>, Aurélie Paquirissamy<sup>1</sup>, Lucia Perugini<sup>32</sup>, Wouter Peters<sup>18</sup>, Roberto Pilli<sup>33</sup>, Julia Pongratz<sup>10,34</sup>, Pierre Regnier<sup>35</sup>, Marko Scholze<sup>15</sup>, Yusuf Serengil<sup>36</sup>, Pete Smith<sup>14</sup>, Efisio Solazzo<sup>24</sup>, Rona L. Thompson<sup>37</sup>, Francesco N. Tubiello<sup>22</sup>, Timo Vesala<sup>38,39</sup>, Sophia Walther<sup>16</sup>

<sup>1</sup>Laboratoire des Sciences du Climat et de l'Environnement, CEA CNRS UVSQ UPSACLAY Orme des Merisiers, Gif-sur-Yvette, France

<sup>2</sup>Department of Earth Sciences, Vrije Universiteit Amsterdam, 1081HV, Amsterdam, the Netherlands

<sup>3</sup>CICERO Center for International Climate Research, Oslo, Norway

<sup>4</sup>Environment Agency Austria, Spittelauer Lände 5 1090, Vienna, Austria

<sup>5</sup>European Commission, Joint Research Centre, Via E. Fermi, 2749, TP 26/A, 21027, Ispra, Italy

<sup>6</sup>International Institute for Applied Systems Analysis (IIASA), 2361 Laxenburg, Austria

<sup>7</sup>Science Partners, 75010 Paris, France

<sup>8</sup>Geophysical Institute, University of Bergen, Bergen, Norway

<sup>9</sup>Bjerknes Centre for Climate Research, Bergen, Norway

<sup>10</sup>Department of Geography, Ludwig-Maximilians-Universität München, Luisenstraße 37, 80333 München, Germany

<sup>11</sup>National Centre for Atmospheric Science (NCAS), University of East Anglia, Norwich, United Kingdom; and Climatic Research Unit, School of Environmental Sciences, University of East Anglia, Norwich, United Kingdom

<sup>12</sup>Tyndall Centre for Climate Change Research, School of Environmental Sciences, University of East Anglia, Norwich Research Park, Norwich NR4 7TJ, United Kingdom

<sup>13</sup>Hawkesbury Institute for the Environment, Western Sydney University, Locked Bag 1797, Penrith, NSW 2751, Australia

<sup>14</sup>Institute of Biological and Environmental Sciences, University of Aberdeen, 23 St Machar Drive, Aberdeen, AB24 3UU, United Kingdom

<sup>15</sup>Dept. of Physical Geography and Ecosystem Science, Lund University, Sweden

<sup>16</sup>Max Planck Institute for Biogeochemistry, Hans-Knöll-Strasse 10, 07745 Jena, Germany

<sup>17</sup>School of GeoSciences, University of Edinburgh, Edinburgh, United Kingdom

<sup>18</sup>Wageningen Environmental Research, Wageningen University and Research (WUR), Wageningen, 6708PB, the Netherlands

<sup>19</sup>Science and Innovation Department, World Meteorological Organization (WMO), Geneva, Switzerland

<sup>20</sup>Università degli Studi di Milano, Milano, Italy

<sup>21</sup>Land Use Change & Climate Research Group, IMK-IFU, Karlsruhe Institute of Technology (KIT), Karlsruhe, Germany

<sup>22</sup>European Centre for Medium-Range Weather Forecasts (ECMWF), Reading, RG2 9AX, United Kingdom

<sup>23</sup>FAO, Statistics Division, Via Terme di Caracalla, Rome 00153, Italy

<sup>24</sup>UniSystems Company, Milan, Italy

<sup>25</sup>Department of Climate, Air and Sustainability, TNO, Princetonlaan 6, 3584 CB Utrecht, the Netherlands

<sup>26</sup>College of Engineering, Mathematics and Physical Sciences, University of Exeter, Exeter EX4 4QF, United Kingdom

<sup>27</sup>Norwegian Meteorological Institute, Oslo, Norway

<sup>28</sup>Umweltbundesamt (UBA), 14193 Berlin, Germany

<sup>29</sup>Woodwell Climate Research Center, Falmouth, Massachusetts, United States of America

<sup>30</sup>Université Paris-Saclay, INRAE, AgroParisTech, UMR ECOSYS, Thiverval-Grignon, France

<sup>31</sup>ARTTIC, 39 rue des Mathurins, 75008 Paris, France

<sup>32</sup>Centro Euro-Mediterraneo sui Cambiamenti Climatici (CMCC), Viterbo, Italy

<sup>33</sup>Scientific consultant, Padua, Italy

<sup>34</sup>Max Planck Institute for Meteorology, Bundesstrasse 53, 20146 Hamburg, Germany

<sup>35</sup>Biogeochemistry and Modeling of the Earth System, Université Libre de Bruxelles, 1050 Bruxelles, Belgium

<sup>36</sup>Istanbul University, Faculty of Forestry, Department of Watershed Management, 34473 Sariyer, Istanbul, Turkey

<sup>37</sup>Norwegian Institute for Air Research (NILU), Kjeller, Norway

<sup>38</sup>University of Helsinki, Institute for Atmospheric and Earth System Research/Physics, Faculty of Science, 00560 Helsinki, Finland

60 <sup>39</sup>Institute for Atmospheric and Earth System Research,/Forest Sciences, Faculty of Agriculture and Forestry, University of  
61 Helsinki, Helsinki, Finland

62  
63  
64  
65

*Correspondence to:* M.J. McGrath (matthew.mcgrath@lsce.ipsl.fr)

## 66 **Abstract**

67 Quantification of land surface-atmosphere fluxes of carbon dioxide (CO<sub>2</sub>) fluxes and their trends and  
68 uncertainties is essential for monitoring progress of the EU27+UK bloc as it strives to meet ambitious targets  
69 determined by both international agreements and internal regulation. This study provides a consolidated synthesis of  
70 fossil sources (CO<sub>2</sub> fossil) and natural (including formally managed ecosystems) sources and sinks over land (CO<sub>2</sub>  
71 land) using bottom-up (BU) and top-down (TD) approaches for the European Union and United Kingdom  
72 (EU27+UK), updating earlier syntheses (Petrescu et al., 2020, 2021b). Given the wide scope of the work and the  
73 variety of approaches involved, this study aims to answer essential questions identified in the previous syntheses and  
74 understand the differences between datasets, particularly for poorly characterized fluxes from managed and  
75 unmanaged ecosystems. The work integrates updated emission inventory data, process-based model results, data-  
76 driven categorical model results, and inverse modeling estimates, extending the previous period 1990-2018 to the year  
77 2020 to the extent possible. BU and TD products are compared with the European National Greenhouse Gas Inventory  
78 (NGHGI) reported by Parties including the year 2019 under the United Nations Framework Convention on Climate  
79 Change (UNFCCC). The uncertainties of the EU27+UK NGHGI were evaluated using the standard deviation reported  
80 by the EU Member States following the guidelines of the Intergovernmental Panel on Climate Change (IPCC) and  
81 harmonized by gap-filling procedures. Variation in estimates produced with other methods, such as atmospheric  
82 inversion models (TD) or spatially disaggregated inventory datasets (BU), originate from within-model uncertainty  
83 related to parameterization as well as structural differences between models. By comparing the NGHGI with other  
84 approaches, key sources of differences between estimates arise primarily in activities. System boundaries and  
85 emission categories create differences in CO<sub>2</sub> fossil datasets, while different land use definitions for reporting  
86 emissions from Land Use, Land Use Change and Forestry (LULUCF) activities result in differences for CO<sub>2</sub> land.  
87 The latter has important consequences for atmospheric inversions, leading to inversions reporting stronger sinks in  
88 vegetation and soils than are reported by the NGHGI.

89 **For CO<sub>2</sub> fossil emissions**, after harmonizing estimates based on common activities and selecting the most recent  
90 year available for all datasets, the UNFCCC NGHGI for the EU27+UK accounts for  $926 \pm 13$  Tg C yr<sup>-1</sup>, while eight  
91 other BU sources report a mean value of 948 [937,961] [25<sup>th</sup>,75<sup>th</sup> percentile] Tg C yr<sup>-1</sup>. The sole top-down inversion  
92 of fossil emissions currently available accounts for 875 Tg C in this same year, a value outside the uncertainty of both  
93 the NGHGI and bottom-up ensemble estimates and for which uncertainty estimates are not currently available. **For**  
94 **the net CO<sub>2</sub> land fluxes**, during the most recent five-year period including the NGHGI estimates, the NGHGI  
95 accounted for  $-91 \pm 32$  Tg C yr<sup>-1</sup> while six other BU approaches reported a mean sink of  $-62$  [-117,-49] Tg C yr<sup>-1</sup> and  
96 a 15-member ensemble of dynamic global vegetation models (DGVMs) reported  $-69$  [-152,-5] Tg C yr<sup>-1</sup>. The five-

97 year mean of three TD regional ensembles combined with one non-ensemble inversion of  $-73 \text{ Tg C yr}^{-1}$  has a slightly  
98 smaller spread (0th-100th percentile of  $[-135,+45] \text{ Tg C yr}^{-1}$ ), and was calculated after removing net land-atmosphere  
99  $\text{CO}_2$  fluxes caused by lateral transport of carbon (crop trade, wood trade, river transport, and net uptake from inland  
100 water bodies) resulting in increased agreement with the NGHGI and bottom-up approaches. Results at the category  
101 level (Forestland, Cropland, Grassland) show generally good agreement between the NGHGI and category-specific  
102 models, but results for DGVMs are mixed. Overall, for both  $\text{CO}_2$  fossil and net  $\text{CO}_2$  land fluxes, we find current  
103 independent approaches are consistent with the NGHGI at the scale of the EU27+UK. We conclude that  $\text{CO}_2$   
104 emissions from fossil sources have decreased over the past 30 years in the EU27+UK, while land fluxes are relatively  
105 stable: positive or negative trends larger (smaller) than  $0.07$  ( $-0.61$ )  $\text{Tg C yr}^{-2}$  can be ruled out for the NGHGI. In  
106 addition, a gap on the order of  $1000 \text{ Tg C yr}^{-1}$  between  $\text{CO}_2$  fossil emissions and net  $\text{CO}_2$  uptake by the land exists  
107 regardless of the type of approach (NGHGI, TD, BU), falling well outside all available estimates of uncertainties.  
108 However, uncertainties in top-down approaches to estimate  $\text{CO}_2$  fossil emissions remain uncharacterized and are likely  
109 substantial, in addition to known uncertainties in top-down estimates of the land fluxes. The data used to plot the  
110 figures are available at <https://doi.org/10.5281/zenodo.8148461> (McGrath et al., 2023).

## 111 **1. Introduction**

112 Atmospheric mole fractions of greenhouse gasses (GHGs) reflect a balance between emissions from both  
113 human activities and natural sources, and removals by the terrestrial biosphere, oceans, and atmospheric oxidation.  
114 Increasing levels of GHG in the atmosphere due to human activities have been the major driver of climate change  
115 since the pre-industrial period (IPCC, 2021). In 2020, GHG mole fractions reached record highs, with globally  
116 averaged mole fractions of  $413.2$  parts per million (ppm) for carbon dioxide ( $\text{CO}_2$ ), representing  $149\%$  of the pre-  
117 industrial level (WMO, 2021). The rise in  $\text{CO}_2$  mole fractions in recent decades is caused primarily by  $\text{CO}_2$  emissions  
118 from fossil sources. Globally, fossil emissions in 2020 (excluding the cement carbonation sink) totaled  $9500 \pm 500 \text{ Tg}$   
119  $\text{C yr}^{-1}$ , with expectations to rise in 2021 as the world recovered from the first year of the Covid-19 pandemic  
120 (Friedlingstein et al., 2022). In contrast, global net  $\text{CO}_2$  emissions from land use and land use change (LULUC,  
121 primarily deforestation; see glossary at Table A1 for more details) estimated from bookkeeping models and dynamic  
122 global vegetation models (DGVMs) were estimated to have a small decreasing trend over the past two decades, albeit  
123 with low confidence, and a value in the year 2020 of  $900 \pm 700 \text{ Tg C yr}^{-1}$  (Friedlingstein et al., 2022). This decrease,  
124 however, is almost an order of magnitude less than the growth in fossil emissions over the same period, and therefore  
125 the total fossil and net LULUC flux has still increased.

126 As all countries in the EU27+UK are Annex I Parties<sup>1</sup> to the United Nations Framework Convention on  
127 Climate Change (UNFCCC), they prepare and report national GHG emission inventories (NGHGIs) on an annual

---

<sup>1</sup> Annex I Parties include the industrialized countries that were members of the OECD (Organization for Economic Co-operation and Development) in 1992 plus countries with economies in transition (the EIT Parties), including the Russian Federation, the Baltic States, and several central and eastern European states (UNFCCC, <https://unfccc.int/parties-observers>, last access: February 2022).

128 basis. These inventories contain annual timeseries of each country’s GHG emissions from the 1990 base year<sup>2</sup> until  
129 two years before the year of reporting and were originally set to track progress towards their reduction targets under  
130 the Kyoto Protocol (UNFCCC, 1997). Annex I NGHGs are reported according to the Decision 24/CP.19 of the  
131 UNFCCC Conference of the Parties (COP) which states that the national inventories *shall* be compiled using the  
132 methodologies provided in the *IPCC Guidelines for National Greenhouse Gas Inventories* (IPCC, 2006). The 2006  
133 IPCC Guidelines provide methodological guidance for estimating emissions for well-defined sectors using national  
134 activity and available emission factors. Decision trees indicate the appropriate level of methodological sophistication  
135 (*Tiered methods*) based on the absolute contribution of the sector to the national GHG balance and the country’s  
136 national circumstances (availability and resolution of national activity data and emission factors). Generally, Tier 1  
137 methods are based on global or regional default emission factors that can be used with aggregated activity data, while  
138 Tier 2 methods rely on country-specific factors and/or activity data at a higher category resolution. Tier 3 methods are  
139 based on more detailed process-level modeling or in some cases facility-level emission observations. Annex I Parties  
140 are furthermore required to estimate and report uncertainties in emissions (95 % confidence interval) following the  
141 2006 IPCC guidelines using, as a minimum requirement, the Gaussian error propagation method (approach 1). Annex  
142 I Parties are furthermore encouraged to use Monte-Carlo methods (approach 2) or a hybrid approach. Additional  
143 information on the NGHGs can be found in Appendix A2.

144 In addition to the NGHGs, other research groups and international institutions produce independent  
145 estimates of national GHG emissions with two approaches: atmospheric inversions (top-down, TD) and GHG  
146 inventories based on the same principle as NGHGs but using slightly different methods (tiers), activity data, and/or  
147 emissions factors (bottom-up, BU). The current work has a strong focus on the EU27, and therefore sits within the  
148 context of recent legislation passed by the European Parliament concerning commitments for the LULUCF sector to  
149 achieve the objectives of the Paris Agreement and the reduction target for the Union (EU, 2018a and the proposed  
150 amendments, EU, 2021a). This legislation requires that, “Member States shall ensure that their accounts and other  
151 data provided under this Regulation are accurate, complete, consistent, comparable and transparent”. The TD and BU  
152 methods discussed below include the most up-to-date publicly available spatially explicit information, which can help  
153 provide a quality check and increase public confidence in NGHGs.

154 The work presented in this paper covers dozens of distinct datasets and models, in addition to the individual  
155 country submissions to the UNFCCC of the EU Member States and the UK. As Annex I Parties, the NGHGs of the  
156 EU Member States and the UK are consistent with the general guidance laid out in IPCC (2006) yet still differ in  
157 specific approaches, models, and parameters, in addition to definitional differences in the underlying system  
158 boundaries and activity datasets. For the land-based sector, Member States are only required to report terrestrial  
159 biospheric fluxes from managed lands, instead of distinguishing between direct and indirect human-induced and  
160 natural effects on carbon fluxes for all ecosystems (Grassi et al., 2018a, 2021). This “managed land proxy” avoids

---

<sup>2</sup> For most Annex I Parties, the historical base year is 1990. However, parties included in Annex I with an economy in transition during the early 1990s (EIT Parties) were allowed to choose one year up to a few years before 1990 as reference because of a non-representative collapse during the breakup of the Soviet Union. For the EU27+UK, this includes Bulgaria (1988), Hungary (1985–1987), Poland (1988), Romania (1989), and Slovenia (1986).

161 having to quantify, for example, increased carbon uptake in remote Forest land due to reactive nitrogen emissions  
162 from both natural soils and human-applied synthetic fertilizers. A comprehensive investigation of detailed differences  
163 between all datasets is beyond the scope of this paper, though systematic analyses have been previously made for  
164 specific sectors (e.g. AFOLU<sup>3</sup> - Petrescu et al., 2020; previous synthesis to this work - Petrescu et al., 2021b;  
165 FAOSTAT versus UNFCCC NGHGI - Tubiello et al., 2021, Grassi et al., 2022a; UNFCCC versus bookkeeping  
166 models - Grassi et al, 2023; and UNFCCC versus inversions - Deng et al., 2021) and by the Global Carbon Project  
167 CO<sub>2</sub> syntheses (e.g., Friedlingstein et al., 2022).

168 Every year (time “*t*”) the Global Carbon Project (GCP) in its Global Carbon Budget (GCB) quantifies large-  
169 scale CO<sub>2</sub> budgets up to the previous year (“*t-1*”), bringing in information from global to large latitude bands, including  
170 various observation-based flux estimates from BU and TD approaches (Friedlingstein et al., 2022). The current  
171 manuscript, given the focus on a single region (“Europe”) with extensive data coverage, dives into more detail than  
172 the GCB, including category-specific models related to LULUCF (e.g., Forest land, Grassland, Cropland) and making  
173 heavy use of the EU27+UK NGHGI in an effort to advance a trust-building process by mutual understanding  
174 developed through comparison of both approaches. Compared to Petrescu et al. (2021b), the current work updates  
175 datasets, methods, and uncertainties.

176 BU observation-based approaches used in the GCB rely heavily on statistical data combined with Tier 1 and  
177 Tier 2 approaches. In the current work, focusing on a region that is well-covered with data and models (EU27+UK),  
178 BU also refers to Tier 3 process-based models (see Sect. 2). At regional and country scales, systematic and regular  
179 comparison of these observation-based CO<sub>2</sub> flux estimates with reported fluxes under the UNFCCC is more difficult.  
180 Continuing our previous efforts within the European project VERIFY (VERIFY, 2022), the current study compares  
181 observation-based flux estimates of BU versus TD approaches and compares them with NGHGI for the EU27+UK  
182 bloc and five sub-regions. VERIFY also provides, as a first attempt, similar comparisons for all European countries  
183 (VERIFY Synthesis Plots, 2022). The methodological and scientific challenges to compare these different estimates  
184 have been partly investigated before (Pongratz et al., 2021, Grassi et al., 2018a, for LULUCF; Andrew, 2020, for  
185 fossil sectors) but such comparisons were not done in a systematic and comprehensive way, including both fossil and  
186 land-based CO<sub>2</sub> fluxes, before Petrescu et al. (2021b).

187 As Petrescu et al. (2021b) is the most comprehensive comparison of the NGHGI and research datasets  
188 (including both TD and BU approaches) for the EU27+UK to date, the focus of the current paper is on improvement  
189 of estimates in the most recent version in comparison with the previous one, including changes in the uncertainty  
190 estimates and identification of the knowledge gaps and added value for policy making. Official NGHGI emissions are  
191 compared with research datasets, including necessary harmonization of the latter on total emissions to ensure  
192 consistency. Differences and inconsistencies between emission estimates were analyzed, and recommendations were  
193 made towards future evaluation of NGHGI data. It is important to remember that, while NGHGI include uncertainty  
194 estimates, the “uncertainty analysis should be seen, first and foremost, as a means to help prioritize national efforts to  
195 reduce the uncertainty of inventories in the future, and guide decisions on methodological choice” (Volume 1, Chapter

---

<sup>3</sup> We refer here to AFOLU as defined by the IPCC AR5: Agriculture, Forestry and Other Land Use. For further details on the differences between AFOLU, LULUCF, and LULUC, please see the glossary at Table A1.

196 3, IPCC, 2006) and were therefore not developed to enable comparisons between countries or other datasets. In  
197 addition, individual spatially disaggregated research emission datasets often lack quantification of uncertainty. Here,  
198 we focus on the mean value and various percentiles (0th, 25th, 75th, 100th) of different research products of the same  
199 type to get a first estimate of uncertainty (see Sect. 2). Not all models/inventories provided an update for v2021, and,  
200 therefore, for the non-updated datasets the previously published timeseries are shown.

201 The dataset assembled in this paper (McGrath et al., 2023) provides annual values of carbon dioxide  
202 emissions and sinks in fossil and LULUCF sectors for the EU27+UK across a range of data products based on different  
203 methodologies. This enables, for example, researchers producing datasets based on new methods a source of  
204 evaluation in the form of a best-estimate range of values. Decision makers may also find the results useful for targeting  
205 mitigation efforts in the EU27+UK by providing a more complete subsectorial breakdown. While NGHGs already  
206 provide detailed data-based disaggregation based on activities, the dataset here adds additional constraints from  
207 independent data and models used outside of the inventory community. In addition, this paper outlines a methodology  
208 by which users of country-level CO<sub>2</sub> emission data can compare datasets against NGHGs and identify where  
209 agreement occurs for the right (and wrong) reasons. Section 3.1 highlights the extreme difference between current  
210 fossil emissions and uptake by the land surface. Section 3.2 looks at an ensemble of bottom-up estimates of fossil  
211 CO<sub>2</sub> emissions, in addition to a preliminary inversion using atmospheric NO<sub>2</sub> observations as a constraint. Sections  
212 3.3.2 and 3.3.3 show that better agreement between the NGHGI and other models occurs when the models are driven  
213 strongly by category-specific data in forestry, grasslands, and croplands, as opposed to more generalized models  
214 created to couple to atmospheric models in global climate projections. Section 3.3.4 highlights the challenges  
215 currently facing comparison of atmospheric inversion models with NGHGs, while simultaneously showing  
216 improvement by accounting for net emissions for lateral transfer of carbon between countries. Section 3.4 provides  
217 more discussion around uncertainties in both top-down and bottom-up estimates.

218 A list of acronyms and terminology is provided in Table A1 for easy reference.

219

## 220 **2. CO<sub>2</sub> data sources and estimation approaches**

221 The CO<sub>2</sub> emissions and removals in the EU27+UK estimated by inversions and anthropogenic emission  
222 inventories resolved at the source category level were analyzed. At the time of this work, data of CO<sub>2</sub> fossil emissions  
223 and CO<sub>2</sub> land<sup>4</sup> emissions and removals (Tables 1 and 2) covered the period from 1990 to 2020, with some of the data  
224 only available for shorter time periods. Since then, some datasets have been updated to include 2021, but not all, and

---

<sup>4</sup> The IPCC Good Practice Guidance (GPG) for Land Use, Land Use Change and Forestry (IPCC, 2003) describes a uniform structure for reporting emissions and removals of greenhouse gasses. This format for reporting can be seen as “land based”: all land in the country must be identified as having remained in one of six categories since a previous survey, or as having changed to a different (identified) category in that period. According to IPCC Special Report on Climate Change and Land: Land covers the terrestrial portion of the biosphere that comprises the natural resources (soil, near surface air, vegetation and other biota, and water) the ecological processes, topography, and human settlements and infrastructure that operate within that system”. Some communities prefer “biogenic” to describe these fluxes, while others find this confusing as fluxes from unmanaged forests, for example, are “biogenic” but not included in inventories reported to the UNFCCC. As this comparison is central to our work, we decided that “land” as defined by the IPCC was a good compromise. However, we avoid the word “natural” as much as possible, under the assumption that almost all terrestrial ecosystems are significantly impacted by humans in the current era.

225 we made the decision to stay with the original time window for simplicity. The estimates are available both from  
226 peer-reviewed literature and from new research results from the VERIFY project. BU results are compared to NGHGI  
227 reported in 2021 (which contain the timeseries for 1990-2019). Data sources are summarized in Tables 1 and 2 with  
228 the detailed description of all products provided in Appendices A2-A4. In Appendix A2, the harmonized methodology  
229 for calculation of uncertainties submitted by Member States to the UNFCCC in their National Inventory Reports  
230 (NIRs) is explained. This includes the same 95 % confidence interval as is typically reported, but involved an  
231 extensive gap-filling to cover more categories and more years than available in Petrescu et al. (2021b), which limited  
232 uncertainty estimation to a single year.

233 BU anthropogenic CO<sub>2</sub> fossil estimates include global inventory datasets such as the Emissions Database for  
234 Global Atmospheric Research (EDGAR v6.0.), Statistical Review of World Energy by BP, the Carbon Dioxide  
235 Information Analysis Center (CDIAC), the Global Carbon Project (GCP), the Energy Information Administration's  
236 (EIA) "International" dataset, and the International Energy Agency (IEA) (see Table 1). These datasets are all  
237 described in detail by Andrew (2020). CO<sub>2</sub> land emission estimates are derived from BU biogeochemical models (e.g.,  
238 DGVMs, bookkeeping models, see Table 2). TD approaches include both high spatial resolution regional inversions  
239 (CarboScopeReg, EUROCOM (Monteil et al., 2020), inversions based on the CIF-CHIMERE system (Berchet et al.,  
240 2021) and LUMIA) and coarser spatial resolution global inversions (GCP 2021: Friedlingstein et al., 2022). Most of  
241 the inversions were carried out for CO<sub>2</sub> land emissions, with only a single inversion for CO<sub>2</sub> fossil emissions (CIF-  
242 CHIMERE). Note that CIF-CHIMERE provides estimates for both CO<sub>2</sub> land and CO<sub>2</sub> fossil from separate simulations.  
243 These estimates are described in Sect. 2.3.

244 The sign of the fluxes is defined from an atmospheric perspective: positive values represent a net source to  
245 the atmosphere and negative values a net removal from the atmosphere. As an overview of potential uncertainty  
246 sources, Table C1 presents the use of emission factor data (EF), activity data (AD), and, whenever available,  
247 uncertainty methods used for all CO<sub>2</sub> land data sources in this study, in addition to more details on each model in  
248 Appendices A. The referenced data used for the figures' replicability purposes are available for download (McGrath  
249 et. al, 2023). Upon request, the codes necessary to plot the figures in the same style and layout can be provided. The  
250 focus is on EU27+UK emissions. In the VERIFY project, an additional web tool was developed which allows for the  
251 selection and display of all plots shown in this paper, not only for the EU Member States and UK but for a total of 79  
252 countries and groups of countries in Europe (Table A2, Appendix A). The data is free and can be accessed upon  
253 registration (VERIFY Synthesis Plots, 2022). An overview of the datasets, including contact information, is provided  
254 in Table C1.

255 For the sake of harmonization, we report the mean values of all ensembles. For small sample sizes (e.g., the  
256 regional inversions of CSR with four members), the literature does not give a clear indication on whether the mean or  
257 the median is preferred; a preference for one or the other depends on what one wishes to demonstrate. While the mean  
258 and median converge in the case of independent randomly-distributed data, the median downplays data skewness. We  
259 display the mean for all ensembles. As the number of datasets in some ensembles is small (less than five), we display  
260 the minimum and maximum annual values for every year (i.e., the 0th/100th percentiles) to give an idea of the spread.  
261 For ensembles with more than ten members (i.e., TRENDY), we show the mean and the 0th/100th percentiles along

262 with the 25th/75th percentiles in the figures. This combination demonstrates "more likely" and "possible" behavior;  
263 as only one ensemble has both bars, displaying them does not overwhelm the reader much more than the standard  
264 graphs, and we find the added information to be worth the trade-off. In the text, we report the mean and 0/100th  
265 percentiles for small ensembles and mean along with the 25th/75th for larger ensembles. We make every effort to  
266 limit the number of significant figures as a function of the error bars. In some cases (e.g., asymmetric error bars which  
267 overlap zero), we retain an extra significant figure to improve readability.

268 The current work extends Petrescu et al. (2021b) by updating the included datasets (both increasing the  
269 number of years covered and in some cases updating the model versions), adding datasets, and highlighting changes  
270 in terms of mean annual emissions and trends. For clarity, the data from Petrescu et al. (2021b) is labeled as v2019,  
271 while the latest results are labeled v2021.

272

## 273 **2.1. CO<sub>2</sub> anthropogenic emissions from NGHGI**

274 The UNFCCC NGHGI (2021) estimates for the period 1990 to year  $t-2$  (2019), collected for the EU27 and UK,  
275 are the basis for this dataset. For historical reasons, a few EU countries provide data for a different base year than  
276 1990<sup>5</sup>, yet it should be noted that regardless of the base year all countries of the EU27+UK bloc are obliged to report  
277 estimates for the period 1990 to year  $t-2$ . The Annex I Parties to the UNFCCC are required to report annual GHG  
278 inventories that include a NIR, with qualitative information on data and methods and a Common Reporting Format  
279 (CRF) set of tables that provide quantitative information on GHG emission by category. This annually updated dataset  
280 includes anthropogenic emissions and removals. For the land-based sector, the managed land proxy is used as a way  
281 to report only anthropogenic fluxes (Grassi et al., 2018a, 2021). This proxy allows Member States to report all fluxes  
282 coming from land designed as “managed” without trying to disentangle their natural and anthropogenic origins.  
283 Spatially-explicit maps of managed lands are not currently available, even for the relatively data-rich region of the  
284 European Union and United Kingdom. However, most of the European Union is classified by the Member States as  
285 managed land; current estimates from available country-aggregated data indicates only 5 % of land in the EU is  
286 unmanaged, including some Forest land, Grassland, and Wetlands. Figure B1 shows the annual NGHGI (2021)  
287 anthropogenic CO<sub>2</sub> timeseries disaggregated by sector in order to provide context.

288

## 289 **2.2. CO<sub>2</sub> fossil emissions**

290 CO<sub>2</sub> fossil emissions occur when fossil carbon compounds are broken down via combustion or other non-  
291 combustive industrial processes. Most of these fossil compounds are in the form of fossil fuels, such as coal, oil, and  
292 natural gas. Another source category of fossil CO<sub>2</sub> emissions is fossil carbonates, such as calcium carbonate and  
293 magnesium carbonate, which are used in industrial processes. Because CO<sub>2</sub> fossil emissions are largely connected  
294 with energy, which is a closely tracked commodity group of high economic importance, there is a wealth of underlying

---

<sup>5</sup> For most Annex I Parties, the historical base year is 1990. However, parties included in Annex I with an economy in transition during the early 1990s (EIT Parties) were allowed to choose one year up to a few years before 1990 as reference because of a non-representative collapse during the breakup of the Soviet Union (e.g., Bulgaria, 1988, Hungary, 1985–1987, Poland, 1988, Romania, 1989, and Slovenia, 1986).



295 data that can be used for estimating emissions. However, differences in collection, treatment, interpretation and  
296 inclusion of various factors – such as carbon contents and fractions of the fuel’s carbon that is oxidized – lead to  
297 methodological differences (Appendix A3) resulting in differences of emissions between datasets (Andrew, 2020).  
298 The datasets are also not fully independent, as discussed in Sec. 2.4. Atmospheric inversions for emissions of fossil  
299 CO<sub>2</sub> are not as established as their bottom-up counterparts (Brophy et al., 2019). The main reason is that the types of  
300 atmospheric measurements suitable for fossil CO<sub>2</sub> atmospheric inversions have not yet been widely deployed (Ciais  
301 et al., 2015). One of the rare inversions is presented below.

302 In this analysis, the inventory-based bottom-up CO<sub>2</sub> fossil emissions estimates are separated and presented  
303 per fuel type and reported for the last year when all data products are available (2017). This updates Andrew (2020)  
304 and Petrescu et al. (2021b) which both report the year 2014. In order to provide a quasi-independent estimate of fossil  
305 emissions assimilating satellite observations of the atmosphere subject to current capabilities of atmospheric  
306 inversions, the CIF-CHIMERE model was used to produce a fossil fuel CO<sub>2</sub> emission estimate for the year 2017. CIF-  
307 CHIMERE is a coupling between the variational mode of the Community Inversion Framework (CIF) platform  
308 developed in the VERIFY project (Berchet et al., 2021), the CHIMERE chemistry transport model (Menut et al., 2013)  
309 and the adjoint of this model (Fortems-Cheiney et al., 2021a). To overcome the lack of CO<sub>2</sub> observation networks  
310 suitable for the monitoring of fossil CO<sub>2</sub> emissions at national scale, this inversion is based on the assimilation of  
311 satellite NO<sub>2</sub> data, which are representative of NO<sub>x</sub> emissions, as NO<sub>x</sub> is co-emitted with CO<sub>2</sub> during fossil fuel  
312 combustion. The uncertainties in the anthropogenic activities underlying the fossil fuel combustion are shared by both  
313 CO<sub>2</sub> and co-emitted species. Therefore, in principle, information from co-emitted species such as NO<sub>x</sub> and CO can  
314 be used to decrease the uncertainties in fossil fuel CO<sub>2</sub> emissions. Recent top-down inversions of anthropogenic CO<sub>2</sub>  
315 emissions from Europe indicate that uncertainties using satellite measurements of NO<sub>2</sub> are much lower than for co-  
316 emitted CO when deriving fossil CO<sub>2</sub> emissions (Konovalov et al., 2016). Therefore, results shown below only  
317 incorporate NO<sub>2</sub> and not CO observations. The CHIMERE model includes a full chemistry scheme to enable linkage  
318 of observations of atmospheric NO<sub>2</sub> mole fractions to surface NO<sub>x</sub> emissions. While the spatial and temporal coverage  
319 of the NO<sub>2</sub> observations is large, there are many factors contribute to uncertainty in fossil fuel emission activity data,  
320 including the uncertainties in NO<sub>x</sub> emission factors and thus the ratio of NO<sub>x</sub> to CO<sub>2</sub> emissions. Therefore, the  
321 influence of using NO<sub>2</sub> observations in determining fossil CO<sub>2</sub> emissions is subject to uncertainties which have not  
322 been characterized appropriately yet in the framework of VERIFY. Here, this conversion relies heavily on the  
323 emission ratios per country, month and large sector of activity from the TNO-GHGco-v3 inventory (Dellaert et al.,  
324 2021), which has been partly developed in VERIFY, and which is based on the most recent UNECE-CLRTAP<sup>6</sup> and  
325 UNFCCC official country reporting respectively for air pollutants and greenhouse gasses. The detailed descriptions  
326 of each of the data products are found in Appendix A3.

327  
328 *Table 1: Data sources for the anthropogenic CO<sub>2</sub> fossil emissions included in this study, all updated from Petrescu*  
329 *et al. (2021b):*

---

<sup>6</sup> UNECE Convention on Long-Range Transboundary Air Pollution. <https://unece.org/environment-policy/air>

Anthropogenic CO <sub>2</sub> fossil			
Data/model name	Contact / lab	Species / Period	Reference/Metadata
UNFCCC NGHGI (2021)	Member State inventory agencies  Annual, gap-filled uncertainties provided by the EU GHG inventory team	Anthropogenic fossil CO <sub>2</sub> 1990-2019	IPCC (2006) UNFCCC NIRs/CRFs <a href="https://unfccc.int/ghg-inventories-annex-i-parties/2021">https://unfccc.int/ghg-inventories-annex-i-parties/2021</a> (UNFCCC, 2021a, 2021b)
Compilation of multiple CO <sub>2</sub> fossil emission data sources (Andrew 2020) EDGAR v6.0, BP, EIA, CDIAC, IEA, GCP, CEDS, PRIMAP	CICERO	CO <sub>2</sub> fossil country totals and split by fuel type 1990-2018 (or last available year)	EDGAR v6.0 <a href="https://edgar.jrc.ec.europa.eu/">https://edgar.jrc.ec.europa.eu/</a> BP 2021 report (BP, 2021) EIA <a href="https://www.eia.gov/beta/international/data/browser/views/partials/sources.html">https://www.eia.gov/beta/international/data/browser/views/partials/sources.html</a> CDIAC <a href="https://energy.appstate.edu/CDIAC">https://energy.appstate.edu/CDIAC</a> (Gilfillan and Marland, 2021) IEA : <a href="http://www.iea.org">www.iea.org</a> CEDS <a href="https://github.com/JGCRI/CEDS">https://github.com/JGCRI/CEDS</a> (O'Rourke et al., 2021) GCP (Friedlingstein et al., 2022) PRIMAP-hist (Gütschow et al., 2021) <a href="https://doi.org/10.5281/zenodo.4479171">https://doi.org/10.5281/zenodo.4479171</a>
Fossil fuel CO <sub>2</sub> inversions	LSCE	Inverse fossil fuel CO <sub>2</sub> emissions  2005-2020	Fortems-Cheiney et al. (2021) Fortems-Cheiney and Broquet (2021)

330

### 331 2.3. CO<sub>2</sub> land fluxes

332 Data products from BU and TD CO<sub>2</sub> land fluxes including CO<sub>2</sub> emissions and removals from land use, land  
333 use change, and forestry (LULUCF) activities are summarized in Table 2. All models and approaches produce an

334 estimate of the net carbon flux from the land surface including uptake through photosynthesis and emission through  
335 respiration and/or disturbances. The details may vary significantly between approaches, however. Attempts are made  
336 where possible to harmonize input data and compare results which roughly correspond to similar categories included  
337 in the NGHGI. Further details are described throughout the rest of this article. As with CO<sub>2</sub> fossil fluxes, the primary  
338 distinctions are between the NGHGI, other bottom-up approaches, and top-down approaches. The situation becomes  
339 more complicated for CO<sub>2</sub> land fluxes due to the inclusion of approaches which only address a single land use category  
340 (e.g., Forest land).

341 For the analysis at category level, the CO<sub>2</sub> net emissions from the LULUCF sector that are primarily considered  
342 in this synthesis are from three land use categories<sup>7</sup> (Forest land, Cropland, and Grassland), each split into a land  
343 category remaining in the same land category<sup>8</sup> or a land category converted to another category. The NGHGI is the  
344 only result discussed here which make use of this transition period, but the distinction is important so as to inform  
345 which NGHGI categories to use in the comparison. Wetlands, Settlements, Other land, and Harvested wood products  
346 (HWP) categories are included in the discussion on total LULUCF activities in Sect. 3.3.1 and 3.3.4. Not all the  
347 categories reported to the UNFCCC are present in FAOSTAT or other models. Some models are category-specific  
348 (e.g., Forest land) while other models include a larger subset of the six UNFCCC categories (e.g., DGVMs which  
349 simulate Forest land, Grassland, and Cropland). The notations FL, CL and GL are used to indicate total emissions and  
350 removals from the respective Forest land, Cropland and Grassland land use categories (i.e., the remaining +  
351 conversions to these categories). The notations “FL-FL”, “CL-CL” and “GL-GL” are used to indicate emissions and  
352 removals from respective forest, cropland and grassland areas which have remained in the same category from year  
353 to year, or in the case of NGHGI lands that have not undergone conversion within the aforementioned transition period  
354 (e.g., *t*-20). Uncertainties for FL, CL, and GL are reported as percentages by the European Union, and we use them  
355 directly. An uncertainty greater than 100 % implies that either a sink or a source is possible.

356 The results from category-specific models reporting carbon fluxes for FL-FL (EFISCEN-Space and CBM),  
357 CL and GL (EPIC-IIASA and ECOSSE) are presented separately from the models and datasets including multiple  
358 land use categories and simulating land use changes: FAOSTAT (version 2021), the DGVM ensemble TRENDY v10  
359 (Friedlingstein et al., 2022; Le Quéré et al., 2009), the ORCHIDEE and CABLE-POP DGVMs forced by high  
360 resolution meteorological data as part of the VERIFY project, and the two bookkeeping approaches of H&N  
361 (Houghton & Nassikas, 2017) and BLUE (Hansis et al., 2015). BLUE includes two simulations with different land-  
362 use forcing, one made for the VERIFY H2020 project and one for the GCP 2021 (Friedlingstein et al., 2022). For CL  
363 and GL both the EPIC-IIASA and ECOSSE category-specific models reported updates, although ECOSSE only  
364 updated results for GL. Processes included in all the products are summarized in Appendix A2-A4 and Table C2.

---

<sup>7</sup> According to 2006 IPCC guidelines the LULUCF sector includes six management categories (Forest land, Cropland, Grassland, Wetlands, Settlements and Other land). We have written Land-use categories with a capital letter at the start in order to emphasize that we are talking about land types as defined and reported by the countries (which vary from country to country), and not some generic scientific definition of what constitutes, for example, a grassland.

<sup>8</sup> According to 2006 IPCC guidelines, land converted to a new category should be reported in a “conversion” category for N years and then moved to a “remaining” category, unless a further change occurs. Converted land refers to CO<sub>2</sub> emissions from conversions to and from all six categories that occurred in the previous N years. By default, N is equal to 20, although the guidelines recognize that longer times may be necessary in temperate and boreal environments for the dead biomass and soil carbon pools to reach the new equilibrium. Member States have the freedom to select a length of time appropriate to their own circumstances.

365 The two updated inverse model ensembles presented are the GCP2021 for the period 2010-2020 (Friedlingstein  
366 et al., 2022) and EUROCOM for the period 2009-2018 (Monteil et al., 2020; Thompson et al., 2020). The GCP  
367 inversions are global and include CarbonTracker Europe (CTE: van der Laan-Luijkx et al., 2017), CAMS (Chevallier  
368 et al., 2005), the Jena CarboScope (Rödenbeck, 2005), NIESMON-CO<sub>2</sub> (Niwa et al., 2017), CMS-Flux (Liu et al.,  
369 2021) and UoE (Feng et al., 2016). The EUROCOM inversions are regional, with a domain limited to Europe and  
370 higher spatial resolution atmospheric transport models, with four inversions covering the entire period 2009-2018 as  
371 analyzed in Thompson et al. (2020). All inversions provide Net Ecosystem Exchange (NEE) fluxes. These inversions  
372 make use of more than 30 atmospheric observing stations within Europe, including flask data and continuous  
373 observations and work at typically higher spatial resolution than the global inversion models (Table 2). The prior  
374 anthropogenic emissions provided for all regional inversions reported here (i.e., EUROCOM, EUROCOM drought  
375 2018, VERIFY CSR, VERIFY CIF-CHIMERE, and VERIFY LUMIA) are all based on EDGAR v4.3, BP statistics,  
376 and TNO datasets by generating spatial and temporal distributions through the COFFEE approach (Steinbach et al.,  
377 2011). Small differences exist between exact versions used by the different groups. The prior anthropogenic  
378 emissions for the GCP global inversions, GridFEDv2021 and v2022, are also based on EDGARv4.3.2 (Janssens-  
379 Maenhout et al., 2019). Differences in fossil fuel emissions for the regional inversions only exist for the years 2019  
380 and 2020, and they only concern the temporal variation within the year, not the annual totals per pixel (or  
381 country). Therefore, differences in the prior anthropogenic emissions are not expected to explain the large differences  
382 seen between the different regional biogenic inversions nor between the regional and global biogenic inversions, but  
383 efforts should be continued to harmonize them to the greatest extent possible in future intercomparisons.

384 Additional inversions for Europe from three regional scale inversion systems are analyzed. Two of these  
385 systems are part of the EUROCOM ensemble, but new runs were carried out for the VERIFY project. The  
386 CarboScopeRegional (CSR) inversion system has performed additional runs for VERIFY for the years 2006-2020  
387 with multiple ensemble members differing by biogenic prior fluxes and assimilated observations. The results are  
388 plotted separately to illustrate two points: 1) that the CSR simulations for VERIFY are not identical to those submitted  
389 to EUROCOM (VERIFY runs from CSR included several sites that started shortly before the end of the EURCOM  
390 inversion period), and 2) the CSR model was used in four distinct runs in VERIFY. Note that the ensemble members  
391 differ from previous years (the spatial correlation length is kept constant this year, while more prior fluxes are used).  
392 By presenting CSR separate from the EUROCOM results, one can get an idea of the uncertainty due to various model  
393 parameters in one inversion system with one single transport model. The LUMIA inversion system submitted four  
394 simulation results to the VERIFY project, based on the set-up developed for the 2018 Drought Task Force project  
395 (labeled here as EUROCOM, Thompson et al., 2020), but with a refined definition of both prior and observation  
396 uncertainties. Also, for the years 2019-2020, the transport models (FLEXPART and TM5) were driven by ERA5  
397 meteorological data, whereas for previous years, ERA-Interim data were used. The four different variants include one  
398 reference simulation and three simulations which change spatial correlation lengths, the number of observation sites,  
399 and the magnitude of uncertainties in the boundary conditions. As one of the variants is only available for 2019-2020  
400 (changing the uncertainties in the boundary conditions), this variant was dropped from the results and only the  
401 remaining three simulations are presented, covering the period 2006-2020.

402 An inversion of the NEE over 2005-2020 from the CIF-CHIMERE variational inversion system is also  
 403 analyzed. The configuration of this inversion is close to that of the PYVAR-CHIMERE NEE inversions in the  
 404 EUROCOM ensembles and follows the general principles of Broquet et al. (2013). However, it uses distinct inputs,  
 405 which play a critical role in the inversion, such as a more recent ORCHIDEE simulation as prior estimate of the NEE  
 406 and a more recent CAMS global inversion to impose the regional CO<sub>2</sub> boundary conditions.

407

408 *Table 2: Data sources for the land CO<sub>2</sub> emissions included in this study. Details are found in Appendix A4. The*  
 409 *timesteps 1Y, 1M, 1W, and 3H refer to the availability of the data: “one year”, “one month”, “one week”, and*  
 410 *“three hours”, respectively. An overview of the datasets, including contact information, is provided in Table C1.*

<b>NGHGI net CO<sub>2</sub> land flux</b>				
<b>Data source</b>	<b>Contact / lab</b>	<b>Variables Period (timestep) Resolution</b>	<b>References</b>	<b>Status compared to Petrescu et al. (2021b)</b>
<b>UNFCCC NGHGI (2021)</b>	Member State inventory agencies  Annual, gap- filled uncertainties provided by the EU GHG inventory team	LULUCF Net CO <sub>2</sub> emissions/removals <sup>a</sup> . 1990-2019 (1Y) Country-level	IPCC (2006)  UNFCCC CRFs  <a href="https://unfccc.int/process-and-meetings/transparency-and-reporting/reporting-and-review-under-the-convention/greenhouse-gas-inventories-annex-i-parties/national-inventory-submissions-2021">https://unfccc.int/process-and-meetings/transparency-and-reporting/reporting-and-review-under-the-convention/greenhouse-gas-inventories-annex-i-parties/national-inventory-submissions-2021</a>	Updated
<b>Inventory and model estimates of net CO<sub>2</sub> land flux</b>				
<b>ORCHIDEE</b>	LSCE	CO <sub>2</sub> fluxes from all ecosystems reported as Net Biome Productivity (NBP) <sup>b</sup> . 1990-2020 (3H) 0.125° x 0.125°	Ducoudré et al. (1993) Viovy et al. (1996) Polcher et al. (1998) Krinner et al. (2005)	Updated – significant model revisions
<b>CABLE-POP</b>	Western Sydney University	CO <sub>2</sub> fluxes (NBP). Model includes N cycling. 1990-2020 (1M) 0.125° x 0.125°	Haverd et al. (2018)	New
<b>TRENDY v10</b>	MetOffice UK	CO <sub>2</sub> fluxes (NBP) 15 models (all except ISAM) 1990-2020 (3H-1M) 0.125° x 0.125°	Friedlingstein et al. (2022; Table 4)	Updated – significant differences in ensemble members

<b>CO<sub>2</sub> emissions from inland waters</b>	ULB	Average C fluxes from rivers, lakes and reservoirs, with lateral C transfer from soils. 1990-2018 (-) 0.1° x 0.1°	Lauerwald et al. (2015) Hastie et al. (2019) Raymond et al. (2013)	Not updated
<b>CBM</b>	EC-JRC	CO <sub>2</sub> fluxes (NBP) as historical 2000-2015 and extrapolation for 2017-2020 (1Y) Country-level	Kurz et al. (2009) Pilli et al. (2022)	Updated
<b>ECOSSE</b>	UNIABDN	CO <sub>2</sub> fluxes (NBP) from croplands and grassland ecosystems. Crops: 1990-2020 (1Y) Grass: 1990-2018 (1Y) 0.125° x 0.125°	Bradbury et al. (1993) Coleman (1996) Jenkinson (1977, 1987) Smith et al. (1996, 2010a,b)	Updates only for croplands – significant differences
<b>EFISCEN-Space</b>	WUR	CO <sub>2</sub> fluxes (NBP): single average value for 5 year periods, replicated on a yearly time axis. 0.125° x 0.125°	Verkerk et al. (2016) Schelhaas et al. (2017, 2020) Nabuurs et al. (2018)	Updates for 15 countries
<b>EPIC-IIASA</b>	IIASA	CO <sub>2</sub> fluxes (NBP) from cropland 1991-2020 (1M) 0.125° x 0.125°	Balkovič et al. (2013, 2018, 2020) Izaurrealde et al. (2006) Williams et al. (1990)	Updated for croplands, new estimates for grasslands
<b>BLUE (VERIFY) and BLUE (GCP)</b>	LMU Munich	CO <sub>2</sub> fluxes from land use change. VERIFY: 1990-2019 (1Y) GCP: 1990-2020 (1Y) 0.25° x 0.25°	Hansis et al. (2015) Ganzenmüller et al. (2022) - VERIFY Friedlingstein et al. (2022) - GCP2021	Updated
<b>H&amp;N</b>	Woodwell Climate Research Center	CO <sub>2</sub> fluxes from land use change. 1990-2020 (1Y) Country-level	Houghton and Nassikas (2017)	Updated
<b>FAO</b>	FAOSTAT	CO <sub>2</sub> emissions / removal from LULUCF processes. 1990-2020 (1Y) Country-level	FAO (2021) Federici et al. (2015) Tubiello et al. (2021)	Updated – significant differences for FL
<b>CO<sub>2</sub> atmospheric inversion estimates</b>				

<b>CSR inversions for VERIFY</b>	MPI -Jena	Total CO <sub>2</sub> inverse flux (NBP) <sup>c</sup> 2006-2020 (3H) 0.5° x 0.5°	Kountouris et al. (2018 a,b)	Updated – significant differences
<b>LUMIA</b>	Lund University (INES)	Total CO <sub>2</sub> inverse flux (NBP) <sup>c</sup> 2006-2020 (1W) 0.25° x 0.25°	Monteil and Scholze (2021)	New
<b>CIF-CHIMERE</b>	LSCE	Total CO <sub>2</sub> inverse flux (NBP) <sup>c</sup> 2005-2020 (3H) 0.5° x 0.5°	Berchet et al. (2021) Broquet et al. (2013)	New
<b>GCP 2021 global inversions (CTE, CAMS, CarboScope, NISMOM-CO<sub>2</sub>, UoE, CMS-Flux)</b>	GCP	Total CO <sub>2</sub> inverse flux (NBP) Six inversions 2010-2020 (various)	Friedlingstein et al. (2022) Van der Laan-Luijk et al. (2017) Chevallier et al. (2005) Rödenbeck et al. (2005) Niwa et al. (2017) Feng et al. (2016) Liu et al. (2021)	Updated – significant differences in ensemble members
<b>EUROCOM regional inversions (CSR, LUMIA, PYVAR)</b>	LSCE, ULUND, MPI-Jena, NILU	Total CO <sub>2</sub> inverse flux (NBP) <sup>c</sup> Three inversions 2009-2018 (3H-1M)	Monteil et al. (2020) Thompson et al. (2020)	Updated (also replaced CSR with the mean of the four runs submitted to VERIFY). FLEXINVERT and NAME are not included (Fig. A5)

411 <sup>a</sup> Member States use a mix of gain-loss and stock-change reporting methods (Table 6.12 in EU NIR, 2021). The net flux from a given country  
412 can thus be based on either stock changes or flux changes.

413 <sup>b</sup> The definition of NBP varies from model to model. Most models include harvest, but not necessarily other disturbances. Please refer to Table  
414 C2 for more details.

415 <sup>c</sup> The net carbon flux from regional inversions over land is the residual after fixing fossil CO<sub>2</sub> emissions and CO<sub>2</sub> fluxes from biomass burning.  
416 In other words, any flux not included in those two categories is reflected in the net flux from the inversions. Biomass burning is prescribed in two  
417 of the EUROCOM models (LUMIA and FLEXINVERT+; see Monteil et al., 2020, and Thompson et al., 2020) and ignored (i.e., assumed  
418 negligible in Europe) for the others.

419 All of the bottom-up models in this work require external forcing datasets. In the context of the VERIFY  
420 project (VERIFY, 2022), an effort was made to provide a single, harmonized version of several kinds of data  
421 (meteorological, land use/land cover, and nitrogen deposition) on a high-resolution grid over Europe. These datasets  
422 were then made available to all of the modeling groups to use in their simulations. Such a practice is common in  
423 model intercomparison projects. However, as the models in Table 2 are not all the same type, data harmonization

424 presented more of a challenge in this work as not all models use the same inputs. All of the datasets described in  
425 Appendix A5 were used by at least one modeling group in this work.

426

## 427 **2.4. Independence of estimates**

428 As pointed out by Andrew (2020), bottom-up fossil CO<sub>2</sub> emission datasets are not entirely independent, since  
429 they largely rely on activity data reported by national agencies. However, there is some variation here, particularly in  
430 traded energy products where, for example, activity data may be sourced from either the exporter or the importer  
431 according to some determination of reporting reliability. However, beyond the underlying activity data, other choices  
432 do vary between datasets: emission factors, which specific products lead to emissions, and how the activity data are  
433 used to estimate the amount of energy product that is consumed, among others. Some examples of differences include:  
434 CDIAC avoids using reported energy consumption and relies on estimating apparent consumption from the major  
435 energy flows; CEDS initially used a very different estimate for emissions from international shipping; EDGAR and  
436 IEA use a Tier 1 approach with default emission factors, while PRIMAP-Hist and GCP use officially reported  
437 emissions based on higher Tier methods and country-specific emission factors for selected countries. Further, the  
438 emission sources covered can vary widely between datasets, with the IEA usually limited to emissions from energy  
439 products, while EDGAR, for example, attempts to include all fossil CO<sub>2</sub> sources. With this lack of full independence  
440 between datasets' sources and methods, the uncertainty ranges should be interpreted with caution.

441 In addition to fossil bottom-up methods, the question of dataset independence can be applied to bottom-up  
442 inventories of the land fluxes, as well as both bottom-up and top-down models. The issue is perhaps less relevant for  
443 model results which, despite sharing input data (as done here to facilitate intercomparison) and "genetics" (i.e., model  
444 development history), create independence through choices of model structure, parameterization, and statistical  
445 solvers. This question has been addressed elsewhere for land surface models (e.g., Prentice et al., 2015). For  
446 inventories, the NGHGI and FAOSTAT share some data (e.g., Tubiello et al., 2021, for the case of Forestland, and  
447 Conchedda and Tubiello, 2020, for drained organic soils in Grassland and Cropland). However, the model approaches  
448 can be quite different, with FAOSTAT limited to Tier 1 (applicable to every country in the world based on available  
449 statistics) and the NGHGIs, in particular in Europe, using more Tier 2 (regional and country-specific emission factors)  
450 and Tier 3 (process-based models) approaches, depending on the country and the specific pool. For example, 21  
451 Member States in the European Union report changes of organic carbon stored in mineral soils on Forest land using a  
452 Tier 1 method, while only two (Malta and Cyprus) use a Tier 1 method for estimates of carbon stored in living biomass  
453 on Forest land (EU NIR, 2021).

454 In this work, the uncertainties for the NGHGI were calculated with assumptions of correlation based on the exact  
455 method applied by the country. As detailed in the Appendix A2 (NGHGI uncertainties), subsector values across  
456 countries are assumed to be correlated for all countries applying a Tier.1 approach as they share default emission  
457 factors. The uncertainties calculated for the NGHGI fossil and LULUCF fluxes, therefore, reflect more accurately  
458 spatial dependence between the inventories of each Member State.

459



## 460 **3. Results and discussion**

### 461 **3.1. Overall NGHGI reported anthropogenic CO<sub>2</sub> fluxes**

462 In 2019, the UNFCCC NGHGI (2021) net CO<sub>2</sub> flux estimates for EU27+UK accounted for 820 Tg C from all  
463 sectors (including LULUCF) and 900 ± 10 Tg C excluding LULUCF (Fig. B1), corresponding to a net sink of  
464 LULUCF of -74 ± 30 Tg C, where the uncertainties are 95 % CI calculated in accordance with the gap-filling methods  
465 of Appendix A2 and propagated to the sector level through Gaussian quadrature. In 2019, few large economies  
466 accounted for the majority of EU27+UK emissions, with Germany, UK, Italy and France representing 53 % of the  
467 total CO<sub>2</sub> emissions (excluding LULUCF). For the LULUCF sector, the countries reporting the largest CO<sub>2</sub> sinks in  
468 2019 were Italy, Spain, Sweden, and France accounting for 56 % of the overall EU27+UK sink. Only a few countries  
469 (Czech Republic, The Netherlands, Ireland and Denmark) reported a net LULUCF source in 2019. Some countries,  
470 like Portugal, report sources in some years due to wildfires, with sinks in other years. The NGHGI shows minimal  
471 interannual variability in the LULUCF sector (Fig. B2), largely due to methodology. For example, emissions and  
472 removals from Forest land are typically based on forest statistics and surveys that are only completed every 5-10 years  
473 (see, for example, the national inventory reports and references cited therein of France, Germany, and Sweden). The  
474 largest contributors to IAV in the EU NGHGI forestry fluxes are fires and windstorms (EU NIR, 2021). Consequently,  
475 the 2019 values are indicative of longer-term averages.

476 CO<sub>2</sub> fossil emissions reported by Member States are dominated by the energy sector (energy combustion and  
477 fugitives) representing 92 % of the total EU27+UK CO<sub>2</sub> emissions (excluding LULUCF) or 895 Tg C in 2019. The  
478 Industrial Process and Product Use (IPPU) sector contributes 7.6 % or 68 Tg C (21 Tg C of which is cement  
479 production). CO<sub>2</sub> emissions reported as part of the agriculture sector cover only liming and urea application, UNFCCC  
480 categories 3G and 3H<sup>9</sup> respectively. Together with waste, in 2019 the emissions from agriculture represent 0.4 % of  
481 the total UNFCCC CO<sub>2</sub> emissions in the EU27+UK.

482 An overview of all CO<sub>2</sub> fossil and land datasets in this work (Fig. 1) leads to a series of conclusions: 1) Regardless  
483 of the method used (NGHGI, bottom-up models, top-down models), the timeseries of annual fluxes from fossil CO<sub>2</sub>  
484 emissions rest almost one order of magnitude higher than removals from CO<sub>2</sub> uptake/removal by the land surface and  
485 well outside uncertainty estimates (Figs. 1a-c); 2) Uncertainties are much larger in the LULUCF estimates than in the  
486 fossil CO<sub>2</sub> estimates, regardless if one represents uncertainty by internal random error (i.e., the NGHGI totals in Fig.  
487 1a, and the sub-sector LULUCF fluxes in Fig. 1d) or ensemble spread (i.e., bottom-up models in Fig. 1b, and the sub-  
488 sector LULUCF fluxes in Fig. 1e); 3) Interannual variability (IAV) is much more present in non-NGHGI LULUCF  
489 datasets (colored lines in Figs. 1b,c,e) than in NGHGI LULUCF datasets (Figs. 1a,d) or any of the fossil datasets  
490 (black lines in all subplots). As datasets are not fully independent, the uncertainties in Fig. 1 need to be interpreted  
491 with caution.

492 The overall message that fossil CO<sub>2</sub> emissions exceed the land sink (Figs. 1a-c) is the same as found in the  
493 Global Carbon Budget (Friedlingstein et al., 2022), although the difference is larger in the EU27+UK. Contrary to

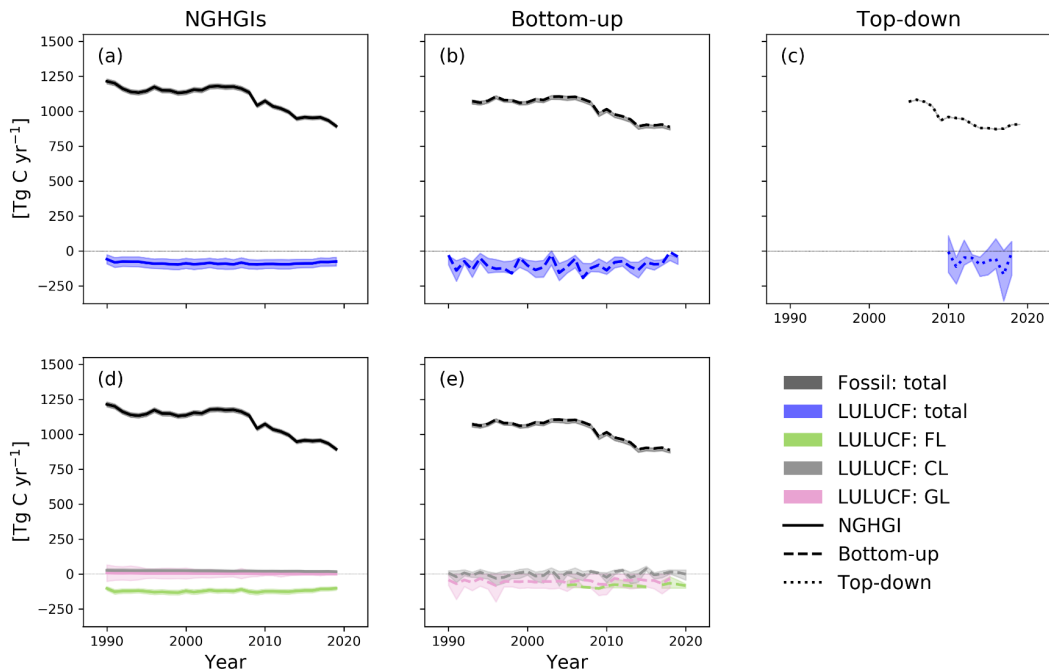
---

<sup>9</sup> 3G and 3H refer to UNFCCC category activities, as reported by the standardized common reporting format (CRF) tables, which contain CO<sub>2</sub> emissions from agricultural activities: liming and urea applications.

494 the GCB, however, fossil CO<sub>2</sub> emissions in the EU27+UK have decreased over the past three decades. Again, this  
 495 finding is supported by the NGHGI, bottom-up models, and a single atmospheric inversion. By applying a Monte  
 496 Carlo analysis and taking each point to be normally distributed around the mean with a width 2σ equal to the given  
 497 95 % CI, we realized 1000 linear regressions of the NGHGI across the 1990-2019 period. From this, we fit a normal  
 498 distribution to the slopes, and can rule out trends greater than 0.07 or less than -0.61 Tg C yr<sup>-2</sup> with 95 % confidence.  
 499 Therefore, any trend over these 30 years is likely less than 1 % of the net carbon uptake, with the vast majority of that  
 500 occurring in forests. While the latter conclusion is clear in the NGHGI (Fig. 1d), very large spreads among bottom-  
 501 up categorical models lead to more uncertainty (bottom-center).

502 The difference in uncertainty between the estimates of fossil CO<sub>2</sub> emissions and CO<sub>2</sub> uptake/removal by the land  
 503 surface is also striking. Eight bottom-up models produce a mean 25-75th percentile spread of 24 Tg C yr<sup>-1</sup> across the  
 504 overlapping timeseries (center-top, gray shading). On the other hand, four models estimating Grassland  
 505 emissions/removals produce an error bar that covers the bottom part of the graph and masks any apparent trend  
 506 (bottom-center, light green shading). A similar conclusion can be drawn from top-down estimates of LULUCF fluxes  
 507 (top-right, blue shading). Additional work on reducing the uncertainty of LULUCF fluxes in the EU27+UK is highly  
 508 welcome.

509



510

511 *Figure 1: A synthesis of all the CO<sub>2</sub> net fluxes shown in the work for the EU27+UK. The estimates are divided by*  
 512 *approach: NGHGI estimates (panels a, d); bottom-up methods (b, e); and top-down methods (c). Panels (d) and (e)*  
 513 *include a breakdown of the [bottom-up] LULUCF flux into three of the dominant components: FL, GL, and CL.*  
 514 *Such a breakdown is not provided for NGHGI CO<sub>2</sub> fossil as partitioning of bottom-up CO<sub>2</sub> fossil datasets*  
 515 *corresponding to UNFCCC NGHGI categories is not currently available. The NGHGI UNFCCC uncertainty is*  
 516 *calculated for submission year 2021 as the relative error of the NGHGI value, computed with the 95 % confidence*

517 *interval method gap-filled and provided for every year of the timeseries, except for FL, GL, and CL which are taken*  
518 *directly from the EU NIR (2021). Shaded areas for the other estimates represent the 0th-100th percentiles for*  
519 *groups with fewer than seven members, and the 25th-75th percentile for groups with seven or more members.*  
520 *Ensembles (e.g., TRENDY v10) are included in the above only their mean values, to avoid more heavily weighting*  
521 *the ensembles compared to the other datasets.*

522

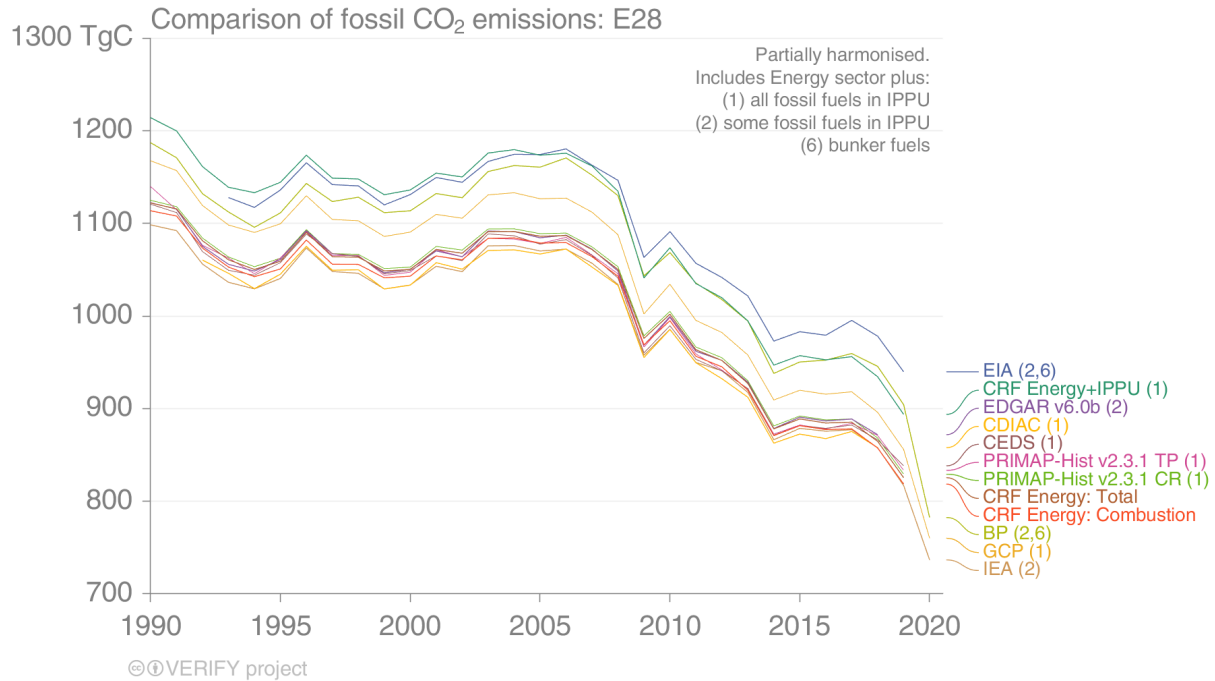
523 Several caveats remain with this overall synthesis. First, the timeseries were combined rather naively in Fig. 1  
524 by taking the mean of annual timeseries for each dataset discussed below. This leads to, for example, the 15-member  
525 TRENDY ensemble being given identical weight as the ORCHIDEE high-resolution simulation over Europe. This  
526 was done to weigh more heavily the regional approaches under the assumption that higher resolution simulations and  
527 more region-specific input data will lead to more accurate results. While the latter assumption appears reasonable,  
528 the first assumption can be disputed. Finer resolution leads to models being exposed to values of input variables (e.g.,  
529 temperature, rainfall) outside the parameterization range, which may result in unexpected behavior. Process  
530 representation can also change with spatial scale. Constant tree mortality, for example, is often used in models at  
531 coarse resolution, while abrupt tree mortality (stand-replacing disturbances) may better describe stand-level dynamics.  
532 Second, only a single top-down result for fossil CO<sub>2</sub> emissions is currently available, preventing an estimate of the  
533 uncertainty for this approach. Third, categorical models were combined disregarding distinctions between those  
534 models estimating “Remain” and “Total” fluxes, where Total indicates all land of a particular type (e.g., Forest land)  
535 regardless of the length of time it has been this type, i.e., Total is the sum of all Remain and Convert. These points  
536 are discussed in more detail in the following sections. However, addressing these points is highly unlikely to alter the  
537 overall conclusions in this section.

538

### 539 **3.2. CO<sub>2</sub> fossil emissions**

540 The inventory-based fossil CO<sub>2</sub> estimates from nine data sources (and some subsets) are presented as timeseries  
541 (1990-last available year) based on Andrew (2020) with the objective to explore differences between datasets and  
542 visualize trends (Fig. 2). Because the emissions source coverage (also called the “system boundary”) of datasets  
543 varies, comparing total emissions from these datasets is not a like-for-like comparison. Therefore, some harmonization  
544 of system boundaries prior to comparison is needed. This harmonization relies on specifying the system boundary of  
545 each dataset and, where possible, removing emission sources to produce a near-common system boundary. For  
546 example, IEA doesn’t include any carbonates, and thus carbonates were removed from all emissions datasets that  
547 include them. UNFCCC (CRFs) Energy+IPPU, CDIAC, CEDS, PRIMAP, and GCP include Energy sector plus all  
548 fossil fuels in IPPU; EIA, EDGAR and BP include some fossil fuels in IPPU, while EIA and BP include bunker fuels  
549 as well. UNFCCC CRFs include Energy total and Energy combustion. Further details on how data sets are harmonized  
550 are provided by Andrew (2020). Because of differing levels of detail provided by datasets, it isn’t possible to do this  
551 perfectly, but the approximate harmonization gives something closer to a like-for-like comparison, with the legend in  
552 Fig. 2 indicating the most significant remaining differences. The pre-harmonization curves are shown in Appendix  
553 A3 (Fig. A1) for reference.

554



556

557 *Figure 2: Comparison of EU27+UK fossil CO<sub>2</sub> emissions from multiple inventory datasets with system boundaries*  
 558 *harmonized as much as possible. Harmonization is limited by the disaggregated information presented by each*  
 559 *dataset. CDIAC does not report emissions prior to 1992 for former-Soviet Union countries. CRF: UNFCCC NGHGI*  
 560 *from the Common Reporting Format tables. The pre-harmonization figure is shown in Fig. A1.*

561 Given the remaining differences in system boundaries after harmonization, most datasets agree well  
 562 (Andrew, 2020). In response to inconsistencies identified in this work, the EIA recently corrected some double-  
 563 counting of emissions from liquid fuels and has revised its estimates of total emissions down about 10 % for the  
 564 EU27+UK (pers. comm., US Energy Information Agency, February 2022). For comparison, applying a similar  
 565 harmonization procedure to the UNFCCC NGHGI and retaining only Fuel combustion (1A), Fugitive emissions (1B),  
 566 Chemical industry (2B), Metal industry (2C), Non-energy products from fuels and solvent use (2D), and Other (2H)  
 567 results in emissions of  $930 \pm 10$  Tg C yr<sup>-1</sup> for the year 2017, where the uncertainty was propagated through quadrature  
 568 using the gap-filled uncertainties described in this work and taking the total sector uncertainty if the category  
 569 uncertainty was not available. This mean value falls within the 25th-75th percentiles of the eight other harmonized  
 570 BU sources ( $[884,928]$  Tg C yr<sup>-1</sup>). Across the overlapping timeseries, the mean value of the 25<sup>th</sup>-75<sup>th</sup> percentile is 24  
 571 Tg C yr<sup>-1</sup>, with a 0<sup>th</sup>-100<sup>th</sup> percentile of 100 Tg C yr<sup>-1</sup>.

572 The sole available inversion for CO<sub>2</sub> fossil fluxes is produced by the CIF-CHIMERE model, shown in Fig. 1c  
 573 and Fig. B3 (for a single year). The inversion yields plausible fossil emission estimates, although it is below NGHGI  
 574 estimates including both Energy and IPPU (Figs. 1a,c,B3) as well as the ensemble of nine bottom-up inventories.  
 575 Uncertainties of CIF-CHIMERE inversion estimate have not yet been quantified, however they are likely largely  
 576 driven by large uncertainties in the input data. The satellite observations of NO<sub>2</sub> have large uncertainties, which partly  
 577 explains the small departure from the prior fluxes during the optimization. Emission ratios between NO<sub>x</sub> and CO<sub>2</sub> are

578 also uncertain (those from the prior are currently used). The atmospheric chemistry surrounding both production and  
579 destruction of NO<sub>2</sub> is another major source of uncertainty. The inversion reports total fossil CO<sub>2</sub> emissions calculated  
580 from NO<sub>x</sub> fossil fuel combustion emissions. However, in principle, the derivation of CO<sub>2</sub> emissions from the NO<sub>x</sub>  
581 inversions should be restricted to derivation of fossil fuel CO<sub>2</sub> emissions based on the fossil fuel CO<sub>2</sub>/NO<sub>x</sub> ratio from  
582 the TNO inventory, since there is no process linking the other fossil CO<sub>2</sub> emissions to the NO<sub>x</sub> fossil fuel emissions.  
583 Future inversions co-assimilating CO<sub>2</sub> data will have to make a clearer distinction in the processing of fossil-fuel and  
584 other anthropogenic emissions in order to exploit the joint fossil fuel signals in CO<sub>2</sub> and NO<sub>2</sub> observations. Finally, it  
585 is important to note that the inversion results are not fully independent of the bottom-up methods, as the prior estimates  
586 and CO<sub>2</sub>/NO<sub>x</sub> emission ratios are based on TNO gridded products. However, part of the lack of departure from the  
587 prior can also be attributed to the general consistency between the prior and the observations, which raise optimistic  
588 perspectives for the co-assimilation of co-emitted species with the data from future CO<sub>2</sub> networks dedicated to  
589 anthropogenic emissions.

590

### 591 **3.3. CO<sub>2</sub> land fluxes**

592

593 This section updates the benchmark data collection of CO<sub>2</sub> emissions and removals from the LULUCF sector in  
594 EU27+UK previously published in Petrescu et al. (2020) and Petrescu et al. (2021b), expanding on the scope of those  
595 works by adding additional datasets and years. The following graphs occasionally show large differences compared  
596 to previously-reported values. This may happen when the model has undergone substantial changes since the work  
597 of Petrescu et al. (2021b), such as the case with ORCHIDEE and the addition of a dynamic nitrogen cycle coupled to  
598 the carbon cycle. Such cases are both identified in the text as appropriate and as well as in Table 2. The countries  
599 analyzed in this study use country-specific activity data and emissions factors for the most important land use  
600 categories and pools (EU NIR 2022, UK NIR 2022). However, several gaps still exist, mainly in non-forest lands and  
601 non-biomass pools (e.g., soil carbon in Forest land mineral soils, dead organic matter on Cropland and Grassland; for  
602 more details, see Table 6.6 in EU NIR, 2021). In addition, since NGHGs largely rely on periodic forest inventories  
603 (carried out every five to ten years) for the most important land use (Forest land), the net CO<sub>2</sub> LULUCF flux often  
604 does not capture the most recent changes, nor the full interannual variability.

605 While the net LULUCF CO<sub>2</sub> flux was relatively stable from 1990 to 2016, staying mostly between -80 to -95 Tg  
606 C yr<sup>-1</sup>, in the past three years the sink has weakened to around -70 Tg C yr<sup>-1</sup> in 2020 (black dotted line in Fig. B2,  
607 Appendix B1; Abad-Viñas, pers. comm, 2022). This weakening occurred mostly in Forest land, due to a combination  
608 of increased natural disturbances, forest aging and increased wood demand (Nabuurs et al., 2013; EU NIR, 2022).  
609 Natural disturbances, including fires (especially in the southern Mediterranean), windthrows, droughts and insect  
610 infestations (especially in central and northern European countries), have increased in recent years (e.g., Seidl et al.,  
611 2014) which explains most of the interannual variability of the NGHGI. Forest aging affects the net sink both through  
612 the forest growth (net increment) - which tends to level off or decline after a certain age - and the harvest, because a  
613 greater area of forest reaches forest maturity (Grassi et al., 2018b). Although the exact increase in total harvest in  
614 Europe in recent years is still subject to debate (Ceccherini et al., 2020; Palahi et al. et al., 2021), demand for fuelwood

615 at least has increased (Camia et al., 2021). The impacts of aging on mortality, another process which affects the net  
616 sink through reduced production and increased respiration, are less clear (e.g., Gray et al., 2016; Senf et al., 2018).

617 Net carbon uptake as seen by the atmosphere may occur on either managed or unmanaged land, and results from  
618 the balance of processes such as photosynthesis, respiration, and disturbances (e.g., fire, pests, harvest). As discussed  
619 by Petrescu et al. (2020), the fluxes reported in NGHGs relate to emissions and removals from direct LULUCF  
620 activities (clearing of vegetation for agricultural purposes, regrowth after agricultural abandonment, wood harvesting  
621 and recovery after harvest and management) but also indirect CO<sub>2</sub> fluxes due to processes such as responses to  
622 environmental drivers on managed land (e.g., long-term changes in CO<sub>2</sub>, air temperature, and water availability).  
623 Additional CO<sub>2</sub> fluxes occur on unmanaged land, but the fraction of unmanaged land in the European Union is only  
624 around 5 % and divided between Forest land, Grassland, and Wetlands. According to Table 4.1 in the EU27 and UK  
625 NGHGs (2021) CRF, almost all land (~95 %) in the EU27+UK is considered managed. France and Greece report  
626 some unmanaged Forest land (1.1 % and 16.6 %, respectively). Hungary and Malta report unmanaged Grassland of  
627 33 % and 100 %, respectively, and Nordic and Baltic countries plus Ireland, Slovakia and Romania report sometimes  
628 quite large (up to 100 %) unmanaged Wetlands.

629 The indirect CO<sub>2</sub> fluxes on managed and unmanaged land due to changing climate, increasing atmospheric  
630 carbon dioxide mole fractions, and nitrogen deposition, are part of the (natural) land sink in the definition used in  
631 IPCC Assessment Reports and the Global Carbon Project’s annual global carbon budget (Friedlingstein et al., 2022),  
632 while the direct LULUCF fluxes are termed “net land-use change flux”, as discussed by Grassi et al. (2018a, 2021,  
633 2022a), Petrescu et al. (2020, 2021b) and Pongratz et al. (2021). Results should thus be interpreted with caution due  
634 to these definitional differences, but as most of the land in Europe is managed and the indirect effects are small, the  
635 definitional differences should be modest compared to other sources of uncertainty (Petrescu et al., 2020). Other  
636 relatively recent studies have already analyzed the European land carbon budget using GHG budgets from fluxes,  
637 inventories and inversions (Luyssaert et al., 2012) and from forest inventories (Pilli et al., 2017; Nabuurs et al., 2018).  
638

### 639 3.3.1. Estimates of CO<sub>2</sub> land fluxes from bottom-up approaches

640

641 In this section we present annual total net CO<sub>2</sub> land emissions between 1990-2020 i.e., induced by both  
642 LULUCF and natural processes (e.g., environmental changes) from category-specific models as well as from models  
643 that simulate multiple land cover/land use categories. The definitions of the categories may differ from the IPCC  
644 definitions of LULUCF (e.g., FL, CL, GL) where, according to IPCC 2006 guidelines, to become accountable in the  
645 NGHGI under “remaining” categories, a land-use type must be in that category for at least N years (where N is the  
646 length of the transition period; 20 years by default). In an effort to create the most accurate comparison possible in  
647 terms of categories and processes included, total Forest land (FL) has been divided up into Forest land remaining  
648 forest land (FL-FL) and Land converted to forest land (X-FL), while only total Grassland (GL) and Cropland (CL) are  
649 reported. This is largely due to the non-forest categorical models explored here only considering net land use change,  
650 which prevents separating out the “converted” component.

651

### 652 3.3.2. Bottom-up estimates of CO<sub>2</sub> from Forest land

653

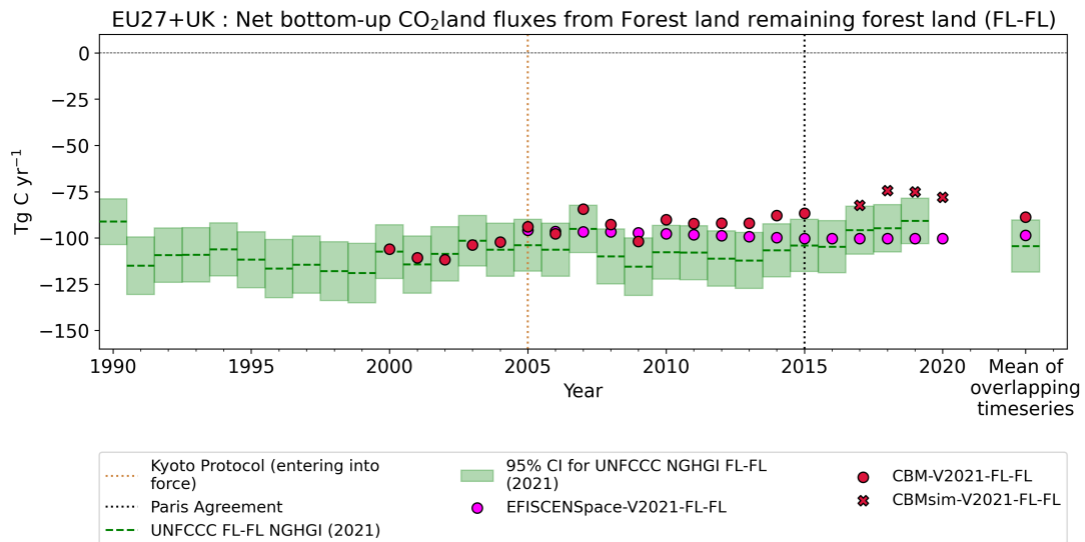
654 Fluxes from Forest land which remain in this category (FL-FL) are shown in Fig. 3 (top). These fluxes were  
655 simulated with ecosystem models (CBM and EFISCEN-Space, described in more detail in the Appendices) and  
656 countries' official inventory statistics reported to UNFCCC. The results show that the differences between models are  
657 systematic, with CBM having slightly weaker sinks than EFISCEN-Space. CBM updated its historical data (1990-  
658 2015) and presents new NBP estimates based on extrapolation of historical timeseries (see Appendix A4) for 2017-  
659 2020 (CBMsim). Both CBM and EFISCEN-Space use national forest inventory (NFI) data as the main source of input  
660 to describe the current structure and composition of European forests. NFIs are also the main source of input data for  
661 most countries in the EU27+UK for NGHGIs (EU NIR, 2021), including data for carbon stock changes in various  
662 pools as well as the estimation of forest areas. Given that EFISCEN-Space does not cover all countries in the  
663 EU27+UK (Austria, Bulgaria, Denmark, Hungary, Lithuania, Portugal and Slovenia are missing), the results were  
664 scaled by 1/0.74 to account for the fact that the available countries comprise around 74 % of the forest NBP for the  
665 EU27+UK, according to previous EFISCEN results (Petrescu et al., 2021b). As noted above, EU regulations are  
666 driving Member States to report spatially explicit NGHGIs. Unlike the original EFISCEN, EFISCEN-Space is a  
667 spatially explicit model, in addition to being able to simulate a wider variety of stand structures, species mixtures and  
668 management options. Note that EFISCEN-Space reports only a single mean value for forest fluxes from 2005-2020;  
669 the annually varying value shown in Fig. 3 (top) arises from scaling by annually varying forest areas.

670 The bottom panel in Fig. 3 presents CO<sub>2</sub> land estimates for total Forest land (FL, including both remain and  
671 convert classes). For the total Forest land, the results were simulated with an ecosystem model (ORCHIDEE) and a  
672 global dataset (FAOSTAT) as it is not possible for these two approaches to separate out the "remain" and "convert"  
673 land use category. This obstacle arises due to the use of net land use/land cover information which does not include  
674 detailed information on the nature of the conversions. Consequently, Fig. 3 (bottom) compares flux estimates to those  
675 on all Forest land from the countries' official inventory statistics (UNFCCC NGHGI, 2021).

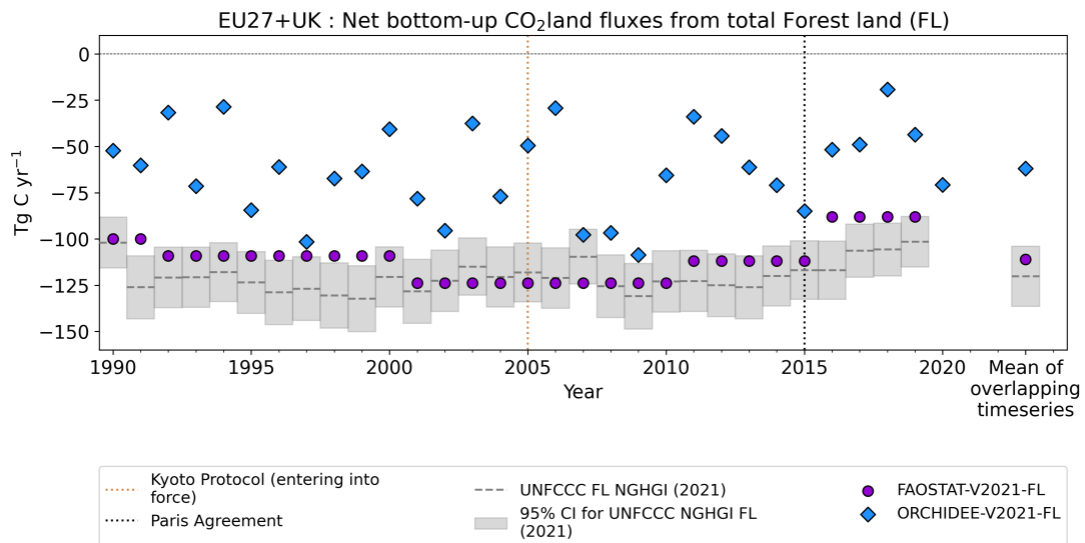
676 The top and bottom panels in Fig. 3 are not directly comparable due to different quantities being displayed (FL-  
677 FL vs. FL). For the NGHGI, the value in the bottom panel is simply the value from the top panel with the addition of  
678 emissions/removals on land converted to Forest land within the past 20 years. The sink gets stronger by around 20  
679 Tg C yr<sup>-1</sup> when considering FL, which is to be expected as abandonment of Cropland or Grassland and subsequent  
680 regrowth of forest results in a net uptake of carbon due to storage in woody biomass. The UNFCCC NGHGI  
681 uncertainty of CO<sub>2</sub> estimates from Forest land across the EU27+UK, computed with the error propagation method (95  
682 % confidence interval, see IPCC, 2006), is 13.5 % for the year 2019 (EU NIR, 2021). This percentage is applied  
683 across all years for both FL and FL-FL, and in year 2019 it translates into an uncertainty of 12 Tg C for FL-FL.

684 Differences within the top panel of Fig. 3 are small, perhaps because all three approaches (NGHGI, CBM,  
685 EFISCEN-Space) rely heavily on forest inventory statistics. The same can be said for FAOSTAT FL fluxes in the  
686 bottom panel of Fig. 3. Among all the data plotted on the two graphs, ORCHIDEE stands out. Despite site-level  
687 evaluation (e.g., Vuichard et al., 2019), the vegetation classes in ORCHIDEE are fairly broad (e.g., temperate  
688 needleleaf evergreen) and parametrized to reproduce global fluxes, which means ORCHIDEE may be less suitable for

689 regional simulations without further adjustments. As trends in forest carbon strongly result from management, the  
 690 lack of explicit management in this version of ORCHIDEE also likely contributes, given the importance of  
 691 management across Europe.  
 692  
 693



CC BY VERIFY Project



CC BY VERIFY Project

694  
 695 *Figure 3: Net CO<sub>2</sub> land flux from Forest land remaining forest land (FL-FL, top panel) and total Forest land (FL,*  
 696 *bottom) for EU27+UK. Means are given for 2005-2019 (top) and 1990-2019 (bottom) on the right side of both*  
 697 *plots. CBM FL-FL historical estimates include 25 EU and UK countries (excl. Cyprus and Malta), in addition to*  
 698 *new estimates for 2017-2020 (red crosses). EFISCEN-Space results have been scaled up from available countries as*



699 *described in the text. FAOSTAT data does not include Romanian inventory estimates. The relative error on the*  
700 *UNFCCC value represents the UNFCCC NGHGI (2021) MS-reported uncertainty with no gap-filling (EU NIR,*  
701 *2021). The fluxes follow the atmospheric convention, where negative values represent a sink while positive values*  
702 *represent a source.*

703 Romanian estimates for FL in FAOSTAT (Fig. 3, bottom) have been removed due to a reporting inconsistency,  
704 which had not yet been corrected at the time of this analysis. In general, FAOSTAT results match well the NGHGI  
705 results, despite differences in models and even occasionally underlying data reported by countries to both  
706 organizations (Tubiello et al., 2021). ORCHIDEE was updated to include a dynamic nitrogen cycle coupled to the  
707 carbon cycle in this work. As shown in Appendix A4, the coupled nitrogen cycle results in a stronger sink, even if  
708 identical forcing is used. ORCHIDEE shows a higher inter-annual variability in carbon fluxes for forests than the  
709 NGHGI in Fig. 3 (bottom) because it incorporates meteorological data at sub-monthly timescales, while methods  
710 based on forest inventories are generally updated only every few years (e.g, five years for FRA), which results in a  
711 more climatological perspective. ORCHIDEE results indicate that climatic perturbations and extreme events (multi-  
712 month droughts, in particular) can have significant impacts on the net carbon fluxes depending on their timing in  
713 relation to the growing season. Flux tower measurements show that carbon sink strength in a European forest may  
714 weaken by 50 % during a summer drought, or a loss of 15 % of net carbon uptake over the course of the year (Ciais  
715 et al., 2005). This is also to some extent supported by dendrometer data although such data varies greatly among sites  
716 and tree species which obscures a significant net effect (Scharnweber et al., 2020). It should also be noted that  
717 dendrometer data measures carbon stored in individual trees, while the NBP reported in figures in this paper include  
718 respiratory fluxes from litter and soil. The variability of the weather affects the carbon dynamics of all components of  
719 the ecosystems (hence NBP), which, for instance, impacts on carbon assimilation rates, length of the growing season,  
720 dynamics of respiration rates and allocation of the carbon in the plant (cf. Fig. 1 and 2 in Reichstein et al. (2013) and  
721 Bastos et al. (2020b)).

722

### 723 3.3.3. Bottom-up estimates of CO<sub>2</sub> from Cropland and Grassland

724

725 Cropland (CL, UNFCCC subsector 4B) and Grassland (GL, UNFCCC sector 4C) include net CO<sub>2</sub> emissions  
726 from or removals by soil organic carbon (SOC) under "remaining" and "conversion" categories, and are shown in the  
727 top and bottom panels of Fig. 4, respectively, for the EU27+UK along with four other approaches: one bottom-up  
728 inventory (FAOSTAT), two category-specific models (EPIC-IIASA, ECOSSE), and one DGVM (ORCHIDEE). The  
729 previous synthesis of Petrescu et al. (2021b) compared models against NGHGI results for CL-CL and GL-GL. For  
730 the current work, we compare against the total Cropland (CL) and Grassland (GL) values. The reason for this is that  
731 FAOSTAT, ECOSSE, EPIC-IIASA, and ORCHIDEE all use land use/land cover maps generated by Approach 1 in  
732 IPCC (2006), which only records the total amount of land in a category for each year; information on transitions  
733 between categories is unknown. Therefore, it is not possible to separate out "remain" and "convert" categories.

734 For CL during common period (1990-2019), ORCHIDEE simulates a mean sink of -26 Tg C yr<sup>-1</sup>, while  
735 ECOSSE, EPIC-IIASA, and FAOSTAT all simulate mean sources of 21 Tg C yr<sup>-1</sup>, 10 Tg C yr<sup>-1</sup> and 16 Tg C yr<sup>-1</sup>,  
736 respectively. With the exception of ORCHIDEE, all models are in line with the NGHGI results (22 ± 14 Tg C yr<sup>-1</sup>).

737 The sink in ORCHIDEE arises from the soil, as no simulated biomass in croplands remains from year to year; carbon  
738 is assimilated into biomass growth during the growing season, after which the biomass dies, is partitioned between  
739 litter and harvest (50 % to each), and either decays or vaporizes, respectively. In other words, no woody or perennial  
740 crops are simulated. Given more favorable growing conditions due to climatic changes and CO<sub>2</sub> fertilization,  
741 increased litter leads to more carbon entering the soil in ORCHIDEE in recent decades, which is driving the calculated  
742 CL sink observed in the model.

743 In the NGHGI, the reported source for the EU27+UK is mostly attributed to emissions from Cropland on  
744 organic soils<sup>16</sup> in the northern part of Europe where CO<sub>2</sub> is emitted due to carbon oxidation from tillage activities and  
745 drainage of peat. In general, annual crops are assumed to be in carbon balance: any carbon assimilated during the year  
746 is respired in the same location. Woody crops (e.g., apple or olive orchards), however, are an exception, and Cropland  
747 on mineral soils uptake carbon in both France and Spain. Romania reports a strong sink on Cropland due to the  
748 inclusion of some forest plantations. Overall, emissions from organic soils on Land converted to cropland dominate,  
749 however; despite accounting for only 9 % of total Cropland area in the EU27+UK, they are responsible for 73 % of  
750 Cropland emissions (EU NIR, 2021). The fact that FAOSTAT values are similar to the UNFCCC values points to the  
751 primary role of drained organic soils, as this is the only flux included for the FAOSTAT dataset in Fig. 4. Finland  
752 and Sweden are of particular importance, as they together account for more than half of the total area of organic soil  
753 in Europe. Organic soils are an important source of emissions when they are under management practices that disturb  
754 the organic matter stored in the soil. In general, the NGHGI emissions from these soils are reported using country-  
755 specific values when they represent an important source within the total budget of GHG emissions.

756 ORCHIDEE also shows a much larger year-to-year variation than EPIC-IIASA and ECOSSE. This is unlikely  
757 to be caused by model timesteps (EPIC-IIASA and ECOSSE at daily, ORCHIDEE at half-hourly) as both EPIC-  
758 IIASA and ECOSSE use minimum and maximum temperatures during the course of the day as input, not simply the  
759 mean daily temperature. Therefore, all three models should see similar extremes, and crop vegetation may simply be  
760 more sensitive to meteorological forcing in ORCHIDEE. FAOSTAT and NGHGIs are mostly insensitive to inter-  
761 annual variability as the estimations are mainly based on statistical data for surfaces/activities and emission factors  
762 that do not vary with changing environmental conditions.

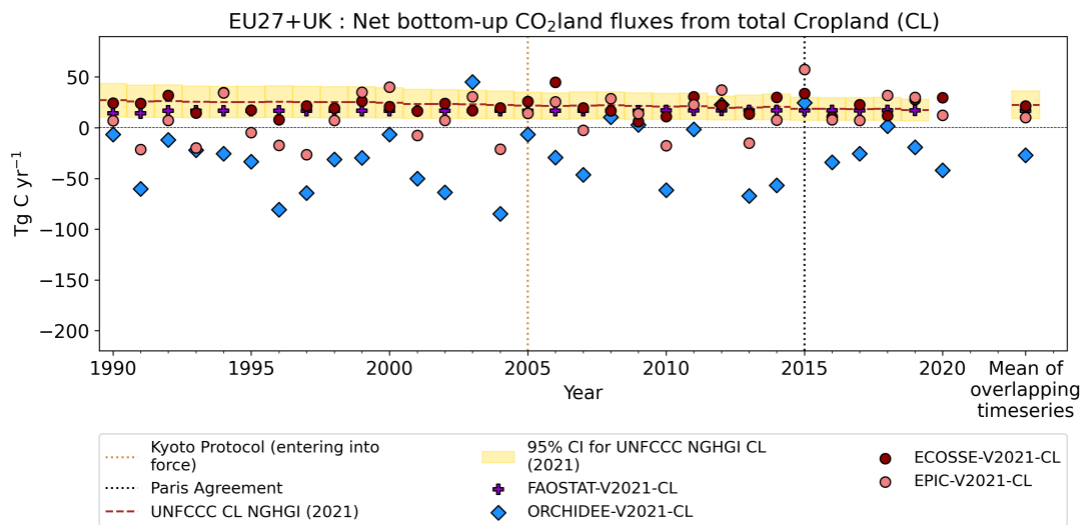
763 Both ECOSSE and EPIC show a striking improvement in agreement with the NGHGI between V2019 (Fig.  
764 B5, top) and the current work (Fig. B5, bottom). For ECOSSE, this is the result of improved data, in particular around  
765 residue management using the external tool MIAMI and more realistic fertilizer data (Mueller et al., 2012). For EPIC,  
766 the shifts in net CO<sub>2</sub> fluxes in the current EPIC results stem from the updated soil organic carbon and nitrogen module  
767 (Balkovič et al., 2020) and updates in meteorological forcing. Firstly, the updated soil module resulted in higher  
768 heterotrophic respiration across many EU regions. Besides attributing more carbon to the soil surface emissions,  
769 enhanced respiration leads to higher NPP and yields in regions with low fertilization rates as more nitrogen is released

---

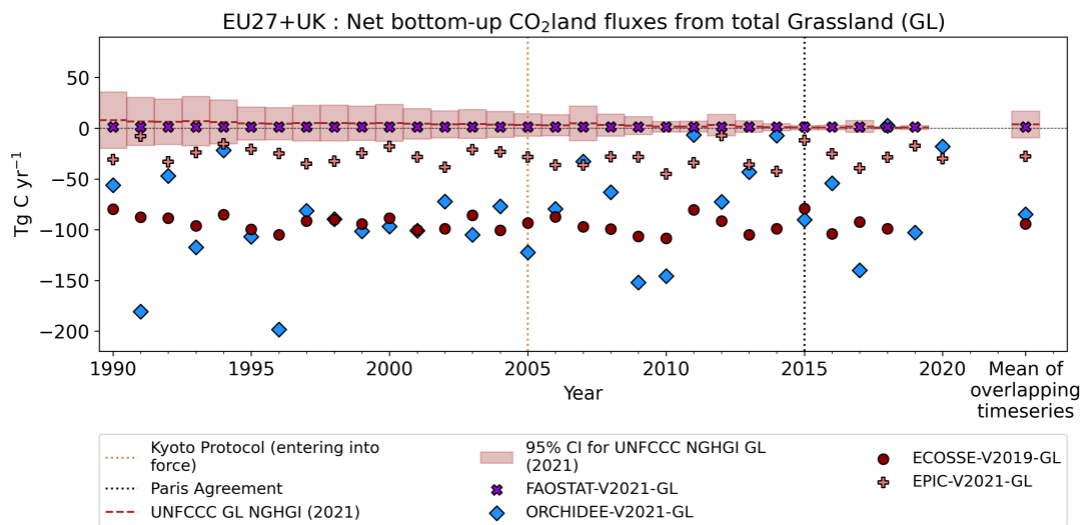
<sup>16</sup>The 2006 IPCC Guidelines largely follow the definition of Histosols by the Food and Agriculture Organization (FAO), but have omitted the thickness criterion from the FAO definition to allow for often historically determined, country-specific definitions of organic soils (see Annex 3A.5, Chapter 3, Volume 4 of IPCC (2006) and Chapter 1, Section 1.2 (Note 3) of IPCC (2014)).

770 from the SOM pool. Secondly, altered solar radiation and air temperature data affected the full range of carbon  
 771 variables in EPIC, including NPP, harvested biomass, heterotrophic respiration, and leached carbon.

772 ORCHIDEE, EPIC-IIASA, and ECOSSE have previously been compared to measurements of net carbon fluxes  
 773 and soil organic carbon changes at the site level (e.g., Balkovič et al., 2020; Chen et al., 2019; Zhang et al., 2018;  
 774 Vuichard et al., 2019). Further comparison is outside the scope of this work, given site heterogeneities and the  
 775 challenges in upscaling such data to a regional level as presented here. We note that this version of ORCHIDEE only  
 776 includes management implicitly, which makes direct comparison to specific sites less informative.  
 777



CC BY VERIFY Project



CC BY VERIFY Project

778  
 779 *Figure 4: Net CO<sub>2</sub> land flux from total Cropland (top plot) and total Grassland (bottom panel) estimates for the*  
 780 *EU27+UK. Total Cropland (CL) data comes from the UNFCCC NGHGI (2021) submissions; ORCHIDEE,*

781 *ECOSSE and EPIC-IIASA process-based models; and the FAOSTAT inventory. Total Grassland (GL) data comes*  
782 *from the same sources, with the caveat that ECOSSE has not been updated and is therefore identical to Petrescu et*  
783 *al. (2021b). Values on the far right in both plots indicate the mean of 1990-2019. The relative error on the*  
784 *UNFCCC value represents the UNFCCC NGHGI (2021) MS-reported uncertainty with no gap-filling (EU NIR,*  
785 *2021). The fluxes follow the atmospheric convention, where negative values represent a sink while positive values*  
786 *represent a source.*

787

788 Differences between mean values may also arise from definitions for each Land type, which vary between  
789 Member States (see Tables 6.18 and 6.22 for Cropland and Grassland, respectively, in EU NIR, 2021). Woody and  
790 annual crops are included in NGHGI Cropland, although annual crops are generally assumed to be in carbon balance  
791 and thus to not contribute to the net flux. This also means that no spatial displacement of emissions ("lateral fluxes")  
792 due to crop trade are taken into account. Grassland includes rangeland and pastureland which is not classified as  
793 Cropland. Urban green spaces, on the other hand, are often included in the Settlements category (EU NIR, 2021),  
794 which is not explicitly simulated by any bottom-up model reported here.

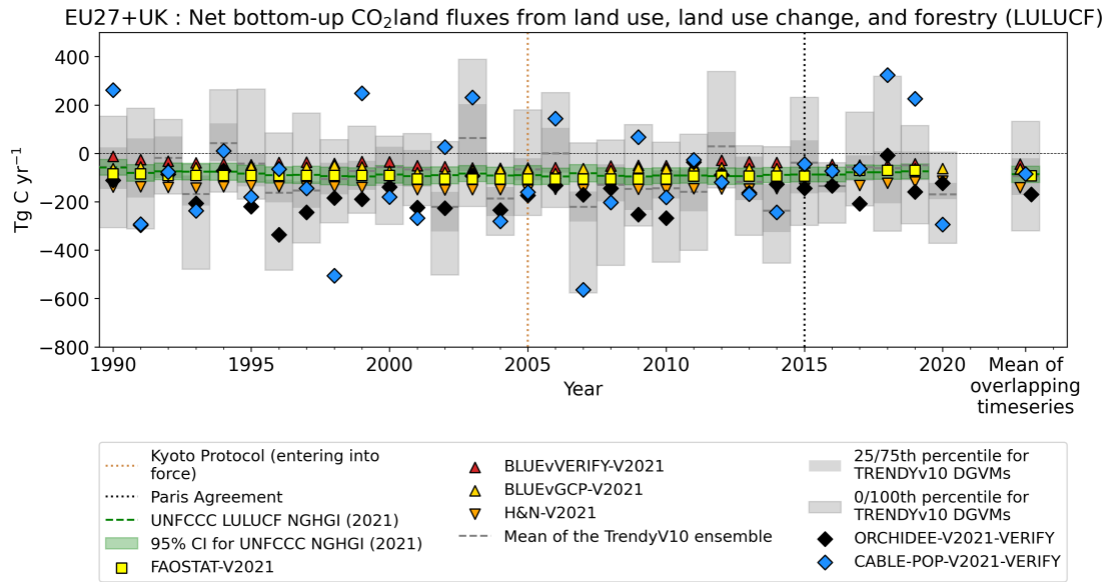
795 For Grassland, the NGHGI reports a slightly positive net flux over 1990-2019, although with a much larger  
796 uncertainty than for either Forest land or Cropland ( $4 \pm 13 \text{ Tg C yr}^{-1}$ ). While increased uncertainty compared to Forest  
797 land emissions is understandable given the emphasis on collecting accurate forestry statistics due to their economic  
798 importance, the increased uncertainty in Grassland compared to Cropland is more puzzling. Uncertainty estimates for  
799 the EU27+UK come from a synthesis of estimates for each of the 28 Member States, and are applied to each year  
800 individually based on the data provided for a single year (2019). The apparent drastic change in uncertainty from  
801 1990 to 2019 is due to the emissions getting much closer to zero (i.e., 7.8 Tg in 1990 compared to 0.5 Tg in 2019),  
802 which itself is due primarily to changes in the way Grassland is treated in the United Kingdom, Bulgaria, and Sweden  
803 (EU NIR, 2021). Additional analysis will be needed to elucidate this issue.

804 In addition to the NGHGI, updated results for GL are available for ORCHIDEE (using a coupled C-N cycle)  
805 and FAOSTAT. For the first time, EPIC-IIASA contributed estimates for Grassland fluxes using five different  
806 grassland types and simulating carbon export due to herbivores (see Appendix A4 for more details). Both of these  
807 models exhibit a strong sink in Grassland. For ORCHIDEE, this is likely due to the same reasons as the sink in  
808 croplands: more suitable growing conditions due to climate change, CO<sub>2</sub> fertilization, and nitrogen deposition leading  
809 to increased inputs into the soil which are not lost during tillage due to the lack of explicit management in the version  
810 reported here. For EPIC-IIASA, this results from manure left on site and incorporated into the soil. A Tier 1 IPCC  
811 approach, used in both the FAOSTAT inventory and many NGHGIs in the EU27+UK, assumes no changes in either  
812 living or dead biomass pools on Grassland. In addition, it only considers organic soils which have been drained for  
813 grazing, and it only considers mineral soils which have undergone a change in management. This greatly reduces or  
814 eliminates mechanisms which promote sinks in ORCHIDEE and EPIC-IIASA. On the other hand, FAOSTAT reports  
815 a slight source in Grasslands, in line with the NGHGI. This is because, as is the case for Cropland, FAOSTAT data  
816 only considers emissions from drained organic soils. As incorporation of manure in EPIC-IIASA changes grasslands  
817 from a net source to a net sink, consideration of CO<sub>2</sub> from manure input in other inventories may have a similar effect.

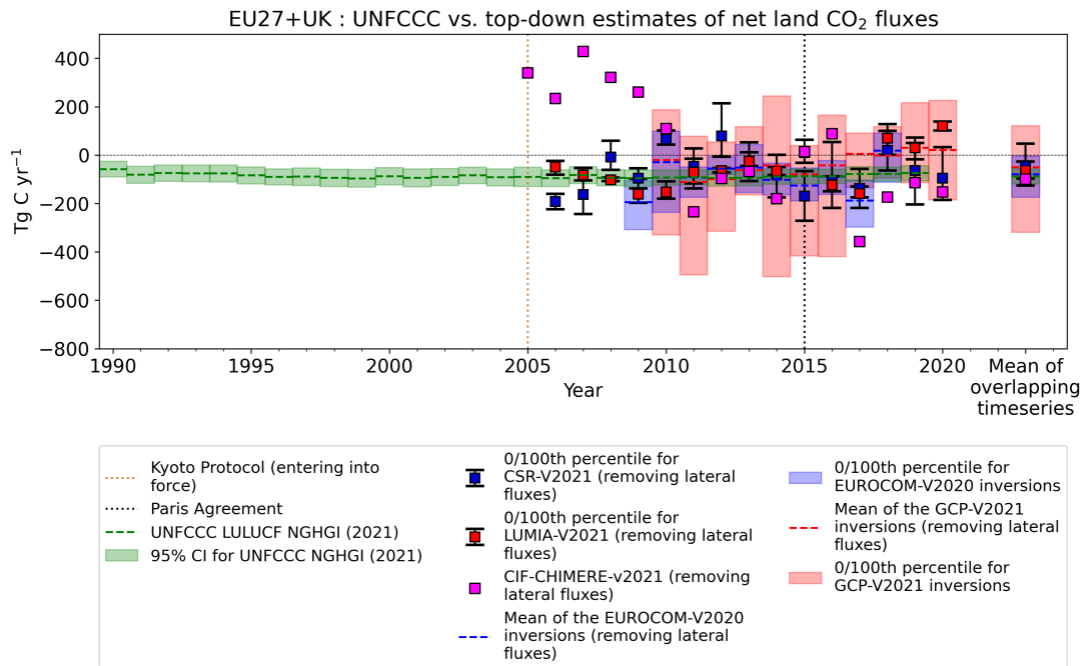
818

819 3.3.4. Total bottom-up and top-down LULUCF CO<sub>2</sub> estimates

820  
821 This section analyzes CO<sub>2</sub> emissions and sinks for the LULUCF sector, including NGHGI categories (from Fig.  
822 B4) and a suite of different bottom-up and top-down approaches. This comparison is challenging due to differences  
823 in terms of activities covered in the different estimates, as well as differences in terminology (see, for example,  
824 Petrescu et al., 2020, Fig. 12, and Petrescu et al., 2021b, Sec 3.3.4). Given the differences noted in those references,  
825 the comparison in this section should be considered as a rough overview that highlights both important aspects of the  
826 carbon cycle and questions that need to be addressed in the future. Going towards a more specific comparison of only  
827 net land-use change (LUC) fluxes would require additional considerations. In GCP's annual global carbon budget, the  
828 net LUC term is estimated by global DGVMs as the difference between a run with and a run without land-use change  
829 (i.e., the S3 and S2 simulations from TRENDY, respectively) and by bookkeeping models (Friedlingstein et al., 2022).  
830 Such an estimate is given in Fig. 13 in Petrescu et al. (2020) for Forest land. However, even taking S3-S2 does not  
831 permit an apples-to-apples comparison between DGVMs, bottom-up inventories, and bookkeeping models. In  
832 particular, questions remain about net vs. gross land use change, managed vs. unmanaged land, and emissions from  
833 wood harvest. In addition, UNFCCC "convert" emissions (i.e., emissions resulting from land that has been converted  
834 from one type to another) are reported within 20 years following conversion in the "convert" category (biomass losses  
835 are typically reported in the year of conversion, while net changes in soil organic carbon are reported during the entire  
836 conversion period). FAOSTAT, DGVMs, and bookkeeping models usually only include "convert" fluxes from the  
837 year following conversion, although bookkeeping models and DGVMs which deal with gross transitions may be able  
838 to include this transition period more easily.



CC BY VERIFY Project



CC BY VERIFY Project

839

840 *Figure 5: Net CO<sub>2</sub> fluxes from total LULUCF activities in the EU27+UK from bottom-up (top) and top-down*  
 841 *(bottom) methods compared to UNFCCC NGHGI (2021). The bottom-up methods include: BLUE (vVERIFY),*  
 842 *BLUE (vGCP2021), H&N (GCP2021), DGVMs (TRENDY v10), FAOSTAT (2021), as well as ORCHIDEE and*  
 843 *CABLE-POP with high-spatial-resolution (0.125 °) meteorological forcing (both models are also part of the*  
 844 *TRENDY ensemble at 0.5 °). The spread of the gray bars represents the individual model data for the DGVMs. Top-*

845 *down inversion results are the global GCB2021 ensemble, as well as several regional inversions: the EUROCOM*  
846 *ensemble, the CarboScopeReg model with multiple variants, the LUMIA model with multiple variants, and CIF-*  
847 *CHIMERE. The colored area represents the min/max of top-down model ensemble estimates. Emissions due to*  
848 *lateral fluxes of carbon through rivers, crop trade, and wood trade are removed from the top-down estimates. The*  
849 *mean values of the timeseries for the overlapping periods of 1990-2019 (top) and 2010-2018 (bottom) are shown on*  
850 *the right. The UNFCCC estimate includes all categories (remain and convert), as well as HWP. The relative error*  
851 *of the UNFCCC values represent the UNFCCC NGHGI (2021) Member States reported uncertainty computed with*  
852 *the error propagation method (95 % confidence interval), gap-filled and provided for each year of the timeseries.*  
853 *The fluxes follow the atmospheric convention, where negative values represent a sink while positive values represent*  
854 *a source.*

855 Figure 5 (top) shows CO<sub>2</sub> fluxes from the NGHGI LULUCF sector compared to all other comparable bottom-  
856 up (BU) estimates in this work: high-resolution S3 simulations for both ORCHIDEE and CABLE-POP; the median  
857 of 15 S3 simulations from the TRENDYv10 DGVM ensemble; three bookkeeping models; and FAOSTAT. As  
858 mentioned above, taking the difference of the TRENDY S2 and S3 simulations does not permit a fully-consistent  
859 comparison between DGVMs, bottom-up inventories, and bookkeeping models for LULUCF fluxes, and for  
860 simplicity we simply report S3 NBP from DGVMs in Fig. 5. Further research is needed in order to establish which  
861 approach (S3-S2, or simply S3) leads to the most consistent comparison. For the overlapping period 1990-2019, the  
862 means of two out of the three bookkeeping models (BLUE vGCP (-61 Tg C yr<sup>-1</sup>) and BLUE vVERIFY (-43 Tg C yr<sup>-1</sup>,  
863 using the Hilda+ land use forcing)) along with the mean of FAOSTAT (without Romanian forestry fluxes) (-93 Tg C  
864 yr<sup>-1</sup>) fall within the 95 % confidence interval of the UNFCCC NGHGI estimate of  $-86 \pm 33$  Tg C yr<sup>-1</sup>. Only H&N rests  
865 apart with a stronger sink (-142 Tg C yr<sup>-1</sup>), although it's difficult to say how different it is from the NGHGI without  
866 uncertainty estimates.

867 Bookkeeping models like BLUE and H&N always regrow biomass at the same rate. In the bookkeeping  
868 approaches used here, regrowth curves are representative for present-day conditions and kept the same throughout  
869 history, which is the same approach used in the Global Carbon Budget. NGHGIs, on the other hand, include legacy  
870 effects from changing environmental conditions, in particular in soil pools. Recent work by Grassi et al. (2023)  
871 demonstrates that including the sink associated with varying human-induced indirect effects (as estimated by the S2  
872 simulations from the TRENDY DGVM ensemble) into results by bookkeeping models can largely reconcile estimates  
873 of net global LULUCF fluxes between the NGHGIs and bookkeeping models. At the level of the EU27+UK, the  
874 inclusion of this sink results in an overcompensation; the BMs estimate a net sink of -56 Tg C yr<sup>-1</sup> compared to the  
875 NGHGI estimate of -88 Tg C yr<sup>-1</sup>, while the BMs+DGVMs results in -112 Tg C yr<sup>-1</sup>. However, both of these estimates  
876 fall inside the NGHGI uncertainty range in Fig. 5.

877 The primary difference between the NGHGI and DGVMs is the interannual variability, with only a small  
878 difference in the means even if there is a substantial amount of spread with the DGVMs:  $-86 \pm 33$  Tg C yr<sup>-1</sup> and  $-81 [-$   
879  $172, -20]$  Tg C yr<sup>-1</sup> for the NGHGI and DGVMs, respectively, where the range for the DGVMs indicates the 25th-75th  
880 percentile of the models in the ensemble. The UNFCCC LULUCF estimates contain CO<sub>2</sub> emissions from all land use  
881 categories and HWP, where a simple analysis shows that for the EU27+UK almost 90 % of the gross flux arises from  
882 only six categories (Table A4). DGVMs currently explicitly include more of these categories than the other methods  
883 (Table C2), which may help explain the closeness between the mean values. ORCHIDEE and CABLE-POP provide  
884 a nice test case of the impact of high spatial resolution forcing on net carbon fluxes in the EU27+UK, as they are

885 present in both the TRENDY ensemble (0.5 °) as well as the VERIFY results (0.125 °). Using one standard deviation  
886 of the mean annual net CO<sub>2</sub> flux as a measure of the IAV, CABLE-POP indeed shows a much higher IAV at high  
887 resolution ( $-40 \pm 142 \text{ Tg C yr}^{-1}$  and  $-92 \pm 214 \text{ Tg C yr}^{-1}$  for TRENDY and this work across 1990-2019), while the  
888 results for ORCHIDEE are almost identical between the two resolutions. More analysis is therefore required to  
889 confirm the relationship between spatial resolution and interannual variability in DGVMs for the EU27+UK.

890 The differences between bookkeeping models and UNFCCC and FAOSTAT are discussed in detail  
891 elsewhere, and focus on the inclusion of unmanaged land in bookkeeping models but not FAOSTAT and UNFCCC  
892 methodologies (Petrescu et al., 2020; Grassi et al., 2018a, 2021). ORCHIDEE, CABLE-POP and the TRENDY v10  
893 ensemble means show much higher inter-annual variability as they simulate sub-annual responses of carbon fluxes to  
894 climate, while the climate responses of inventories and bookkeeping models are averaged over multiple years. A  
895 comparison including categorical-specific models (e.g., ECOSSE, EFISCEN-Space, EPIC-IIASA, CBM) where  
896 multiple model results are harmonized and aggregated to produce a “total” LULUCF flux comparable to DGVMs and  
897 bookkeeping models would be insightful; however, such a comparison requires extensive analysis which is beyond  
898 the scope of the current work.

899 The bottom panel in Figure 5 highlights the range of estimates from global and regional atmospheric inversions  
900 (GCP2021, EUROCOM, CSR, LUMIA, and CIF-CHIMERE; see Table 2 and Appendix A4 for more details) against  
901 bottom-up total annual EU27+UK CO<sub>2</sub> land emissions/removals from the UNFCCC NGHGI (2021). Notice that  
902 unlike other works (e.g., Deng et al., 2022), we have not applied a managed-land mask to the inversions or bottom-up  
903 models in order to be compatible with the managed land proxy in the NGHGIs. The reasons for this are two-fold.  
904 One, most of the land in the European Union is managed, as noted above. Second, no such mask currently exists,  
905 even for the relatively data-rich EU. A managed land mask created solely based on non-intact forests (e.g., Deng et  
906 al., 2022) neglects that Grassland and Wetlands contribute significantly to unmanaged areas in the EU. Including  
907 fluxes from the 5 % of unmanaged land in the EU is unlikely to change any conclusions in this work given the  
908 uncertainties in the LULUCF methods presented here. As soon as a reasonably accurate managed land mask is  
909 available, however, it should be used.

910 One significant change between this work and Petrescu et al. (2021b) is the removal of emissions and sinks from  
911 inversion results due to lateral transport of carbon from crop trade, wood trade, and inland waters. Bottom-up methods  
912 (including all the NGHGIs for European countries) do not consider emissions and removal of atmospheric CO<sub>2</sub> due  
913 to lateral transport of biomass carbon, while inversions calculate geographically resolved net land-atmosphere CO<sub>2</sub>  
914 fluxes without regard to the original location of photosynthetic assimilation. Some lateral transport of soil organic  
915 carbon may be taken into account by measuring stock changes, but given the mix of stock-change and gain-loss  
916 methods used in NGHGIs in the EU, and the presence of methods ranging from Tier 1 to Tier 3, exactly how much is  
917 far from trivial to determine.

918 Net emissions from lateral transport of carbon (“lateral fluxes”) were prepared generally following the approach  
919 described by Ciais et al. (2021), where crop and wood product fluxes are derived from country-level trade statistics  
920 compiled by the FAO. Inland water emissions and riverine export of terrestrial carbon use spatially explicit  
921 climatological data and a statistical model combined with estimates of gas transfer velocities. A more complete



922 description is given in Appendix A4. This adjustment accounts for a combined mean of  $-140 \text{ Tg C yr}^{-1}$  over the 2010-  
923 2018 common period of the inversions, and has been applied using Eq. 1 in Deng et al. (2021) (without a managed  
924 land mask) to all top-down fluxes reported here unless indicated otherwise.

925         Uncertainties for net emissions of  $\text{CO}_2$  due to lateral transport of carbon are not yet available. However, FAO  
926 and IEA statistics form the basis of calculated fluxes due to wood and crop trade. FAO estimates an uncertainty of 50  
927 % on carbon emissions and removals from forested land (Tubiello et al., 2021). Even if uncertainties in trade fluxes  
928 are not available, 50 % therefore works as a first order approximation given the similarities between the two fluxes  
929 (i.e., a well-tracked value multiplied by an uncertain emission factor). Uncertainties in net carbon uptake by rivers  
930 and lakes are estimated to also be on the order of 50 % due to the fact that these fluxes can only be calculated based  
931 on budget closure including estimates of river exports to the coast, emissions of carbon from the water surface to the  
932 atmosphere, and burial of carbon in aquatic sediments (Battin et al., 2023). Combined, this results in an uncertainty  
933 of around  $70 \text{ Tg C yr}^{-1}$  for the lateral fluxes, which is on the same order as the ensemble spread for the regional  
934 inversions as shown in Fig 5, though still lower than that of the global inversions.

935         Flux estimates from inversion methods for  $\text{CO}_2$  land show much more variability than the NGHGI, both on  
936 the interannual scale as well as for any given year (Fig. 5, bottom). The mean values from 2010-2018 show good  
937 agreement but with an order of magnitude more variability in the inversions:  $-88 \pm 60 \text{ Tg C yr}^{-1}$  for EUROCOM and  
938  $-80 \pm 6 \text{ Tg C yr}^{-1}$  for the NGHGI, where the uncertainty here is the standard deviation of the annual mean values for  
939 each. For any given year, the spread between the inversions is also much greater ( $170 \pm 70 \text{ Tg C yr}^{-1}$  for EUROCOM  
940 versus  $63 \pm 3 \text{ Tg C yr}^{-1}$  for the NGHGI, which represents the mean and standard deviation of the 0-100th percentiles  
941 for the inversions and the 95% CI for the NGHGI). This large spread per year can be linked to uncertainty in  
942 atmospheric transport modeling, inversion methods and assumptions, and to limitations of the observation system.  
943 Furthermore, the EUROCOM inversions were designed for the European geographical domain (which is larger than  
944 the EU27+UK) and are still being developed in particular to better constrain the latitudinal and longitudinal boundary  
945 conditions.

946         The annual mean (overlapping period 2010-2018) of the EUROCOM v2021 inversions ( $-80 [-175,-4] \text{ Tg C yr}^{-1}$ )  
947 is the closest inversion estimate to the timeseries mean of the NGHGI estimates ( $-88 \pm 31 \text{ Tg C yr}^{-1}$ ), where the  
948 error bars for the inversion indicate the  $[0^{\text{th}}, 100^{\text{th}}]$  percentiles due to the small size of the ensembles. The ensemble of  
949 all regional inversions is consistent with the NGHGI estimates, assuming the spread of the inverse model results is an  
950 accurate proxy of the structural uncertainties. The impact of the net emissions of lateral fluxes due to wood trade,  
951 crop trade, and rivers is clear: without factoring in their contribution of the approximately  $-140 \text{ Tg C yr}^{-1}$ , the sink  
952 from regional inversions, in particular, would be much stronger than even the strongest estimate of the NGHGI (i.e.,  
953 the lower boundary on the green bar in Fig. 5). The mean of the global GCP2021 inversions ( $-50 [-320,+122] \text{ Tg C}$   
954  $\text{yr}^{-1}$ ) and regional inversions, CSR ( $-46 [-126,+47] \text{ Tg C yr}^{-1}$ ) and LUMIA ( $-65 [-97,-27] \text{ Tg C yr}^{-1}$ ) show a lower  
955 absolute value, but report larger interannual variability (min/max). The new CIF-CIMERE product has a mean of  $-99$   
956  $\text{Tg C yr}^{-1}$ , showing a trend towards more negative fluxes since 2010, which is not seen in other models and is still  
957 under investigation.

958 The comparison of past and current versions of the inversions shows changes in specific top-down models  
959 (Fig. B5). A reduction in the spread of the estimates is noted over the two past versions of CSR, resulting in a small  
960 source in the most recent estimates. The CSRv2021 (bottom-plot) predicts in 2018 (last common year of both versions)  
961 a small source of 19 [-64, +100] Tg C yr<sup>-1</sup> compared to the previous CSRv2019 which simulated a very strong sink of  
962 -253 [-280, -194] Tg C yr<sup>-1</sup>. This smaller source appears more in line with more positive fluxes expected in years of  
963 extreme drought (e.g., 2018 in Northern Europe, even if this did not impact the whole EU27+UK (Toreti et al., 2019)).

964 As can be seen in Fig. 5 (bottom), there is also improved agreement between the EUROCOM ensemble and  
965 the NGHGI, including a greatly reduced IAV compared to the previous version. The small EUROCOM ensemble  
966 mean sink for the 2009-2015 period of -1.9 [-335,+322] Tg C yr<sup>-1</sup> (top panel) strengthened to -93 [-187,-15] Tg C yr<sup>-1</sup>  
967 in the v2021 version (bottom panel). The UNFCCC total LULUCF mean is  $-92 \pm 33$  Tg C yr<sup>-1</sup> for the same time  
968 period. The IAV of EUROCOM was dramatically reduced by removing the FLEXINVERT model from the v2021  
969 ensemble as a clear outlier of annual means due to a slightly shifted seasonal cycle (Appendix A4).

970 Despite an apparent trend in the mean of the new GCP2021 inversions towards a source near 2017, the spread  
971 of the models precludes significance; following 1000 realizations of a Monte Carlo analysis assuming the min-max  
972 ensemble spread represents  $3\sigma$  in a normal distribution, the only period of at least four consecutive years for which  
973 the 95% confidence interval comes close to excluding zero is 2015-2018 ( $26 \pm 28$  Tg C yr<sup>-2</sup>). The large variability  
974 and high sink observed in the upper plot of Fig. 5 (bottom) shifted to a source in 2019 ( $21 [-185, +226]$  Tg C yr<sup>-1</sup>) due  
975 to the extreme climatic response of the TD models to the drought year, which can also be observed in the BU  
976 simulations (e.g., TRENDY v10, ORCHIDEE, and CABLE-POP in the top panel of Fig. 5). Out of the GCP2021  
977 models, CAMS was the model responsible for the strongest sink in the ensemble during most years (data not shown),  
978 which may be due partly to changes in the stations assimilated.

979

### 980 **3.4. Uncertainties in top-down and bottom-up estimates**

981

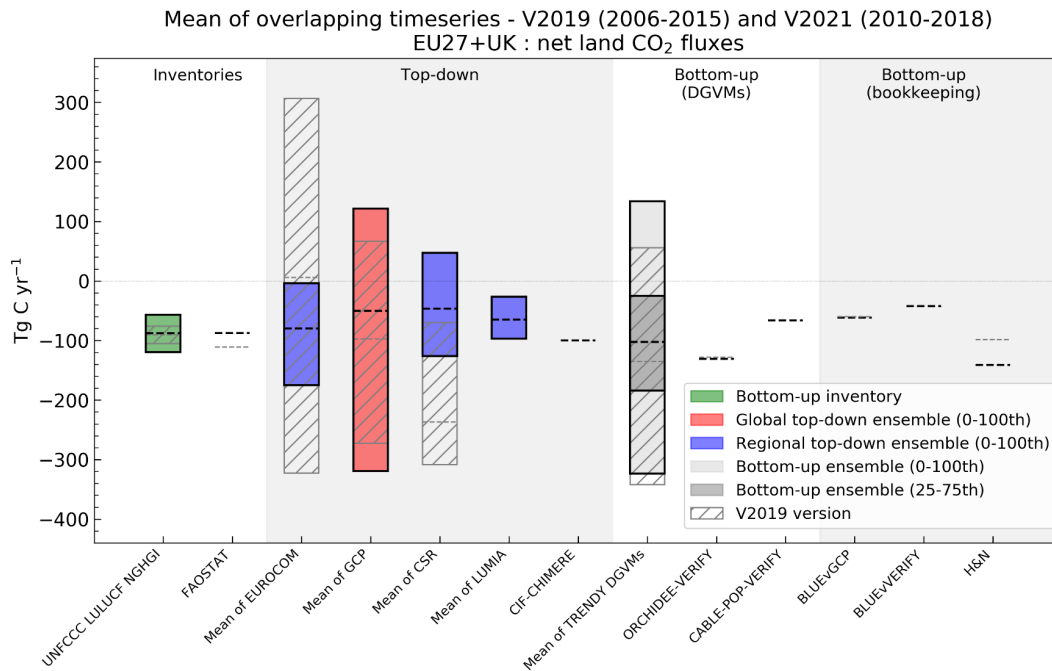
982 Uncertainties are essential for complete comparisons between models and approaches. This section  
983 summarizes the main sources of uncertainty estimates interwoven throughout the above text. We also provide a  
984 comparison of available uncertainties between the previous synthesis (V2019) and the current synthesis (V2021) for  
985 both bottom-up and top-down methods. Finally, we give an overview of two important advances in uncertainty  
986 estimation included in this work (one for the NGHGI, and one for top-down approaches), referring the interested  
987 reader to the Appendix A4 for more information.

988 Several sources of uncertainty arise from the synthesis of bottom-up (BU) inventories and models of carbon  
989 fluxes, which can be summarized as: (a) differences due to input data and structural/parametric uncertainty of models  
990 (Houghton et al., 2012) and (b) differences in definitions (Pongratz et al., 2014; Grassi et al., 2018b, 2021; Petrescu  
991 et al., 2020, 2021b). Posterior uncertainties in top-down (TD) estimates mostly come from: 1) errors in the modeled  
992 atmospheric transport; 2) aggregation errors, i.e., errors arising from the way the flux variables are discretized in space  
993 and time and error correlations in time; 3) errors in the background mole fractions, in particular for regional inversions;  
994 and 4) incomplete information from the observations and hence the dependence on the prior fluxes. The multi-model

995 ensemble approach is being used as a proxy for estimation of systematic error. Calculation of random error is generally  
996 difficult when using the most common inverse model flux optimization approaches.

997 Figure 6 summarizes the quantifiable uncertainties in this work, compared to previous results from Petrescu  
998 et al. (2021b). With the exception of the NGHGI, all the other uncertainties are calculated from ensembles of  
999 simulations using either: 1) multiple models of the same general type, either using model-specific inputs or attempting  
1000 to harmonize inputs as much as possible (e.g., TRENDY), or 2) multiple simulations with the same model, varying  
1001 input parameters and/or forcing data (e.g., CarboScopeRegional, LUMIA). As a complete characterization of model  
1002 uncertainty involves exploring the full parameter, input data, and model structure space, none of the uncertainties  
1003 reported here can be considered “complete”, but they represent best estimates given realistic constraints of resources  
1004 and knowledge. The uncertainties represent the mean of overlapping periods for the previous V2019 (overlapping  
1005 period: 2006-2015) versus the current V2021 (2010-2018). In general, the differences in mean behaviors between the  
1006 two versions falls within uncertainty estimates. Note, however, that this graph can hide certain behaviors. For  
1007 example, the similarity in the means for ORCHIDEE-VERIFY for both periods (-129 and -131 Tg C yr<sup>-1</sup> for V2019  
1008 and V2021, respectively) is likely a coincidence, given the wide fluctuation of annual values and the differences in  
1009 the multi-decennial means seen in Fig. 5.

1010 Figure 6 shows notable reductions in the spread of two ensembles: EUROCOM and CSR. Both of these are  
1011 regional ensembles. In addition, the CSR results show a weaker sink in the current V2021 version compared to the  
1012 previous V2019 version. As noted in Appendix A4, the change for CSR is explained by the inclusion of a corrected  
1013 observation dataset for an isolated station in southeastern Europe which heavily influenced the regional results. The  
1014 reduction in the spread of the EUROCOM ensemble results from the exclusion of a single member which produces  
1015 annual flux results that are clear outliers compared to the remaining three members. More details of this analysis can  
1016 be found in Appendix A4. The remaining ensembles retain similar model spread compared to the previous versions.



1017

1018 *Figure 6: Mean annual values of overlapping time periods (2006-2015) from Petrescu et al. (2021b) (transparent*  
 1019 *boxes and light gray lines) and new means for the 2010-2018 period from the current study (Fig. 5, Sect. 3.3.4). The*  
 1020 *hashed boxes and colored boxes depict the “old” and “new” values for ensembles of multiple models, with the top*  
 1021 *and bottom of the boxes corresponding to minimum and maximum mean values of the overlapping period. For non-*  
 1022 *ensemble models (e.g., CIF-CHIMERE, FAOSTAT) the mean of the old and new overlapping periods are given by*  
 1023 *gray dotted and black dashed lines, respectively. The NGHGI UNFCCC uncertainty is calculated for submission*  
 1024 *year 2021 as the relative error of the NGHGI value, computed with the 95 % confidence interval method gap-filled*  
 1025 *and provided for every year of the timeseries. Inversions for both V2019 and V2021 have been corrected for net*  
 1026 *emissions of CO<sub>2</sub> from lateral transport of carbon using identical datasets to enable a fair comparison. The fluxes*  
 1027 *follow the atmospheric convention, where negative values represent a sink while positive values represent a source.*

1028

1029 Three advances in uncertainty estimation were made in this study, involving all three classes of models:  
 1030 NGHGI, bottom-up, and top-down. In Petrescu et al. (2021b), percentage uncertainties for the NGHGI (2019)  
 1031 LULUCF sector and land use categories were taken from reported uncertainties of the EU Member States and UK that  
 1032 are used for compiling the National Inventory Reports (NIR) of the EU27+UK bloc, as well as the aggregate  
 1033 uncertainties for the block reported in the EU NIR. Uncertainty estimates were only given for a single year and were  
 1034 also partially incomplete due to missing uncertainty estimates for some sectors/subsectors of some countries. For the  
 1035 current work, we use values compiled by the EU inventory team involving a recently developed procedure to  
 1036 harmonize and gap-fill uncertainties reported by the Member States at the sector level (see EU NIR, 2021). Error  
 1037 correlations are accounted for, in addition to year-to-year variations in sub-sectoral contributions to the overall  
 1038 uncertainty. Extensive details are found in Appendix A2, and permit estimates of uncertainty on an annual basis, as  
 1039 opposed to the single value used in the previous synthesis. Note, however, that this procedure was not applied to sub-  
 1040 sectoral categories (FL, CL, and GL), for which values were taken directly from EU NIR (2021) and applied across

1041 the whole timeseries. Synthesis plots created for individual countries and reported on the VERIFY website (VERIFY  
1042 Synthesis Plots, 2022) take percentages directly from the respective country's NIR.

1043 The second advance relates to the impact of forcing data on bottom-up models, in particular DGVMs. Figure  
1044 A3 (Appendix A4) shows how the ORCHIDEE model responds to both changes in meteorological forcing (for  
1045 ORCHIDEE) and nitrogen forcing (for ORCHIDEE-N) over the past several decades. The impact of both is relatively  
1046 small compared to interannual variability. This is likely due to at least two reasons. The first reason is that  
1047 meteorological forcing used in this work has been re-aligned to the CRU observational dataset at 0.5 degrees and  
1048 monthly resolution, thus removing large-scale and long-term differences between the original meteorological datasets.  
1049 In addition, extensive spin-up and transient simulations are run for ORCHIDEE before reaching the point at which  
1050 the forcing changes (1981 for the meteorological forcing, and 1995 for the nitrogen forcing). Such lengthy simulations  
1051 enable woody biomass and soil carbon pools to develop a significant amount of inertia in response to additional  
1052 changes. Greater differences may be seen for models where modified forcing data covers the entire length of the pre-  
1053 production simulation steps.

1054 The final advance relates to uncertainty characterization in the regional inversion model CSR following the  
1055 methodology of Chevallier et al. (2007). Spatially explicit estimates of the uncertainty reduction achieved from the  
1056 flux optimization were prepared through a Monte Carlo approach using an ensemble of 40 members. The uncertainty  
1057 reduction is then calculated based on the ratio of the prior errors and the posterior spread of the ensemble members,  
1058 using a formula such that 0 indicates no reduction and 1 indicates a complete elimination of uncertainty. A preliminary  
1059 analysis showed that a considerable reduction may be achieved through the inclusion of more observation stations,  
1060 although additional work is needed. For the moment, these maps only reflect random uncertainties, and systematic  
1061 uncertainties remain poorly characterized. More information can be found in Appendix A4.

1062

## 1063 **4. Data availability**

1064 Annual timeseries for the EU27+UK used in creation of the figures in this work for V2019 and V2021 are  
1065 available for public download at <https://doi.org/10.5281/zenodo.8148461> (McGrath et al., 2023). This excludes CO<sub>2</sub>  
1066 fossil data for the IEA, which is subject to license restrictions. Most sector-level data from IEA are available for a  
1067 fee, although some high-level emissions data can be accessed free-of-charge. The data are reachable with one click  
1068 (without the need for entering login and password), and downloadable with a second click, consistent with the two  
1069 click access principle for data published in ESSD (Carlson and Oda, 2018). The data and the DOI number are subject  
1070 to future updates and only refers to this version of the paper. In addition, figures and annual timeseries for EU27+UK  
1071 as well as other countries and regions are available from VERIFY Synthesis Plots (2022) as well as a number of  
1072 gridded data files submitted to the VERIFY project listed in Table C1. Access to the data files requires free registration  
1073 to obtain a username and password. Alternatively, interested users are invited to contact the persons listed in Table  
1074 C1 to request gridded datafiles directly from them. We do not provide access to data already made freely available

1075 elsewhere, as we prefer users use mechanisms put in place by the original providers so that they are able to ensure  
1076 their continued funding for their work.  
1077

## 1078 **5. Summary and concluding remarks**

1079 This work represents an update of the Petrescu et al. (2021b) European CO<sub>2</sub> synthesis paper presenting and  
1080 investigating differences between the UNFCCC NGHGI, BU data-based inventories, both coarse and high resolution  
1081 process-based BU models, and TD approaches represented by both global and regional inversions. Datasets used in  
1082 the previous work have been updated by extending the temporal coverage and updating the models and data behind  
1083 the calculations. In addition, several new models to expand the number of independent approaches compared have  
1084 been added. Additional efforts have been made to improve uncertainty characterization in two approaches, along with  
1085 a first attempt to present as many datasets as possible in a clear single figure to draw overarching conclusions.

1086 CO<sub>2</sub> fossil emissions dominate the anthropogenic CO<sub>2</sub> flux in the EU27+UK, regardless of the approach  
1087 employed and irrespective of uncertainties, although the datasets are not fully independent, which complicates  
1088 uncertainty estimation. Fossil CO<sub>2</sub> emissions are more straightforward to estimate than ecosystem fluxes due to  
1089 extensive data collection around fuel production and trade, assuming that fuel statistics and accurate emission factors  
1090 are available. A suite of eight BU methods for fossil CO<sub>2</sub> emissions are within the uncertainty of the NGHGI when  
1091 methods are harmonized to include similar categories. The remaining differences can often be attributed to definitions,  
1092 assumptions about activity data or emission factors, and the allocation of fuel types to different sectors (see Sect. 3.2  
1093 and Fig. B3). The one available TD method, a regional European inversion system (CIF-CHIMERE) using an NO<sub>x</sub>  
1094 proxy to determine CO<sub>2</sub> fossil emissions, shows broad agreement with the BU estimates. However, this initial TD  
1095 inversion is not yet capable of distinguishing the minor differences between the various BU estimates and does not  
1096 yet quantify uncertainties, unlike, for example, Basu et al. (2020), which presents fossil fuel combustion and cement  
1097 production emission including uncertainty estimates for the United States. However, a substantial decrease in the level  
1098 of uncertainty of the inverse modeling system is expected in the near-term with the large-scale deployment of  
1099 observation networks dedicated to detecting fossil fuel emissions (e.g., with launch of the CO<sub>2</sub>M<sup>19</sup> satellite mission in  
1100 2025). In the short-term, the CoCO<sub>2</sub> project (CoCO<sub>2</sub>, 2022) aims to advance methodology around co-assimilation of  
1101 existing CO<sub>2</sub> satellite data (from the OCO-2/3 instruments) and to provide new analysis of the CO/FFCO<sub>2</sub> and  
1102 NO<sub>x</sub>/FFCO<sub>2</sub> ratios in order to significantly decrease uncertainty in the fossil CO<sub>2</sub> estimates.

1103 The CO<sub>2</sub> land fluxes belong to the LULUCF sector, which is one of the most uncertain sectors in UNFCCC  
1104 reporting. The IPCC guidelines prescribe methodologies that are used to estimate the CO<sub>2</sub> fluxes in the NGHGI, but  
1105 grant countries significant freedom to adopt methods appropriate to their national circumstances. Even in the European  
1106 Union, Member States use a wide variety of stock-change and gain-loss methods ranging from Tier 1 to Tier 3  
1107 depending on the specific LULUCF flux being estimated (EU NIR, 2021). When analyzing the different estimates

---

<sup>19</sup> CO<sub>2</sub>M : Copernicus Anthropogenic Carbon Dioxide Monitoring,  
[https://esamultimedia.esa.int/docs/EarthObservation/CO2M\\_MRD\\_v3.0\\_20201001\\_Issued.pdf](https://esamultimedia.esa.int/docs/EarthObservation/CO2M_MRD_v3.0_20201001_Issued.pdf)

1108 from multiple BU sources (inventories and models) similar sources of uncertainties are observed such as: (a)  
1109 differences due to input data and structural/parametric uncertainty of models (Houghton et al., 2012; Pongratz et al.,  
1110 2021) and (b) differences in definitions (Pongratz et al., 2014; Grassi et al., 2018b; Petrescu et al., 2020, 2021b; Grassi  
1111 et al., 2021). Reducing uncertainties in LULUCF estimates is needed given the increasing importance of the sector to  
1112 EU climate policy over the next decades. In contrast to the previous 2020 climate and energy package, the LULUCF  
1113 sector will now formally contribute to the binding emission reduction targets of the Unions 2030 climate and energy  
1114 framework (EU, 2018a; 2018b). Furthermore, the European Climate Law explicitly states that LULUCF, together  
1115 with all sectors of the economy, should contribute to achieving climate neutrality within the Union by 2050 (EU,  
1116 2021b).

1117 The LULUCF sector in NGHGs is composed of six land use categories. Of these, Forest land provides the  
1118 most important contribution to the net CO<sub>2</sub> land flux in the EU27+UK, followed by Cropland and Grassland. HWP  
1119 and “Land converted to settlements” also have non-negligible contributions, and changes in HWP strongly influence  
1120 variations in decennial mean net LULUCF fluxes for the region. Of these, all except “Land converted to settlements”  
1121 are represented in general ecosystem models, while Forestland, Cropland, and Grassland are simulated by category-  
1122 specific process-based and data-driven models. Top-down inversions are capable of simulating net CO<sub>2</sub> fluxes to the  
1123 atmosphere, but cannot yet attribute them between different categories.

1124 Differences in the detailed category-specific and inversion model results (Fig. 3-5) often come from choices in  
1125 the simulation setup and the type of model used: bookkeeping models, process-based DGVMs, inventory-based  
1126 statistical methods, or atmospheric inversions. Results also differ based on whether fluxes are attributed to LULUCF  
1127 emissions due to the cause or location of occurrence. For example, indirect fluxes resulting from long-term changes  
1128 in growing conditions, such as CO<sub>2</sub>, air temperature, and water availability on managed land are included in NGHGI  
1129 and FAOSTAT. Additional sink capacity compared to pre-industrial conditions (also called the “amplification effect”,  
1130 e.g., Gasser and Ciais, 2013) occurs on Forest land in process-based models (e.g., ORCHIDEE or TRENDY DGVMs)  
1131 due to improved growing conditions resulting from CO<sub>2</sub> fertilization, climate change, and anthropogenic nitrogen  
1132 deposition, while this is not included in bookkeeping models which use the same regrowth curves for pre-industrial  
1133 and modern times. The use of gross land use changes fluxes (e.g., in the NGHGI, bookkeeping models, and CABLE-  
1134 POP) as opposed to net fluxes also likely plays an important role. We found that adjusting top-down models by  
1135 emissions/removals resulting from later transport of carbon through trade and the inland water network improves the  
1136 agreement with the NGHGI of the EU27+UK (Fig. 5, compared to Petrescu et al., 2021b).

1137 Observation-based BU estimates of LULUCF provide large year-to-year flux variability (Figs. 3-4, in particular  
1138 for DGVMs like ORCHIDEE, CABLE-POP and the TRENDY ensemble), contrary to the NGHGI, primarily due to  
1139 the effect of varying meteorology. In particular, the duration and intensity of the summer growing season can vary  
1140 significantly between years (e.g., Bastos et al., 2020a; Thompson et al., 2020). In the framework of periodic NGHGI  
1141 assessments, the choice of a reference period (such as 2015-2019, as used here) or the use of a moving window to  
1142 calculate the means may be critical to smooth out high inter-annual variability and facilitate comparisons. One can  
1143 also imagine incorporating IAV into NGHGs through the use of annual anomalies of emission factors calculated from  
1144 Tier 3 observation-based approaches (either BU or TD). TD estimates also show very large inter-annual variability

1145 and uncertainty (Fig. 5). Uncertainties in the inversion results are primarily due to uncertainties in atmospheric  
1146 transport modeling, boundary conditions, technical simplifications and uncertainty inherent to the limitation of the  
1147 observation network. Currently, regional inversions (LUMIA, CSR and EUROCOM) are still under development and  
1148 face different challenges from the coarser resolution global systems used here to represent regional results (GCP). As  
1149 seen in Fig. 6, the mean of the regional inversions appears to agree better with the NGHGI than that of the global  
1150 inversions, after the net carbon fluxes from lateral transfers are taken into account. In addition, the inter-model spread  
1151 of the regional inversions is smaller. Based on this work, it is difficult to claim that one or the other provides a more  
1152 accurate result for the net CO<sub>2</sub> land fluxes across the EU27+UK, although two regional inversion ensembles  
1153 (EUROCOM and CSR) dramatically reduced their uncertainties between the previous and current versions of this  
1154 synthesis, with CSR showing much more overlap now with the NGHGI (Fig. 6).

1155         Uncertainties can be reflected in space as well as in time. Reconciling differences across aggregated EU  
1156 regions may be challenging due to diverse methodologies and drivers in each country. On the other hand, the analysis  
1157 of smaller regions or individual countries may represent a productive first step towards monitoring the current state  
1158 of emissions as national data and experts can be used to help clarify differences across models. Country-level case  
1159 studies may help inform the design of future monitoring and verification systems (MVS) for CO<sub>2</sub> which aim to supply  
1160 additional evidence for the emissions levels and trends, coupling anthropogenic activities and associated emissions  
1161 with the atmospheric patterns of greenhouse gas mole fractions, and perform data assimilation and modeling over a  
1162 wide variety of environmental conditions (Pinty et al., 2017).

1163         As seen in figures throughout this work, reducing uncertainties of both individual models and classes of  
1164 models remains a priority. Some categories (Forestland, Cropland) produce results for multiple category-specific  
1165 models which lie within the uncertainty of the NGHGI. This likely reflects the use of data-driven models and the  
1166 relatively high quality of data that is available due to the economic importance of these categories. On the other hand,  
1167 generalized ecosystem models (the DGVMs, like ORCHIDEE and CABLE-POP) may create mean estimates which  
1168 fall within uncertainties, but fall outside of NGHGI uncertainties for any given year due to the sensitivity of processes  
1169 in these models to rapidly changing meteorology and the necessity for these models to operate globally, including in  
1170 data-poor regions for which parameterization may be impossible. Two advances in characterizing uncertainty were  
1171 presented here: one for the case of the NGHGI, and one for the case of the TD model CSR. Additional characterization  
1172 of uncertainty both within and across models will enable more fair comparisons between methods.

1173         A more detailed analysis of LULUCF fluxes at the regional/country level is foreseen as part of projects linked  
1174 to VERIFY including the RECCAP2 initiative (RECCAP2, 2022) and current and future Horizon Europe funded  
1175 projects (e.g., CoCO<sub>2</sub>, EYE-CLIMA, AVENGERS, PARIS) which will highlight examples of good practice in  
1176 LULUCF flux monitoring amongst European countries. Sect. 3.4 presents a summary of uncertainties to provide  
1177 insight into ground observation systems assimilated by inversions. This lays the basis of future improvements for  
1178 establishing best practices on how to configure atmospheric inversions and systematically quantify uncertainties. For  
1179 the overall estimation of emissions from LULUCF activities on all land types (Fig. 5, top), the comparison is made  
1180 more challenging as results from both land use and land use changes are presented. Comparing only the “effect of



1181 land use change” (conversion) is non-trivial. A methodology for reconciling LULUCF country estimates from the  
1182 FAOSTAT datasets with the NGHGIs is presented in Grassi et al. (2022a) for the global scale.

1183 The next steps needed to improve and facilitate the reconciliation between BU and TD estimates are the same  
1184 as those discussed in Petrescu et al. (2021b): 1) BU process-based models incorporating unified protocols and  
1185 guidelines for uniform definitions should be able to disaggregate their estimates to facilitate comparison to NGHGI  
1186 and 2006 IPCC practices (e.g., managed vs. unmanaged land, 20-year legacy for categories remaining in the same  
1187 category, distinction of fluxes arising solely from land use change, Grassi et al. (2022a)); 2) for category-specific  
1188 models, in particular for cropland and grassland, improving treatment of the contribution of soil organic carbon  
1189 dynamics to the budget; 3) for TD estimates, using the recently developed Community Inversion Framework (Berchet  
1190 et al., 2021) to better assess the different sources of uncertainties from the inversion set-ups (model transport, prior  
1191 fluxes, observation networks), 4) standardize methods to compare datasets with and without interannual variability,  
1192 and 5) develop a clear way to report key system boundary, data, or definitional issues, as it often necessary to have  
1193 deep understanding of each estimate to know how to do a like-for-like comparison.

1194 Similar to Petrescu et al. (2021b), this updated study concludes that a complete, ready-for-purpose monitoring  
1195 system providing annual carbon fluxes across Europe is still under development, but data sources are beginning to  
1196 show improved agreement compared to previous estimates. Significant effort must still be undertaken to robustly  
1197 quantify and then reduce uncertainties (both in the models themselves as well as in their input data) used in such a  
1198 system so that differences in the central values can be identified and understood (e.g., Maenhout et al., 2020). Future  
1199 activities in the CoCO<sub>2</sub> project (CoCO<sub>2</sub>, 2022) will investigate the one and five-year carbon budgets across the data-  
1200 rich area of the EU27+UK and deepen the analysis for both global and regional/local (city level) estimates.

1201 Achieving the well-below 2°C temperature goal of the Paris Agreement requires consideration of, among  
1202 other things, low-carbon energy technologies, forest-based mitigation approaches, and engineered carbon dioxide  
1203 removal (Grassi et al., 2018a; Nabuurs et al. 2017). Currently, the EU27+UK reports a sink for LULUCF and forest  
1204 management will continue to be the main driver affecting the productivity of European forests for the next decades  
1205 (Koehl et al., 2010), shown as well by the domination of Forestland CO<sub>2</sub> fluxes to the LULUCF sector in the NGHGI  
1206 for the bloc. Forest management changes forest composition and structure, which affects the exchange of energy with  
1207 the atmosphere (Naudts et al., 2016), and therefore the potential of mitigating climate change (Luyssaert et al., 2018;  
1208 Grassi et al., 2019). Meteorological extremes can also affect the efficiency of the sink (Thompson et al., 2020). The  
1209 EU forest sink is projected to decrease in the near future (Vizzarri et al., 2021). Consequently, for the EU to meet its  
1210 ambitious climate targets, it is necessary to maintain and even strengthen the LULUCF sink (EU, 2020).  
1211 Understanding the evolution of the CO<sub>2</sub> land fluxes is critical to enable the EU27+UK to meet its ambitious climate  
1212 goals.

1213

## 1214 **6. Appendices**

1215

## 1216 **Appendix A. Data sources, methodology and** 1217 **uncertainty descriptions**

1218 Plots for all countries in Europe as well as dozens of country groups and some countries outside of Europe are available  
1219 following a simple registration (VERIFY Synthesis Plots, 2022).

1220

### 1221 **A1. VERIFY project**

1222

1223 VERIFY's primary aim is to develop scientifically robust methods to assess the accuracy and potential biases in  
1224 national inventories reported by the parties through an independent pre-operational framework. "Pre-operational"  
1225 seeks to bridge the gap between pure research efforts and those aiming to provide regular (e.g., annual) updates of a  
1226 product. The main concept is to provide observation-based estimates of anthropogenic and terrestrial biospheric GHG  
1227 emissions and sinks as well as associated uncertainties. The proposed approach is based on the integration of  
1228 atmospheric measurements, improved emission inventories, ecosystem data, and satellite observations, and on an  
1229 understanding of processes controlling GHG fluxes (ecosystem models, GHG emission models).

1230 Two complementary approaches relying on observational data-streams were combined in VERIFY to  
1231 quantify GHG fluxes:

1232 1) atmospheric GHG mole fractions from satellites and ground-based networks (top-down atmospheric inversion  
1233 models), and

1234 2) bottom-up activity data (e.g., fuel use and emission factors, as represented in inventories) and ecosystem  
1235 measurements (e.g., aboveground biomass and net ecosystem fluxes, as assimilated into bottom-up and top-down  
1236 models)

1237 For CO<sub>2</sub>, a specific effort was made to separate fossil fuel emissions from ecosystem fluxes.

1238

1239 The objectives of VERIFY were:

1240 **Objective 1.** Integrate the efforts between the research community, national inventory compilers, operational centers  
1241 in Europe, and international organizations towards the definition of future international standards for the verification  
1242 of GHG emissions and sinks based on independent observation.

1243 **Objective 2.** Enhance the current observation and modeling ability to accurately and transparently quantify the sinks  
1244 and sources of GHGs in the land-use sector for the tracking of land-based mitigation activities.

1245 **Objective 3.** Develop new research approaches to monitor anthropogenic GHG emissions in support of the EU  
1246 commitment to reduce its GHG emissions by 40 % by 2030 compared to the year 1990.

1247 **Objective 4.** Produce periodic scientific syntheses of observation-based GHG balance of EU countries and practical  
1248 policy-oriented assessments of GHG emission trends, and apply these methodologies to other countries.

1249

1250 For more information on the project team and products/results please visit the VERIFY website (VERIFY, 2022).

1251

1253 *Table A1: A short glossary of terminology and acronyms used in this work. Note that nuances may be lost due to*  
 1254 *space limitations, and therefore these definitions should be considered as a guide.*

Terminology/Acronym	Brief description
additional sink capacity	A term referring to a general increased capacity of forests to uptake carbon due to improved growing conditions compared to pre-industrial times, in particular after the year 1950.
AFOLU	Agriculture, forestry, and land use. Includes all LULUCF fluxes (Sector 4) and also fluxes from Agriculture (Sector 3, e.g., CO <sub>2</sub> emissions from applications of urea to fields).
Annex I Parties	A designation of countries under the UNFCCC. Includes most industrialized countries and economies in transition as determined in 1992. Required to submit more regular and complete inventories to the UNFCCC.
bottom-up (BU)	A model which estimates fluxes by through physical processes and/or data without explicit consideration of atmospheric gas mole fractions. Often subdivided into "data-driven" and "process-based", and include "inventories".
category	Land-use category: Forest land, Cropland. Be careful to avoid confusion with categories. For example, "net emissions from Forest land" (subsector 4A) and the classification of land into Forest land (a category).
CL	Total Cropland (including both "remain" and "convert")
CL-CL	Cropland which remains Cropland from year to year
class	In some IPCC documents, appears to be used in the same manner as "category". We avoid its use here in the same context. However, "class" is used in general to indicate several types of an object ("classes of models", for example).
convert	Land which has been converted to this category in the previous N years (by default, N is equal to 20)
decay	Gradual breakdown and respiration of organic matter
DGVM	Dynamical global vegetation model, a form of bottom-up model.
FL	Total Forest land (including both "remain" and "convert")
FL-FL	Forest land which remains Forest land from year to year
GCB	Global Carbon Budget
GHG	Greenhouse gas (generally CO <sub>2</sub> in this work)
GL	Total Grassland (including both "remain" and "convert")
GL-GL	Grassland which remains Grassland from year to year
HWP	Harvested wood products. Carbon in timber removed from Forest land is counted here and allowed to slowly decompose (i.e., release CO <sub>2</sub> to the atmosphere).
IPPU	Industrial processes and product use
LUC	Land use change
LULCC	Land use and land cover change. Includes changes from one land cover type to another without necessarily a change in use (e.g., a change from C3 to C4 species during natural succession of a grassland).
LULUC	Land use and land use change. Does not include fluxes from activities on Forest land remaining Forest land (e.g., thinning).
LULUCF	Land use, land use change, and forestry. "Sector 4" in NGHGI terminology, representing fluxes from Forest land, Grassland, Cropland, Wetlands, Settlements, and Other land, though not all of these Land types are present in other bottom-up models. Note the use of capital letters for Land types to indicate the definitions changes from country to country.
managed land proxy	An assumption used in the NGHGIs which permits Member States to only report fluxes on lands deemed to be "managed" by the MS
mole fraction	The number of molecules of a substance per unit of total molecules. A measure of concentration that is independent of temperature and pressure.

MS	Member State (generally a sovereign country)
net flux (NBP, NEE)	The definition of the net carbon flux varies from approach to approach. In general, in this work, use of “net biome production” includes harvest but perhaps no other disturbances. Regional inversions generally fix fossil emissions and biomass burning (or assume the latter to be negligible). NGHGI are calculated through both stock-change and gain-loss methods, and therefore what is explicit/implicitly included varies from country to country. Table C2 has more details.
NGHGI	National greenhouse gas inventory
remain	Land which has remained in the same category for the past N years (by default, N is equal to 20)
subsector	Divisions of sectors (e.g., Sector 1A is Fuel combustion in the Energy sector). In the case of LULUCF, subsectors may be confused with categories.
sector	The most highly-aggregated level of emission reporting in the NGHGI: Energy (Sector 1), IPPU (Sector 2), Agriculture (Sector 3), LULUCF (Sector 4), and Waste (Sector 5). The word is occasionally used in the more generalized sense of a sector of the economy, e.g., the forest sector.
tier	Refers to the level of specificity used to calculate emissions. Tier 1 is the default, for which the IPCC provides generic emission factors and equations. Tier 2 uses the same equations, but region- or country-specific emission factors. Tier 3 uses more complex equations, possibly including process-based modeling.
top-down (TD)	A model which solves for fluxes by optimizing a prior guess based on observed atmospheric mole fractions. Also called an “atmospheric inversion”.
UNFCCC	United Nations Framework Convention on Climate Change
VERIFY	A project funded by the European Commission to build a pre-operational greenhouse gas monitoring system (see Appendix A1)
volatilize	Immediate release of carbon to the atmosphere, similar to instantaneous and complete combustion

1255

1256 *Table A2: Country grouping used for comparison purposes between BU and TD emissions as reported for the*  
1257 *country- and regional-level synthesis plots available through the VERIFY web portal.*

Country name – geographical Europe	BU-ISO3	Aggregation from TD-ISO3
Luxembourg	LUX	
Belgium	BEL	BENELUX
Netherlands	NLD	BNL
Bulgaria	BGR	BGR
Switzerland	CHE	
<i>Lichtenstein</i>	<i>LIE</i>	<i>CHL</i>
Czech Republic	CZE	Former Czechoslovakia
Slovakia	SVK	CSK
Austria	AUT	AUT
Slovenia	SVN	North Adriatic countries
Croatia	HRV	NAC

Romania	ROU	ROU
Hungary	HUN	HUN
Estonia	EST	
Lithuania	LTU	Baltic countries
Latvia	LVA	BLT
Norway	NOR	NOR
Denmark	DNK	
Sweden	SWE	
Finland	FIN	DSF
Iceland	ISL	ISL
Malta	MLT	MLT
Cyprus	CYP	CYP
France (Corsica incl.)	FRA	FRA
<i>Monaco</i>	<i>MCO</i>	
<i>Andorra</i>	<i>AND</i>	
Italy (Sardinia, Vatican incl.)	ITA	ITA
<i>San Marino</i>	<i>SMR</i>	
United Kingdom (Great Britain + N Ireland)	GBR	UK
<i>Isle of Man</i>	<i>IMN</i>	
Iceland		
Ireland	IRL	IRL
Germany	DEU	DEU
Spain	ESP	IBERIA
Portugal	PRT	IBE
Greece	GRC	GRC
<i>Russia (European part)</i>	<i>RUS European</i>	
<i>Georgia</i>	<i>GEO</i>	<i>RUS European+GEO</i>
<i>Russian Federation</i>	<i>RUS</i>	<i>RUS</i>
Poland	POL	POL
<i>Turkey</i>	<i>TUR</i>	<i>TUR</i>

EU27+UK (Austria, Belgium, Bulgaria, Cyprus, Czech Republic, Germany, Denmark, Spain, Estonia, Finland, France, Greece, Croatia, Hungary, Ireland, Italy, Lithuania, Latvia, Luxembourg, Malta, Netherlands, Poland, Portugal, Romania, Slovakia, Slovenia, Sweden, United Kingdom)	AUT, BEL, BGR, CYP, CZE, DEU, DNK, ESP, EST, FIN, FRA, GRC, HRV, HUN, IRL, ITA, LTU, LVA, LUX, MLT, NDL, POL, PRT, ROU, SVN, SVK, SWE, GBR	E28
Western Europe (Belgium, France, United Kingdom, Ireland, Luxembourg, Netherlands)	BEL, FRA, UK, IRL, LUX, NDL	WEE
Central Europe (Austria, Switzerland, Czech Republic, Germany, Hungary, Poland, Slovakia)	AUT, CHE, CZE, DEU, HUN, POL, SVK	CEE
Northern Europe (Denmark, Estonia, Finland, Lithuania, Latvia, Norway, Sweden)	DNK, EST, FIN, LTU, LVA, NOR, SWE	NOE
<i>South-Western Europe (Spain, Italy, Malta, Portugal)</i>	<i>ESP, ITA, MLT, PRT</i>	<i>SWN</i>
<i>South-Eastern Europe (all) (Albania, Bulgaria, Bosnia and Herzegovina, Cyprus, Georgia, Greece, Croatia, Macedonia, the former Yugoslav, Montenegro, Romania, Serbia, Slovenia, Turkey)</i>	<i>ALB, BGR, BIH, CYP, GEO, GRC, HRV, MKD, MNE, ROU, SRB, SVN, TUR</i>	<i>SEE</i>
<i>South-Eastern Europe (Albania, Bosnia and Herzegovina, Macedonia, the former Yugoslav, Georgia, Turkey, Montenegro, Serbia)</i>	<i>ALB, BIH, MKD, MNE, SRB, GEO, TUR</i>	<i>SEA</i>
<i>South-Eastern Europe (EU) (Bulgaria, Cyprus, Greece, Croatia, Romania, Slovenia)</i>	<i>BGR, CYP, GRC, HRV, ROU, SVN</i>	<i>SEZ</i>
<i>Southern Europe (all) (SOE) (Albania, Bulgaria, Bosnia and Herzegovina, Cyprus, Georgia, Greece, Croatia, Macedonia, the former Yugoslav, Montenegro, Romania, Serbia, Slovenia, Turkey, Italy, Malta, Portugal, Spain)</i>	<i>ALB, BGR, BIH, CYP, GEO, GRC, HRV, MKD, MNE, ROU, SRB, SVN, TUR, ITA, MLT, PRT, ESP</i>	<i>SOE</i>
<i>Southern Europe (SOY) Albania, Bosnia and Herzegovina, Georgia, Macedonia, the former Yugoslav, Montenegro, Serbia, Turkey)</i>	<i>ALB, BIH, GEO, MKD, MNE, SRB, TUR,</i>	<i>SOY</i>
Southern Europe (EU) (SOZ) (Bulgaria, Cyprus, Greece, Croatia, Romania, Slovenia, Italy, Malta, Portugal, Spain)	BGR, CYP, GRC, HRV, ROU, SVN, ITA, MLT, PRT, ESP	SOZ
Eastern Europe (Belarus, Moldova, Republic of, Russian Federation, Ukraine)	BLR, MDA, RUS, UKR	EAE
<i>EU-15 (Austria, Belgium, Germany, Denmark, Spain, Finland, France, United Kingdom, Greece, Ireland, Italy, Luxembourg, Netherlands, Portugal, Sweden)</i>	<i>AUT, BEL, DEU, DNK, ESP, FIN, FRA, GBR, GRC, IRL, ITA, LUX, NDL, PRT, SWE</i>	<i>E15</i>

<p><i>EU-27 (Austria, Belgium, Bulgaria, Cyprus, Czech Republic, Germany, Denmark, Spain, Estonia, Finland, France, Greece, Croatia, Hungary, Ireland, Italy, Lithuania, Latvia, Luxembourg, Malta, Netherlands, Poland, Portugal, Romania, Slovakia, Slovenia, Sweden)</i></p>	<p><i>AUT, BEL, BGR, CYP, CZE, DEU, DNK, ESP, EST, FIN, FRA, GRC, HRV, HUN, IRL, ITA, LTU, LVA, LUX, MLT, NDL, POL, PRT, ROU, SVN, SVK, SWE</i></p>	<p><i>E27</i></p>
<p><i>All Europe (Aaland Islands, Albania, Andorra, Austria, Belgium, Bulgaria, Bosnia and Herzegovina, Belarus, Switzerland, Cyprus, Czech Republic, Germany, Denmark, Spain, Estonia, Finland, France, Faroe Islands, United Kingdom, Guernsey, Greece, Croatia, Hungary, Isle of Man, Ireland, Iceland, Italy, Jersey, Liechtenstein, Lithuania, Luxembourg, Latvia, Moldova, Republic of, Macedonia, the former Yugoslav, Malta, Montenegro, Netherlands, Norway, Poland, Portugal, Romania, Russian Federation, Svalbard and Jan Mayen, San Marino, Serbia, Slovakia, Slovenia, Sweden, Turkey, Ukraine)</i></p>	<p><i>ALA, ALB, AND, AUT, BEL, BGR, BIH, BLR, CHE, CYP, CZE, DEU, DNK, ESP, EST, FIN, FRA, FRO, GBR, GGY, GRC, HRV, HUN, IMN, IRL, ISL, ITA, JEY, LIE, LTU, LUX, LVA, MDA, MKD, MLT, MNE, NDL, NOR, POL, PRT, ROU, RUS, SJM, SMR, SRB, SVK, SVN, SWE, TUR, UKR</i></p>	<p><i>EUR</i></p>

1258 \*countries highlighted in *italic* are not discussed in the current 2021 synthesis mostly because unavailability of UNFCCC NGHGI reports (non-  
1259 Annex I countries<sup>21</sup>) but are present on the web-portal (VERIFY Synthesis Plots, 2022).

1260

<sup>21</sup>Non-Annex I countries are mostly developing countries. The reporting to UNFCCC is implemented through national communications (NCs) and biennial update reports (BURs): <https://unfccc.int/national-reports-from-non-annex-i-parties>

1261 *Table A3: An overview of major changes of the current study with respect to the original (Petrescu et al., 2020) and*  
 1262 *most recent (Petrescu et al., 2021b) studies of this series; n/a means a dataset was not used or available. **Bold** text*  
 1263 *indicates changes in this study with respect to the most recent version.*

1264

Dataset	Petrescu et al. (2020)	Petrescu et al. (2021b)	This study
<b>NGHGI Fossil CO<sub>2</sub></b>			
Emissions	n/a	Common reporting framework (CRF), submitted in 2019 1990-2017	Common reporting framework (CRF), submitted in <b>2021 1990-2019</b>
Uncertainties	n/a	Uncertainty exists for 2016 (error propagation, 95 % confidence interval)	Uncertainty exists for <b>1990-2019</b> (error propagation, 95 % confidence interval, <b>gap-filling</b> )
<b>Bottom-up fossil CO<sub>2</sub></b>			
BP	n/a	n/a	<b>Version 2021 1971-2020</b>
CDIAC	n/a	2005-2018	Version 2021v2 <b>1992-2018</b>
CEDS	n/a	2005-2014	Version 2021_04_21 <b>1750-2019</b>
EDGAR	n/a	Version 5.0 1990-2018	<b>Version 6.0b 1970-2018</b>
EIA	n/a	2005-2016	Version 220216 <b>1993-2019</b>
GCP	n/a	2005-2018	Version 2021v40 <b>1750-2020</b>
IEA	n/a	1990-2017	1990- <b>2020</b>
PRIMAP-hist	n/a	2005-2017	Version <b>2.3.1 1750-2019</b>
<b>Top-down fossil CO<sub>2</sub></b>			
Emissions	n/a	IAP RAS fast-track inversion EU11+CHE	<b>CIF-CHIMERE fast-track inversion EU27+UK 2005-2020</b>
<b>NGHGI land CO<sub>2</sub></b>			
Emissions	CRF, submitted in 2018 LULUCF : 1990-2016 FL : 1995, 2000, 2005, 2010, 2015 GL : 1990, 2005, 2010, 2016 CL : 1990, 2005, 2010, 2016	CRF, submitted in 2019 LULUCF: 1990-2017 FL : 1990-2017 GL: 1990-2017 CL: 1990-2017	CRF, submitted in <b>2021</b> LULUCF: 1990- <b>2019</b> FL : 1990- <b>2019</b> GL: 1990- <b>2019</b> CL: 1990- <b>2019</b>
Uncertainties	Uncertainty exists for 2016 (error propagation, 95 % confidence interval)	Uncertainty exists for 2016 (error propagation, 95 % confidence interval)	LULUCF: Uncertainty exists for <b>1990-2019</b> (error propagation, 95 % confidence interval, <b>gap-filling</b> ) FL, GL, CL: Uncertainty exists for <b>2018</b> (error propagation, 95 % confidence interval)
<b>Bottom-up terrestrial biosphere CO<sub>2</sub></b>			
BLUE	Version GCP 1990-2017	Version GCP 1990-2018	Version GCP 1990- <b>2020</b> <b>Version VERIFY 1990-2020</b>



CABLE-POP	n/a	n/a	<b>1990-2020</b>
CBM	2000, 2005, 2010, 2015	1990-2015	2000-2015 <b>2017-2020 (estimate)</b>
ECOSSE	n/a	1990-2018 (grassland) 1990-2018 (cropland)	1990-2018 (grassland) 1990-2020 (cropland)
EFISCEN	1995, 2000, 2010, 2015 Country totals EU27+UK	2005-2018 Country Totals EU27+UK	2005-2020 <b>Spatially-explicit 15 countries</b>
EPIC-IIASA	n/a	1990-2018 (cropland)	1990-2020 (cropland) <b>1990-2020 (grassland)</b>
FAOSTAT	1990-2016	1990-2017	1990-2019
H&N	1990-2015	1990-2018	1990-2020
Lateral fluxes	n/a	(not accounted for in inversions) Emissions from inland waters	<b>(accounted for in inversions)</b> Emissions from inland waters <b>Wood trade Crop trade 1990-2019</b>
ORCHIDEE	n/a	version 2.2 1990-2018	version 3.0 <b>1990-2020</b>
TRENDY DVGMs	Version 6 1990-2017	Version 7 1990-2018	Version 10 <b>1990-2020</b>
<b>Top-down terrestrial biosphere CO<sub>2</sub> (global)</b>			
Global Carbon Project	n/a	version 2019 2000-2018	version 2021 2010-2020
<b>Top-down terrestrial biosphere CO<sub>2</sub> (regional)</b>			
CarboScopeRegional	n/a	2006-2018	2006-2020
CIF-CHIMERE	n/a	n/a	<b>2005-2020</b>
EUROCOM	n/a	Original version 2006-2015	<b>Drought Version 2009-2018</b>
LUMIA	n/a	n/a	<b>2006-2020</b>

1265

1266

## 1267 **A2. UNFCCC NGHGI (2021)**

1268

1269 Annex I NGHGIs should follow principles of transparency, accuracy, consistency, completeness and  
1270 comparability (TACCC) under the guidance of the UNFCCC (UNFCCC, 2014) and as mentioned above, shall be  
1271 completed following the 2006 IPCC guidelines (IPCC, 2006). In addition, the IPCC 2019 Refinement (IPCC, 2019),  
1272 which may be used to complement the 2006 IPCC guidelines, has updated sectors with additional emission sources  
1273 and provides guidance on the use of atmospheric data for independent verification of GHG inventories.

1274 Both approaches (BU and TD) provide useful insights on emissions from two different points of view. First,  
1275 as outlined in Volume 1, Chapter 6 of the 2019 IPCC Refinement (IPCC, 2019), TD approaches act as an additional  
1276 quality check for BU and NGHGI approaches, and facilitate a deeper understanding of the processes driving changes  
1277 in different elements of GHG budgets. Second, while independent BU methods do not follow prescribed standards  
1278 like the IPCC Guidelines, they do provide complementary information based on alternative input data at varying  
1279 temporal, spatial, and sectoral resolution. This complementary information helps build trust in country GHG estimates,  
1280 which form the basis of national climate mitigation policies. Additionally, BU estimates are needed as input for TD  
1281 estimates. As there is no formal guideline to estimate uncertainties in TD or BU approaches, uncertainties are usually

1282 assessed from the spread of different estimates within the same approach, though some groups or institutions report  
1283 uncertainties for their individual estimates using a variety of methods, for instance, by performing Monte Carlo  
1284 sensitivity simulation by varying input data parameters. However, this can be logistically and computationally difficult  
1285 when dealing with complex process-based models.

1286         Despite the important insights gained from complementary BU and TD emission estimates, it should be noted  
1287 that comparisons with the NGHGI are not always straightforward. BU estimates often share common methodology  
1288 and input data, and through harmonization, structural differences between BU estimates and NGHGIs can be  
1289 interpreted. However, the use of common input data restricts the independence between the datasets and, from a  
1290 verification perspective, may limit the conclusions drawn from the comparisons. On the other hand, TD estimates are  
1291 constrained by independent atmospheric observations and can serve as an additional, potentially independent quality  
1292 check for NGHGIs. Nonetheless, structural differences between NGHGIs (what sources and sinks are included, and  
1293 where and when emissions/removals occur) and the actual fluxes of GHGs to the atmosphere must be taken into  
1294 account during comparison of estimates. While NGHGIs go through a central QA/QC review process, the UNFCCC  
1295 reporting requirements do not mandate large-scale observation-derived verification. Nevertheless, the individual  
1296 countries may use atmospheric data and inverse modeling within their data quality control, quality assurance and  
1297 verification processes, with expanded and updated guidance provided in chapter 6 of the 2019 Refinement of IPCC  
1298 2006 Guidelines (IPCC, 2019). So far, only a few countries (e.g. Switzerland, UK, New Zealand and Australia) have  
1299 used atmospheric observations to constrain national emissions and documented these verification activities in their  
1300 national inventory reports (Bergamaschi et al., 2018), and none do so for CO<sub>2</sub>.

1301         Under the UNFCCC convention and its Kyoto Protocol, national GHG inventories are the most important  
1302 source of information to track progress and assess climate protection measures by countries. In order to build mutual  
1303 trust in the reliability of GHG emission information provided, national GHG inventories are subject to standardized  
1304 reporting requirements, which have been continuously developed by the Conference of the Parties (COP)<sup>22</sup>. The  
1305 calculation methods for the estimation of greenhouse gasses in the respective sectors is determined by the methods  
1306 provided by the 2006 IPCC Guidelines for National Greenhouse Gas Inventories (IPCC, 2006). These Guidelines  
1307 provide detailed methodological descriptions to estimate emissions and removals, as well as recommendations to  
1308 collect the activity data needed. As a general overall requirement, the UNFCCC reporting guidelines stipulate that  
1309 reporting under the Convention and the Kyoto Protocol must follow the five key principles of transparency, accuracy,  
1310 completeness, consistency and comparability (TACCC).

1311         The reporting under UNFCCC shall meet the TACCC principles. The three main GHGs are reported in  
1312 timeseries from 1990 up to two years before the due date of the reporting. The reporting is strictly source category  
1313 based and is done under the Common Reporting Format tables (CRF), downloadable from the UNFCCC official  
1314 submission portal: <https://unfccc.int/ghg-inventories-annex-i-parties/2021>.

1315

---

<sup>22</sup> The last revision has been made by COP 19 in 2013 (UNFCCC, 2013)

## 1316 NGHGI uncertainties

1317

1318           The presented uncertainties in the reported emissions of the individual countries and the EU27+UK bloc  
1319 were calculated by using the methods and data used to compile the official GHG emission uncertainties that are  
1320 reported by the EU under the UNFCCC (NIRs, 2022). The EU uncertainty analysis reported in the bloc's National  
1321 Inventory Report (NIR) is based on country-level, Approach 1 uncertainty estimates (IPCC, 2006, Vol. 1, Chap. 3)  
1322 that are reported by EU Member States, Iceland and United Kingdom under Article 7(1)(p) of EU (2013). These  
1323 country-level uncertainty estimates are typically reported at beginning of a submission cycle and are not always  
1324 revised with updated CRF submissions later in the submission cycle. Furthermore, the compiled uncertainties of some  
1325 countries are incomplete (e.g., uncertainties not estimated for LULUCF and/or indirect CO<sub>2</sub> emissions, certain  
1326 subsector emissions are confidential) and the sector and gas resolution at which uncertainties are provided varies  
1327 between the countries. The EU inventory team therefore implements a procedure to harmonize and gap-fill these  
1328 uncertainty estimates. A processing routine reads the individual country uncertainty files that are pre-formatted  
1329 manually to assign consistent sector and gas labels to the respective estimates of emissions/removals and uncertainties.  
1330 The uncertainty values are then aggregated to a common sector resolution, at which the emissions and removals  
1331 reported in the uncertainty tables of the countries are then replaced with the respective values from the final CRF  
1332 tables of the countries. Due to the issue of incompleteness mentioned above, the country-level data are then screened  
1333 to identify residual GHG emissions and removals for which no uncertainty estimates have been provided. Where  
1334 sectors are partially complete, the residual net emission is quantified in CO<sub>2</sub> equivalents and incorporated. An  
1335 uncertainty is then estimated, by calculating the overall sector uncertainty of the sources and sinks that were included  
1336 in that country's reported uncertainties estimates and assigning this percentage average to the residual net emission.  
1337 In cases where for certain sectors no uncertainties have been provided at all (e.g., indirect CO<sub>2</sub> emissions, LULUCF),  
1338 an average (median) sector uncertainty in percent is calculated from all the countries for which complete sectoral  
1339 emissions and uncertainties were reported, and this average uncertainty is assigned to the country's sector GHG total  
1340 reported in its final CRF tables.

1341           The country-level uncertainties presented in this paper, have been compiled using this same processing  
1342 routine and using the uncertainties and CRF data reported by the countries in the 2021 submission. However, here the  
1343 method has been expanded to gap-fill at the individual greenhouse gas level (CO<sub>2</sub> emissions and removals only) rather  
1344 than at the aggregate GHG level. Furthermore, the expanded method here assigns the sub-sectoral uncertainties to the  
1345 emissions and removals of the entire timeseries (1990-2019), rather than just the base year and latest year of the  
1346 respective timeseries. This allows uncertainties to be sensitive to the sub-sectoral contributions to sectoral and national  
1347 total emissions, which of course change over time. For each year of the timeseries, uncertainties in the total and  
1348 sectoral CO<sub>2</sub> emissions are calculated using Gaussian error propagation, by summing the respective sub-sectoral  
1349 uncertainties (expressed in kt CO<sub>2</sub>) in quadrature and assuming no error correlation. In contrast, for the EU27+UK  
1350 bloc, uncertainties in the total and sectoral CO<sub>2</sub> emissions were calculated to take into account error correlations  
1351 between the respective country estimates at the subsector level. This was done by applying the same methods and  
1352 assumptions described in the 2022 EU NIR (UNFCCC NIR, 2022). The subsector resolution applied for gap-filling

1353 allows the routine to access respective data on emission factors from CRF Table *Summary 3* and apply correlation  
1354 coefficients ( $r$ ) when aggregating the uncertainties. For a given subsector, it is assumed that the errors of countries  
1355 using default factors are completely correlated ( $r = 1$ ), while errors of countries using country-specific factors are  
1356 assumed uncorrelated ( $r = 0$ ). For countries using a mix of default and country-specific factors at the given subsector  
1357 level, it is assumed that these errors are partially correlated ( $r = 0.5$ ) with one another and with the errors of countries  
1358 using the default factors only.

1359 Based on these correlation assumptions, the routine then aggregates CO<sub>2</sub> emissions/removals and  
1360 uncertainties for the specified subsector resolution at the EU27+UK level. Uncertainties at sector total level are then  
1361 aggregated from the subsector estimates assuming no correlation between subsectors. However, for countries reporting  
1362 very coarse resolution estimates (e.g., total sector CO<sub>2</sub> emissions/removals) or where the sector has been partially or  
1363 completely gap-filled, it is assumed that these uncertainties are partially correlated ( $r = 0.5$ ) with one another and with  
1364 the other reported subsector level estimates. Level uncertainties on the total EU27+UK CO<sub>2</sub> emissions and removals  
1365 (with and without LULUCF) are then aggregated from the sector estimates assuming no error correlation between  
1366 sectors.

1367 Note that the above procedure does not apply to LULUCF categories (FL, CL, and GL). Estimates for these  
1368 values were taken directly from the EU NIR (2021) without gap-filling or consideration of correlations. An  
1369 uncertainty greater than 100 % implies that either a sink or a source is possible. As the values are given for only one  
1370 single year, this value is applied uniformly across the whole timeseries.

1371

### 1372 **A3. Fossil CO<sub>2</sub> emissions**

1373

#### 1374 **A3.1. Bottom-up emission estimates**

1375

1376 For further details of all datasets, see Andrew (2020).

1377

#### 1378 *UNFCCC NGHGI (2021)*

1379

1380 The UNFCCC NGHGI CO<sub>2</sub> emissions/removals include estimates from five key sectors for the EU27+UK:  
1381 1 Energy, 2 Industrial processes and product use (IPPU), 3 Agriculture, 4 LULUCF and 5 Waste. The tiers method a  
1382 country applies depends on the national circumstances and the individual conditions of the land, which explains the  
1383 variability of uncertainties among the sector itself as well as among EU countries. This annual published dataset  
1384 includes all CO<sub>2</sub> emissions sources for those countries, and for most countries for the period 1990 to t-2. Some eastern  
1385 European countries' submissions began in the 1980s.

1386 Information on uncertainty calculation in the NGHGI is found above in the general section on the NGHGI.

1387

1388 *EDGAR v6.0*

1389

1390 The first edition of the Emissions Database for Global Atmospheric Research was published in 1995. The  
1391 dataset now includes almost all sources of fossil CO<sub>2</sub> emissions, is updated annually, and reports data for 1970 to year  
1392 n-1. Estimates for v6.0 are provided by sector. Emissions are estimated fully based on statistical data from 1970 till  
1393 2018 <https://data.jrc.ec.europa.eu/dataset/97a67d67-c62e-4826-b873-9d972c4f670b>.

1394 **Uncertainties:** EDGAR uses emission factors (EFs) and activity data (AD) to estimate emissions. Both EFs and AD  
1395 are uncertain to some degree, and when combined, their uncertainties need to be combined too. To estimate EDGAR's  
1396 uncertainties (stemming from lack of knowledge of the true value of the EF and AD), the methodology devised by  
1397 IPCC (2006, Chapter 3) is adopted (Solazzo et al., 2021), including the use of default uncertainties. The overall  
1398 relative uncertainty in emissions is thus given by simple error propagation for the product of two variables, where the  
1399 overall relative uncertainty is the square root of the sum of squares of the relative uncertainties of the EF and AD. A  
1400 log-normal probability distribution function is assumed in order to avoid negative values, and uncertainties are  
1401 reported as the 95 % confidence interval according to IPCC (2006, chapter 3, equation 3.7). For emission uncertainty  
1402 in the range 50 % to 230 % a correction factor is adopted as suggested by Frey et al. (2003) and IPCC (2006, chapter  
1403 3, equation 3.4). Uncertainties are published in Solazzo et al. (2021).

1404

1405 *BP*

1406

1407 BP releases its Statistical Review of World Energy annually in June, the first report being published in 1952.  
1408 Primarily an energy dataset, BP also includes estimates of fossil-fuel CO<sub>2</sub> emissions derived from its energy data (BP  
1409 2011, 2017). The emissions estimates are totals for each country starting in 1965 to year n-1.

1410

1411 *CDIAC*

1412

1413 The original Carbon Dioxide Information Analysis Center included a fossil CO<sub>2</sub> emissions dataset that was  
1414 long known as CDIAC. This dataset is now produced at Appalachian State University, and has been renamed CDIAC-  
1415 FF (CDIAC, 2022). It includes emissions from fossil fuels (including gas flaring) and cement production from 1751  
1416 to year n-3. Fossil-fuel emissions are derived from UN energy statistics, and cement emissions from USGS production  
1417 data.

1418

1419 *EIA*

1420

1421 The US Energy Information Administration publishes international energy statistics and from these derives  
1422 estimates of CO<sub>2</sub> emissions from energy combustion based on energy consumption. Data are currently available for  
1423 the period 1980-2016.

1424

1425 *IEA*

1426

1427           The International Energy Agency publishes international energy statistics and from these derives estimates  
1428 of CO<sub>2</sub> emissions from energy combustion. In addition, IEA also estimates emissions from the use of coal in the iron  
1429 and steel industry, while not providing any other IPPU estimates. Emissions estimates start in 1960 for OECD  
1430 members and 1971 for non-members, and run through n-1 for OECD members' totals, and year n-2 for members'  
1431 details and non-members. Most subsector-level data from IEA are available for a fee, although some high-level  
1432 emissions data can be accessed free-of-charge

1433

1434 *GCP*

1435

1436           The Global Carbon Project includes estimates of fossil CO<sub>2</sub> emissions in its annual Global Carbon Budget  
1437 publication. These include emissions from fossil fuels and cement production for the period 1750 to year n-1. GCP's  
1438 fossil CO<sub>2</sub> dataset was once entirely derived solely from CDIAC's dataset, with some extension using BP data, but  
1439 this has since changed as described in Andrew and Peters (2022).

1440

1441 *CEDS*

1442

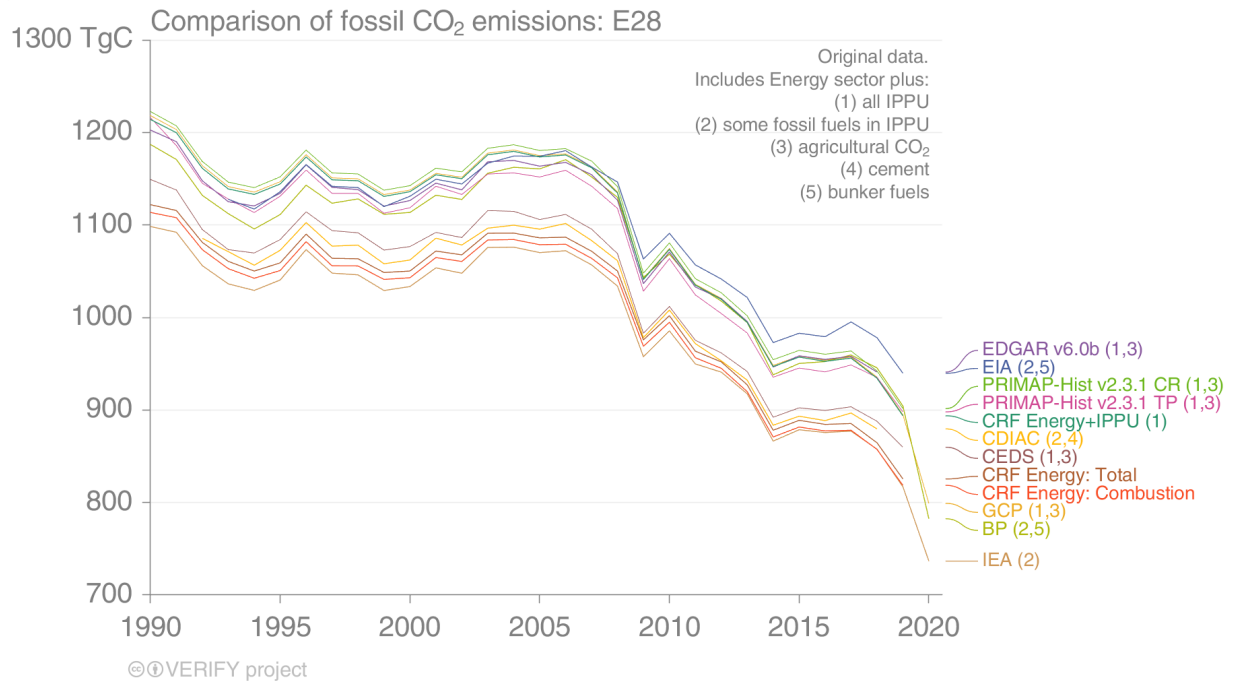
1443           The Community Emissions Data System has included estimates of fossil CO<sub>2</sub> emissions since 2018, with an  
1444 irregular update cycle (CEDS, 2022). Energy data are directly from IEA, but emissions are scaled to higher-priority  
1445 sources, including national inventories. Almost all emissions sources are included and estimates are published for the  
1446 period 1750 to year n-1. Estimates are provided by subsector.

1447

1448 *PRIMAPv2.2*

1449

1450           The PRIMAP-hist dataset combines several published datasets to create a comprehensive set of greenhouse  
1451 gas emission pathways for every country and Kyoto gas, covering the years 1850 to 2018, and all UNFCCC (United  
1452 Nations Framework Convention on Climate Change) member states as well as most non-UNFCCC territories. The  
1453 data resolves the main IPCC (Intergovernmental Panel on Climate Change) 2006 categories. For CO<sub>2</sub>, CH<sub>4</sub>, and N<sub>2</sub>O  
1454 subsector data for Energy, Industrial Processes and Product Use (IPPU), and Agriculture is available. Due to data  
1455 availability and methodological issues, version 2.2 of the PRIMAP-hist dataset does not include emissions from Land  
1456 Use, Land-Use Change, and Forestry (LULUCF). More info at <https://zenodo.org/record/4479172#.YUsc6p0zbIU>.



1457

1458 *Figure A1: Comparison of EU27+UK fossil CO<sub>2</sub> emissions from multiple inventory datasets. Identical to Fig. 2,*  
 1459 *except that no system boundaries harmonization has been done. CDIAC does not report emissions prior to 1992 for*  
 1460 *former-Soviet Union countries. CRF: UNFCCC NGHGI from the Common Reporting Format tables.*

1461

1462

### 1463 A3.2. Top-down CO<sub>2</sub> emission estimates

1464

#### 1465 *CIF-CHIMERE - fossil CO<sub>2</sub> emission inversion*

1466

1467 CIF-CHIMERE is used for both CO<sub>2</sub> land and CO<sub>2</sub> fossil emission estimates, and this section only describes  
 1468 the CO<sub>2</sub> fossil estimates. The product is explained in more detail by Fortems-Cheiney and Broquet, 2021.

1469 Results from previous atmospheric inversions of the European fossil CO<sub>2</sub> emissions indicated that there were  
 1470 much larger uncertainties associated with the assimilation of CO data than with that of NO<sub>2</sub> data for such a purpose  
 1471 (Konovalov et al, 2016; Konovalov and Llova, 2018). In this context, we have developed an atmospheric inversion  
 1472 configuration quantifying monthly to annual budgets of the national emissions of fossil CO<sub>2</sub> in Europe based on the  
 1473 assimilation of the long-term series of NO<sub>2</sub> spaceborne observations; the Community Inversion Framework (CIF); the  
 1474 CHIMERE regional chemistry transport model (CTM); corrections to the TNO-GHGco-v3 inventory of NO<sub>x</sub>  
 1475 anthropogenic emissions at 0.5° horizontal resolution; and the conversion of NO<sub>x</sub> anthropogenic emission estimates  
 1476 into CO<sub>2</sub> fossil emission estimates. For the first time, to our knowledge, variational regional inversions have been  
 1477 performed to estimate the European CO<sub>2</sub> fossil emissions using NO<sub>x</sub> emissions from OMI satellite observations.  
 1478 Particular attention is paid in the analysis assessing the consistency between the fossil CO<sub>2</sub> emissions estimates from

1479 our processing chain with the fossil CO<sub>2</sub> emission budgets provided by the TNO-GHGco-v3 inventory based on the  
1480 emissions reported by countries to UNFCCC, which are assumed to be accurate in Europe. The algorithm first  
1481 optimizes NO<sub>x</sub> emissions and then assumes a fixed ratio of NO<sub>x</sub> to fossil CO<sub>2</sub> emissions. However, long-term plans  
1482 include the simultaneous inversion of all three gasses (CO<sub>2</sub>, NO<sub>2</sub>, and CO).

1483 The analysis is conducted over the period 2005 to 2020. CHIMERE is run over a 0.5°×0.5° regular grid and  
1484 17 vertical layers, from the surface to 200hPa, with 8 layers within the first two kilometers. The domain includes 101  
1485 (longitude) x 85 (latitude) grid-cells (15.25°W-35.75°E; 31.75°N-74.25°N) and covers Europe. CHIMERE is driven  
1486 by the European Centre for Medium-Range Weather Forecasts (ECMWF) meteorological forecast (Owens and  
1487 Hewson, 2018). The chemical scheme used in CHIMERE is MELCHIOR-2, with more than 100 reactions (Lattuati,  
1488 1997; CHIMERE 2017), including 24 for inorganic chemistry. Climatological values from the LMDZ-INCA global  
1489 model (Szopa et al., 2008) are used to prescribe mole fractions at the lateral and top boundaries and the initial  
1490 atmospheric composition in the domain. Considering the short NO<sub>2</sub> lifetime, we do not consider its import from outside  
1491 the domain: its boundary conditions are set to zero. Nevertheless, we take into account peroxyacetyl nitrate (PAN) for  
1492 the large-scale transport of NO<sub>x</sub>. Due to atmospheric chemistry, it represents an important and the associated NO<sub>x</sub>  
1493 reservoir and has a significant impact on the regional NO<sub>2</sub> tropospheric columns observed by OMI.

1494 Several critical aspects of this workflow need to be highlighted: (i) Fortems-Cheiney and Broquet (2021)  
1495 have not yet reported estimates of the uncertainty in the fossil CO<sub>2</sub> emissions (this requires the derivation of the  
1496 uncertainties in the NO<sub>x</sub> emission inversions and in the NO<sub>x</sub>-to-FFCO<sub>2</sub> emission conversion), and (ii) the fossil CO<sub>2</sub>  
1497 emission budgets provided by the TNO-GHGco-v3 inventory are based on the emissions reported by countries to  
1498 UNFCCC, which are assumed to be accurate in Europe, and therefore the NO<sub>x</sub> inversion prior estimate is consistent  
1499 with the inventory estimates (with respect to the NO<sub>x</sub>-to-FFCO<sub>2</sub> emission conversion used to infer fossil CO<sub>2</sub>  
1500 emissions from the NO<sub>x</sub> inversions).

1501 **Uncertainty:** There is no uncertainty estimate currently available for this product.

1502

## 1503 **A4. Land CO<sub>2</sub> emissions/removals**

1504

### 1505 **A4.1. Bottom-up CO<sub>2</sub> estimates**

1506

#### 1507 **UNFCCC NGHGI 2021 - LULUCF**

1508

1509 For the biogenic CO<sub>2</sub> emissions from LULUCF (Sector 4 in the terminology of the NGHGIs), methods for the  
1510 estimation of CO<sub>2</sub> removals differ enormously among countries and land use categories. Each country uses its own  
1511 country specific method which takes into account specific national circumstances (as long as they are in accordance  
1512 with the 2006 IPCC guidelines), as well as IPCC default values, which are a "compromise between the level of detail  
1513 that would be needed to create the most accurate estimates for each country, and the input data likely to be available



1514 or readily obtainable in most countries" (Volume 1, Chapter 3 of IPCC, 2006). They may, therefore, result in higher  
 1515 uncertainties. The EU GHG inventory underlies the assumption that the individual use of national country specific  
 1516 methods leads to more accurate GHG estimates than the implementation of a single EU wide approach (UNFCCC,  
 1517 2018b). Key categories for the EU27 are 4.A.1 Forest Land: Land Use CO<sub>2</sub>, 4.A.2. Forest Land: Land Use CO<sub>2</sub>, 4.B.1  
 1518 Cropland Land Use CO<sub>2</sub>, 4.B.2 Cropland Land Use CO<sub>2</sub>, 4.C.1 Grassland Land Use CO<sub>2</sub>, 4.C.2 Grassland Land Use  
 1519 CO<sub>2</sub>, 4.D.1 Wetlands Land Use CO<sub>2</sub>, 4.E.2 Settlements Land Use CO<sub>2</sub>, and 4.G Harvested Wood Production Wood  
 1520 product CO<sub>2</sub>. The tiered method a country applies depends on the national circumstances and the individual conditions  
 1521 of the land, which explains the variability of uncertainties among the sector itself as well as among EU countries.

1522 Table A4 shows the mean values of all LULUCF categories for the EU27+UK NGHGI (2021). The  
 1523 contribution is calculated as the percentage of the sum of the absolute values of all the categories, in order to account  
 1524 for differing signs.

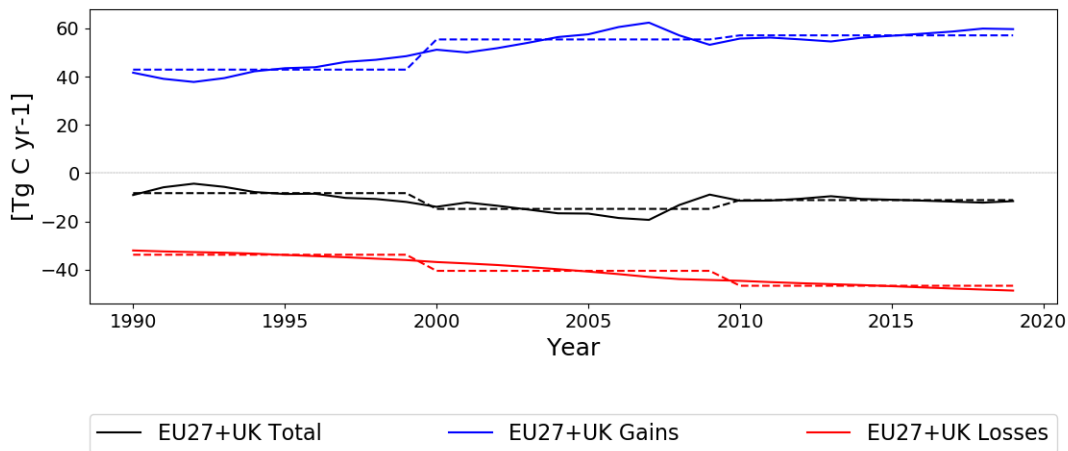
1525

1526 *Table A4: LULUCF categories for the EU27+UK NGHGI (2021)*

Category	Mean value for 1990-2020 [Tg C]	Contribution to gross LULUCF flux [%]
Forest land remaining forest land	-107	56.0
Land converted to forest land	-13.0	6.80
Cropland remaining cropland	8.45	4.41
Land converted to cropland	14.0	7.33
Grassland remaining grassland	11.8	6.16
Land converted to grassland	-8.22	4.23
Wetlands remaining wetlands	2.89	1.51
Land converted to wetlands	1.09	0.567
Settlements remaining settlements	1.42	0.744
Land converted to settlements	11.8	6.15
Other land remaining other land	N/A	N/A
Land converted to other land	0.135	0.0706
Harvested wood products	-11.5	5.99

1527

1528



1529

1530 *Figure A2: The gains, losses, and total HWP pools from the Common Reporting Format tables for the European*  
 1531 *Union (Convention), which covers the EU27+UK. Dashed lines show the averages for 1990-1999, 2000-2009, and*  
 1532 *2010-2019 for easy comparison with Fig. B4.*

1533

1534 **Uncertainty:** Methodology for the NGHGI UNFCCC submissions are based on Chapter 3 of 2006 IPCC Guidelines  
 1535 for National Greenhouse Gas Inventories and is the same as described in Appendix A2.

1536

1537 *ORCHIDEE*

1538

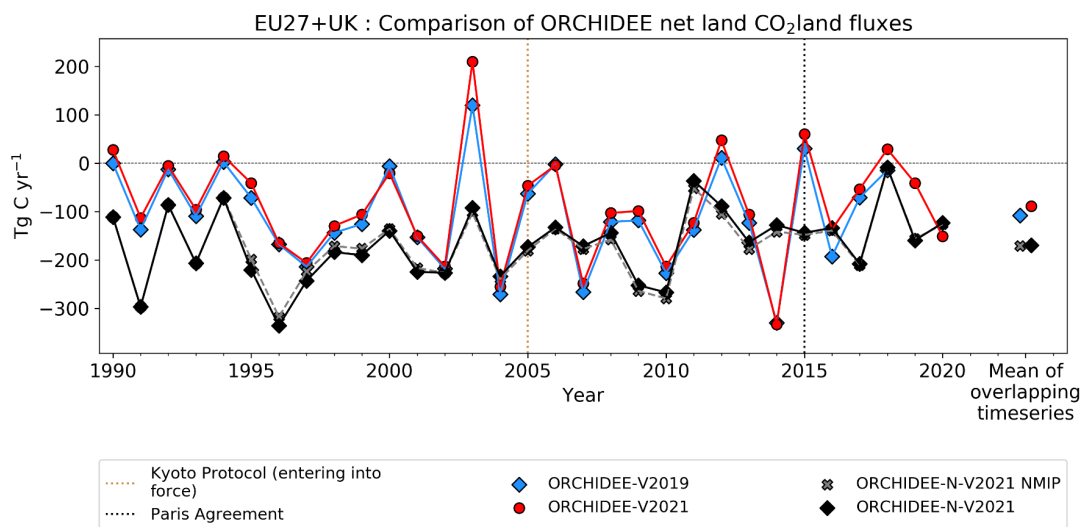
1539 ORCHIDEE is a general ecosystem model designed to be coupled to an atmospheric model in the context of  
 1540 modeling the entire Earth system. As such, ORCHIDEE calculates its prognostic variables (i.e., a multitude of carbon,  
 1541 water, and energy fluxes) from the following environmental drivers: air temperature, wind speed, solar radiation, air  
 1542 humidity, precipitation and atmospheric CO<sub>2</sub> mole fraction. As the run progresses, vegetation grows on each pixel,  
 1543 divided into fifteen generic types (e.g., broadleaf temperate forests, C3 crops), which cycle carbon between the soil,  
 1544 land surface, and atmosphere, through such processes such as photosynthesis, litter fall, and decay. Limited human  
 1545 activities are included through the form of generic wood and crop harvests, which remove aboveground biomass on  
 1546 an annual basis. The version reported here, ORCHIDEE-N v3, includes a dynamic nitrogen cycle coupled to the  
 1547 vegetation carbon cycle which results in, among other things, limitations on photosynthesis in nitrogen-poor  
 1548 environments (Vuichard et al., 2019)


1549 Among other environmental indicators, ORCHIDEE simulates positive and negative CO<sub>2</sub> emissions from  
 1550 plant uptake, soil decomposition, and harvests across forests, grasslands, and croplands. Activity data is based on land  
 1551 use and land cover maps. For VERIFY, pixel land cover/land use fractions were based on a combination of the land  
 1552 use map LUH2v2h and the land cover project of the Climate Change Initiative (CCI) program of the European Space

1553 Agency (ESA). The latter is based on purely remotely sensed methods, while the former makes use of national harvest  
 1554 data from the U.N. Food and Agricultural Organization.

1555 **LUH2v2-ESACCI:** quoted directly from Lurton et al. (2020): “We describe here the input data and algorithms used  
 1556 to create the land cover maps specific for our CMIP6 simulations using the historical/future reconstruction of land use  
 1557 states provided as reference datasets for CMIP6 within the land use harmonization database LUH2v2h (Hurtt et al.,  
 1558 2020). More details are provided on the devoted web page <https://orchidas.lsce.ipsl.fr/dev/lccci> which shows further  
 1559 tabular, graphical and statistical data. The overall approach relies on the combination of the LUH2v2 data with present-  
 1560 day land cover distribution derived from satellite observations for the past decades. The main task consists in allocating  
 1561 the land-use types from LUH2v2 in the different PFTs for the historical period and the future scenarios. The terrestrial  
 1562 biospheric vegetation in each grid cell is defined as the PFT distribution derived from the ESA-CCI land cover product  
 1563 for the year 2010 to which pasture fraction and crop fraction from LUH2v2 (for the year 2010) have been subtracted  
 1564 from grass and crop PFTs. This characterization of the terrestrial biospheric vegetation in terms of PFT distribution is  
 1565 assumed invariant in time and is used for both the historical period and the different future scenarios”.

1566



1567  VERIFY Project

1568 *Figure A3: A comparison of the version of ORCHIDEE used in previous synthesis of Petrescu et al. (2021b)*  
 1569 *compared to the same version using the forcing prepared for this work (ORCHIDEE-V2021) and the version with*  
 1570 *the coupled C-N cycle from this work (ORCHIDEE-N-V2021). For the current work, both the version shown with*  
 1571 *the Europe-specific nitrogen forcing prepared under VERIFY for the years 1995-2018 (ORCHIDEE-N-V2021) and*  
 1572 *that using the standard nitrogen forcing from the N<sub>2</sub>O Model Intercomparison Project (NMIP; Tian et al., 2018) as*  
 1573 *supplied to the TRENDY model intercomparison is shown (ORCHIDEE-N-V2021 NMIP).*

1574

1575 **Uncertainty:** In the ORCHIDEE model, uncertainty arises from three primary sources: parameters, forcing data  
 1576 (including spatial and temporal resolution), and model structure. Some researchers argue that the initial state of the  
 1577 model (i.e., the values of the various carbon and water pools at the beginning of the production run, following model  
 1578 spinup) represents a fourth area. However, the initial state of this version of ORCHIDEE is defined by its equilibrium

1579 state, and therefore a strong function of the parameters, forcing data, and model structure, with the only independent  
1580 choice being the target year of the initial state. Out of the three primary areas of uncertainty, the climate forcing data  
1581 is dictated by the VERIFY project itself, thus removing that source from explaining observed differences among the  
1582 models, although it can still contribute to uncertainty between the ORCHIDEE results and the national inventories.  
1583 The land use/land cover maps, another major source of uncertainty for ORCHIDEE carbon fluxes, have also been  
1584 harmonized to a large extent between the bottom-up carbon budget models in the project. Parameter uncertainty and  
1585 model structure thus represent the two largest sources of potential disagreement between ORCHIDEE and the other  
1586 bottom-up carbon budget models. Computational cost prevents a full characterization of uncertainty due to parameter  
1587 selection in ORCHIDEE (and dynamic global vegetation models in general), and uncertainties in model structure  
1588 require the use of multiple models of the same type but including different physical processes. Such a comparison has  
1589 not been done in the context of VERIFY, although the results from the TRENDY suite of models shown in Fig. 5 give  
1590 a good indication of this. Figure A3 shows a small influence from the nitrogen forcing, likely because the European  
1591 nitrogen forcing is only available from 1995-2018 and ORCHIDEE carries out almost 500 years of simulation prior  
1592 to this point. Many major carbon pools (i.e., woody biomass, soil carbon) have built up a large amount of inertia over  
1593 that time and are unlikely to undergo dramatic changes for any realistic forcing over the past. A similar conclusion  
1594 can be reached from simulations ORCHIDEE-V2019 and ORCHIDEE-V2021 in Fig. A3, which only differ in  
1595 meteorological forcing from 1981-2020.

1596

#### 1597 *CABLE-POP*

1598

1599 CABLE-POP (Haverd et al., 2018) is a global terrestrial biosphere model developed around a  
1600 core biogeophysics module (Wang & Leuning, 1998) and a biogeochemistry module including cycles of nitrogen and  
1601 phosphorus (Wang et al., 2010). Only nitrogen cycling was turned on for the present simulations. The model also  
1602 includes modules simulating woody demography (Haverd et al., 2013) as well as land use change and land  
1603 management (Haverd et al., 2018). The model distinguishes seven plant functional types which can co-occur in a given  
1604 grid cell. CABLE-POP does not simulate (natural) dynamic vegetation and the distribution and cover fraction of PFTs  
1605 is only affected by land use change. Forest demography (establishment, age class distribution, mortality) is accounted  
1606 for in the simulations, as are natural disturbances and forest management (wood harvest).

1607 For the simulations described here, a baseline land cover map was created from the HILDA+ dataset for the year 1901  
1608 and vegetation classes in the dataset were reclassified to correspond to PFTs represented in CABLE-POP. Land use  
1609 transitions as well as land management (harvest) were prescribed from the LUH2v2h dataset over the entire simulation  
1610 period. Crops and pastures are treated as C3 grasses but are subject to agricultural harvest fluxes as given by LUH2v2h.  
1611 The use of HILDA+ data for the land cover distribution and the LUH2v2h for the representation of land cover/land  
1612 use change likely introduced additional uncertainties resulting from a potential mismatch between the two data sets.

1613

1614 *CBM*

1615

1616 The Carbon Budget Model developed by the Canadian Forest Service (CBM-CFS3), can simulate the  
1617 historical and future stand- and landscape-level C dynamics under different scenarios of harvest and natural  
1618 disturbances (fires, storms), according to the standards described by the IPCC (Kurz et al., 2009). Since 2009, the  
1619 CBM has been tested and validated by the Joint Research Centre of the European Commission (JRC), and adapted to  
1620 the European forests. It is currently applied to 26 EU Member States, both at country and NUTS2 level (Pilli et al.,  
1621 2016).

1622 Based on the model framework, each stand is described by area, age and land use classes and up to 10  
1623 classifiers based on administrative and ecological information and on silvicultural parameters (such as forest  
1624 composition and management strategy). A set of yield tables define the merchantable volume production for each  
1625 species while species-specific allometric equations convert merchantable volume production into aboveground  
1626 biomass at stand-level. At the end of each year the model provides data on the net primary production (NPP), carbon  
1627 stocks and fluxes, as the annual C transfers between pools and to the forest product sector.

1628 The model can support policy anticipation, formulation and evaluation under the LULUCF sector, and it is  
1629 used to estimate the current and future forest C dynamics, both as a verification tool (i.e., to compare the results with  
1630 the estimates provided by other models) and to support the EU legislation on the LULUCF sector (Grassi et al., 2018a).  
1631 In the biomass sector, the CBM can be used in combination with other models, to estimate the maximum wood  
1632 potential and the forest C dynamic under different assumptions of harvest and land use change (Jonsson et al., 2018).  
1633 **Uncertainty:** Quantifying the overall uncertainty of CBM estimates is challenging because of the complexity of each  
1634 parameter. The uncertainty in CBM arises from three primary sources: parameters, forcing data (including spatial and  
1635 temporal resolution) and model structure. It is linked to both activity data and emission factors (area, biomass volume  
1636 implied by species specific equation to convert the merchantable volume to total aboveground biomass (used as a  
1637 biomass expansion factor)) as well to the capacity of each model to represent the original values, in this case estimated  
1638 through the mean percentage difference between the predicted and observed values. A detailed description of the  
1639 uncertainty methodology is found in Pilli et al. (2017).

1640

1641 **Explanatory note on the extrapolation of Net Biome Productivity for the period 2017-2020** (Matteo Vizzarri,  
1642 Roberto Pilli, Giacomo Grassi, EC-JRC)

1643 *Background*

1644 We performed a linear extrapolation of forest Net Biome Productivity (NBP) by country (EU 25 Member States and  
1645 UK) in the period 2017-2020 based on the correlation between NBP and harvest from the period 2000-2015. Cyprus  
1646 and Malta are excluded from the analysis because of missing historical data.

1647 *Input data*

1648 Table A5 reports a summary of input data sources.

1649 *Table A5: main input data used in the extrapolation of NBP for the period 2017-2020.*

	Unit	Temporal resolution	Source
<b>Wood removals (HWP pool)</b>	t C	Annual (2000-2015)	CBM calibration run
<b>Forest area</b>	ha	Annual (2000-2020)	FAOSTAT <sup>25</sup>
<b>Roundwood amount</b>	m <sup>3</sup>	Annual (2000-2020)	FAOSTAT <sup>26</sup>
<b>NBP</b>	t C	Annual (2000-2015)	CBM calibration run

1650

1651 *Assessment procedure*

1652 The extrapolation of the NBP for the period 2017-2020 was obtained throughout the following steps:

- 1653 1. For each country (EU 25 Member States + UK), we first calculated the **average conversion factor** –  
 1654 representing a correspondence between one ton of biomass carbon removed and one cubic meter of wood per  
 1655 hectare – for the period 2000-2015 through equation [1]:

1656 
$$CF_{2000-2015} = \sum_{t=2000}^{2015} \frac{HWP_t}{\frac{RW_t}{A_{2015}}} \quad \text{eq. (1)}$$

1657 where:  $CF_{2000-2015}$  is the average conversion factor per hectare in the period 2000-2015 (t C m<sup>-3</sup> ha<sup>-1</sup>);  $HWP_t$   
 1658 is the carbon content per ha in harvested wood products in year  $t$  (t C year<sup>-1</sup>), as derived from the CBM model run;  
 1659  $RW$  is the total roundwood removals in year  $t$  (m<sup>3</sup> year<sup>-1</sup>) (source: FAOSTAT<sup>27</sup>);  $A_{2015}$  is the managed forest area in  
 1660 year 2015 (ha; source: Forest Europe 2015).

- 1661 2. Using the average conversion factor estimated in eq. 1, we converted, for each country, the total roundwood  
 1662 removals per ha derived from FAOSTAT for the period 2017-2020, to the corresponding amount of carbon  
 1663 removals per ha, through equation [2]:

1664 
$$HWP_{conv} = CF_{2000-2015} \cdot \left( \frac{RW_t}{A_{2015}} \right) [\forall t = 2017 \div 2020] \quad \text{eq. (2)}$$

1666 where:  $HWP_{conv}$  is the amount of carbon removals per hectare in year  $t$  (t C ha<sup>-1</sup> year<sup>-1</sup>);  $CF_{2000-2015}$  is the  
 1667 average conversion factor per hectare in the period 2000-2015 (t C m<sup>-3</sup> ha<sup>-1</sup>);  $RW_t$  is the total roundwood in year  $t$   
 1668 (m<sup>3</sup> year<sup>-1</sup>) (source: FAOSTAT<sup>28</sup>);  $A_{2015}$  is the managed forest area in the year 2015 (ha).

- 1669 3. Then, for each country and the period 2000-2015, we performed a **linear regression** to search for significant  
 1670 correlation between the harvest amount (i.e., HWP in t C ha<sup>-1</sup> yr<sup>-1</sup>) and NBP, according to the generalized  
 1671 equation:

1672 
$$NBP = a + b \cdot (HWP) \quad \text{eq. (3)}$$

<sup>25</sup> <https://www.fao.org/faostat/en/#data/RL>

<sup>26</sup> <https://www.fao.org/faostat/en/#data/FO>

<sup>27</sup> <https://www.fao.org/faostat/en/#data/FO>

<sup>28</sup> <https://www.fao.org/faostat/en/#data/FO>

1673 In this case, we assumed NBP as the dependent variable ( $t \text{ C ha}^{-1} \text{ year}^{-1}$ ), the amount of harvest ( $t \text{ C ha}^{-1} \text{ year}^{-1}$ ) as the main driver affecting the short term evolution of NBP, in absence of other exogenous natural  
 1674 disturbances;  $a$  is the intercept of the linear trendline;  $b$  is the coefficient of the independent variable harvest  
 1675 amount (i.e. HWP) ( $\text{m}^3 \text{ ha}^{-1} \text{ year}^{-1}$ ). This approach is consistent with the methodological assumptions reported  
 1676 in Jonsson et al. (2021).  
 1677

- 1678 4. We finally calculated the **NBP in the period 2017-2020** for each country through equation [4]:

1679 
$$NBP_{t,m} = (a + b \cdot HWP_{conv})_{t,m} \quad \text{eq. (4)}$$

1680 where:  $NBP_{t,m}$  is the Net Biome Productivity for year  $t$ , country  $m$  ( $t \text{ C ha}^{-1} \text{ year}^{-1}$ );  $a_{t,m}$  is the intercept  
 1681 of the linear trendline for year  $t$ , country  $m$ ;  $b_{t,m}$  is the coefficient of the independent variable in the trendline;  
 1682  $HWP_{conv(t,m)}$  is the amount of carbon removal per ha for year  $t$ , country  $m$  ( $t \text{ C ha}^{-1} \text{ year}^{-1}$ ).

1683 Forest area and parameters used in equation [4] by country are reported in Table A6.

1684 *Table A6: country-based forest area in 2015 and parameters used in equation [4]. \*: significant ( $p < 0.05$ ); NS: not*  
 1685 *significant ( $p > 0.05$ ).*

EU 25 + UK	CF (2000-2015)	Intercept (a)	Coefficient (b)	$p < 0.05$
<b>Austria</b>	0.28	2.60	-1.57	*
<b>Belgium</b>	0.18	2.97	-1.54	*
<b>Bulgaria</b>	0.22	1.17	-2.13	*
<b>Croatia</b>	0.28	1.42	-1.27	*
<b>Czechia</b>	0.22	2.55	-1.21	*
<b>Denmark</b>	0.16	1.92	-1.21	*
<b>Estonia</b>	0.20	1.16	-1.08	*
<b>Finland</b>	0.23	1.15	-1.20	*

<b>EU 25 + UK</b>	<b>CF (2000-2015)</b>	<b>Intercept (a)</b>	<b>Coefficient (b)</b>	<b><i>p</i>&lt;0.05</b>
<b>France</b>	0.19	1.63	-1.17	*
<b>Germany</b>	0.21	2.55	-1.23	*
<b>Greece</b>	0.20	1.17	-1.75	ns
<b>Hungary</b>	0.27	1.50	-1.54	*
<b>Ireland</b>	0.18	6.12	-5.45	*
<b>Italy</b>	0.23	0.69	0.39	ns
<b>Latvia</b>	0.19	2.00	-1.77	*
<b>Lithuania</b>	0.22	1.11	-0.89	*
<b>Luxembourg</b>	0.20	1.79	-1.40	*
<b>Netherlands</b>	0.22	2.44	-2.01	*
<b>Poland</b>	0.21	2.49	-2.16	*
<b>Portugal</b>	0.29	1.39	-1.01	*
<b>Romania</b>	0.32	1.54	-1.65	*
<b>Slovakia</b>	0.28	2.57	-1.42	*
<b>Slovenia</b>	0.24	2.07	-1.55	*
<b>Spain</b>	0.28	0.26	0.18	ns
<b>Sweden</b>	0.23	1.02	-1.20	*



<b>EU 25 + UK</b>	<b>CF (2000-2015)</b>	<b>Intercept (a)</b>	<b>Coefficient (b)</b>	<b><i>p</i>&lt;0.05</b>
<b>United Kingdom</b>	0.19	2.27	-1.34	*

1686

1687 *Additional notes*

1688 Because of biased estimates, values for the year 2016 were excluded from this analysis.

1689 Extrapolated NBP for Czech Republic, Ireland and Netherlands were negative (thus showing emissions) because of  
 1690 an increase of harvest in the corresponding years (2017-2020) compared to the previous period 2000-2015. Estonia  
 1691 shows negative extrapolated NBP only for the year 2018.

1692 *EFISCEN-Space*

1693

1694 The European Forest Information SCENario Model (EFISCEN) is a large-scale forest model that projects  
 1695 forest resource development on a regional to European scale. The model uses aggregated national forest inventory  
 1696 data as a main source of input to describe the current structure and composition of European forest resources. The  
 1697 model projects the development of forest resources, based on scenarios for policy, management strategies and climate  
 1698 change impacts. With the help of biomass expansion factors, stem wood volume is converted into whole-tree biomass  
 1699 and subsequently to whole tree carbon stocks. Information on litter fall rates, felling residues and natural mortality is  
 1700 used as input into the soil module YASSO (Liski et al., 2005), which is dynamically linked to EFISCEN and delivers  
 1701 information on forest soil carbon stocks. The core of the EFISCEN model was developed by Prof. Ola Sallnäs at the  
 1702 Swedish Agricultural University (Sallnäs, 1990). It has been applied to European countries in many studies since then,  
 1703 dealing with a diversity of forest resource and policy aspects. A detailed model description is given by Verkerk et al.  
 1704 (2016), with online information on availability and documentation of EFISCEN at <http://efiscen.efi.int>. The model  
 1705 and its source code are freely available, distributed under the GNU General Public License conditions  
 1706 ([www.gnu.org/licenses/gpl-3.0.html](http://www.gnu.org/licenses/gpl-3.0.html)).

1707 In this report the follow-up of the EFISCEN model was used, called EFISCEN-Space. EFISCEN-Space  
 1708 simulates the development of the forest at the level of the plots as measured in the national forest inventories, thereby  
 1709 providing a much higher spatial detail. The simulation is based on the distribution of trees over diameter classes rather  
 1710 than age as in the old EFISCEN model. This allows the simulation of a wider variety of stand structures, species  
 1711 mixtures and management options. Similar to the EFISCEN model, biomass expansion factors and the YASSO soil  
 1712 carbon model are used to provide carbon balances for the forest. For use within VERIFY, individual plot results are  
 1713 aggregated to a 0.125 degree grid. For the moment only 15 European member states are included, partly due to the  
 1714 lack of an appropriate national forest inventory in the other member states, or because the data could not be shared.  
 1715 No formal sensitivity and uncertainty analysis has been conducted yet.

1716 Figure 3 shows results which vary from year-to-year. In practice, the model was initialized with starting  
1717 years depending on the country, assuming that all data applied to this year. The model then produced stock and flux  
1718 changes for the subsequent five-year period, reporting a single mean value per pixel. To compute timeseries for the  
1719 EU27+UK, it was further assumed that these values were valid across 2005-2020. As the fluxes were given per square  
1720 meter of forest, they were scaled by the total area of the forest in each pixel found on the land use/land cover maps  
1721 used by the ORCHIDEE DGVM. This explains why the numbers vary from year to year; the flux per square meter of  
1722 forest does not change, but the total amount of forest area changes slightly. It should be noted that country-level values  
1723 available on the VERIFY website are only available for the five-year period for which the model produces a mean  
1724 result.

1725  
1726 **Uncertainties:** A sensitivity analysis of EFISCEN v3 is described in detail in Chapter 6 of the user manual (Schelhaas  
1727 et al., 2007). Total sensitivity is caused by especially young forest growth, width of volume classes, age of felling and  
1728 few other variables. Scenario uncertainty comes on top of this when projecting in future. Within VERIFY, a full  
1729 uncertainty analysis has been completed, enabling the estimation of uncertainty ranges of the various output variables  
1730 (Schelhaas et al., 2020).

1731  
1732 *EPIC-IIASA*  
1733

1734 The Environmental Policy Integrated Climate (EPIC) model is a field-scale process-based model (Izaurrealde  
1735 et al., 2006; Williams, 1990) which calculates, with a daily time step, crop growth and yield, hydrological, nutrient  
1736 and carbon cycling, soil temperature and moisture, soil erosion, tillage, and plant environment control. Potential crop  
1737 biomass is calculated from photosynthetically active radiation using the radiation-use-efficiency concept modified for  
1738 vapor pressure deficit and atmospheric CO<sub>2</sub> mole fraction effect. Potential biomass is adjusted to actual biomass  
1739 through daily stress caused by extreme temperatures, water and nutrient deficiency, or inadequate aeration. The  
1740 coupled organic C and N module in EPIC (Izaurrealde et al., 2006) distributes organic C and N between three pools of  
1741 soil organic matter (active, slow and passive) and two litter compartments (metabolic and structural). EPIC calculates  
1742 potential transformations of the five compartments as regulated by soil moisture, temperature, oxygen, tillage and  
1743 lignin content. Daily potential transformations are adjusted to actual transformations when the combined N demand  
1744 in all receiving compartments exceeds the N supply from the soil. The transformed components are partitioned into  
1745 CO<sub>2</sub> (heterotrophic respiration), dissolved C in leaching (DOC) and the receiving SOC pools. EPIC also calculates  
1746 SOC loss with erosion.

1747 The EPIC-IIASA (version EU) modeling platform was built by coupling the field-scale EPIC version 0810  
1748 with large-scale data on land cover (cropland and grasslands), soils, topography, field size, crop management practices  
1749 and grassland cutting intensity aggregated at a 1x1 km grid covering European countries (Balkovič et al., 2018, 2013).  
1750 In VERIFY, a total of 10 major European crops including winter wheat, winter rye, spring barley, grain maize, winter  
1751 rapeseed, sunflower, sugar beet, potatoes, soybean and rice were used to represent agricultural production systems in  
1752 European cropland. Crop fertilization and irrigation were estimated for NUTS2 statistical regions between 1995 and

1753 2010 (Balkovič et al., 2013). For VERIFY, the simulations were carried out assuming conventional tillage, consisting  
1754 of two cultivation operations and moldboard plowing prior to sowing and an offset disking after harvesting of cereals.  
1755 Two row cultivations during the growing season were simulated for maize and one ridging operation for potatoes. It  
1756 was assumed that 20 % of crop residues are removed in the case of cereals (excluding maize), while no residues are  
1757 harvested for other crops.

1758 A total of five managed grassland types with distinct temperature requirements, biomass productivity, and  
1759 phenology were used to represent the C-cycle in European grasslands. High-productive generic winter pasture and tall  
1760 fescue-based grasslands were used for Atlantic Europe, low fescue grasslands for the cool climates of Nordic regions  
1761 and high mountains, high-productive tall fescue-based grasslands and low-productive bluegrass types for continental  
1762 Europe, and low-productive brome grass and high-productive winter pastures in the Mediterranean regions. Annual  
1763 nitrogen and carbon inputs, including inorganic and manure fertilization, and atmospheric N deposition, were obtained  
1764 from ISIMIP3 (Jägermeyr et al., 2021). In this dataset, the annual manure production and the fraction of manure from  
1765 livestock applied to cropland and rangeland were used from Zhang et al. (2017). The original manure data were re-  
1766 gridded to half-degree spatial resolution in ISMIP3. In the model, manure is applied as an organic fertilizer with a  
1767 C:N ration of 14.5:1. The organic carbon and nitrogen are added to the fresh organic litter pool where they decompose  
1768 in a manner identical to the fresh litter from vegetation, while mineral N from manure is added to the soil nitrate and  
1769 ammonium pools. The distribution of herbage biomass export intensity was constructed based on (Chang et al., 2016).

1770 **Uncertainty:** In EPIC, uncertainties arise from three primary sources which were described in detail by ORCHIDEE.  
1771 A detailed sensitivity and uncertainty analysis of EPIC-IIASA regional carbon modeling is presented in (Balkovič et  
1772 al., 2020).

1773

#### 1774 *ECOSSE (grasslands)*

1775

1776 ECOSSE is a biogeochemical model that is based on the carbon model ROTH-C (Jenkinson and Rayner,  
1777 1977; Jenkinson et al. 1987; Coleman and Jenkinson, 1996) and the nitrogen-model SUNDIAL (Bradbury et al., 1993;  
1778 Smith et al., 1996). All major processes of the carbon and nitrogen dynamics are considered (Smith et al., 2010a,b).  
1779 Additionally, in ECOSSE processes of minor relevance for mineral arable soils are implemented as well (e.g., methane  
1780 emissions) to have a better representation of processes that are relevant for other soils (e.g., organic soils). ECOSSE  
1781 can run in different modes and for different time steps. The two main modes are site specific and limited data. In the  
1782 later version, basic assumptions/estimates for parameters can be provided by the model. This increases the uncertainty  
1783 but makes ECOSSE a universal tool that can be applied for large scale simulations even if the data availability is  
1784 limited. To increase the accuracy in the site-specific version of the model, detailed information about soil properties,  
1785 plant input, nutrient application and management can be added as available.

1786 During the decomposition process, material is exchanged between the SOM pools according to first order  
1787 rate equations, characterized by a specific rate constant for each pool, and modified according to rate modifiers  
1788 dependent on the temperature, moisture, crop cover and pH of the soil. The model includes five pools with one of  
1789 them being inert. The N content of the soil follows the decomposition of the SOM, with a stable C:N ratio defined for

1790 each pool at a given pH, and N being either mineralized or immobilized to maintain that ratio. Nitrogen released from  
1791 decomposing SOM as ammonium (NH<sub>4</sub><sup>+</sup>) or added to the soil may be nitrified to nitrate (NO<sub>3</sub><sup>-</sup>).

1792 For spatial simulations the model is implemented in a spatial model platform. This allows to aggregate the  
1793 input parameter for the desired resolution. ECOSSE is a one-dimensional model and the model platform provides the  
1794 input data in a spatial distribution and aggregates the model outputs for further analysis. While climate data are  
1795 interpolated, soil data are represented by the dominant soil type or by the proportional representation of the different  
1796 soil types in the spatial simulation unit (this is in VERIFY a grid cell).

1797 **Uncertainty:** In ECOSSE, uncertainty arises from three primary sources: parameters, forcing data (including spatial  
1798 and temporal resolution), and model structure. These uncertainties are not yet quantified.

1799

### 1800 *Bookkeeping models*

1801

1802 We make use of data from two bookkeeping models: **BLUE** (Hansis et al., 2015) and **H&N** (Houghton &  
1803 Nassikas, 2017).

1804 The **BLUE** model provides a data-driven estimate of the net land use change fluxes. BLUE stands for  
1805 “bookkeeping of land use emissions”. Bookkeeping models (Hansis, 2015; Houghton, 1983) calculate land-use change  
1806 CO<sub>2</sub> emissions (sources and sinks) for transitions between various natural vegetation types and agricultural lands. The  
1807 bookkeeping approaches keep track of the carbon stored in vegetation, soils, and products before and after the land-  
1808 use change. In BLUE, land-use forcing is taken from the Land Use Harmonization, LUH2, for estimates within the  
1809 annual global carbon budget. The model provides data at annual time steps and 0.25 degree resolution. Temporal  
1810 evolution of carbon gain or loss, i.e., how fast carbon pools respire or regrow following a land-use change, is based  
1811 on response curves derived from literature. The response curves describe gradual respiration of vegetation and soil  
1812 carbon, including transfer to product pools of different lifetimes, as well as carbon uptake due to regrowth of  
1813 vegetation and subsequent refilling of soil carbon pools. In this report we present two versions of BLUE:  
1814 BLUEvVERIFY and BLUEvGCP. The BLUEvVERIFY version is a set of runs made for VERIFY, using the Hilda<sup>29</sup>  
1815 product (Ganzenmüller et al., 2022).

1816 The **H&N** model (Houghton et al., 1983) calculates land-use change CO<sub>2</sub> emissions and uptake fluxes for  
1817 transitions between various natural vegetation types and agricultural lands (croplands and pastures). The original  
1818 bookkeeping approach of Houghton (2003) keeps track of the carbon stored in vegetation and soils before and after  
1819 the land-use change. Carbon gain or loss is based on response curves derived from literature. The response curves  
1820 describe gradual respiration of vegetation and soil carbon, including transfer to product pools of different life-times,  
1821 as well as carbon uptake due to regrowth of vegetation and consequent re-filling of soil carbon pools. Natural  
1822 vegetation can generally be distinguished into primary and secondary land. For forests, a primary forest that is cleared  
1823 can never return back to its original carbon density. Instead, long-term degradation of primary forest is assumed and  
1824 represented by lowered standing vegetation and soil carbon stocks in the secondary forests. Apart from land use

---

<sup>29</sup><https://landchangestories.org/hildaplus/>

1825 transitions between different types of vegetation cover, forest management practices in the form of wood harvest  
1826 volumes are included. Different from dynamic global vegetation models, bookkeeping models ignore changes in  
1827 environmental conditions (climate, atmospheric CO<sub>2</sub>, nitrogen deposition and other environmental factors). Carbon  
1828 densities at a given point in time are only influenced by the land use history, but not by the preceding changes in the  
1829 environmental state. Carbon densities are taken from observations in the literature and thus reflect environmental  
1830 conditions of the last decades. In this study an updated H&N version submitted to the GCP2021 is used.

1831 **Uncertainty:** Uncertainties can be captured through simulations varying uncertain parameters, input data, or process  
1832 representation. A large contribution of uncertainty can be expected from various input datasets. Apparent uncertainties  
1833 arise from the land-use forcing data (Gasser et al., 2020; Hartung et al., 2021; Ganzenmüller et al., 2022), the  
1834 equilibrium carbon densities of soil and vegetation and allocation of material upon a land-use transition (Bastos et al.,  
1835 2021), and the response curves built to reflect carbon pool decay and regrowth after land-use transitions. Furthermore,  
1836 studies have shown that different accounting schemes (Hansis et al., 2015) and initialization settings at the start of the  
1837 simulations (Hartung et al., 2021) lead to different emission estimates even decades later.

1838

#### 1839 *FAOSTAT*

1840

1841 FAOSTAT: Statistics Division of the Food and Agricultural Organization of the United Nations provides  
1842 updates for the LULUCF CO<sub>2</sub> emissions for the period 1990-2019, available at:  
1843 <https://www.fao.org/faostat/en/#data/GT> and its sub-domains. The FAOSTAT emissions land use database is  
1844 computed following a Tier 1 approach of IPCC (2006). Geospatial data are the source of AD for the estimates of  
1845 emissions from cultivation of organic soils, biomass and peat fires. GHG emissions are provided by countries, regions  
1846 and special groups, with global coverage, relative to the period 1990-present (with annual updates). Land Use Total  
1847 contains all GHG emissions and removals produced in the different Land Use sub-domains, representing four IPCC  
1848 Land Use categories, of which three land use categories: forest land, cropland, grassland and biomass burning.  
1849 LULUCF emissions consist of CO<sub>2</sub> associated with land use and change, including management activities. CO<sub>2</sub>  
1850 emissions/removals are computed at Tier 3 using carbon stock change. To this end, FAOSTAT uses Forest area and  
1851 carbon stock data from FRA (2015), gap-filled and interpolated to generate annual time-series. As a result CO<sub>2</sub>  
1852 emissions/removals are computed for forest land and net forest conversion, representing respectively IPCC categories  
1853 “Forest land” and “Forest land converted to other land uses”. CO<sub>2</sub> emissions are provided as by country, regions and  
1854 special groups, with global coverage, relative to the period 1990-most recent available year (with annual updates),  
1855 expressed as net emissions/removals as Gg CO<sub>2</sub>, by underlying land use emission sub-domain and by aggregate (land  
1856 use total).

1857 **Uncertainty:** FAOSTAT uncertainties are not available.

1858

#### 1859 *TRENDY DGVMs*

1860

1861 The TRENDY (Trends in net land-atmosphere carbon exchange over the period 1980-2010) project  
1862 represents a consortium of dynamic global vegetation models (DGVMs) following identical simulation protocols to  
1863 investigate spatial trends in carbon fluxes across the globe over the past century. As DGVMs, the models require  
1864 climate, carbon dioxide, and land use change input data to produce results. In TRENDY, all three of these are  
1865 harmonized to make the results across the whole suite of models more comparable. In the case of VERIFY, 15 of the  
1866 16 models for TRENDY v10 (except for ISAM, which after visual inspection showed several outlier years) were used.  
1867 While describing the details of all the models used here is clearly not possible, DGVMs calculate prognostic variables  
1868 (i.e., a multitude of carbon, water, and energy fluxes) from the following environmental drivers: air temperature, wind  
1869 speed, solar radiation, air humidity, precipitation and atmospheric CO<sub>2</sub> mole fraction. As the run progresses, vegetation  
1870 grows on each pixel, divided into generic types which depend on the model (e.g., broadleaf temperate forests, C3  
1871 crops), which cycle carbon between the soil, land surface, and atmosphere, through such processes such as  
1872 photosynthesis, litter fall, and decay. Limited human activities are included depending on the model, typically  
1873 removing aboveground biomass on an annual basis.

1874 Among other environmental indicators, DGVMs simulate positive and negative CO<sub>2</sub> emissions from plant  
1875 uptake, soil decomposition, and harvests across forests, grasslands, and croplands. Activity data is based on land use  
1876 and land cover maps and generally follows Approach 1 as described by the IPCC 2006 guidelines (enabling calculation  
1877 of only net changes from year to year). For TRENDY, pixel land cover/land use fractions were based on the land use  
1878 map LUH2 (Hurtt et al., 2020) and the HYDE land-use change data set (Klein Goldewijk et al., 2017a, b). Both of  
1879 these maps rely on FAO statistics on agricultural land area and national harvest data.

1880 **Uncertainty:** In TRENDY v10 uncertainties are model specific and described by Friedlingstein et al. (2022). The  
1881 spread of the 15 TRENDY models used by this study (Fig. 5) gives an idea of the uncertainty due to model structure  
1882 in dynamic global vegetation models, as the forcing data was harmonized for all models.

1883

#### 1884 *Net emissions from lateral transport of carbon (crops, wood, and inland waters)*

1885

1886 Net carbon flux due to lateral transport includes both carbon imported into a country/pixel and respired and carbon  
1887 assimilated in a country/pixel and then transported to a different country/pixel before respiration.

1888

1889 Production and consumption of carbon do not always occur on the same grid points. This is particularly relevant for  
1890 the land surface in the case of crops, wood products, and carbon transfers through the inland water network. The  
1891 purpose of the work here is primarily to convert the flux changes of the top-down inversions into NGHGI-like stock  
1892 changes. To convert the flux changes of the inversions (where a positive number represents a flux to the atmosphere,  
1893 i.e., a source) into NGHGI-like stock changes, one needs to add the crop sink and remove the crop source. The crop  
1894 sink comes from production numbers in the FAO food balance sheets, while the source is estimated by production  
1895 plus import minus export (all from the FAO food balance sheets), and both terms make use of conversion factors for  
1896 each commodity. We take the forestry balance sheets of FAO (production, import and export per commodity), and  
1897 convert to C mass. For a given year, the fraction of this mass that is released later in the atmosphere in each country

1898 is modeled with an e-folding decrease driven by experimental data per country (Mason Earles et al., 2012). Lateral  
1899 transfers of carbon through inland waters also need to be removed from the inversion results as the terrestrial  
1900 biospheric CO<sub>2</sub> uptake leached into the inland water network represents a carbon sink, while the fraction that is  
1901 subsequently re-emitted as CO<sub>2</sub> before reaching the ocean is a carbon source. The inland water CO<sub>2</sub> outgassing  
1902 originates from carbon imported with runoff as dissolved CO<sub>2</sub> or produced in-situ from the decomposition of terrestrial  
1903 carbon inputs. Note further that a fraction of the net-uptake of atmospheric CO<sub>2</sub> over the continents does not  
1904 accumulate on land, but is instead exported through the inland water network to the oceans; this fraction is included  
1905 in the calculation. For regional carbon budgets, any river carbon export outside the boundaries of the region of interest  
1906 (in this case, EU27+UK) needs to be known to separate net uptake of atmospheric C from the actual land C sink.

1907 Carbon fluxes to the atmosphere from rivers and lakes were obtained from maps described in Zscheischler  
1908 et al. (2017). These methods are similar to those described previously in Petrescu et al. (2021b). The primary difference  
1909 is that the updated estimates include smaller lakes and reservoirs not represented in the Global Lakes and Wetland  
1910 Database through the use of a scaling law, in addition to the older results being created specifically for Europe, while  
1911 the newer results are part of a global product. The emissions from the previous work totaled 25.5 Tg C yr<sup>-1</sup> for the  
1912 EU27+UK, while those used here are 19.8 Tg C yr<sup>-1</sup> (with no variability from year-to-year). This difference is  
1913 therefore small compared to the river C export, which is included this year for the first time and averages -73.8 Tg for  
1914 the period 1990-2020.

1915 One important difference between the fluvial carbon exports reported here and those from a previous work  
1916 (Ciais et al., 2021) are that those reported here are rescaled to reasonable global flux reflecting bias in inter-  
1917 hemispheric exchange. Similar to Bastos et al. (2020), the dissolved organic carbon (DOC) and particulate organic  
1918 carbon (POC) exports were rescaled per basin to match the estimates of Resplandy et al. (2018). The global total  
1919 organic C was finally rescaled to 500 Tg C/yr, which is considered a reasonable global number based on different  
1920 reviews and synthesis efforts (Regnier et al., 2013).

1921  
1922

#### 1923 A4.2. Top-down CO<sub>2</sub> emissions estimates

1924

1925 For the regional inversions, atmospheric observations of CO<sub>2</sub> were taken from multiple sources. For  
1926 CarboScopeRegional, atmospheric observations were taken from the ICOS 2021.1 ATC (ICOS RI, 2021) and the  
1927 GlobalViewPlus 6.1 product (Schuldt et al., 2021a). For the CIF-CHIMERE inversions, atmospheric observations of  
1928 CO<sub>2</sub> for the period 2005-2020 were taken from the ICOS 2021.1 ATC (ICOS RI, 2021) and SNO\_SIFA L2 (SNO-  
1929 IFA, 2023) releases, along with data distributed through the GlobalViewPlus 6.1 product (Schuldt et al., 2021a). For  
1930 LUMIA inversions, atmospheric observations of CO<sub>2</sub> for the period 2006-2018 were taken from the dataset prepared  
1931 for the 2018 drought task force initiative (Thompson et al., 2020). For the more recent years, data were used from the  
1932 ICOS 2021.1 ATC release (ICOS RI, 2021), along with data distributed through the GlobalViewPlus 7.0 product  
1933 (Schuldt et al., 2021b), and, for four sites, data distributed through the World Data Center for Greenhouse Gases.

1934

1935 *CarboScope-Regional*

1936

1937 CarboScopeRegional (CSR) (Munassar et al., 2022): CSR is a Bayesian Framework inversion system that employs a-  
1938 priori knowledge of the surface-atmosphere carbon fluxes to regularize the solution of the ill-posed inverse problem  
1939 arising from the sparseness of observations sampled over limited geographical locations throughout the domain of  
1940 interest. Due to the heterogeneity of biogenic fluxes, the convention in CSR is to optimize Net Ecosystem Exchange  
1941 (NEE) against measurements of CO<sub>2</sub> dry model fraction at 3-hourly temporal and 0.5° horizontal resolutions, while  
1942 ocean fluxes and anthropogenic emissions are prescribed given their better knowledge available compared with NEE.  
1943 The prior flux uncertainty is assumed to have a uniform shape in space and time and its spatial correlation is fitted to  
1944 a hyperbolic decay function following the assumption of Kountouris et al. (2018a, b). Model-data mismatch  
1945 uncertainty is defined weekly in the measurement covariance matrix varying over sites from 0.5 to 4 (ppm) according  
1946 to the ability for atmospheric transport models to sample the true mole fraction at such locations (Rödenbeck, 2005).  
1947 This uncertainty implicitly encompasses the combinations of atmospheric transport, representation, and measurement  
1948 errors and is assumed to be independent at different locations. To separate the lateral influences originating from  
1949 outside of the regional domain, the two-step scheme inversion (Rödenbeck et al., 2009) is applied to run a global  
1950 inversion with the Eulerian model TM3 at coarse resolutions to provide the lateral boundary conditions to the regional  
1951 inversion. In the regional inversion runs, the Lagrangian model STILT (Lin et al., 2003), forced by IFS data from  
1952 ECMWF, is used to calculate the surface sensitivities “footprints” over the regional site network (receptors) at hourly  
1953 temporal and 0.25° spatial resolutions. Typically, the prior fluxes of CO<sub>2</sub> are obtained from bottom-up model  
1954 estimations. Thus, the diagnostic biosphere model VPRM calculates the biogenic fluxes at hourly temporal resolution  
1955 preserving the diurnal cycle. Ocean fluxes are obtained from the CarboScope ocean-based fluxes developed in-house  
1956 by Rödenbeck et al. (2014). Emissions of fossil fuel are taken from EDGAR\_v4.3 inventories updated every year  
1957 based on the British Petroleum statistics (BP), and are distributed in space and time using the COFFEE approach  
1958 (Steinbach et al., 2011) according to fuel-type and sector.

1959 The v2021 CSR inversions underwent updates in comparison with the previous v2019:

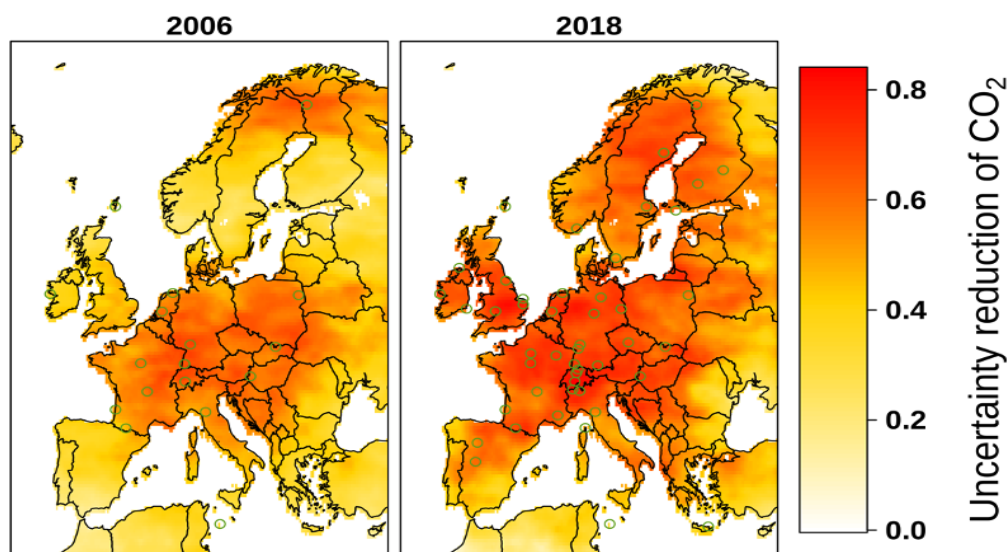
- 1960
- 1961 • v2019 from Petrescu et al. (2021b) excluded observations from two sites: La Muela (LMU) in Spain because  
1962 of inconsistent datasets between releases, and Finokalia (FKL) in Greece due to errors in the dataset. These  
1963 exclusions resulted in a larger C sink from 2013 onwards (Fig. 5, lower plot). FKL observations start at this  
1964 time and are the dominant impact over south-east Europe, as it is the only site located there. In v2021  
1965 inversions, we included corrected datasets from the FKL site.
  - 1966 • Two new flask sites were included in the v2021 inversions: Shetland Islands in the UK and Centro  
1967 Investigacion Baja in Spain. These sites are also used in the CarboScope global inversion that provides the  
1968 far-field contributions to the EU domain.

1968



1969 **Uncertainty:** Uncertainties from top-down (TD) estimates can be reported as posterior Bayesian uncertainties.  
1970 Following the methodology of Chevallier et al. (2007) the CSR inversion system computed maps of uncertainty  
1971 reductions for 2006 and 2018 (Fig. A4). The reduction is carried out through an ensemble of 40 members of inversions  
1972 using error realizations following a Monte Carlo (MC) approach. Circles on maps refer to locations of stations. In the  
1973 inversion system, a MC method is used to generate N ensembles of realizations of prior errors and model-data  
1974 mismatch errors. The inversion is repeated for each ensemble member starting from each set of prior and model-data  
1975 mismatch errors to generate posterior fluxes. The posterior uncertainty is calculated as the spread over the optimized  
1976 fluxes across the whole ensemble. The uncertainty reduction is then calculated as  $1 - (\sigma_{\text{post}} / \sigma_{\text{prior}})$ . It is clear that  
1977 larger ensembles will lead to better convergence of the error reduction. However, due to computational limitations, 40  
1978 ensemble members were selected as a good compromise.

1979



1980

1981 *Figure A4: CSR uncertainty reduction maps computed as  $1 - (\sigma_{\text{post}} / \sigma_{\text{prior}})$  for 2006 and 2018 using a Monte Carlo*  
1982 *approach focused on prior errors. The circles represent the observation stations network.*

1983 Figure A4 represents a preliminary attempt at how the inclusion of additional observation stations (additional  
1984 circles in the right-side figure for Germany, Switzerland, Finland compared to the left-side figure) might reduce the  
1985 uncertainty. However, the two different simulation years (2006 and 2018) might also differ in terms of other factors  
1986 which may lead to lower uncertainties in a given year (e.g., climatological conditions, such as the 2018 drought year).

1987 Several caveats remain. When comparing the uncertainty over pixels or subregions in the domain of interest,  
1988 the maps of uncertainty reduction should be interpreted together with the maps of posterior uncertainty to give a better  
1989 illustration of the magnitude of uncertainty. The maps of uncertainty reduction reflect only the random uncertainties.  
1990 The systematic uncertainties are still poorly characterized, including uncertainties due to atmospheric transport  
1991 modeling, dependence on the prior fluxes, and the weighting between the prior and observation uncertainties. To  
1992 improve knowledge of the systematic uncertainties, dedicated studies with controlled comparisons between inversions  
1993 using different atmospheric transport models (such as planned with the Community Inversion Framework, Berchet et

1994 al., 2021) are still needed. Furthermore, the posterior uncertainty and uncertainty reductions between inversions  
1995 depend on internal parameterizations, e.g., the weighting of prior and observation uncertainties. Future efforts should  
1996 focus on establishing best practices on how to set-up inversions and quantification of systematic uncertainties,  
1997 including as well tests of the fidelity of models against data (Simmonds et al., 2021).

1998  
1999

## 2000 *LUMIA*

2001

2002 The LUMIA inversion system (Monteil and Scholze, 2021) is a regional atmospheric inversion system, which  
2003 was designed to produce estimates of the land-atmosphere carbon exchanges based on in-situ CO<sub>2</sub> observations from  
2004 the ICOS network. It relies on the FLEXPART 10.4 Lagrangian transport model (Pisso et al., 2019) to compute the  
2005 transport of CO<sub>2</sub> fluxes within a regional domain (15°W; 33°N to 35°E, 73°N) at a 0.5°, 3-hourly resolution. Boundary  
2006 conditions are provided in the form of timeseries of far-field contributions at the observation sites, obtained from a  
2007 global TM5-4DVAR inversion (using the 2-step inversion approach of Rödenbeck et al., 2009). Both transport models  
2008 were driven by ECMWF ERA-Interim data, up to 2018, and by ECMWF ERA5 data afterwards.

2009 The inversions solve for weekly offsets to the prior NEE/NBP estimate, at a variable spatial resolution,  
2010 highest where the observational coverage is better (up to 0.5° upwind of the observation sites). The optimal solution  
2011 is searched for using a variational inversion approach (preconditioned conjugate gradient). The inversions were  
2012 constrained by in-situ and flask observations from 66 European observation sites, although only a subset of these sites  
2013 is usually available at a given time. The observation uncertainties were set to 1 ppm/week at all sites (the uncertainty  
2014 of a single observation is therefore higher, on average 5.2 ppm, and given by  $\sqrt{n}$ , with n the number of assimilated  
2015 observations at the same site in a  $\pm 3.5$  day window around the observation time). The prior NEE was produced using  
2016 the LPJ-GUESS model (Smith et al., 2014), driven by ECMWF ERA5 meteorological data.

2017 The inversion also accounts for (prescribed) anthropogenic CO<sub>2</sub> fluxes from the EDGAR/TNO product  
2018 (<https://doi.org/10.18160/Y9QV-S113>) and for atmosphere-ocean CO<sub>2</sub> exchanges from the Jena-CarboScope  
2019 oc\_v2021 product ([https://www.bgc-jena.mpg.de/CarboScope/oc/oc\\_v2021.html](https://www.bgc-jena.mpg.de/CarboScope/oc/oc_v2021.html)). The uncertainties on the prior NEE  
2020 were set proportional to the sum of the absolute value of the 3-hourly fluxes in each 7-day optimization interval (so  
2021 the uncertainty is not zero even if the net flux is zero), and scaled to a total value of 0.45 PgC/year, accounting for  
2022 covariances based on Gaussian (spatial) and exponential (temporal) correlation decay functions, with correlation  
2023 lengths of respectively 500 km and 1 month (see Monteil and Scholze, 2021, for details).

2024 The main differences from the LUMIA setup used in Thompson et al. (2014) are the specification of prior  
2025 and observation uncertainties (here made, on purpose, more comparable to those used in the CSR inversions), and the  
2026 implementation of flux optimization at a variable spatial resolution (which has negligible impact on the results but  
2027 improves the model performance).

2028

## 2029 *CIF-CHIMERE - land CO<sub>2</sub>*

2030

2031 CIF-CHIMERE is used for both CO<sub>2</sub> land and CO<sub>2</sub> fossil emission estimates, and this section only describes  
2032 the CO<sub>2</sub> land estimates.

2033 The CIF-CHIMERE inversions have been generated with the variational mode of the Community Inversion  
2034 Framework (CIF, Berchet et al., 2021) coupled to the regional Eulerian atmospheric chemistry-transport model  
2035 CHIMERE (Menut et al., 2013; Mailler et al., 2017) and to its adjoint code. They are set-up in a manner that is close  
2036 to that of the PYVAR-CHIMERE inversions of Broquet et al. (2013), of Thompson et al. (2020) and of Monteil et al.  
2037 (2020).

2038 A European configuration of CHIMERE is used; this configuration covers latitudes 31.75-73.25 °N and  
2039 longitudes 15.25 °W -34.75 °E with a 0.5 ° × 0.5 ° horizontal resolution and 17 vertical layers up to 200 hPa.  
2040 Meteorological forcing for CHIMERE is generated using the European Center for Medium Range Weather  
2041 Forecasting (ECMWF) operational forecasts. Initial, lateral and top boundary conditions for CO<sub>2</sub> mole fractions are  
2042 generated from the new CAMS global CO<sub>2</sub> inversions v20r2 (Chevallier et al., 2010).

2043 The inversion assimilates in situ CO<sub>2</sub> data from continuous measurements stations compiled in the VERIFY  
2044 Deliverable D3.12 and in the Table A1 from the VERIFY CIF Inversion Protocol (Thompson et al., 2021). More  
2045 specifically, the inversion assimilates 1-hour averages of the measured CO<sub>2</sub> mole fractions during the time window  
2046 12:00-18:00 UTC for low altitude stations (below 1000 masl) and 0:00-6:00 UTC for high altitude stations (above  
2047 1000 masl). The inversion optimizes 6-hourly mean NEE and ocean fluxes at the 0.5°×0.5° resolution of CHIMERE.  
2048 The anthropogenic CO<sub>2</sub> emissions, considered as perfect and consequently not optimized in the inversions, are based  
2049 on the spatial distribution of the EDGAR-v4.2 inventory, on national and annual budgets from the BP (British  
2050 Petroleum) Statistics and on temporal profiles at hourly resolution derived with the COFFEE approach (Steinbach et  
2051 al., 2011).

2052 The prior estimate of NEE and its uncertainty covariance matrix are specified using ORCHIDEE model  
2053 simulations of NEE and respiration, respectively, following the general approach of Broquet et al. (2011). The  
2054 temporal and spatial correlation scales for the prior uncertainty in NEE are set to ~1 month and 200 km (following the  
2055 diagnostics of Kountouris et al., 2015), with no correlation between the four 6-hour windows of the same day. The  
2056 ocean prior fluxes come from a hybrid product of the University of Bergen coastal ocean flux estimate and the  
2057 Rödenbeck global ocean estimate (Rodenbeck et al., 2014). Fluxes from biomass burning are ignored. The observation  
2058 error covariance matrix is set-up to be diagonal, ignoring the correlations between errors for different hourly averages  
2059 of the CO<sub>2</sub> measurements (which has been justified by the analysis of Broquet et al., 2011). The variances for hourly  
2060 data are based on the values from Broquet et al. (2013), which vary depending on the sites and season, and which are  
2061 derived from Radon model-data comparisons.

2062 About 12 iterations are needed to reduce the norm of the gradient of J by 95 %, using the M1QN3 limited  
2063 memory quasi-Newton minimisation algorithm (Gilbert et Lemaréchal, 1989). To cover the whole analysis period  
2064 (2005-2020), a series of 7-month (including an overlapping of 15 days between consecutive periods) inversions is  
2065 performed. Posterior estimates of NEE at 1-hourly and 0.5°×0.5° spatial resolution are generated for the full period of  
2066 analysis.

2067

2068 **Uncertainty:** Estimates of the uncertainty of regional inversions over Europe can be found by comparing against the  
2069 results of the other regional inversions in this work (the ensembles of EUROCOM, CarboScopeRegional, and  
2070 LUMIA).

2071

2072 *GCP 2021*

2073

2074 Top-down estimates of land biosphere fluxes are provided by a number of different inverse modeling systems  
2075 that use atmospheric mole fraction data as input, as well as prior information on fossil emissions, ocean fluxes, and  
2076 land biosphere fluxes. The land biosphere fluxes, and in some systems the ocean fluxes, are estimated using a statistical  
2077 optimization involving atmospheric transport models. The inversion systems differ in the transport models used,  
2078 optimization methods, spatiotemporal resolution, boundary conditions, and prior error structure (spatial and temporal  
2079 correlation scales), thus using ensembles of such systems is expected to result in more robust top-down estimates.

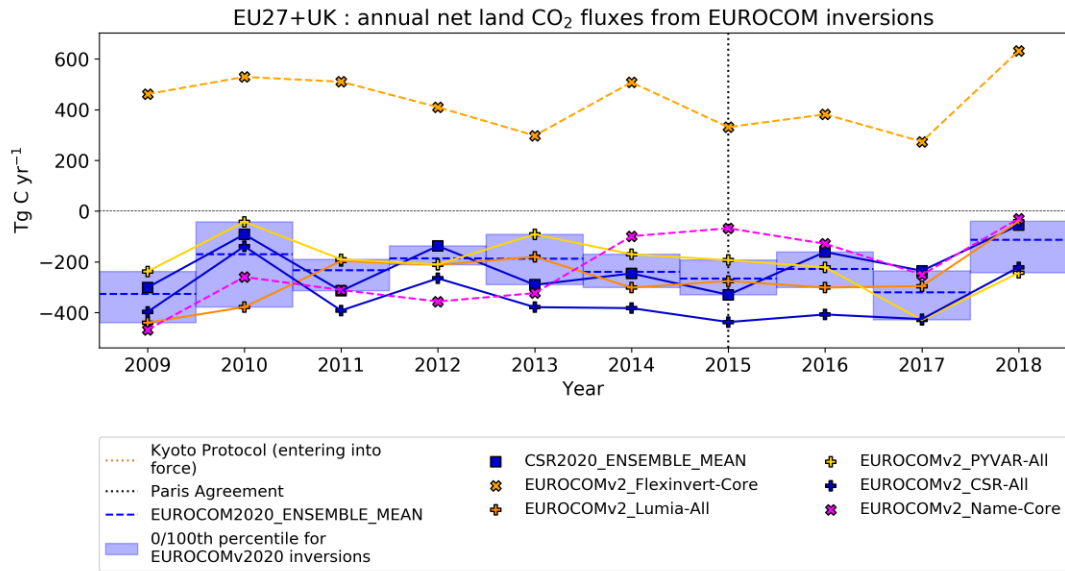
2080 For this study, the global inversion results are taken from all six of the models reported in the GCP 2021:  
2081 CTE (CarbonTracker Europe), CAMS (Copernicus Atmosphere Monitoring Service), CMS-Flux, JENA, NIES-  
2082 NIWA, and UoE, with spatial resolutions ranging from  $1^\circ \times 1^\circ$  for certain regions to  $4^\circ \times 5^\circ$ . For details see Friedlingstein  
2083 et al. (2022), in particular Table A4. Atmospheric observations for most model systems are taken from Cox et al.  
2084 (2021) and Di Sarra et al. (2021). Note that one of the ensemble members (CMS-Flux) only covers the period 2010-  
2085 2020, and therefore the ensemble results are only shown from 2010 until the last year common between all models  
2086 (2018).

2087

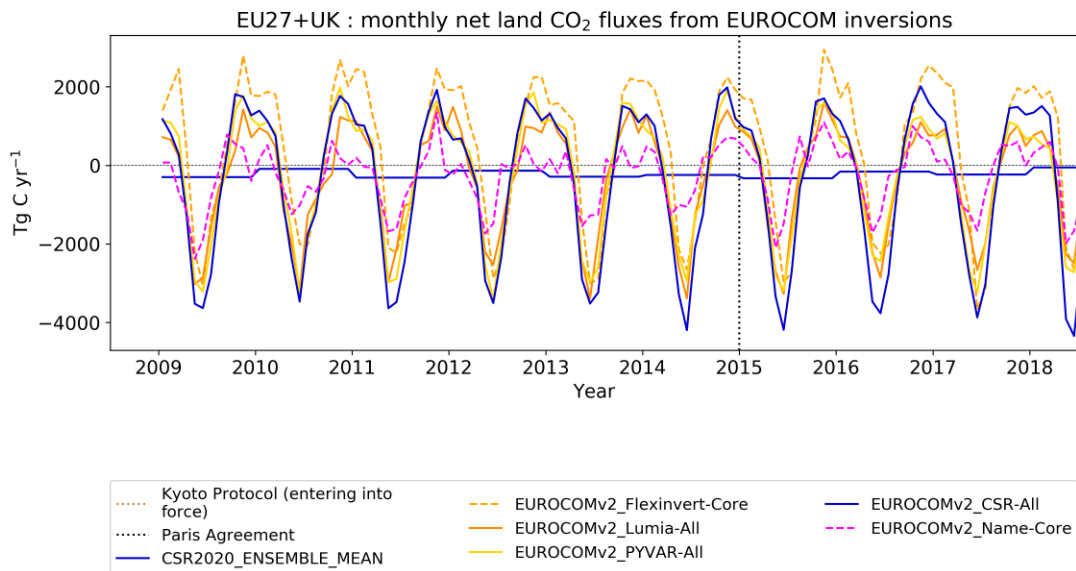
2088 *EUROCOM*

2089

2090 Top-down estimates at regional scales (up to  $0.25^\circ \times 0.25^\circ$  resolution) for the period 2009 – 2018 are taken from  
2091 three models used within EUROCOM (Monteil et al., 2020; Thompson et al., 2020): LUMIA, PYVAR, and CSR.  
2092 The NAME model was excluded as visual inspection of monthly values identified it as a clear outlier. FLEXINVERT  
2093 was excluded after visual inspection of annual values identified it as a clear outlier (Fig. A5). These inversions make  
2094 use of more than 30 atmospheric observing stations within Europe, including flask data and continuous observations.  
2095 The CarboScope-Regional (CSR) inversion system results were re-run for VERIFY using the extended period 2009-  
2096 2020 using four different settings: three network configurations using 15, 40, or 46 sites, and one using all 46 sites but  
2097 a factor two larger prior error correlation length scale (200 instead of 100 km). The CSR results reported to  
2098 EUROCOM were not used, being instead replaced by the mean of the four updated CSR runs. The observational  
2099 dataset used for the EUROCOM drought ensemble is accessible on the ICOS Carbon Portal (Drought 2018 Team and  
2100 ICOS Atmosphere Thematic Centre, 2020).



CC BY VERIFY Project



CC BY VERIFY Project

2101

2102 *Figure A5: Annual (top) and monthly (bottom) timeseries for inversions in EUROCOM (Monteil et al., 2020).*  
 2103 *Inversions with solid lines were retained for the ensemble used in this work (shown in blue in the top figure for*  
 2104 *clarity). Note that the CSR values from EUROCOM have been replaced by the mean of four CSR simulations*  
 2105 *submitted under the VERIFY project (Appendix A1). Negative fluxes represent a sink into the land surface.*

2106

2107

2108

2109

2110 **A5. Input data**

2111

2112 **CRUERA**

2113

2114 The ERA5-Land (Muñoz-Sabater, 2019; 2021) dataset at 0.1-degree resolution over the global land surface  
2115 at hourly resolution was aggregated to three-hourly resolution and extracted for a 0.125 degree grid over Europe  
2116 (35N:73N, 25W:45E) to match the grid used in previous efforts within the VERIFY project. The variables extracted  
2117 are: air temperatures, wind components, surface pressure, downwelling longwave radiation, downwelling shortwave  
2118 radiation, snowfall, and total precipitation. From these, additional variables were calculated: total windspeed, specific  
2119 humidity, relative humidity, and rainfall. Of these, the air temperature, downwelling shortwave radiation, specific  
2120 humidity, and total precipitation were re-aligned with the CRU observation dataset (Harris et al., 2020) from 1901–  
2121 2020 so that monthly means at 0.5 degree pixels correspond exactly. Variation from observations is therefore present  
2122 only on sub-monthly temporal scales and sub-0.5 degree spatial scales. At the time of the model intercomparison,  
2123 ERA5-Land was only available from 1981-2020. Consequently, the years 1901-1980 were taken from the UERRA  
2124 HARMONIE-V1 dataset from ECMWF re-aligned with CRU observations under the VERIFY project and used in  
2125 Petrescu et al. (2021b). For both datasets, results were aggregated to daily and monthly temporal resolution for use  
2126 as needed in some models.

2127

2128 **HILDA+**

2129

2130 The full Hilda+ dataset is described in detail elsewhere (Winkler et al., 2020; Winkler et al., 2021). Hilda+  
2131 is available at 1x1km spatial and annual temporal resolution across the whole globe from 1960-2019 for six land use  
2132 classes (urban, cropland, pasture/rangeland, forest, unmanaged grass/shrubland, and sparse/no vegetation). The  
2133 algorithm uses earth observation data and land use statistics to generate annual land use/cover maps and transitions.  
2134 Probability maps for land use change categories are generated by using multiple earth-observation-based data  
2135 estimates of the extent of a given land cover category on a given pixel. The VERIFY project requires additional work  
2136 to satisfy the needs of the various modeling groups. For example, the maps were extended back to 1900 to meet the  
2137 needs of the DGVM groups. As observational data is lacking for the years pre-1960, the temporal trend of the  
2138 probability maps and the FAO land use database were used for extrapolation. In addition, forest areas were further  
2139 subdivided into six forest types (Evergreen, needle leaf; Evergreen, broad leaf; Deciduous, needle leaf; Deciduous,  
2140 broad leaf; Mixed; Unknown/Other) based on the ESA CCI land cover dataset (ESA 2017). Spatiotemporal forest type  
2141 dynamics within the forest category were included for 1992-2015. Before 1992 and after 2015, the static forest type  
2142 distribution as found in the years 1992 and 2015 in the ESA CCI land cover was assumed, respectively.

2143

## 2144 NITROGEN DEPOSITION

2145

2146 Wet and dry deposition maps of ammonium and nitrate covering Europe from 1995-2018 were calculated at  
2147 0.5 degree spatial and monthly temporal resolution by the EMEP MSC-W model (“EMEP model” hereafter). The  
2148 EMEP model is a 3-D Eulerian chemistry transport model (CTM) developed at the EMEP Centre MSC-W under the  
2149 Framework of the UN Convention on Long-Range Transboundary Air Pollution (CLRTAP). The EMEP model has  
2150 traditionally been used to assess acidification, eutrophication and air quality over Europe, to underpin air quality policy  
2151 decisions (e.g., the Gothenburg Protocol), and has been under continuous development reflecting new scientific  
2152 knowledge and increasing computer power. The model was described in detail by Simpson et al. (2012) and later  
2153 updated as described in the annual EMEP status reports (Simpson et al., 2022, and references therein). For the  
2154 VERIFY project, output from the EMEP model version rv4.33 was used (Simpson et al., 2019), and averaged to annual  
2155 temporal resolution. In these simulations, the model was driven by meteorological data from the ECWMF IFS  
2156 (European Centre for Medium-Range Weather Forecasts – Integrated Forecast System) version cy40r1. Land-use data  
2157 were taken from the CORINE land-cover maps (de Smet and Hettelingh, 2001), the Stockholm Environment Institute  
2158 at York (SEIY), the Global Land Cover (GLC2000) database, and the Community Land Model (Oleson et al., 2010;  
2159 Lawrence et al., 2011). For more details see Simpson et al. (2017).

2160

## 2161 COASTAL OCEAN FLUXES

2162

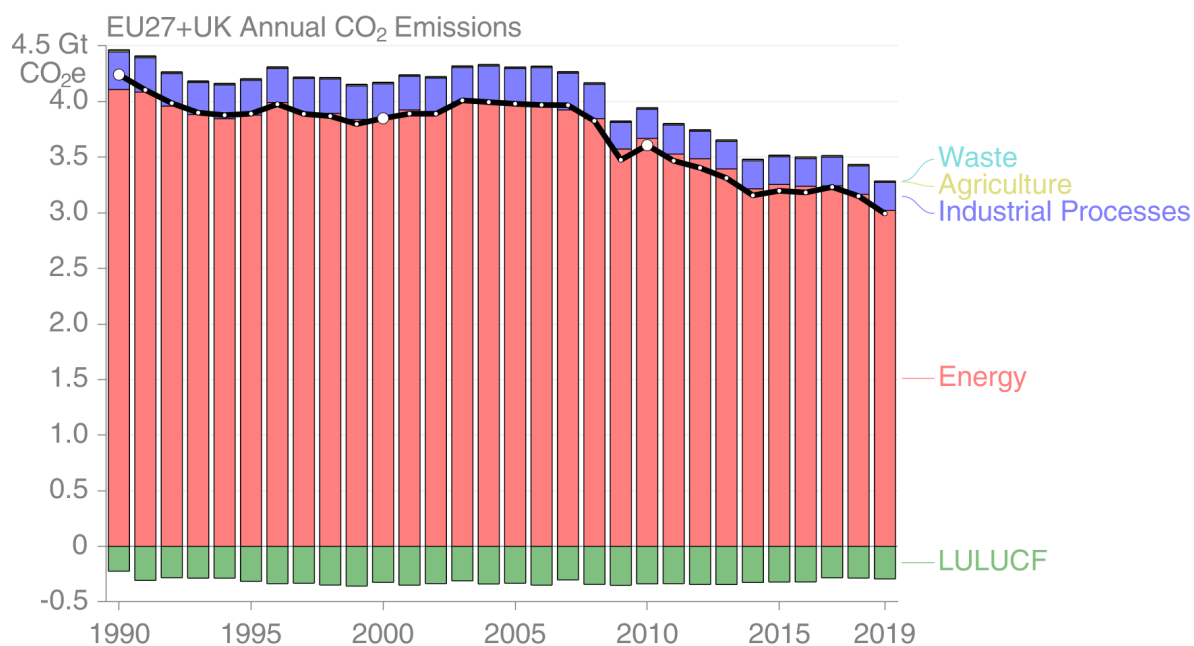
2163 Ocean CO<sub>2</sub> fluxes were prepared for use as prior estimates in the regional inversions by combining the Rödenbeck  
2164 global ocean estimate (Rödenbeck et al., 2014) with coastal ocean fluxes for Europe prepared under the VERIFY  
2165 project. The combined dataset was prepared by choosing the coastal flux map when available and otherwise the open  
2166 ocean map. The coastal ocean fluxes were generated for an area extending from the western Mediterranean to the  
2167 Barents Sea and cover shelf areas down to 500 m water depth or 100 km distance from shore. First, surface ocean  
2168 fCO<sub>2</sub> observations are taken from the annually updated SOCAT database (Bakker et al., 2016; Bakker et al., 2022)  
2169 and gridded to a monthly 0.125°x0.125° grid. pCO<sub>2</sub> maps are created based on fitting a set of driver data (including  
2170 sea surface temperature, mixed layer depth, chlorophyll concentration, and ice concentration) against the gridded fCO<sub>2</sub>  
2171 observations. Both random forest and multi-linear regressions were used. The general procedure is described  
2172 elsewhere (Becker et al., 2021), but for the version reported here, random forest regressions were used instead of  
2173 multi-linear regression and the region was extended to the south. The dataset was divided into seven subregions  
2174 (Barents Sea, Norwegian Coast, North Sea, Baltic Sea, Northern Atlantic Coast/Celtic Sea, Southern Atlantic  
2175 coast/Bay of Biscay, western Mediterranean) and each region was fitted separately (leaf size: 20, bag size: 500). The  
2176 root mean square error (RMSE) of the random forest regressions was determined to be between 34 micro-atm (Baltic  
2177 Sea) and 10 micro-atm (Barents Sea). Random forest regressions consist of many regression trees, each based on a  
2178 random subset of data. Due to this internal structure, the overall RMSE can be seen as an out-of-box error estimate.  
2179 The final fluxes are calculated from the pCO<sub>2</sub> maps with the atmospheric xCO<sub>2</sub> in the marine boundary layer and six-  
2180 hourly wind speed data using the gas transfer coefficient and the Schmidt number after Wanninkhoff (2014), the

2181 coefficient  $a_q$  of 0.2814 calculated after Naegler (2009) and 6-hourly winds from the NCEP-DOE Reanalysis 2 product  
2182 (Kanamitsu et al., 2002).  
2183  
2184

## 2185 Appendix B. Additional figures

2186

### 2187 B1. Overview figures

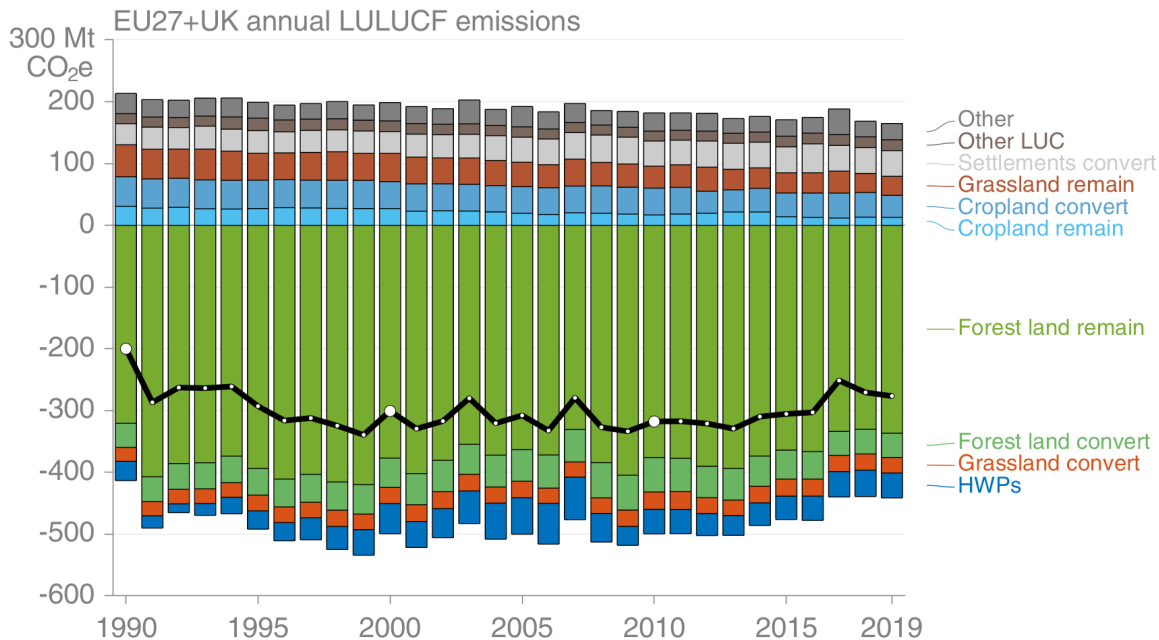


2188

2189 *Figure B1: EU27+UK total annual GHG emissions from UNFCCC NGHGI (2021) submissions split per sector.*

2190





2191

2192 *Figure B2: EU27+UK total annual GHG emissions from the LULUCF sector split in categories and sub-categories,*  
 2193 *according to UNFCCC NGHGI (2021).*

2194

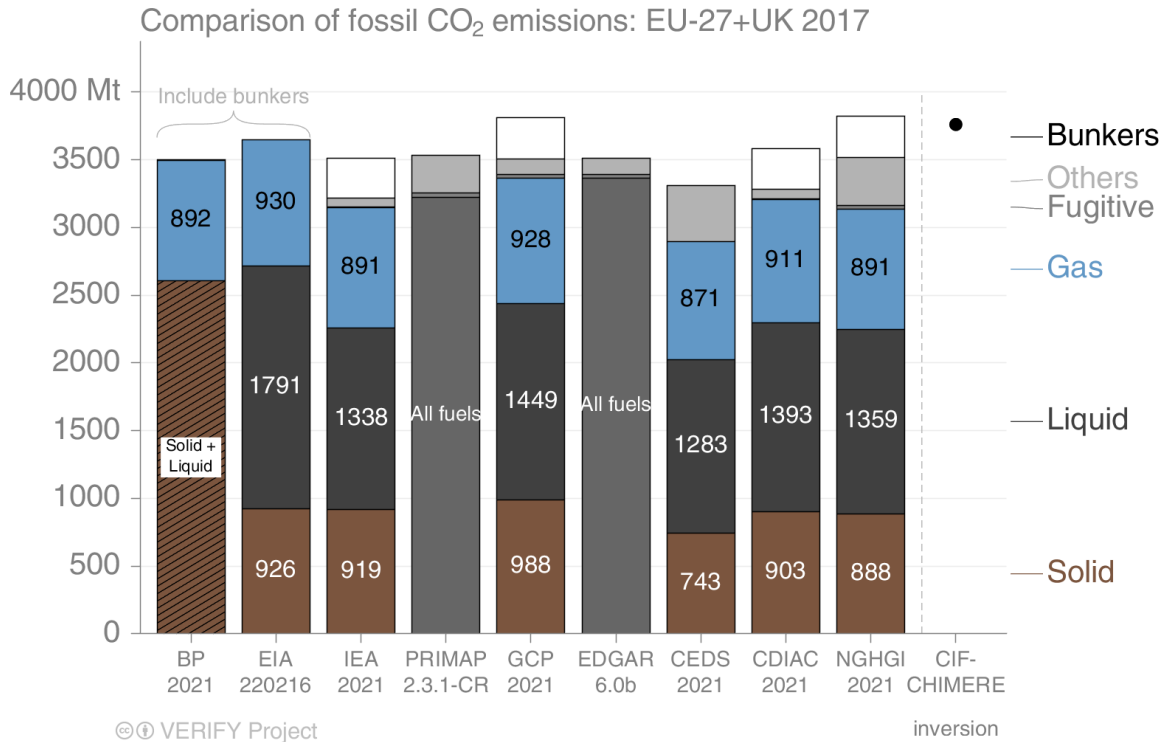
## 2195 B2. CO<sub>2</sub> fossil

2196

2197 Figure B3 shows the CO<sub>2</sub> fossil emission estimates from EU27+UK split by major source categories for each  
 2198 dataset for a single year. Sectors 1, 2, 3, and 5 are included for the UNFCCC NGHGI (2021) total, without indirect  
 2199 emissions. A breakdown of the nine other fossil BU data sources corresponding to UNFCCC NGHGI sectors or  
 2200 categories is not currently available.

2201 As in Andrew (2020), we observe good agreement for the EU27+UK between all BU data sources and the  
 2202 UNFCCC NGHGI (2021) data. The figure presents updated estimates for the year 2017, the most recent year when  
 2203 all datasets reported estimates. Sectors 1, 2, 3, and 5 are included for the UNFCCC NGHGI (2021) total, without  
 2204 indirect emissions.

2205 While most datasets agree well on total emissions, there are some differences. Both BP and the EIA include  
 2206 bunker fuels and exclude most industrial process emissions. CEDS appears to be underestimating emissions from solid  
 2207 fuels, for example lignite in Germany and oil shale in Estonia. IEA's emissions are lower because they exclude most  
 2208 industrial processes. GCP's total matches the NGHGI exactly by design but remaps some of the fossil fuels used in  
 2209 non-energy processes from "Others" to the fuel types used. CDIAC, PRIMAP, and EDGAR v6.0 all report total  
 2210 emissions very similar to the UNFCCC NGHGI (2021). Larger differences are seen in the disaggregation of fuel types,  
 2211 generally because of differing definitions.



2212

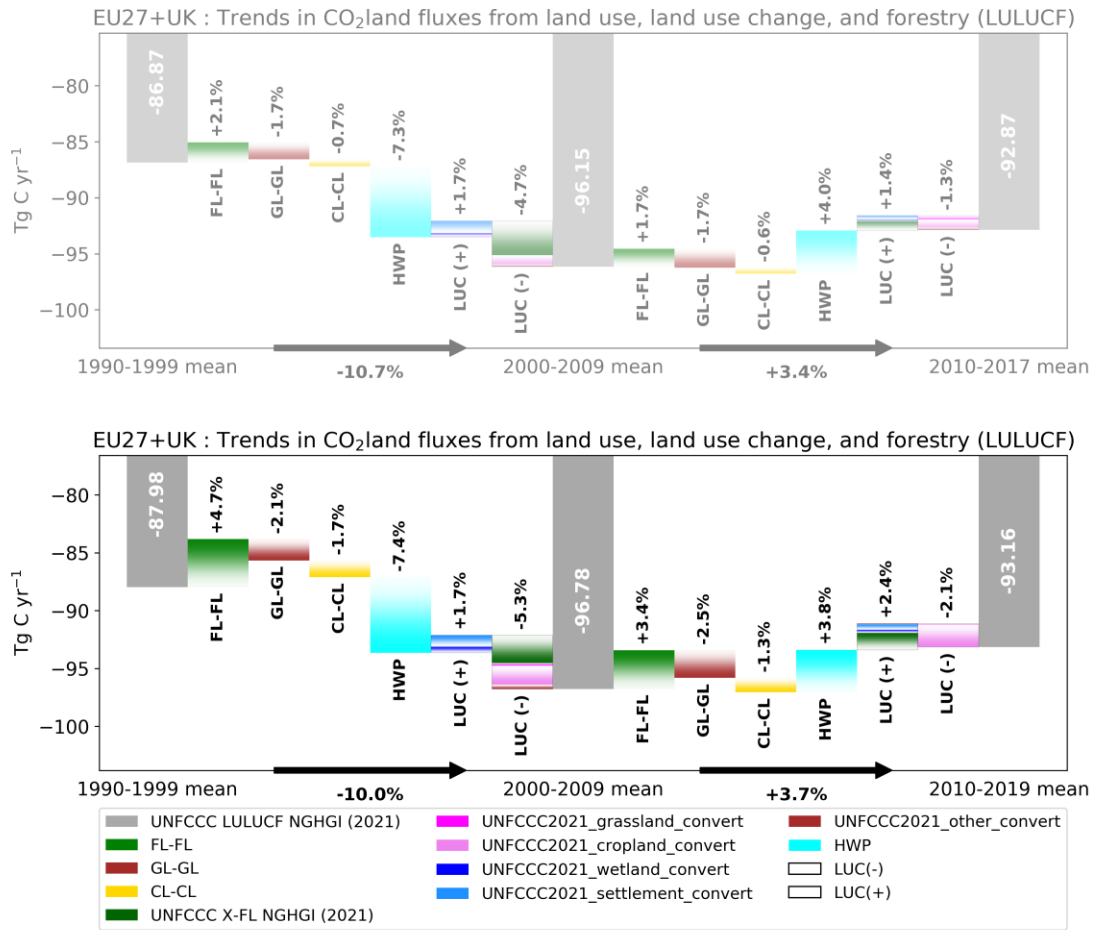
2213 *Figure B3: EU27+UK total CO<sub>2</sub> fossil emissions, as reported by nine bottom-up data sources: BP, EIA, CEDS,*  
 2214 *EDGAR v6.0, GCP, IEA, CDIAC, PRIMAPv2.3.1-CR and the UNFCCC NGHGI (2021) along with a top-down CIF-*  
 2215 *CHIMERE atmospheric inversion (black dot) (Fortems-Cheiney and Broquet, 2021). This figure presents the split*  
 2216 *per fuel type for year 2017. “Others” is other emissions in the UNFCCC’s IPPU, and international bunker fuels*  
 2217 *(the white boxes) are not usually included in total emissions at sub-global level. Neither EDGAR<sup>30</sup> (v6.0) nor*  
 2218 *PRIMAP publish a break-down by fuel type, so only the total is shown. For BP, the method description allows for*  
 2219 *emissions from natural gas to be calculated from BP’s energy data, but the data for solid and liquid fuels are*  
 2220 *insufficiently disaggregated to allow replication of BP’s emissions calculation method for those fuels.*

2221

### 2222 B3. CO<sub>2</sub> land

2223

<sup>30</sup>EDGAR v6.0 provides significant sectoral disaggregation of emissions, but not by fuel type due to license restrictions with the underlying energy data from the IEA.

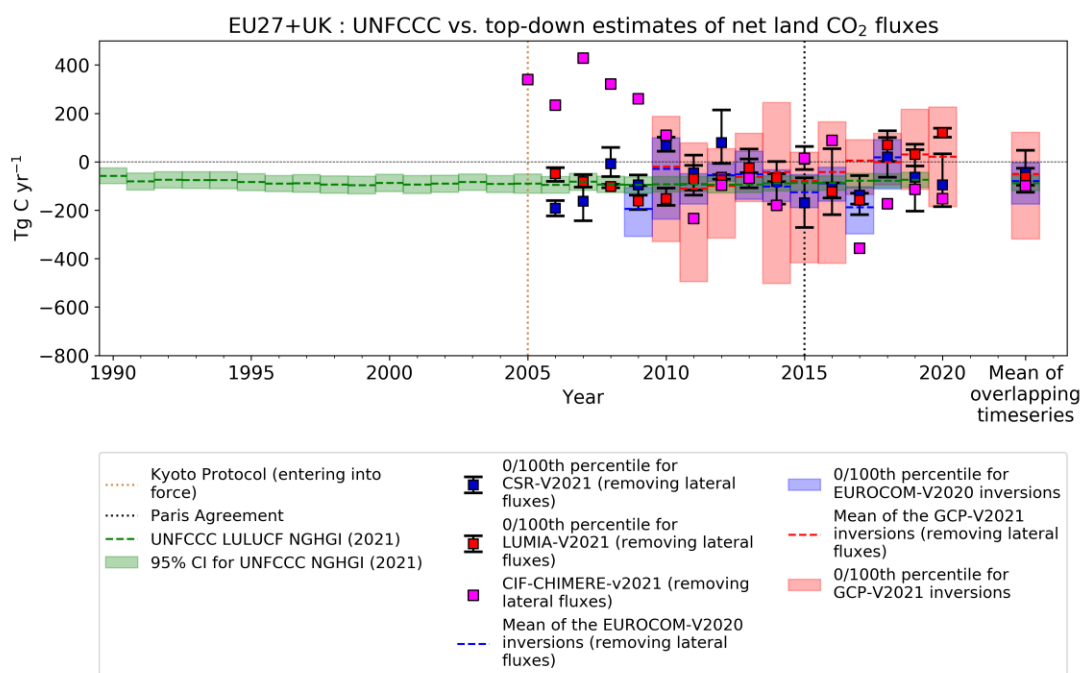
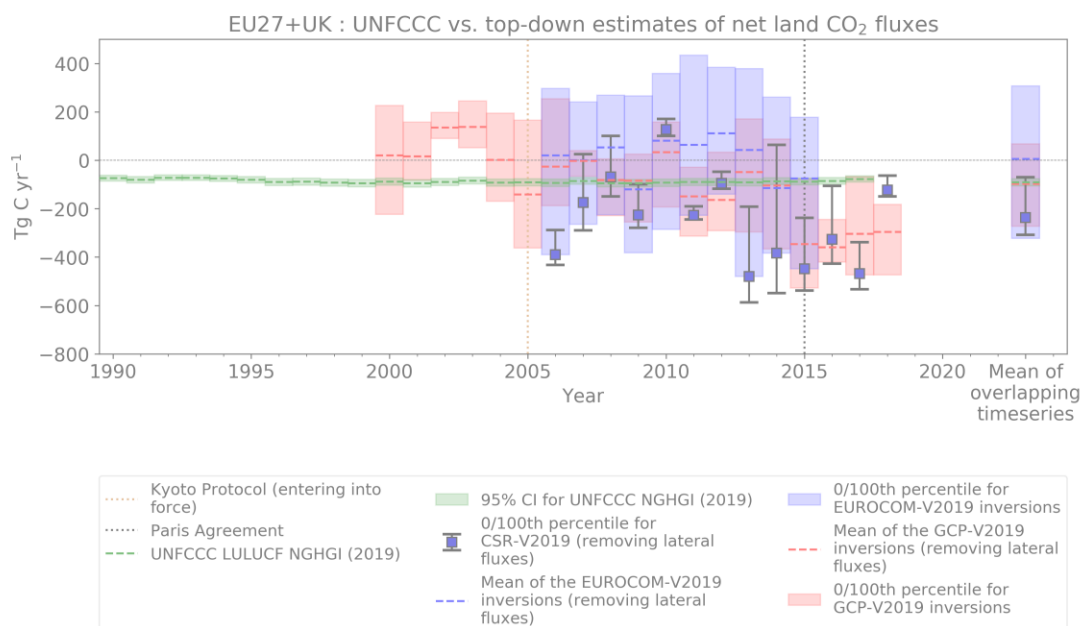


2224



2225 *Figure B4: The contribution of changes (%) in CO<sub>2</sub> land fluxes from various LULUCF categories to the overall*  
 2226 *change in decadal mean for the EU27+UK as reported by Member States to the UNFCCC. The top plot shows the*  
 2227 *previous NGHGI data from Petrescu et al. (2021b) and the bottom plot illustrates data from UNFCCC NGHGI*  
 2228 *(2021). Changes in land categories converted to other land are grouped to show net gains and net losses in the*  
 2229 *same column, with the bar color dictating which category each emission belongs to; note that the composition of the*  
 2230 *“LUC(+)” and “LUC(-)” bars can change between time periods. Not shown are emissions from “Wetlands*  
 2231 *remaining wetlands”, “Settlements remaining settlements”, and “Other land remaining other land” as none of the*  
 2232 *BU models used distinguish these categories. The fluxes follow the atmospheric convention, where negative values*  
 2233 *represent a sink while positive values represent a source. The color bars are shaded to guide the eye in the*  
 2234 *direction of the change (white-to-color).*

2235



2236



2237 *Figure B5: Comparison of inventories and atmospheric inversions for the total EU27+UK biogenic CO<sub>2</sub> fluxes from*  
 2238 *Petrescu et al. (2021b) (top plot) and updated data from current study (bottom plot). Top-down inversion results*  
 2239 *are: the global GCB2021 ensemble, the regional EUROCOM ensemble, the regional CarboScopeReg model with*  
 2240 *multiple variants, the regional LUMIA model with multiple variants, and CIF-CHIMERE. The relative error in the*  
 2241 *UNFCCC values represents the UNFCCC NGHGI (2021) Member states reported uncertainty computed with the*

2242 error propagation method (95 % confidence interval) gap-filled and provided for every year of the timeseries. The  
 2243 timeseries mean overlapping period is 2010-2018. The colored area represents the min/max of model ensemble  
 2244 estimates. The same emissions due to lateral fluxes of carbon through rivers, crop trade, and wood trade are  
 2245 removed from the top-down estimates in both the top and bottom graphs for consistency. The fluxes follow the  
 2246 atmospheric convention, where negative values represent a sink while positive values represent a source. Note that  
 2247 Petrescu et al. (2021b) presented the top plot including a suite of bottom-up models, which have been removed here  
 2248 for clarity.

2249  
 2250

## 2251 Appendix C. Source specific methodologies: AD, EFs and 2252 uncertainties

2253

2254 Table C1: Source specific activity data (AD), emission factors (EF) and uncertainty methodology for all current  
 2255 VERIFY and non-VERIFY 2021 data products.

<i>Data sources CO<sub>2</sub> emission calculation</i>	<i>AD/Tier</i>	<i>EFs/Tier</i>	<i>Uncertainty assessment method</i>	<i>Emission data availability</i>
<b>UNFCCC NGHGI (2021)</b>	Country-specific information consistent with the IPCC Guidelines	IPCC guidelines / Country specific information for higher Tiers	IPCC guidelines ( <a href="https://www.ipcc-nggip.iges.or.jp/public/2006gl/">https://www.ipcc-nggip.iges.or.jp/public/2006gl/</a> ) for calculating the uncertainty of emissions based on the uncertainty of AD and EF, two different approaches: 1. Error propagation, 2. Monte Carlo Simulation  The EU GHG inventory team provided yearly harmonized and gap-filled uncertainties.	NGHGI official data (CRFs) are found at <a href="https://unfccc.int/ghg-inventories-annex-i-parties/2021">https://unfccc.int/ghg-inventories-annex-i-parties/2021</a> (last access: June 2022).

2256

*Fossil CO<sub>2</sub>*

<p><b>BP</b> <b>CDIAC</b> <b>EIA</b> <b>IEA</b> <b>GCP</b> <b>CEDS</b> <b>PRIMAP-Hist</b></p>	<p><i>For further details, see Andrew (2020)</i></p>			
<p><b>EDGAR v6.0</b></p>	<p>International Energy Agency (IEA) for fuel combustion Food and Agricultural Organisation (FAO) for agriculture US Geological Survey (USGS) for industrial processes (e.g., cement, lime, ammonia and ferroalloys production) GGFR/NOAA for gas flaring World Steel Association for iron and steel production International Fertilisers Association (IFA) for urea consumption and production Complete description of the data sources can be found in Janssens-Maenhout et al. (2019) and in Crippa et al. (2019)</p>	<p>IPCC (2006): Tier 1 or Tier 2 depending on the sector</p>	<p>Tier 1 with error propagation by fuel type for CO<sub>2</sub> and accounting for covariances.</p>	<p><a href="https://edgar.jrc.ec.europa.eu/datas_et_ghg60">https://edgar.jrc.ec.europa.eu/datas_et_ghg60</a></p>
<p><b>CIF-CHIMERE</b></p>	<p>Tier 3 top-down 0.1° x 0.1° resolution maps of annual averages of fossil CO<sub>2</sub> anthropogenic emissions from EDGAR v4.3.2 Assimilation of satellite atmospheric mole fraction data: total column CO from IASI, and tropospheric column NO<sub>2</sub> from OMI</p>	<p>Tier 3 top-down regional inversions of CO and NO<sub>x</sub> emissions using EMEP/CEIP as prior knowledge of the emissions and CO<sub>2</sub>/CO and CO<sub>2</sub>/NO<sub>x</sub> emission ratios associated with the combustion of fossil fuel from EDGARv4.3.2.</p>	<p>Bayesian analysis in the CO and NO<sub>x</sub> inversions along with propagation of uncertainties in fCO<sub>2</sub>/CO and fCO<sub>2</sub>/NO<sub>x</sub> emission ratios</p>	<p>Detailed gridded data can be obtained by contacting the data providers: Gregoire Broquet gregoire.broquet@lsce.ipsl.fr <a href="https://verifydb.lsce.ipsl.fr/thredds/fileServer/verify/VERIFY_OUTPUT/FCO2/CO2_Tier3TD_FossilFuel_CIF-CHIMERE_LSCE_ALL_EUR-85x101_1M_V2021_20210628_FORTEMSCHEINEY_2D.nc">https://verifydb.lsce.ipsl.fr/thredds/fileServer/verify/VERIFY_OUTPUT/FCO2/CO2_Tier3TD_FossilFuel_CIF-CHIMERE_LSCE_ALL_EUR-85x101_1M_V2021_20210628_FORTEMSCHEINEY_2D.nc</a></p>

2257

**CO<sub>2</sub> land: bottom-up**

<p><b>BLUEvGCP</b></p> <p><b>BLUEvVERIFY</b></p>	<p>From LUH2: data on wood harvest, land cover types (primary, secondary, pasture, crop), and gross land use transitions (e.g. from secondary to pasture and back); Based on Pongratz et al. (2008) and Ramankutty and Foley (1999): Plant functional types (PFTs) of natural vegetation types</p> <p>Same as above with land cover from HILDA+ (Ganzenmüller et al., 2022)</p>	<p>Tier 3 (IPCC, 2006); PFT and land-cover type specific response curves describing the decay and regrowth of vegetation and soil carbon</p>	<p>N/A</p>	<p>Detailed gridded data can be obtained by contacting the data provider:          Julia Pongratz:  <a href="mailto:julia.pongratz@lmu.de">julia.pongratz@lmu.de</a>  <a href="https://verifydb.lsce.ipsl.fr/thredds/fileServer/verify/VERIFY_OUTPUT/FCO2/CO2_Tier3BUPB_LandFlux_BLU E-2021_bgc-jena LAND_GLO-720x1440_1M_V2021_20211014_Pongratz_2D.nc">https://verifydb.lsce.ipsl.fr/thredds/fileServer/verify/VERIFY_OUTPUT/FCO2/CO2_Tier3BUPB_LandFlux_BLU E-2021_bgc-jena LAND_GLO-720x1440_1M_V2021_20211014_Pongratz_2D.nc</a>  <a href="https://verifydb.lsce.ipsl.fr/thredds/fileServer/verify/VERIFY_OUTPUT/FCO2/CO2_Tier3BUPB_LandFlux_BLU E-GCB-2021_bgc-jena LAND_GLO-720x1440_1M_V2021_20211014_Pongratz_2D.nc">https://verifydb.lsce.ipsl.fr/thredds/fileServer/verify/VERIFY_OUTPUT/FCO2/CO2_Tier3BUPB_LandFlux_BLU E-GCB-2021_bgc-jena LAND_GLO-720x1440_1M_V2021_20211014_Pongratz_2D.nc</a></p>
<p><b>H&amp;N</b></p>	<p>Simple assumptions about C-stock densities (per biome or per biome/country) based on literature</p>	<p>Transient change in C-stocks following a given transition (time dependent EF after an land use transition)</p>	<p>N/A</p>	<p>Detailed gridded data can be obtained by contacting the data provider:          Richard A. Houghton  <a href="mailto:rhougton@woodwellclimate.org">rhougton@woodwellclimate.org</a></p>
<p><b>ECOSSE</b></p>	<p>Tier 3 approach. The model is a point model, which provides spatial results by using spatial distributed input data (lateral fluxes are not considered). The model is a Tier 3 approach that is applied on grid map data, polygon organized input data or study sites.</p>	<p>IPCC (2006): Tier 3</p> <p>The simulation results will be allocated due to the available information (size of spatial unit, representation of considered land use, etc.).</p>	<p>N/A</p>	<p>Detailed gridded data can be obtained by contacting the data providers:          Kuhnert, Matthias  <a href="mailto:matthias.kuhnert@abdn.ac.uk">matthias.kuhnert@abdn.ac.uk</a>          Pete Smith:  <a href="mailto:pete.smith@abdn.ac.uk">pete.smith@abdn.ac.uk</a>  <a href="https://verifydb.lsce.ipsl.fr/thredds/fileServer/verify/VERIFY_OUTPUT/FCO2/CO2_Tier3BUPB_GrassFluxes_ECOSSE-lim-S1_UAbdn_CRP_EUR-304x560_1M_V2019_20200923_KUHNERT_2D.nc">https://verifydb.lsce.ipsl.fr/thredds/fileServer/verify/VERIFY_OUTPUT/FCO2/CO2_Tier3BUPB_GrassFluxes_ECOSSE-lim-S1_UAbdn_CRP_EUR-304x560_1M_V2019_20200923_KUHNERT_2D.nc</a>  <a href="https://verifydb.lsce.ipsl.fr/thredds/fileServer/verify/VERIFY_OUTPUT/FCO2/CO2_Tier3BUPB_CropFluxes_ECOSSE-SX_ABDN_CRP_EUR-142x179_1M_V2021_20220506_KUHNERT_2D.nc">https://verifydb.lsce.ipsl.fr/thredds/fileServer/verify/VERIFY_OUTPUT/FCO2/CO2_Tier3BUPB_CropFluxes_ECOSSE-SX_ABDN_CRP_EUR-142x179_1M_V2021_20220506_KUHNERT_2D.nc</a></p>

<p><b>EPIC-IIASA Croplands</b></p>	<p>Tier 3 approach. Cropland: static 1×1 km cropland mask from CORINE-PELCOM. Initial SOC stock from the Map of organic carbon content in the topsoil (Lugato et al., 2014). “Static” crop management and input intensity by NUTS2 calibrated for 1995-2010 (Balkovič et al., 2013). Crop harvested areas by NUTS2 from EUROSTAT. Parameterization of soil carbon routine was updated based on Balkovič et al. (2020).</p>	<p>IPCC (2006): Tier 3  Land management and input factors for the cropland remaining cropland category as simulated by the EPIC-IIASA modeling platform, assuming the business-as-usual crop management calibrated for the 1995-2010 period. A 50-ha field is considered in each grid cell.</p>	<p>Sensitivity and uncertainty analysis of EPIC-IIASA regional soil carbon modeling (Balkovič et al, 2020).</p>	<p>Detailed gridded data can be obtained by contacting the data provider: Balkovič Juraj balkovic@iiasa.ac.at <a href="https://verifydb.lsce.ipsl.fr/thredds/fileServer/verify/VERIFY_OUTP_UT/FCO2/CO2_Tier3BUPB_CropFluxes_EPIC-S1_IIASA_CRP_EUR-304x560_IM_V2021_20211026_BALKOVIC_2D.nc">https://verifydb.lsce.ipsl.fr/thredds/fileServer/verify/VERIFY_OUTP_UT/FCO2/CO2_Tier3BUPB_CropFluxes_EPIC-S1_IIASA_CRP_EUR-304x560_IM_V2021_20211026_BALKOVIC_2D.nc</a></p>
<p><b>EPIC-IIASA grasslands</b></p>	<p>Tier 3 approach. Grassland: static 1x1 km mask from CORINE &amp; PELCOM 2000, including pastures, herbaceous vegetation, heterogeneous agricultural areas, and permanent cropland. Initial SOC stock from the map of organic carbon content in the topsoil (Lugato et al., 2014) with a spin-up. Static grassland management and input intensity as adopted from (Chang et al., 2016) and ISIMIP (Jägermeyr et al., 2021).</p>	<p>IPCC (2006): Tier 3 Land management and input factors for the grassland remaining grassland category as simulated by the EPIC-IIASA modeling platform, calibrated for the 1995–2020 period.</p>	<p>N/A</p>	<p>Detailed gridded data can be obtained by contacting the data provider: Juraj Balkovič: balkovic@iiasa.ac.at <a href="https://verifydb.lsce.ipsl.fr/thredds/fileServer/verify/VERIFY_OUTP_UT/FCO2/CO2_Tier3BUPB_GrassFluxes_EPIC-S1_IIASA_GRS_EUR-304x560_IM_V2021_20220427_BALKOVIC_2D.nc">https://verifydb.lsce.ipsl.fr/thredds/fileServer/verify/VERIFY_OUTP_UT/FCO2/CO2_Tier3BUPB_GrassFluxes_EPIC-S1_IIASA_GRS_EUR-304x560_IM_V2021_20220427_BALKOVIC_2D.nc</a></p>
<p><b>ORCHIDEE</b></p>	<p>For the land cover/land use input maps: data on wood harvest from the FAO</p>	<p>Tier 3 model, process based. Any emission factors enter in the form of generic parameters for a given ecosystem type fit against observational data (both site-level and remotely sensed).</p>	<p>None, though some information on uncertainty due to model structure is given by looking at the spread from the TRENDY suite of models, of which ORCHIDEE is a member.</p>	<p>Detailed gridded data can be obtained by contacting the data providers: Matthew McGrath <a href="mailto:matthew.mcgrath@lsce.ipsl.fr">matthew.mcgrath@lsce.ipsl.fr</a> Philippe Peylin: <a href="mailto:peylin@lsce.ipsl.fr">peylin@lsce.ipsl.fr</a> <a href="https://verifydb.lsce.ipsl.fr/thredds/fileServer/verify/VERIFY_OUTP_UT/FCO2/CO2_Tier3BUPB_CarbonCycle_ORCHIDEE-N-V32-VNDEP-S3_LSCE_LAND_EUR-304x560_IM_V2021_20211209_BASTRIKOV_2D.nc">https://verifydb.lsce.ipsl.fr/thredds/fileServer/verify/VERIFY_OUTP_UT/FCO2/CO2_Tier3BUPB_CarbonCycle_ORCHIDEE-N-V32-VNDEP-S3_LSCE_LAND_EUR-304x560_IM_V2021_20211209_BASTRIKOV_2D.nc</a></p>



<b>CABLE-POP</b>	For the land cover/land use input maps: data on wood harvest and agricultural land from the FAO	Tier 3 model, process based. Any emission factors enter in the form of generic parameters for a given ecosystem type fit against observational data (both site-level and remotely sensed).	None, though some information on uncertainty due to model structure is given by looking at the spread from the TRENDY suite of models, of which CABLE-POP is a member.	Model output (gridded data) can be obtained by contacting the data provider:  Jürgen Knauer:  J.Knauer@westernsydney.edu.au  <a href="https://verifydb.lsce.ipsl.fr/thredds/fileServer/verify/VERIFY_OUTPUT/FCO2/CO2_Tier3BUPB_Land_Flux_CABLE-POP_UWESTSYDNEY_LAND_GLO-304x560_1M_V2021_20220510_KNAUER_2D.nc">https://verifydb.lsce.ipsl.fr/thredds/fileServer/verify/VERIFY_OUTPUT/FCO2/CO2_Tier3BUPB_Land_Flux_CABLE-POP_UWESTSYDNEY_LAND_GLO-304x560_1M_V2021_20220510_KNAUER_2D.nc</a>
<b>TRENDY v10</b>	For the land cover/land use input maps: data on wood harvest and agricultural land from the FAO	Tier 3 models, process based. Any emission factors enter in the form of generic parameters for a given ecosystem type fit against observational data (both site-level and remotely sensed).	The spread of the 15 TRENDY models used gives an idea of the uncertainty due to model structure in dynamic global vegetation models, as the forcing data was harmonized for all models.	Detailed gridded data can be obtained by contacting the data provider: Sitch, Stephen S.A.Sitch@exeter.ac.uk
<b>Statistical prediction model for CO<sub>2</sub> in inland waters</b>	Hydrosheds 15s (Lehner et al., 2008) and Hydro1K (USGS, 2000) for river network, HYDROLAKES for lakes and reservoirs network and surface area (Messenger et al., 2016); river pCO <sub>2</sub> data from GloRiCh (Hartmann et al., 2014), lake pCO <sub>2</sub> database from Sobek et al. (2005); river channel slope and width calculated from GLOBE-DEM (GLOBE-Task-Team et al., 1999) and runoff data from Fekete et al. (2002). Geodata for predictors of pCO <sub>2</sub> and gas transfer coefficient include air temperature, precipitation and wind speed (Hijmans et al., 2005), population density (CIESIN and CIAT), catchment slope	N/A	Monte Carlo runs (uncertainty on pCO <sub>2</sub> and gas transfer velocity)	Detailed gridded data can be obtained by contacting the data providers: Ronny Lauerwald <a href="mailto:Ronny.Lauerwald@ulb.ac.be">Ronny.Lauerwald@ulb.ac.be</a> Pierre Regnier <a href="mailto:Pierre.Regnier@ulb.ac.be">Pierre.Regnier@ulb.ac.be</a>

	gradient (Hydrosheds 15s), and terrestrial NPP (Zhao et al., 2005)			
<b>CBM</b>	National forest inventory data, Tier 2	EFs directly calculated by model, based on specific parameters (i.e., turnover and decay rates) defined by the user	N/A used from IPCC	Detailed gridded data can be obtained by contacting the data providers: Giacomo Grassi <a href="mailto:Giacomo.GRASSI@ec.europa.eu">Giacomo.GRASSI@ec.europa.eu</a> Matteo Vizzarri <a href="mailto:Matteo.VIZZARRI@ec.europa.eu">Matteo.VIZZARRI@ec.europa.eu</a> Roberto Pilli <a href="mailto:roberto.pilli713@gmail.com">roberto.pilli713@gmail.com</a>
<b>EFISCEN-Space</b>	National forest inventory data, Tier 3	emission factor is calculated from net balance of growth minus harvest	Sensitivity analysis on EFISCEN V3 in the user manual (Schelhaas et al., 2007). Total sensitivity is caused by esp. young forest growth, width of volume classes, age of felling and few more. Scenario uncertainty comes on top of this when projecting in future.	Detailed gridded data can be obtained by contacting the data providers: Gert-Jan Nabuurs <a href="mailto:gert-jan.nabuurs@wur.nl">gert-jan.nabuurs@wur.nl</a> Mart-Jan Schelhaas <a href="mailto:martjan.schelhaas@wur.nl">martjan.schelhaas@wur.nl</a>
<b>FAOSTAT</b>	FAOSTAT Land Use Domain; Harmonized world soil; ESA CCI; MODIS 6 Burned area products	IPCC guidelines	IPCC (2006, Vol.4, p.10.33) - confidential Uncertainties in estimates of GHG emissions are due to uncertainties in emission factors and activity data. They may be related to, inter alia, natural variability, partitioning fractions, lack of spatial or temporal coverage, or spatial aggregation.	Agriculture total and subdomain specific GHG emissions are found for download at <a href="http://www.fao.org/faostat/en/#data/GT">http://www.fao.org/faostat/en/#data/GT</a> (last access: April 2022).
<b>CO<sub>2</sub> land: Top-down</b>				
<b>CSR</b> <b>GCP ensemble</b> (CTE, CAMS, CarboScope) <b>EUROCOM</b> (PYVAR-CHIMERE, LUMIA, FLEXINVERT, CSR, CTE-Europe) <b>LUMIA</b> <b>CIF-CHIMERE</b>	Tier 3 top-down approach, prior information from fossil emissions, ocean fluxes, and biosphere-atmosphere exchange Spatial resolutions ranging from 1°x1° for certain regions to 4°x5°. EUROCOM uses more than 30 atmospheric stations. CSR uses four different settings (as described in Appendix A4)	Tier 3 top-down Inversion systems based on atmospheric transport models	<b>CSR</b> - Gaussian probability distribution function, where the error covariance matrix includes errors in prior fluxes, observations and transport model representations. <b>GCP</b> : the different methodologies, the land-use and land-cover data set, and the different processes represented trigger the uncertainties between models. a semi-quantitative measure of uncertainty for annual and decadal emissions as best value judgment = at least a 68 % chance ( $\pm 1\sigma$ ) <b>EUROCOM</b> : account for source of uncertainties via	Detailed gridded data can be obtained by contacting the data providers:  <b>CSR</b> : Christoph Gerbig <a href="mailto:cgerbig@bgc-jena.mpg.de">cgerbig@bgc-jena.mpg.de</a> Saqr Munassar <a href="mailto:smunas@bgc-jena.mpg.de">smunas@bgc-jena.mpg.de</a>  <b>GCP</b> : Pierre Friedlingstein <a href="mailto:P.Friedlingstein@exeter.ac.uk">P.Friedlingstein@exeter.ac.uk</a>  <b>EUROCOM</b> : Marko Scholze <a href="mailto:marko.scholze@nateko.lu.se">marko.scholze@nateko.lu.se</a> Gregoire Broquet <a href="mailto:gregoire.broquet@lscce.ipsl.fr">gregoire.broquet@lscce.ipsl.fr</a>

			<p>prior and model and observation error covariance matrices; assessment of the resulting uncertainties in fluxes based on spread</p> <p><b>LUMIA:</b> The prior uncertainties are constructed using standard deviations proportional to the sum of the absolute value of the hourly NEE aggregated in each weekly optimization interval (so, in essence, uncertainties are large when the daily cycle of NEE is large), spatial correlation lengths of 500 km (Gaussian) and temporal correlation lengths of 1 month (Exponential).</p>	<p><b>LUMIA:</b> Guillaume Monteil <a href="mailto:guillaume.monteil@nateko.lu.se">guillaume.monteil@nateko.lu.se</a></p> <p><b>CIF-CHIMERE:</b> Gregoire Broquet <a href="mailto:gbroquet@lsce.ipsl.fr">gbroquet@lsce.ipsl.fr</a></p>
--	--	--	--	--

2260

2261

2262 *Table C2: Comparison of the processes included in the inventories, bottom-up models and inversions.*

Description	NGHGI	Global database	Process-based models				DGVMs			Bookkeeping Models			Inversions <sup>#</sup>
			E	E	C	E	C	T	O	B	B	H	
	U N F C C C <sup>a</sup>	F A O S T A T <sup>a</sup>	E C O S S E	E P I C - I I A S A	C B M	E F I S C E N - Space	C A B L E - P O P	T R E N D Y V I 0	O R C H I D E	B L U E I V G C P	B L U E V E R I F Y	H & N	
Forest total	E	E	N	N	E	E	E	Acc. table A1 in GCB 2021 (Friedling et al., 2022)	E	E <sup>h</sup>	E <sup>h</sup>	E <sup>h</sup>	
Split FL-FL / FL-X / X-FL	E	E	N	N	E	E/N/N	E		E	E <sup>h</sup> /E/E	E <sup>h</sup> /E/E	E <sup>h</sup> /E/E	
Cropland total	E	N	E	E	N	N	I		E	E <sup>h</sup>	E <sup>h</sup>	E <sup>h</sup>	
Split CL-CL / CL-X / X-CL	E	N	E	E/N/N	N	N	I		E	N/E/E	N/E/E	N/E/E	
Grassland total	E	N	E	N	N	N	E		E	E	E	E	
Split GL-GL /	E	N	E	N	N	N	E		E	N/E/E	N/E/E	N/E/E	

GL-X / X-GL														
Peatland accounting	E	E	N	N	N	N	N		N	N	N	N		
CO <sub>2</sub> fertilization	I	I	N	E	N	N	E	Acc. table A1 in GCB 2021 (Friedling et al., 2022)	E	N <sup>i</sup>	N <sup>i</sup>	N <sup>i</sup>		
Climate induced impacts	I	I	N	E <sup>f</sup>	I <sup>b</sup>	I <sup>c</sup>	E		E	N <sup>i</sup>	N <sup>i</sup>	N <sup>i</sup>		
Natural disturbances (fires, insect, wind)	I	I	N	N	E	N	E		N	N <sup>i</sup>	N <sup>i</sup>	N <sup>i</sup>		
Soil Organic C dynamic	I		E	E	E	E	E		E	N	N	N		
Lateral C transport (river)	N	N	N	N	N	N	N		N	N	N	N		
Flux from Harvested Wood Products	E	N	N	N	I	N <sup>d</sup>	E		Acc. table A1 in GCB 2021 (Friedling et al., 2022)	E	E	E	E	
Flux from Crop/Grass harvest	?	N	E	E <sup>c</sup>	N	N	E	E		I <sup>i</sup>	I <sup>i</sup>	I <sup>i</sup>		
Biomass burning	E	E	E	N <sup>g</sup>	E	N	N	N		E <sup>j</sup>	E <sup>j</sup>	E <sup>j</sup>		
N fertilization (with N dep)	I	N	E	N	N	N	E	N		N	N	N		
Flux from drained organic soils	I	E	E	N	I	N	N	I		E <sup>j</sup>	E <sup>j</sup>	E <sup>j</sup>		

Not included : N, Explicitly modeled : E, Implicitly modeled: I, Partly modeled : P

2263

2264

2265

2266

2267

2268

2269

2270

2271

<sup>a</sup> UNFCCC and FAOSTAT are ensemble of country estimates calculated with specific methodology for each country, following some guidelines

<sup>b</sup> The climate effects can be estimated indirectly by CBM, using external additional input provided by other models

<sup>c</sup> EFISCEN Space: Increment is sensitive to weather, but average weather

<sup>d</sup> EFISCEN has only production in m<sup>3</sup> but doesn't have a direct HWP module

<sup>e</sup> Crop yield and residue harvest from cropland (20 % of residues harvested in case of cereals, no residue harvest for other crops)

<sup>f</sup> EPIC-IIASA partly accounts for soil drought, i.e., plant growth limitation due to a lack of water in the soils. Heat stress and floods are not

accounted for, though

2272 <sup>g</sup> In principle, burning of crop residues on cropland can be explicitly simulated by EPIC-IIASA. However, not done for VERIFY as it is not a  
2273 relevant scenario for the business as usual cropland management in Europe  
2274 <sup>h</sup> forest/cropland/grassland exist and have carbon stocks, but have carbon fluxes only through change to management. FL-FL includes all land-use  
2275 induced effects (harvest slash and product decay, regrowth after agricultural abandonment and harvesting)  
2276 <sup>i</sup> implicit by using observation-based carbon densities that reflect harvest/climate/natural disturbances  
2277 <sup>j</sup> peat burning and peat drainage are not bookkeeping model output, but are added from various data sources during post processing  
2278 <sup>\*</sup> According to Table 2 in Monteil et al. (2020) and Table A3 in Friedlingstein et al. (2019)  
2279 <sup>#</sup> These categories are inputs to the inversions, not a result; the inversions adjust the total land-atmosphere C flux, regardless of what went into the  
2280 prior, and the posterior flux cannot really be disaggregated into contributions from separate processes. In a sense, as long as a process is  
2281 sufficiently significant to influence the CO<sub>2</sub> observations, it will have an impact on the inversion results  
2282  
2283

2284

## 2285 **Author contributions**

2286

2287 MJM processed original data, made Fig. 1, 3-6, A2, A3, A5, B4, and B5, edited the final manuscript, and coordinated  
2288 the response to reviewers; AMRP designed the initial research, led the discussions, wrote the initial draft of the paper  
2289 and helped edit all the following versions; RMA made Fig. 2, A1, B3; BM provided the new UNFCCC gap-filled  
2290 uncertainties and provided extensive support on questions related to NGHGs; PP, VB, and MJM processed the  
2291 original data submitted to the VERIFY portal; PP, PB, and MJM designed and are managing the web portal; GP  
2292 provided Figs. B1 and B2; GP, RMA, FD, BM, and GG made detailed reviews; SM made Fig. A4; PC, GB, PIP, MJ,  
2293 RL, MK, JK, FC, OT, JP, RG, FNT, JB and GG gave detailed comments and advice on previous versions of the  
2294 manuscript; all remaining co-authors provided data and commented on specific parts of the text related to their data  
2295 sets.

2296

## 2297 **Competing interests**

2298 Francesco N. Tubiello is a member of the editorial board of ESSD.

2299

## 2300 **Acknowledgements**

2301 We thank Aurélie Paquirissamy, Géraud Moulas and all ARTTIC team, for the great managerial support offered during  
2302 the VERIFY project. FAOSTAT statistics are produced and disseminated with the support of its member countries  
2303 to the FAO regular budget. The views expressed in this publication are those of the author(s) and do not necessarily  
2304 reflect the views or policies of FAO. Annual, gap-filled and harmonized NGHGI uncertainty estimates for the EU and  
2305 its member states were provided by the EU GHG inventory team (European Environment Agency and its European  
2306 Topic Centre on Climate change mitigation). We acknowledge the work of other members of the EDGAR group  
2307 (Edwin Schaaf, Jos Olivier). We acknowledge Stephen Sitch and the authors of the DGVMs TRENDY v10 ensemble  
2308 models for providing us with the data. We thank all the national forest inventories that have made their data available:  
2309 Ireland (John Redmond), Norway (Rasmus Astrup), Sweden (Jonas Fridman), Poland (Andrzej Talarczyk), Germany  
2310 (BMEL), The Netherlands (WUR & Stichting Probos), Belgium (Flanders: Leen Govaere), Luxembourg (Thierry  
2311 Palgen), France (IGN), Spain (MAPA), Switzerland (Esther Thürig), Italy (CREA), Czech Republic (Emil Cienciala),  
2312 Slovak Republic (Vladimír Šebeň). We thank all the NFI field crews for their hard work. Timo Vesala thanks ICOS-  
2313 Finland, University of Helsinki. Ingrid T. Luijkx and Wouter Peters thank the HPC cluster Aether at the University of

2314 Bremen, financed by DFG within the scope of the Excellence Initiative. MJM and VB were granted access to the  
2315 HPC resources of GENCI-TGCC under the allocation A0130106328.

2316

2317

### 2318 **Financial support**

2319 This research has been supported by the European Commission, Horizon 2020 Framework Programme (VERIFY,  
2320 grant no. 776810, for AB, AFC, AMRP, AP, CG, GB, GJM, GJN, GM, GP, HACDG, JB, LP, MJ, MJM, MK, MV,  
2321 PP, PR, PS, RG, RMA, SD). MJM and GM also acknowledge funding from the European Union's Horizon 2020  
2322 research and innovation programme under Grant Agreement No. 958927 (CoCO2). Philippe Ciais acknowledges  
2323 the support of European Research Council Synergy project SyG-2013-610028 IMBALANCE-P and from the ANR  
2324 CLand Convergence Institute. Ronny Lauerwald thanks the CLand Convergence Institute. Pierre Regnier  
2325 acknowledges the ESM 2025. Gert-Jan Nabuurs thanks the Dutch National Forest Inventory funded by the Ministry  
2326 Agriculture Nature Management and Food Quality. Guillaume Monteil's model computations were enabled by  
2327 resources provided by the Swedish National Infrastructure for Computing (SNIC) at NSC partially funded by the  
2328 Swedish Research Council through grant agreement no. 2018-05973.

2329

### 2330 **References**

2331 Andrew, R. M.: A comparison of estimates of global carbon dioxide emissions from fossil carbon sources, *Earth Syst.*  
2332 *Sci. Data*, 12, 1437–1465, <https://doi.org/10.5194/essd-12-1437-2020>, 2020.

2333

2334 Andrew, R. M., Peters, G.: The Global Carbon Project's fossil CO<sub>2</sub> emissions dataset. Global Carbon Project. Dataset.  
2335 <https://doi.org/10.5281/zenodo.5569234>. Accessed 01 Oct 2021.

2336

2337 Arneth, A., Sitch, S., Pongratz, J., Stocker, B. D., Ciais, P., Poulter, B., Bayer, A. D., Bondeau, A., Calle, L., Chini,  
2338 L. P., Gasser, T., Fader, M., Friedlingstein, P., Kato, E., Li, W., Lindeskog, M., Nabel, J. E. M. S., Pugh, T. A. M.,  
2339 Robertson, E., Viovy, N., Yue, C., and Zaehle, S.: Historical carbon dioxide emissions caused by land-use changes  
2340 are possibly larger than assumed. *Nature Geosci*, 10, 79–84, <https://doi.org/10.1038/ngeo2882>, 2017.

2341

2342 Bakker, D. C. E., Alin, S. R., Becker, M., Bittig, H. C., Castaño-Primo, R., Feely, R. A., Gkritzalis, T., Kadono, K.,  
2343 Kozyr, A., Lauvset, S. K., Metzl, N., Munro, D. R., Nakaoka, S., Nojiri, Y., O'Brien, K. M., Olsen, A., Pfeil, B.,  
2344 Pierrot, D., Steinhoff, T., Sullivan, K. F., Sutton, A. J., Sweeney, C., Tilbrook, B., Wada, C., Wanninkhof, R.,  
2345 Willstrand Wranne, A., Akl, J., Apelthun, L. B., Bates, N., Beatty, C. M., Burger, E. F., Cai, W.-J., Cosca, C. E.,  
2346 Corredor, J. E., Cronin, M., Cross, J. N., De Carlo, E. H., DeGrandpre, M. D., Emerson, S., Enright, M. P., Enyo, K.,  
2347 Evans, W., Frangoulis, C., Fransson, A., García-Ibáñez, M. I., Gehrung, M., Giannoudi, L., Glockzin, M., Hales, B.,  
2348 Howden, S. D., Hunt, C. W., Ibáñez, J. S. P., Jones, S. D., Kamb, L., Körtzinger, A., Landa, C. S., Landschützer, P.,  
2349 Lefèvre, N., Lo Monaco, C., Macovei, V. A., Maenner Jones, S., Meinig, C., Millero, F. J., Monacci, N. M., Mordy,  
2350 C., Morell, J. M., Murata, A., Musielewicz, S., Neill, C., Newberger, T., Nomura, D., Ohman, M., Ono, T., Passmore,  
2351 A., Petersen, W., Petihakis, G., Perivoliotis, L., Plueddemann, A. J., Rehder, G., Reynaud, T., Rodriguez, C., Ross,  
2352 A. C., Rutgersson, A., Sabine, C. L., Salisbury, J. E., Schlitzer, R., Send, U., Skjelvan, I., Stamatakis, N., Sutherland,  
2353 S. C., Sweeney, C., Tadokoro, K., Tanhua, T., Telszewski, M., Trull, T., Vandemark, D., van Ooijen, E., Voynova,  
2354 Y. G., Wang, H., Weller, R. A., Whitehead, C., Wilson, D.: Surface Ocean CO<sub>2</sub> Atlas Database Version 2022  
2355 (SOCATv2022) (NCEI Accession 0253659). Subset v2021. NOAA National Centers for Environmental Information.  
2356 Dataset. <https://doi.org/10.25921/1h9f-nb73>. Accessed 01 July 2021.

2357

2358 Balkovič, J., Madaras, M., Skalský, R., Folberth, C., Smatanová, M., Schmid, E., van der Velde, M., Kraxner, F.,  
2359 Obersteiner, M.: Verifiable soil organic carbon modeling to facilitate regional reporting of cropland carbon change:  
2360 A test case in the Czech Republic, *J. Environ. Manage.*, 274, 111206, <https://doi.org/10.1016/j.jenvman.2020.111206>,  
2361 2020.

2362

2363 Balkovič, J., Skalský, R., Folberth, C., Khabarov, N., Schmid, E., Madaras, M., Obersteiner, M., van der Velde, M.:  
2364 Impacts and Uncertainties of +2°C of Climate Change and Soil Degradation on European Crop Calorie Supply, *Earths*  
2365 *Future*, 6, 373–395, <https://doi.org/10.1002/2017EF000629>, 2018.

2366

2367 Balkovič, J., van der Velde, M., Schmid, E., Skalský, R., Khabarov, N., Obersteiner, M., Stürmer, B., Xiong, W.: Pan-  
2368 European crop modeling with EPIC: Implementation, up-scaling and regional crop yield validation, *Agric. Syst.*, 120,  
2369 61–75, <https://doi.org/10.1016/j.agry.2013.05.008>, 2013.

2370

2371 Bastos, A., Ciais, P., Friedlingstein, P., Sitch, S., Pongratz, J., Fan, L., Wigneron, J. P., Weber, U., Reichstein, M., Fu,  
2372 Z., Anthoni, P., Arneth, A., Haverd, V., Jain, A. K., Joetzjer, E., Knauer, J., Lienert, S., Loughran, T., McGuire, P. C.,  
2373 Tian, H., Viovy, N., and Zaehle, S.: Direct and seasonal legacy effects of the 2018 heat wave and drought on European  
2374 ecosystem productivity, *Science Advances*, 6, eaba2724, DOI: 10.1126/sciadv.aba27, 2020a.  
2375  
2376 Bastos, A., O'Sullivan, M., Ciais, P., Makowski, D., Sitch, S., Friedlingstein, P., Chevallier, F., Rödenbeck, C.,  
2377 Pongratz, J., Lujikx, I. T., Patra, P. K., Peylin, P., Canadell, J. G., Lauerwald, R., Li, W., Smith, N. E., Peters, W.,  
2378 Goll, D. S., Jain, A. K., Kato, E., Lienert, S., Lombardozzi, D. L., Haverd, V., Nabel, J. E. M. S., Poulter, B., Tian,  
2379 H., Walker, A. P., and Zaehle, S.: Sources of uncertainty in regional and global terrestrial CO<sub>2</sub> exchange estimates,  
2380 *Global Biogeochemical Cycles*, 34, e2019GB006393, <https://doi.org/10.1029/2019GB006393>, 2020b.  
2381  
2382 Basu, S., Lehman, S. J., Miller, J. B., Andrews, A. E., Sweeney, C., Gurney, K. R., Xu, X., Southon, J., and Tans, P.  
2383 P.: Estimating US fossil fuel CO<sub>2</sub> emissions from measurements of <sup>14</sup>C in atmospheric CO<sub>2</sub>, *Proc. Nat. Acad. Sci.*,  
2384 117, 13300-13307, <https://doi.org/10.1073/pnas.1919032117>, 2020.  
2385  
2386 Battin, T. J., Lauerwald, R., Bernhardt, E. S., Bertuzzo, E., Gener, L. G., Hall Jr, R. O., Hotchkiss, E. R., Maavara, T.,  
2387 Pavelsky, T. M., Ran, L., Raymond, P., Rosentreter, J. A., and Regnier, P.: River ecosystem metabolism and carbon  
2388 biogeochemistry in a changing world, *Nature*, 613, 449-459, <https://doi.org/10.1038/s41586-022-05500-8>, 2023.  
2389  
2390 Becker, M., Olsen, A., Landschützer, P., Omar, A., Rehder, G., Rödenbeck, C., and Skjelvan, I.: The northern  
2391 European shelf as an increasing net sink for CO<sub>2</sub>, *Biogeosciences*, 18, 1127–1147, [https://doi.org/10.5194/bg-18-](https://doi.org/10.5194/bg-18-1127-2021)  
2392 1127-2021, 2021.



2393

2394 Berchet, A., Sollum, E., Thompson, R. L., Pison, I., Thanwerdas, J., Broquet, G., Chevallier, F., Aalto, T., Berchet,  
2395 A., Bergamaschi, P., Brunner, D., Engelen, R., Fortems-Cheiney, A., Gerbig, C., Groot Zwaaftink, C. D., Haussaire,  
2396 J.-M., Henne, S., Houweling, S., Karstens, U., Kutsch, W. L., Lujckx, I. T., Monteil, G., Palmer, P. I., van Peet, J. C.  
2397 A., Peters, W., Peylin, P., Potier, E., Rödenbeck, C., Saunio, M., Scholze, M., Tsuruta, A., and Zhao, Y.: The  
2398 Community Inversion Framework v1.0: a unified system for atmospheric inversion studies, *Geosci. Model Dev.*, 14,  
2399 5331–5354, <https://doi.org/10.5194/gmd-14-5331-2021>, 2021.

2400

2401 BP: 60 Years BP Statistical Review of World Energy: 1951–2011, available at:  
2402 <https://www.bp.com/en/global/corporate/energy-economics/statistical-review-of-world-energy/downloads.html> (last  
2403 access: 8 February 2019), 2011.

2404

2405 BP: BP Statistical Review of World Energy June 2018, available at: [https://www.bp.com/en/global/corporate/energy-](https://www.bp.com/en/global/corporate/energy-economics/statistical-review-of-world-energy/downloads.html)  
2406 [economics/statistical-review-of-world-energy/downloads.html](https://www.bp.com/en/global/corporate/energy-economics/statistical-review-of-world-energy/downloads.html), (last access: 14 June 2018).

2407

2408 BP: Methodology for calculating CO<sub>2</sub> emissions from energy use, available at:  
2409 <https://www.bp.com/en/global/corporate/energy-economics/statistical-review-of-world-energy/co2-emissions.html>  
2410 (last access: 8 February 2019), 2017.

2411

2412 Bradbury, N. J., Whitmore, A. P., Hart, P. B. S., and Jenkinson, D. S.: Modelling the fate of nitrogen in crop and soil  
2413 in the years following application of <sup>15</sup>N-labelled fertilizer to winter wheat, *J. Agr. Sci.*, 121, 363-379,  
2414 doi:10.1017/S0021859600085567, 1993.

2415

2416 Brophy, K., Graven, H., Manning, A. J., White, E., Arnold, T., Fischer, M. L., Jeong, S., Cui, X., and Rigby, M.:  
2417 Characterizing uncertainties in atmospheric inversions of fossil fuel CO<sub>2</sub> emissions in California, *Atmos. Chem.*  
2418 *Phys.*, 19, 2991–3006, <https://doi.org/10.5194/acp-19-2991-2019>, 2019.

2419

2420 Broquet, G., Chevallier, F., Rayner, P., Aulagnier, C., Pison, I., Ramonet, M., Schmidt, M., Vermeulen, A. T., and  
2421 Ciais, P.: A European summertime CO<sub>2</sub> biogenic flux inversion at mesoscale from continuous in situ mixing ratio  
2422 measurements,  
2423 *J. Geophys. Res.*, 116, D23303, doi:10.1029/2011JD016202, 2011.

2424

2425 Broquet, G., Chevallier, F., Bréon, F.-M., Kadygrov, N., Alemanno, M., Apadula, F., Hammer, S., Haszpra, L.,  
2426 Meinhardt, F., Morguí, J. A., Necki, J., Piacentino, S., Ramonet, M., Schmidt, M., Thompson, R. L., Vermeulen, A.  
2427 T., Yver, C., and Ciais, P.: Regional inversion of CO<sub>2</sub> ecosystem fluxes from atmospheric measurements: reliability  
2428 of the uncertainty estimates, *Atmos. Chem. Phys.*, 13, 9039–9056, <https://doi.org/10.5194/acp-13-9039-2013>, 2013.

2429

2430 CDIAC, <https://energy.appstate.edu/CDIAC> (last access: 10 November 2022).

2431

2432 Ceccherini, G, Duveiller, G, Grassi, G, Lemoine, G, Avitabile, V, Pilli, R, and Cescatti, A.: Abrupt increase in  
2433 harvested forest area over Europe after 2015, *Nature*, 583, 72–77, <https://doi.org/10.1038/s41586-020-2438-y>, 2020.

2434

2435 CEDS v\_2019\_12\_23, <https://www.pnnl.gov/projects/ceds> (last access: 10 November 2022).

2436

2437 Chang, J., Ciais, P., Herrero, M., Havlik, P., Campioli, M., Zhang, X., Bai, Y., Viovy, N., Joiner, J., Wang, X., Peng,  
2438 S., Yue, C., Piao, S., Wang, T., Hauglustaine, D. A., Soussana, J.-F., Peregón, A., Kosykh, N., and Mironycheva-  
2439 Tokareva, N.: Combining livestock production information in a process-based vegetation model to reconstruct the  
2440 history of grassland management, *Biogeosciences*, 13, 3757–3776, <https://doi.org/10.5194/bg-13-3757-2016>, 2016.

2441

2442 Chen, J., Wang, S., Kraxner, F., Balkovič, J., Xu, X., and Sun, L.: Spatial Analysis of the Soil Carbon Sequestration  
2443 Potential of Crop-Residue Return in China Based on Model Simulation, *J. Resour. Ecol.*, 10, 184-195,  
2444 <https://doi.org/10.5814/j.issn.1674-764x.2019.02.009>, 2019.

2445

2446 Chevallier, F., Fisher, M., Peylin, P., Serrar, S., Bousquet, P., Bréon, F.-M., Chédin, A., and Ciais, P.: Inferring CO<sub>2</sub>  
2447 sources and sinks from satellite observations: Method and application to TOVS data, *J. Geophys. Res.*, 110, D24309,  
2448 doi:10.1029/2005JD006390, 2005.

2449

2450 Chevallier, F., F.-M. Bréon, F.-M., and Rayner, P. J.: Contribution of the Orbiting Carbon Observatory to the  
2451 estimation of CO<sub>2</sub> sources and sinks: Theoretical study in a variational data assimilation framework, *J. Geophys. Res.*,  
2452 112, D09307, doi:10.1029/2006JD007375, 2007.

2453

2454 Chevallier, F., Ciais, P., Conway, T. J., Aalto, T., Anderson, B. E., Bousquet, P., Brunke, E. G., Ciattaglia, L., Esaki,  
2455 Y., Fröhlich, M., Gomez, A. J., Gomez-Pelaez, A. J., Haszpra, L., Krummel, P., Langenfelds, R., Leuenberger, M.,  
2456 Machida, T., Maignan, F., Matsueda, H., Morguí, J. A., Mukai, H., Nakazawa, T., Peylin, P., Ramonet, M., Rivier, L.,  
2457 Sawa, Y., Schmidt, M., Steele, P., Vay, S. A., Vermeulen, A. T., Wofsy, S., and Worthy, D. : CO<sub>2</sub> surface fluxes at  
2458 grid point scale estimated from a global 21-year reanalysis of atmospheric measurements. *J. Geophys. Res.*, 115,  
2459 D21307, doi:10.1029/2010JD013887, 2010.

2460

2461 Ciais, P., Reichstein, M., Viovy, N., Granier, A., Ogée, J., Allard, V., Aubinet, M., Buchmann, N., Bernhofer Chr.,  
2462 Carrara, A., Chevallier, F., De Noblet, N., Friend, A. D., Friedlingstein, P., Grünwald, T., Heinesch, B., Keronen, P.,  
2463 Knohl, A., Krinner, G., Loustau, D., Manca, G., Matteucci, G., Miglietta, F., Ourcival, J. M., Papale, D., Pilegaard,  
2464 K., Rambal, S., Seufert, G., Soussana, J. F., Sanz, M. J., Schulze, E. D., Vesala, T. and Valentini, R.: Europe-wide  
2465 reduction in primary productivity caused by the heat and drought in 2003. *Nature*, 437, 529–533,  
2466 <https://doi.org/10.1038/nature03972>, 2005.

2467

2468 Ciais, P., Crisp, D., Denier van der Gon, H., Engelen, R., Janssens-Maenhout, G., Heimann, M., Rayner, P., and  
2469 Scholze, M.: Towards a European Operational Observing System to Monitor Fossil CO<sub>2</sub> emissions - Final Report  
2470 from the expert group, [https://www.copernicus.eu/sites/default/files/2019-09/CO2\\_Blue\\_report\\_2015.pdf](https://www.copernicus.eu/sites/default/files/2019-09/CO2_Blue_report_2015.pdf), 2015.

2471

2472 Ciais, P., Yao, Y., Gasser, T., Baccini, A., Wang, Y., Lauerwald, R., Peng, S., Bastos, A., Li, W., Raymond, P.A. and  
2473 Canadell, J.G., Peters, G. P., Andres, R. J., Chang, J., Yue, C., Dolman, A. J., Haverd, V., Hartmann, J., Laruelle, G.,  
2474 Konings, A. G., King, A. W., Liu, Y., Luyssaert, S., Maignan, F., Patra, P. K., Peregón, A., Regnier, P., Pongratz, J.,  
2475 Poulter, B., Shvidenko, A., Valentini, R., Wang, R., Brouquet, G., Yin, Y., Zscheischler, J., Guenet, B., Goll, D. S.,  
2476 Ballantyne, A.-P., Yang, H., Qiu, C., and Zhu, D.: Empirical estimates of regional carbon budgets imply reduced  
2477 global soil heterotrophic respiration, *National Science Review*, 8, nwaa145, <https://doi.org/10.1093/nsr/nwaa145>,  
2478 2021.

2479

2480 CoCO2: <https://coco2-project.eu/>, last access: 21 November 2022.

2481

2482 Coleman, K., Jenkinson, D. S.: RothC-26.3 - A model the turnover of carbon in soil. In: Powlson DS, Smith P, Smith

2483 JU (ed) Evaluation of soil organic matter models using existing long-term datasets, NATO ASI Series I, vol. 38.

2484 Springer, Berlin, pp 237–246, 1996.

2485

2486 Conchedda, G. and Tubiello, F. N.: Drainage of organic soils and GHG emissions: validation with country data, Earth

2487 Syst. Sci. Data, 12, 3113–3137, <https://doi.org/10.5194/essd-12-3113-2020>, 2020.

2488

2489 Cox, A., Di Sarra, A. G., Vermeulen, A., Manning, A., Beyersdorf, A., Zahn, A., Manning, A., Watson, A., Karion,  
2490 A., Hensen, A., Arlyn A., Frumau, A., Colomb, A., Scheeren, B., Law, B., Baier, B., Munger, B., Paplawsky, B.,  
2491 Viner, B., Stephens, B., Daube, B., Labuschagne, C., Myhre, C. L., Hanson, C., Miller, C. E., Plass-Duelmer, C.,  
2492 Gerbig, C., Sloop, C. D., Sweeney, C., Kubistin, D., Goto, D., Jaffe, D., Say, D., Van Dinter, D., Bowling, D., Lam,  
2493 D. H. Y., Munro, D., Dickon Y., Worthy, D., Dlugokencky, E., Kozlova, E., Gloor, E., Cuevas, E., Reyes-Sanchez,  
2494 E., Hints, E., Kort, E., Morgan, E., Obersteiner, F., Apadula, F., Gheusi, F., Meinhardt, F., Moore, F., Vitkova, G.,  
2495 Chen, G., Bentz, G., Manca, G., Brailsford, G., Forster, G., Boenisch, H., Riris, H., Meijer, H., Timas, H., Matsueda,  
2496 H., Huilin C., Levin, I., Lehner, I., Mammarella, I., Bartyzel, J., Abshire, J. B., Elkins, J. W., Levula, J., Necki, J.,  
2497 Pichon, J. M., Peischl, J., Müller-Williams, J., Turnbull, J., Miller, J. B., Lee, J., Lin, J., Morgui, J.-A., DiGangi, J.  
2498 P., Lavric, J., Hatakka, J., Coletta, J. D., Worsley, J., Holst, J., Kominkova, K., McKain, K., Saito, K., Aikin, K., Davis,  
2499 K., Thoning, K., Tørseth, K., Haszpra, L., Mitchell, L., Gatti, L.V., Emmenegger, L., Chmura, M., Merchant, L., Sha,  
2500 M. K., Delmotte, M., Fischer, Marc L., Schumacher, M., Torn, M., Leuenberger, M., Heimann, M., Steinbacher, M.,  
2501 De Mazière, M., Sargent, M., Lindauer, M., Mölder, M., Martin, M. Y., Shook, M., Galkowski, M., Heliasz, M.,  
2502 Marek, M. V., Ramonet, M., Miroslaw Z., Lopez, M., Sasakawa, M., Mihalopoulos, N., Miles, N., Lee, O. S.M.,  
2503 Laurent, O., Peltola, O., Hermanssen, O., Trisolino, P., Cristofanelli, P., Kolari, P., Krummel, P., Shepson, P., Smith,  
2504 P., Rivas, P. P., Bakwin, P., Bergamaschi, P., Keronen, P., Tans, P., Van Den Bulk, P., Keeling, R., Ramos, R.,  
2505 Langenfels, R., Leppert, R., Curcoll, R., Commane, R., Newman, S., Piacentino, S., Hammer, S., Richardson, S.,  
2506 Biraud, S. C., Conil, S., Clark, S., Morimoto, S., Shuangxi F., Aoki, S., O'Doherty, S., Sites Climadat, Zachle, S., De  
2507 Wekker, S., Kawa, S. R., Montzka, S., Walker, S., Piper, S., Wofsy, S., Nichol, S., Schuck, T., Lauvaux, T., Ryerson,  
2508 T., Seifert, T., Griffis, T., Biermann, T., Gehrlein, T., Machida, T., Laurila, T., Aalto, T., Gomez-Trueba, V., Kazan,  
2509 V., Ivakhov, V., Joubert, W., Niwa, Y., and Loh, Z.: Multi-laboratory compilation of atmospheric carbon dioxide data  
2510 for the period 1957–2019; obspack\_CO2\_1\_GLOBALVIEWplus\_v6.1\_2021-03-01, NOAA Global Monitoring  
2511 Laboratory [data set], <https://doi.org/10.25925/20201204>, 2021.

2512

2513 Crippa, M., Oreggioni, G., Guizzardi, D., Muntean, M., Schaaf, E., Lo Vullo, E., Solazzo, E., Monforti-Ferrario, F.,  
2514 Olivier, J.G.J., and Vignati, E.: Fossil CO<sub>2</sub> and GHG emissions of all world countries - 2019 Report, EUR 29849 EN,  
2515 Publications Office of the European Union, Luxembourg, 2019, ISBN 978-92-76-11100-9, doi:10.2760/687800,  
2516 JRC117610, 2019.

2517

2518 Deng, Z., Ciais, P., Tzompa-Sosa, Z. A., Saunio, M., Qiu, C., Tan, C., Sun, T., Ke, P., Cui, Y., Tanaka, K., Lin, X.,  
2519 Thompson, R. L., Tian, H., Yao, Y., Huang, Y., Lauerwald, R., Jain, A. K., Xu, X., Bastos, A., Sitch, S., Palmer, P.  
2520 I., Lauvaux, T., d'Aspremont, A., Giron, C., Benoit, A., Poulter, B., Chang, J., Petrescu, A. M. R., Davis, S. J., Liu,  
2521 Z., Grassi, G., Albergel, C., Tubiello, F. N., Perugini, L., Peters, W., and Chevallier, F.: Comparing national  
2522 greenhouse gas budgets reported in UNFCCC inventories against atmospheric inversions, *Earth Syst. Sci. Data*, 14,  
2523 1639–1675, <https://doi.org/10.5194/essd-14-1639-2022>, 2022.

2524

2525 Di Sarra, A. G., Karion, A., Arlyn Andrews, Colomb, A., Scheeren, B., Viner, B., Myhre, C. L., Miller, C. E., Plass-  
2526 Duclmer, C., Plass-Duclmer, C., Sloop, C. D., Sweeney, C., Kubistin, D., Jaffe, D., Dlugokencky, E., Vitkova, G.,  
2527 Manca, G., Huilin Chen, Lehner, I., Mammarella, I., Pichon, J. M., Müller-Williams, J., Miller, J. B., Lee, J., Hatakka,  
2528 J., Holst, J., Kominkova, K., McKain, K., Thoning, K., Tørseth, K., Emmenegger, L., Sha, M. K., Delmotte, M.,  
2529 Fischer, M. L., Schumacher, M., Leuenberger, M., Steinbacher, M., De Mazière, M., Lindauer, M., Mölder, M.,  
2530 Heliasz, M., Marek, M. V., Ramonet, M., Lopez, M., Laurent, O., Hermanssen, O., Trisolino, P., Cristofanelli, P.,  
2531 Smith, P., Bakwin, P., Bergamaschi, P., Keronen, P., Tans, P., Piacentino, S., Biraud, S. C., Conil, S., De Wekker, S.,  
2532 Biermann, T., Laurila, T., Aalto, T., and Kazan, V.: Multi-laboratory compilation of atmospheric carbon dioxide data  
2533 for the years 2020–2021; *obspack\_CO2\_1\_NRT\_v6.1.1\_2021-05-17*, NOAA Global Monitoring Laboratory [data  
2534 set], <https://doi.org/10.25925/20210517>, 2021.

2535

2536 Drought 2018 Team, ICOS Atmosphere Thematic Centre: Drought-2018 atmospheric CO<sub>2</sub> Mole Fraction product for  
2537 48 stations (96 sample heights), Integrated Carbon Observation System [data set], <https://doi.org/10.18160/ERE9-9D85>, 2020.

2538

2539

2540 Ducoudré, N. I., Laval, K., and Perrier, A.: SECHIBA, a new set of parameterizations of the hydrologic exchanges at  
2541 the land-atmosphere interface within the LMD atmospheric general circulation model, *Journal of Climate*, 6, 248–  
2542 273, <https://www.jstor.org/stable/26197219>, 1993.

2543

2544 ESA: Land Cover CCI Product User Guide Version 2. ESA. <http://maps.elie.ucl.ac.be/CCI/viewer/index.php>, (last  
2545 access: 10 November 2022), 2017.

2546

2547 EU: REGULATION (EU) No 525/2013 OF THE EUROPEAN PARLIAMENT AND OF THE COUNCIL of 21 May  
2548 2013 on a mechanism for monitoring and reporting greenhouse gas emissions and for reporting other information at  
2549 national and Union level relevant to climate change and repealing Decision No 280/2004/EC, [https://eur-  
2550 lex.europa.eu/legal-content/EN/TXT/PDF/?uri=CELEX:32013R0525&from=EN](https://eur-lex.europa.eu/legal-content/EN/TXT/PDF/?uri=CELEX:32013R0525&from=EN), 2013.

2551

2552 EU: Regulation (EU) 2018/841 of the European Parliament and of the Council of 30 May 2018 on the inclusion of  
2553 greenhouse gas emissions and removals from land use, land use change and forestry in the 2030 climate and energy  
2554 framework, and amending Regulation (EU) No 525/2013 and Decision No 529/2013/EU, [https://eur-  
2555 lex.europa.eu/legal-content/EN/TXT/?uri=uriserv:OJ.L\\_.2018.156.01.0001.01.ENG](https://eur-lex.europa.eu/legal-content/EN/TXT/?uri=uriserv:OJ.L_.2018.156.01.0001.01.ENG), 2018a.

2556

2557 EU: Regulation (EU) 2018/842 of the European Parliament and of the Council of 30 May 2018 on binding annual  
2558 greenhouse gas emission reductions by Member States from 2021 to 2030 contributing to climate action to meet  
2559 commitments under the Paris Agreement and amending Regulation (EU) No 525/2013, [https://eur-  
2560 lex.europa.eu/legal-content/EN/TXT/?uri=CELEX:32018R0842](https://eur-lex.europa.eu/legal-content/EN/TXT/?uri=CELEX:32018R0842), 2018b.

2561

2562 EU: Communication COM/2020/562: Stepping up Europe’s 2030 climate ambition Investing in a climate-neutral  
2563 future for the benefit of our people, [https://knowledge4policy.ec.europa.eu/publication/communication-com2020562-  
2564 stepping-europe%E2%80%99s-2030-climate-ambition-investing-climate\\_en](https://knowledge4policy.ec.europa.eu/publication/communication-com2020562-stepping-europe%E2%80%99s-2030-climate-ambition-investing-climate_en), (last access: 10 November 2022), 2020.

2565

2566 EU: Procedure 2021/0201/COD, COM (2021) 554: Proposal for a REGULATION OF THE EUROPEAN  
2567 PARLIAMENT AND OF THE COUNCIL amending Regulations (EU) 2018/841 as regards the scope, simplifying  
2568 the compliance rules, setting out the targets of the Member States for 2030 and committing to the collective  
2569 achievement of climate neutrality by 2035 in the land use, forestry and agriculture sector, and (EU) 2018/1999 as  
2570 regards improvement in monitoring, reporting, tracking of progress and review, [https://eur-](https://eur-lex.europa.eu/procedure/EN/2021_201)  
2571 [lex.europa.eu/procedure/EN/2021\\_201](https://eur-lex.europa.eu/procedure/EN/2021_201), 2021a.

2572

2573 EU: Regulation (EU) 2021/1119 of the European Parliament and of the Council of 30 June 2021 establishing the  
2574 framework for achieving climate neutrality and amending Regulations (EC) No 401/2009 and (EU) 2018/1999  
2575 ('European Climate Law'), <https://eur-lex.europa.eu/legal-content/EN/TXT/?uri=CELEX:32021R1119>, 2021b.

2576

2577 EU NIR: Annual European Union greenhouse gas inventory 1990–2019 and inventory report 2021, Submission to the  
2578 UNFCCC Secretariat, EEA/PUBL/2021/066, 2021.

2579

2580 EU NIR: Annual European Union greenhouse gas inventory 1990–2020 and inventory report 2022, Submission to the  
2581 UNFCCC Secretariat, EEA/PUBL/2022/023, 2022.

2582

2583 Federici, S., Tubiello, F. N., Salvatore, M., Jacobs, H., and Schmidhuber, J.: New estimates of CO<sub>2</sub> forest emissions  
2584 and removals: 1990–2015, *Forest Ecol. Manage.*, 352, 89–98, <https://doi.org/10.1016/j.foreco.2015.04.022>, 2015.

2585

2586 Feng, L., Palmer, P. I., Parker, R. J., Deutscher, N. M., Feist, D. G., Kivi, R., Morino, I., and Sussmann, R.: Estimates  
2587 of European uptake of CO<sub>2</sub> inferred from GOSAT XCO<sub>2</sub> retrievals: sensitivity to measurement bias inside and outside  
2588 Europe, *Atmos. Chem. Phys.*, 16, 1289–1302, <https://doi.org/10.5194/acp-16-1289-2016>, 2016.

2589

2590 Fortems-Cheiney, A., Pison, I., Broquet, G., Dufour, G., Berchet, A., Potier, E., Coman, A., Siour, G., and Costantino,  
2591 L.: Variational regional inverse modeling of reactive species emissions with PYVAR-CHIMERE-v2019, *Geosci.*  
2592 *Model Dev.*, 14, 2939–2957, <https://doi.org/10.5194/gmd-14-2939-2021>, 2021.

2593

2594 Fortems-Cheiney, A and Broquet, G.: D2.12: Final re-analysis of the national scale CO<sub>2</sub> anthropogenic emissions  
2595 over 2005-2015, [https://projectsworkspace.eu/sites/VERIFY/Deliverables/WP2/VERIFY\\_D2.12\\_Final%20re-](https://projectsworkspace.eu/sites/VERIFY/Deliverables/WP2/VERIFY_D2.12_Final%20re-)



2596 analysis%20of%20the%20national%20scale%20CO2%20anthropogenic%20emissions%20over%202005-  
2597 2015\_v1.pdf, 2021.

2598

2599 FRA: Global Forest Resources Assessment 2015: How are the world's forest changing?, 2015, Rome, Italy, available  
2600 at: <http://www.fao.org/3/a-i4793e.pdf> (last access: 10 December 2019), 2015.

2601

2602 Frey, H.C.: Evaluation of an Approximate Analytical Procedure for Calculating Uncertainty in the Greenhouse Gas  
2603 Version of the Multi-Scale Motor Vehicle and Equipment Emissions System, Prepared for Office of Transportation  
2604 and Air Quality, U.S. Environmental Protection Agency, Ann Arbor, MI, May 30, 2003.

2605

2606 Friedlingstein, P., O'Sullivan, M., Jones, M. W., Andrew, R. M., Hauck, J., Olsen, A., Peters, G. P., Peters, W.,  
2607 Pongratz, J., Sitch, S., Le Quéré, C., Canadell, J. G., Ciais, P., Jackson, R. B., Alin, S., Aragão, L. E. O. C., Arneeth,  
2608 A., Arora, V., Bates, N. R., Becker, M., Benoit-Cattin, A., Bittig, H. C., Bopp, L., Bultan, S., Chandra, N., Chevallier,  
2609 F., Chini, L. P., Evans, W., Florentie, L., Forster, P. M., Gasser, T., Gehlen, M., Gilfillan, D., Gkritzalis, T., Gregor,  
2610 L., Gruber, N., Harris, I., Hartung, K., Haverd, V., Houghton, R. A., Ilyina, T., Jain, A. K., Joetzer, E., Kadono, K.,  
2611 Kato, E., Kitidis, V., Korsbakken, J. I., Landschützer, P., Lefèvre, N., Lenton, A., Lienert, S., Liu, Z., Lombardozzi,  
2612 D., Marland, G., Metzl, N., Munro, D. R., Nabel, J. E. M. S., Nakaoka, S.-I., Niwa, Y., O'Brien, K., Ono, T., Palmer,  
2613 P. I., Pierrot, D., Poulter, B., Resplandy, L., Robertson, E., Rödenbeck, C., Schwinger, J., Séférian, R., Skjelvan, I.,  
2614 Smith, A. J. P., Sutton, A. J., Tanhua, T., Tans, P. P., Tian, H., Tilbrook, B., van der Werf, G., Vuichard, N., Walker,  
2615 A. P., Wanninkhof, R., Watson, A. J., Willis, D., Wiltshire, A. J., Yuan, W., Yue, X., and Zaehe, S.: Global Carbon  
2616 Budget 2020, *Earth Syst. Sci. Data*, 12, 3269–3340, <https://doi.org/10.5194/essd-12-3269-2020>, 2020.

2617

2618 Friedlingstein, P., Jones, M. W., O'Sullivan, M., Andrew, R. M., Bakker, D. C. E., Hauck, J., Le Quéré, C., Peters, G.  
2619 P., Peters, W., Pongratz, J., Sitch, S., Canadell, J. G., Ciais, P., Jackson, R. B., Alin, S. R., Anthoni, P., Bates, N. R.,  
2620 Becker, M., Bellouin, N., Bopp, L., Chau, T. T. T., Chevallier, F., Chini, L. P., Cronin, M., Currie, K. I., Decharme,  
2621 B., Djeutchouang, L. M., Dou, X., Evans, W., Feely, R. A., Feng, L., Gasser, T., Gilfillan, D., Gkritzalis, T., Grassi,  
2622 G., Gregor, L., Gruber, N., Gürses, Ö., Harris, I., Houghton, R. A., Hurtt, G. C., Iida, Y., Ilyina, T., Luijkx, I. T., Jain,  
2623 A., Jones, S. D., Kato, E., Kennedy, D., Klein Goldewijk, K., Knauer, J., Korsbakken, J. I., Körtzinger, A.,  
2624 Landschützer, P., Lauvset, S. K., Lefèvre, N., Lienert, S., Liu, J., Marland, G., McGuire, P. C., Melton, J. R., Munro,  
2625 D. R., Nabel, J. E. M. S., Nakaoka, S.-I., Niwa, Y., Ono, T., Pierrot, D., Poulter, B., Rehder, G., Resplandy, L.,  
2626 Robertson, E., Rödenbeck, C., Rosan, T. M., Schwinger, J., Schwingshackl, C., Séférian, R., Sutton, A. J., Sweeney,

2627 C., Tanhua, T., Tans, P. P., Tian, H., Tilbrook, B., Tubiello, F., van der Werf, G. R., Vuichard, N., Wada, C.,  
2628 Wanninkhof, R., Watson, A. J., Willis, D., Wiltshire, A. J., Yuan, W., Yue, C., Yue, X., Zaehle, S., and Zeng, J.:  
2629 Global Carbon Budget 2021, *Earth Syst. Sci. Data*, 14, 1917–2005, <https://doi.org/10.5194/essd-14-1917-2022>, 2022.  
2630

2631 Ganzenmüller, R., Bultan, S., Winkler, K., Fuchs, R., Zabel, F., and Pongratz, J.: Land-use change emissions based  
2632 on high-resolution activity data substantially lower than previously estimated: *Environmental Research Letters*, 17,  
2633 64050, DOI 10.1088/1748-9326/ac70d8, 2022.  
2634

2635 Gasser, T. and Ciais, P.: A theoretical framework for the net land-to-atmosphere CO<sub>2</sub> flux and its implications in the  
2636 definition of "emissions from land-use change", *Earth Syst. Dynam.*, 4, 171–186, [https://doi.org/10.5194/esd-4-171-](https://doi.org/10.5194/esd-4-171-2013)  
2637 2013, 2013.  
2638

2639 Gasser, T., Crepin, L., Quilcaille, Y., Houghton, R. A., Ciais, P., and Obersteiner, M.: Historical CO<sub>2</sub> emissions from  
2640 land use and land cover change and their uncertainty, *Biogeosciences*, 17, 4075–4101, [https://doi.org/10.5194/bg-17-](https://doi.org/10.5194/bg-17-4075-2020)  
2641 4075-2020, 2020.  
2642

2643 Grassi, G., House, J., Kurz, W. A., Cescatti, A., Houghton, R. A., Peters, G. P., Sanz, M. J., Vi nas, R. A., Alkama, ..,  
2644 Arneeth, A., Bondeau, A., Dentener, F., Fader, M., Federici, S., Friedlingstein, P., Jain, A. K., Kato, E., Koven, C. D.,  
2645 Lee, D., Nabel, J. E. M. S., Nassikas, A. A., Perugini, L., Rossi, S., Sitch, S., Viovy, N., Wiltshire, A., and Zaehle, S.:  
2646 Reconciling global-model estimates and country reporting of anthropogenic forest CO<sub>2</sub> sinks, *Nat. Clim. Chang.*, 8,  
2647 914–920, <https://doi.org/10.1038/s41558-018-0283-x>, 2018a.  
2648

2649 Grassi, G., Pilli, R., House, J., Federici, S., and Kurz, W. A.: Science-based approach for credible accounting of  
2650 mitigation in managed forests, *Carbon balance Manag.*, 13, 8, <https://doi.org/10.1186/s13021-018-0096-2>, 2018b.  
2651

2652 Grassi, G., Cescatti, A., Matthews, R., Duveiller, G., Amia, A., Federici, S., House, J., de Noblet-Ducoudré, N., Pilli,  
2653 R., and Vizzarri, M.: On the realistic contribution of European forests to reach climate objectives, *Carbon balance*  
2654 *Manag.*, 14, 8, <https://doi.org/10.1186/s13021-019-0123-y>, 2019.  
2655

2656 Grassi, G., Conchedda, G., Federici, S., Abad Viñas, R., Korosuo, A., Melo, J., Rossi, S., Sandker, M., Somogyi, Z.,  
2657 Vizzarri, M., and Tubiello, F. N.: Carbon fluxes from land 2000–2020: bringing clarity to countries' reporting, *Earth*  
2658 *Syst. Sci. Data*, 14, 4643–4666, <https://doi.org/10.5194/essd-14-4643-2022>, 2022a.

2659

2660 Grassi, G., Schwingshackl, C., Gasser, T., Houghton, R. A., Sitch, S., Canadell, J. G., Cescatti, A., Ciais, P., Federici,  
2661 S., Friedlingstein, P., Kurz, W. A., Sanz Sanchez, M. J., Abad Viñas, R., Alkama, R., Bultan, S., Ceccherini, G., Falk,  
2662 S., Kato, E., Kennedy, D., Knauer, J., Korosuo, A., Melo, J., McGrath, M. J., Nabel, J. E. M. S., Poulter, B.,  
2663 Romanovskaya, A. A., Rossi, S., Tian, H., Walker, A. P., Yuan, W., Yue, X., and Pongratz, J.: Harmonising the land-  
2664 use flux estimates of global models and national inventories for 2000–2020, *Earth Syst. Sci. Data*, 15, 1093–1114,  
2665 <https://doi.org/10.5194/essd-15-1093-2023>, 2023.

2666

2667 Gray, A. N., Whittier, T. R., and Harmon, M. E.: Carbon stocks and accumulation rates in Pacific Northwest forests:  
2668 role of stand age, plant community, and productivity, *Ecosphere*, 7, e01224, <https://doi.org/10.1002/ecs2.1224>, 2016.

2669

2670 Hansis, E., Davis, S. J., and Pongratz, J.: Relevance of methodological choices for accounting of land use change  
2671 carbon fluxes, *Glob. Biogeochem. Cy.*, 29, 1230–1246, <https://doi.org/10.1002/2014GB004997>, 2015.

2672

2673 Hartung, K., Bastos, A., Chini, L., Ganzenmüller, R., Havermann, F., Hurtt, G. C., Loughran, T., Nabel, J. E. M. S.,  
2674 Nützel, T., Obermeier, W. A., and Pongratz, J.: Bookkeeping estimates of the net land-use change flux – a sensitivity  
2675 study with the CMIP6 land-use dataset, *Earth Syst. Dynam.*, 12, 763–782, <https://doi.org/10.5194/esd-12-763-2021>,  
2676 2021.

2677

2678 Harris, I., Osborn, T.J., Jones, P., and Lister, D.: Version 4 of the CRU TS monthly high-resolution gridded  
2679 multivariate climate dataset, *Sci Data* 7, 109, <https://doi.org/10.1038/s41597-020-0453-3>, 2020.

2680

2681 Hastie, A., Lauerwald, R., Ciais, P., and Regnier, P. : Aquatic carbon fluxes dampen the overall variation of net  
2682 ecosystem productivity in the Amazon basin: An analysis of the interannual variability in the boundless carbon cycle,  
2683 *Global Change Biology*, 25 (6), pp. 2094-2111, DOI: 10.1111/gcb.14620, 2019.

2684

2685 Haverd, V., Smith, B., Cook, G. D., Briggs, P. R., Nieradzik, L., Roxburgh, S. H., Liedloff, A., Meyer, C. P., and  
2686 Canadell, J. G.: A stand-alone tree demography and landscape structure module for Earth system models, *Geophysical*  
2687 *Research Letters*, 40, 5234–5239, <https://doi.org/10.1002/grl.50972>, 2013.

2688

2689 Haverd, V., Smith, B., Nieradzik, L., Briggs, P. R., Woodgate, W., Trudinger, C. M., Canadell, J. G., and Cuntz, M.:  
2690 A new version of the CABLE land surface model (Subversion revision r4601) incorporating land use and land cover  
2691 change, woody vegetation demography, and a novel optimisation-based approach to plant coordination of  
2692 photosynthesis, *Geosci. Model Dev.*, 11, 2995–3026, <https://doi.org/10.5194/gmd-11-2995-2018>, 2018.

2693

2694 Houghton, R., Hobbie, J., Melillo, J., Moore, B., Peterson, B., Shaver, G., and Woodwell, G.: Changes in the carbon  
2695 content of terrestrial biota and soils between 1860 and 1980: A net release of CO<sub>2</sub> to the atmosphere, *Ecol. Monogr.*,  
2696 53, 235–262, <https://doi.org/10.2307/1942531>, 1983.

2697

2698 Houghton, R. A.: Revised estimates of the annual net flux of carbon to the atmosphere from changes in land use and  
2699 land management 1850–2000, *Tellus B*, 55, 378–390, <https://doi.org/10.3402/tellusb.v55i2.16764>, 2003.

2700

2701 Houghton, R. A., House, J. I., Pongratz, J., van der Werf, G. R., DeFries, R. S., Hansen, M. C., Le Quéré, C., and  
2702 Ramankutty, N.: Carbon emissions from land use and land-cover change, *Biogeosciences*, 9, 5125–5142,  
2703 <https://doi.org/10.5194/bg-9-5125-2012>, 2012.

2704

2705 Houghton, R. A. and Nassikas, A. A.: Global and regional fluxes of carbon from land use and land cover change  
2706 1850–2015, *Glob. Biogeochem. Cy.*, 31, 456–472, <https://doi.org/10.1002/2016GB005546>, 2017.

2707

2708 Hurtt, G. C., Chini, L., Sahajpal, R., Frohling, S., Bodirsky, B. L., Calvin, K., Doelman, J. C., Fisk, J., Fujimori, S.,  
2709 Klein Goldewijk, K., Hasegawa, T., Havlik, P., Heinemann, A., Humpenöder, F., Jungclaus, J., Kaplan, J. O., Kennedy,  
2710 J., Krisztin, T., Lawrence, D., Lawrence, P., Ma, L., Mertz, O., Pongratz, J., Popp, A., Poulter, B., Riahi, K.,  
2711 Shevliakova, E., Stehfest, E., Thornton, P., Tubiello, F. N., van Vuuren, D. P., and Zhang, X.: Harmonization of global  
2712 land use change and management for the period 850–2100 (LUH2) for CMIP6, *Geosci. Model Dev.*, 13, 5425–5464,  
2713 <https://doi.org/10.5194/gmd-13-5425-2020>, 2020.

2714

2715 ICOS RI: ICOS Atmosphere Release 2021-1 of Level 2 Greenhouse Gas Mole Fractions of CO<sub>2</sub>, CH<sub>4</sub>, N<sub>2</sub>O, CO,  
2716 meteorology and 14CO<sub>2</sub> [data set], <https://doi.org/10.18160/WJY7-5D06>, 2021.  
2717

2718 IPCC: Good Practice Guidance for Land use, Land use Change and Forestry, Chapter 3, 3.3, [https://www.ipcc-  
2720 ggip.iges.or.jp/public/gpglulucf/gpglulucf\\_files/GPG\\_LULUCF\\_FULLL.pdf](https://www.ipcc-<br/>2719 ggip.iges.or.jp/public/gpglulucf/gpglulucf_files/GPG_LULUCF_FULLL.pdf), (last access: 10 January 2022), 2003.

2721 IPCC: Guidelines for National Greenhouse Gas Inventories, Prepared by the National Greenhouse Gas Inventories  
2722 Programme. IGES, Japan, <https://www.ipcc-nggip.iges.or.jp/public/2006gl/>, 2006, (last access: 10 January 2022),  
2723 2006.  
2724

2725 IPCC: Refinement to the 2006 IPCC Guidelines for National Greenhouse Gas Inventories, available at:  
2726 <https://www.ipcc.ch/report/2019-refinement-to-the-2006-ipcc-guidelines-for-national-greenhouse-gas-inventories>,  
2727 (last access: 10 January 2022), 2019.  
2728

2729 IPCC: Supplement to the 2006 IPCC Guidelines for National Greenhouse Gas Inventories: Wetlands, edited by:  
2730 Hiraishi, T., Krug, T., Tanabe, K., Srivastava, N., Baasansuren, J., Fukuda, M., and Troxler, T. G., IPCC, Switzerland,  
2731 2014.  
2732

2733 IPCC: Summary for Policymakers. In: Climate Change 2021: The Physical Science Basis. Contribution of Working  
2734 Group I to the Sixth Assessment Report of the Intergovernmental Panel on Climate Change [Masson-Delmotte, V., P.  
2735 Zhai, A. Pirani, S.L. Connors, C. Péan, S. Berger, N. Caud, Y. Chen, L. Goldfarb, M.I. Gomis, M. Huang, K. Leitzell,  
2736 E. Lonnoy, J.B.R. Matthews, T.K. Maycock, T. Waterfield, O. Yelekçi, R. Yu, and B. Zhou (eds.)].Cambridge  
2737 University Press, Cambridge, United Kingdom and New York, NY, USA, pp. 3–32, doi:10.1017/9781009157896.001,  
2738 2021.  
2739

2740 Izaurrealde, R. C., Williams, J. R., McGill, W. B., Rosenberg, N.J., and Jakas, M. C. Q.: Simulating soil C dynamics  
2741 with EPIC: Model description and testing against long-term data, *Ecol. Model.* 192, 362–384,  
2742 <https://doi.org/10.1016/j.ecolmodel.2005.07.010>, 2006.  
2743

2744 Janssens-Maenhout, G., Crippa, M., Guizzardi, D., Muntean, M., Schaaf, E., Dentener, F., Bergamaschi, P., Pagliari,  
2745 V., Olivier, J. G. J., Peters, J. A. H. W., van Aardenne, J. A., Monni, S., Doering, U., Petrescu, A. M. R., Solazzo, E.,

2746 and Oreggioni, G. D.: EDGAR v4.3.2 Global Atlas of the three major greenhouse gas emissions for the period 1970–  
2747 2012, *Earth Syst. Sci. Data*, 11, 959-1002, <https://doi.org/10.5194/essd-11-959-2019>, 2019.

2748

2749 Jägermeyr, J., Müller, C., Ruane, A.C., Elliott, J., Balkovic, J., Castillo, O., Faye, B., Foster, I., Folberth, C., Franke,  
2750 J.A., Fuchs, K., Guarin, J.R., Heinke, J., Hoogenboom, G., Iizumi, T., Jain, A.K., Kelly, D., Khabarov, N., Lange, S.,  
2751 Lin, T.-S., Liu, W., Mialyk, O., Minoli, S., Moyer, E.J., Okada, M., Phillips, M., Porter, C., Rabin, S.S., Scheer, C.,  
2752 Schneider, J.M., Schyns, J.F., Skalsky, R., Smerald, A., Stella, T., Stephens, H., Webber, H., Zabel, F., and  
2753 Rosenzweig, C.: Climate impacts on global agriculture emerge earlier in new generation of climate and crop models.  
2754 *Nat. Food*, 2, 873–885, <https://doi.org/10.1038/s43016-021-00400-y>, 2021.

2755

2756 Jenkinson, D. S., Hart, P. B. S., Rayner, J. H., and Parry, L. C.: Modelling the turnover of organic matter in long-term  
2757 experiments at Rothamsted, *INTECOL Bulletin*, 15, 1987.

2758

2759 Jenkinson, D. S., and Rayner, J. H.: The turnover of organic matter in some of the Rothamsted classical experiments,  
2760 *Soil. Sci.*, 123, 298–305, <https://doi.org/10.1097/00010694-197705000-00005>, 1977.

2761

2762 Jonsson, R., Blujdea, V. N., Fiorese, G., Pilli, R., Rinaldi, F., Baranzelli, C., and Camia, A.: Outlook of the European  
2763 forest-based sector: forest growth, harvest demand, wood-product markets, and forest carbon dynamics implications,  
2764 *iForest*, 11, 315–328, <https://doi.org/10.3832/ifer2636-011>, 2018.

2765

2766 Jonsson, R., Rinaldi, F., Pilli, R., Fiorese, G., Hurmekoski, E., Cazzaniga, N., Robert, N., and Camia, A: Boosting the  
2767 EU forest-based bioeconomy: Market, climate, and employment impacts, *Technological Forecasting and Social*  
2768 *Change*, 163, 120478, <https://doi.org/10.1016/j.techfore.2020.120478>, 2021.

2769

2770 Kanamitsu, M., Ebisuzaki, W., Woollen, J., Yang, S., Hnilo, J. J., Fiorino, M., and Potter, G. L.: NCEP–DOE AMIP-  
2771 II Reanalysis (R-2). *Bulletin of the American Meteorological Society*, 83, 1631-1644, <https://doi.org/10.1175/BAMS->  
2772 [83-11-1631](https://doi.org/10.1175/BAMS-83-11-1631), 2002.

2773

2774 Klein Goldewijk, K., Beusen, A., Doelman, J., and Stehfest, E.: Anthropogenic land-use estimates for the Holocene;  
2775 HYDE 3.2, *Earth Syst. Sci. Data*, 9, 927–953, <https://doi.org/10.5194/essd9-927-2017>, 2017a.

2776

2777 Klein Goldewijk, K., Dekker, S. C., and van Zanden, J. L.: Per capita estimations of long-term historical land use and  
2778 the consequences for global change research, *J. Land Use Sci.*, 12, 313– 337,  
2779 <https://doi.org/10.1080/1747423X.2017.1354938>, 2017b.

2780

2781 Koehl, M., Hildebrandt, R., Olschofsky, K., Koehler, R., Roetzer, T., Mette, T., Pretzsch, H., Koethke, M., Dieter,  
2782 M., Abiy, M., Makeschin, F., and Kenter, B.: Combating the effects of climatic change on forests by mitigation  
2783 strategies, *Carbon Balance and Management*, 5, 8, <https://doi.org/10.1186/1750-0680-5-8>, 2010.

2784

2785 Konovalov, I. B., Berezin, E. V., Ciais, P., Broquet, G., Zhuravlev, R. V., and Janssens-Maenhout, G.: Estimation of  
2786 fossil-fuel CO<sub>2</sub> emissions using satellite measurements of "proxy" species, *Atmos. Chem. Phys.*, 16, 13509–13540,  
2787 <https://doi.org/10.5194/acp-16-13509-2016>, 2016.

2788

2789 Konovalov, I. B., and Lvova, D. A. : First, fast-track, Re-analysis of the national scale CO<sub>2</sub> anthropogenic emissions  
2790 over 2005-2015, internal VERIFY report:  
2791 [https://projectsworkspace.eu/sites/VERIFY/Deliverables/WP2/VERIFY\\_D2.10\\_First,%20fast-track,%20Re-](https://projectsworkspace.eu/sites/VERIFY/Deliverables/WP2/VERIFY_D2.10_First,%20fast-track,%20Re-analysis%20of%20the%20national%20scale%20CO2%20anthropogenic%20emissions%20over%202005-2015.pdf)  
2792 [analysis%20of%20the%20national%20scale%20CO<sub>2</sub>%20anthropogenic%20emissions%20over%202005-2015.pdf](https://projectsworkspace.eu/sites/VERIFY/Deliverables/WP2/VERIFY_D2.10_First,%20fast-track,%20Re-analysis%20of%20the%20national%20scale%20CO2%20anthropogenic%20emissions%20over%202005-2015.pdf),  
2793 (last access: 15 September 2020), 2018.

2794

2795 Kountouris, P., Gerbig, C., Rödenbeck, C., Karstens, U., Koch, T. F., and Heimann, M.: Technical Note: Atmospheric  
2796 CO<sub>2</sub> inversions on the mesoscale using data-driven prior uncertainties: methodology and system evaluation, *Atmos.*  
2797 *Chem. Phys.*, 18, 3027–3045, <https://doi.org/10.5194/acp-18-3027-2018>, 2018a.

2798

2799 Kountouris, P., Gerbig, C., Rödenbeck, C., Karstens, U., Koch, T. F., and Heimann, M.: Atmospheric CO<sub>2</sub> inversions  
2800 on the mesoscale using data-driven prior uncertainties: quantification of the European terrestrial CO<sub>2</sub> fluxes, *Atmos.*  
2801 *Chem. Phys.*, 18, 3047–3064, <https://doi.org/10.5194/acp-18-3047-2018>, 2018b.

2802

2803 Krinner, G., Viovy, N., de Noblet-Ducoudré N., Ogée, J., Polcher, J., Friedlingstein, P., Ciais, P., Sitch, S., and  
2804 Prentice, I. C.: A dynamic global vegetation model for studies of the coupled atmosphere-biosphere system, *Global*  
2805 *Biogeochemical Cycles*, 19, GB1015, doi:10.1029/2003GB002199, 2005.

2806

2807 Kumarathunge, D. P., Medlyn, B. E., Drake, J. E., Tjoelker, M. G., Aspinwall, M. J., Battaglia, M., Cano, F. J., Carter,  
2808 K. R., Cavaleri, M. A., Cernusak, L. A., Chambers, J. Q., Crous, K. Y., De Kauwe, M. G., Dillaway, D. N., Dreyer,  
2809 E., Ellsworth, D. S., Ghannoum, O., Han, Q., Hikosaka, K., Jensen, A. M., Kelly, J. W. G., Kruger, E. L., Mercado,  
2810 L. M., Onoda, Y., Reich, P. B., Rogers, A., Slot, M., Smith, N. G., Tarvainen, L., Tissue, D. T., Togashi, H. F.,  
2811 Tribuzy, E. S., Uddling, J., Vårhammar, A., Wallin, G., Warren, J. M. and Way, D. A.: Acclimation and adaptation  
2812 components of the temperature dependence of plant photosynthesis at the global scale, *New Phytologist*, 222, 768-  
2813 784, <https://doi.org/10.1111/nph.15668>, 2019.

2814

2815 Kurz, W. A., Dymond, C. C., White, T. M., Stinson, G., Shaw, C. H., Rampley, G. J., Smyth, C., Simpson, B. N.,  
2816 Neilson, E. T., Trofymow, J. A., Metsaranta, J., and Apps, M. J.: CBMCF3: a model of carbon dynamics in forestry  
2817 and land use change implementing IPCC standards, *Ecol. Model.*, 220, 480–504,  
2818 <https://doi.org/10.1016/j.ecolmodel.2008.10.018>, 2009.

2819

2820 Lauerwald, R., Laruelle, G. G., Hartmann, J., Ciais, P., and Regnier, P. A. G. :Spatial patterns in CO2 evasion from  
2821 the global river network, *Global Biogeochemical Cycles*, 29, 534–554. <https://doi.org/10.1002/2014GB004941015>,  
2822 2015.

2823

2824 Lawrence, D. M., Oleson, K. W., Flanner, M. G., Thornton, P. E., Swenson, S. C., Lawrence, P. J., Zeng, X., Yang,  
2825 Z.-L., Levis, S., Sakaguchi, K., Bonan, G. B., and Slater, A. G.: Parameterization Improvements and Functional and  
2826 Structural Advances in Version 4 of the Community Land Model, *Journal of Advances in Modeling Earth Systems*,  
2827 3, M03001, DOI 10.1029/2011MS000045, 2011.

2828

2829 Le Quéré, C., Raupach, M. R., Canadell, J. G., Marland, G., Bopp, L., Ciais, P., Conway, T. J., Doney, S. C., Feely,  
2830 R. A., Foster, P., Friedlingstein, P., Gurney, K., Houghton, R. A., House, J. I., Huntingford, C., Levy, P. E., Lomas,  
2831 M. R., Majkut, J., Metz, N., Ometto, J. P., Peters, G. P., Prentice, I. C., Randerson, J. T., Running, S. W., Sarmiento,  
2832 J. L., Schuster, U., Sitch, S., Takahashi, T., Viovy, N., van der Werf, G. R., and Woodward, F. I.: Trends in the sources  
2833 and sinks of carbon dioxide, *Nat. Geosci.*, 2, 831–836, <https://doi.org/10.1038/ngeo689>, 2009.

2834

2835 Liski, J., Palosuo, T., Peltoniemi, M., and Sievänen, R.: Carbon and decomposition model Yasso for forest soils, *Ecol.*  
2836 *Model.*, 189, 168–182, <https://doi.org/10.1016/J.ECOLMODEL.2005.03.005>, 2005.

2837



2838 Liu, J., Baskaran, L., Bowman, K., Schimel, D., Bloom, A. A., Parazoo, N. C., Oda, T., Carroll, D., Menemenlis, D.,  
2839 Joiner, J., Commancin, R., Daube, B., Gatti, L. V., McKain, K., Miller, J., Stephens, B. B., Sweeney, C., and Wofsy,  
2840 S.: Carbon Monitoring System Flux Net Biosphere Exchange 2020 (CMS-Flux NBE 2020), *Earth Syst. Sci. Data*, 13,  
2841 299–330, <https://doi.org/10.5194/essd-13-299-2021>, 2021.

2842

2843 Lugato, E., Panagos, P., Bampa, F., Jones, A., Montanarella, L.: A new baseline of organic carbon stock in European  
2844 agricultural soils using a modeling approach, *Glob. Change Biol.*, 20, 313–326, <https://doi.org/10.1111/gcb.12292>,  
2845 2014.

2846

2847 Lurton, T., Balkanski, Y., Bastrikov, V., Bekki, S., Bopp, L., Braconnot, P., Brockmann, P., Cadule, P., Contoux, C.,  
2848 Cozic, A., Cugnet, D., Dufresne, J.-L., Éthé, C., Foujols, M.-A., Ghattas, J., Hauglustaine, D., Hu, R.-M., Kageyama,  
2849 M., Khodri, M., Lebas, N., Levvasseur, G., Marchand, M., Ottlé, C., Peylin, P., Sima, A., Szopa, S., Thiéblemont,  
2850 R., Vuichard, N., and Boucher, O.: Implementation of the CMIP6 Forcing Data in the IPSL-CM6A-LR Model. *Journal*  
2851 *of Advances in Modeling Earth Systems*, 12(4), e2019MS001940, <https://doi.org/10.1029/2019MS001940>, 2020.

2852

2853 Luysaert, S., Abril, G., Andres, R., Bastviken, D., Bellassen, V., Bergamaschi, P., Bousquet, P., Chevallier, F., Ciais,  
2854 P., Corazza, M., Dechow, R., Erb, K.-H., Etiope, G., Fortems-Cheiney, A., Grassi, G., Hartmann, J., Jung, M.,  
2855 Lathière, J., Lohila, A., Mayorga, E., Moosdorf, N., Njakou, D. S., Otto, J., Papale, D., Peters, W., Peylin, P.,  
2856 Raymond, P., Rödenbeck, C., Saarnio, S., Schulze, E.-D., Szopa, S., Thompson, R., Verkerk, P. J., Vuichard, N.,  
2857 Wang, R., Wattenbach, M., and Zaehle, S.: The European land and inland water CO<sub>2</sub>, CO, CH<sub>4</sub> and N<sub>2</sub>O balance  
2858 between 2001 and 2005, *Biogeosciences*, 9, 3357–3380, <https://doi.org/10.5194/bg-9-3357-2012>, 2012.

2859

2860 Luysaert, S., Marie, G., Valade, A., Chen, Y. Y., Njakou Djomo, S., Ryder, J., Otto, J., Naudts, K., Lansø, A. S.,  
2861 Ghattas, J., and McGrath, M. J.: Trade-offs in using European forests to meet climate objectives, *Nature*, 562, 259–  
2862 262, <https://doi.org/10.1038/s41586-018-0577-1>, 2018.

2863

2864 Mason Earles, J., Yeh, S. and Skog, K.: Timing of carbon emissions from global forest clearance, *Nature Clim Change*,  
2865 2, 682–685, <https://doi.org/10.1038/nclimate1535>, 2012.

2866

2867 McGrath, M. J., Petrescu, A. M. R., Peylin, P., Andrew, R. M., Matthews, B., Dentener, F., Balkovič, J., Bastrikov,  
2868 V., Becker, M., Broquet, G., Ciais, P., Fortems, A., Ganzenmüller, R., Grassi, G., Harris, I., Jones, M., Knauer, J.,

2869 Kuhnert, M., Monteil, G., Munassar, S., Palmer, P. I., Peters, G. P., Qiu, C., Schelhaas, M.-J., Tarasova, O., Vizzarri,  
2870 M., Winkler, K., Balsamo, G., Berchet, A., Briggs, P., Brockmann, P., Chevallier, F., Conchedda, G., Crippa, M.,  
2871 Dellaert, S., Denier van der Gon, H. A. C., Filipek, S., Friedlingstein, P., Fuchs, R., Gauss, M., Gerbig, C., Guizzardi,  
2872 D., Günther, D., Houghton, R. A., Janssens-Maenhout, G., Lauerwald, R., Lerink, B., Luijkx, I. T., Moulas, G.,  
2873 Muntean, M., Nabuurs, G.-J., Paquirissamy, A., Perugini, L., Peters, W., Pilli, R., Pongratz, J., Regnier, P., Scholze,  
2874 M., Serengil, Y., Smith, P., Solazzo, E., Thompson, R. L., Tubiello, F. N., Vesala, T. and Walther, S.: Data for the  
2875 consolidated European synthesis of CO<sub>2</sub> emissions and removals for EU27 and UK: 1990-2020,  
2876 <https://doi.org/10.5281/zenodo.8148461>, 2023.

2877

2878 Menut, L., Bessagnet, B., Khvorostyanov, D., Beekmann, M., Blond, N., Colette, A., Coll, I., Curci, G., Foret, G.,  
2879 Hodzic, A., Mailler, S., Meleux, F., Monge, J.-L., Pison, I., Siour, G., Turquety, S., Valari, M., Vautard, R., and  
2880 Vivanco, M. G.: CHIMERE 2013: a model for regional atmospheric composition modeling, *Geosci. Model Dev.*, 6,  
2881 981–1028, <https://doi.org/10.5194/gmd-6-981-2013>, 2013.

2882

2883 Messenger, M. L., Lehner, B., Grill, G., Nedeva, I. and Schmitt, O.: Estimating the volume and age of water stored in  
2884 global lakes using a geo-statistical approach, *Nat. Commun.*, 7, 13603, doi:10.1038/ncomms13603, 2016.

2885

2886 Monteil, G., Broquet, G., Scholze, M., Lang, M., Karstens, U., Gerbig, C., Koch, F.-T., Smith, N. E., Thompson, R.  
2887 L., Luijkx, I. T., White, E., Meesters, A., Ciais, P., Ganesan, A. L., Manning, A., Mischurow, M., Peters, W., Peylin,  
2888 P., Tarniewicz, J., Rigby, M., Rödenbeck, C., Vermeulen, A., and Walton, E. M.: The regional European atmospheric  
2889 transport inversion comparison, EUROCOM: first results on European-wide terrestrial carbon fluxes for the period  
2890 2006–2015, *Atmos. Chem. Phys.*, 20, 12063–12091, <https://doi.org/10.5194/acp-20-12063-2020>, 2020.

2891

2892 Monteil, G., and Scholze, M.: Regional CO<sub>2</sub> inversions with LUMIA, the Lund University Modular Inversion  
2893 Algorithm, v1.0, *Geoscientific Model Development*, 14, 3383–3406, <https://doi.org/10.5194/gmd-14-3383-2021>,  
2894 2021.

2895

2896 Mueller, N., Gerber, J., Johnston, M., Ray, D. K., Ramankutty, N., and Foley, J. A.: Closing yield gaps through nutrient  
2897 and water management, *Nature*, 490, 254–257, <https://doi.org/10.1038/nature11420>, 2012.

2898

2899 Muñoz-Sabater, J.: ERA5-Land hourly data from 1981 to present, Copernicus Climate Change Service (C3S) Climate  
2900 Data Store (CDS), DOI 10.24381/cds.e2161bac, (last access: 1 May 2021), 2019.  
2901

2902 Muñoz-Sabater, J., Dutra, E., Agustí-Panareda, A., Albergel, C., Arduini, G., Balsamo, G., Boussetta, S., Choulga,  
2903 M., Harrigan, S., Hersbach, H., Martens, B., Miralles, D. G., Piles, M., Rodríguez-Fernández, N. J., Zsoter, E.,  
2904 Buontempo, C., and Thépaut, J.-N.: ERA5-Land: A state-of-the-art global reanalysis dataset for land applications,  
2905 Earth Syst. Sci. Data, 13, 4349–4383, <https://doi.org/10.5194/essd-13-4349-2021>, 2021.  
2906

2907 Nabuurs, G, Lindner, M, Verkerk, H, Gunia, K, Deda, P, Michalak, R, and Grassi, G.: First signs of carbon sink  
2908 saturation in European forest biomass, Nature Climate Change 3, 792-796, <https://doi.org/10.1038/nclimate1853>,  
2909 2013.  
2910

2911 Nabuurs, G. J., Delacote, P., Ellison, D., Hanewinkel, M., Hetemäki, L., Lindner, M., and Ollikainen, M.: By 2050  
2912 the mitigation effects of EU forests could nearly double through climate smart forestry, Forests, 8, 484,  
2913 <https://doi.org/10.3390/f8120484>, 2017.  
2914

2915 Nabuurs, G. J., Arets, E. J. M. M., and Schelhaas, M. J.: Understanding the implications of the EU-LULUCF regulation  
2916 for the wood supply from EU forests to the EU, Carbon Balance Manag., 13, 18, [https://doi.org/10.1186/s13021-018-](https://doi.org/10.1186/s13021-018-0107-3)  
2917 0107-3, 2018.  
2918

2919 Naegler, T.: Reconciliation of excess 14C-constrained global CO2 piston velocity estimates, Tellus B, 61, 372–384,  
2920 <https://doi.org/10.1111/j.1600-0889.2008.00408.x>, 2009.  
2921

2922 Naudts, K., Chen, Y., McGrath, M., Ryder, J., Valade, A., Otto, J., and Luyssaert, S.: Europe’s forest management  
2923 did not mitigate climate warming, Science, 351, 597–600, <https://doi.org/10.1126/science.aad7270>, 2016.  
2924

2925 Niwa, Y., Fujii, Y., Sawa, Y., Iida, Y., Ito, A., Satoh, M., Imasu, R., Tsuboi, K., Matsueda, H., and Saigusa, N.: A  
2926 4D-Var inversion system based on the icosahedral grid model (NICAM-TM 4D-Var v1.0) – Part 2: Optimization  
2927 scheme and identical twin experiment of atmospheric CO2 inversion, Geosci. Model Dev., 10, 2201–2219,  
2928 <https://doi.org/10.5194/gmd-10-2201-2017>, 2017.  
2929

2930 Oleson, K.: Technical Description of the Community Land Model (CLM). NCAR Technical Note. TN-478+STR.  
2931 10.5065/D6RR1W7M, 2010.  
2932  
2933 Petrescu, A. M. R., Peters, G. P., Janssens-Maenhout, G., Ciais, P., Tubiello, F. N., Grassi, G., Nabuurs, G.-J., Leip,  
2934 A., Carmona-Garcia, G., Winiwarter, W., Höglund-Isaksson, L., Günther, D., Solazzo, E., Kiesow, A., Bastos, A.,  
2935 Pongratz, J., Nabel, J. E. M. S., Conchedda, G., Pilli, R., Andrew, R. M., Schelhaas, M.-J., and Dolman, A. J.:  
2936 European anthropogenic AFOLU greenhouse gas emissions: a review and benchmark data, *Earth Syst. Sci. Data*, 12,  
2937 961–1001, <https://doi.org/10.5194/essd-12-961-2020>, 2020.  
2938  
2939 Petrescu, A. M. R., McGrath, M. J., Andrew, R. M., Peylin, P., Peters, G. P., Ciais, P., Broquet, G., Tubiello, F. N.,  
2940 Gerbig, C., Pongratz, J., Janssens-Maenhout, G., Grassi, G., Nabuurs, G.-J., Regnier, P., Lauerwald, R., Kuhnert, M.,  
2941 Balkovič, J., Schelhaas, M.-J., Denier van der Gon, H. A. C., Solazzo, E., Qiu, C., Pilli, R., Konovalov, I. B.,  
2942 Houghton, R. A., Günther, D., Perugini, L., Crippa, M., Ganzenmüller, R., Luijkx, I. T., Smith, P., Munassar, S.,  
2943 Thompson, R. L., Conchedda, G., Monteil, G., Scholze, M., Karstens, U., Brockmann, P., and Dolman, A. J.: The  
2944 consolidated European synthesis of CO<sub>2</sub> emissions and removals for the European Union and United Kingdom: 1990–  
2945 2018, *Earth Syst. Sci. Data*, 13, 2363–2406, <https://doi.org/10.5194/essd-13-2363-2021>, 2021b.  
2946  
2947 Pilli, R., Grassi, G., Kurz, W. A., Moris, J. V., and Viñas, R. A.: Modelling forest carbon stock changes as affected  
2948 by harvest and natural disturbances – II. EU-level analysis including land use changes, *Carbon Balance and*  
2949 *Management*, 11, 20, <https://doi.org/10.1186/s13021-016-0059-4>, 2016.  
2950  
2951 Pilli, R., Grassi, G., Kurz, W. A., Fiorese, G., and Cescatti, A.: The European forest sector: past and future carbon  
2952 budget and fluxes under different management scenarios, *Biogeosciences*, 14, 2387–2405, [https://doi.org/10.5194/bg-](https://doi.org/10.5194/bg-14-2387-2017)  
2953 [14-2387-2017](https://doi.org/10.5194/bg-14-2387-2017), 2017.  
2954  
2955 Pilli, R., Alkama, R., Cescatti, A., Kurz, W. A., and Grassi, G.: The European forest carbon budget under future  
2956 climate conditions and current management practices, *Biogeosciences*, 19, 3263–3284, [https://doi.org/10.5194/bg-19-](https://doi.org/10.5194/bg-19-3263-2022)  
2957 [3263-2022](https://doi.org/10.5194/bg-19-3263-2022), 2022.  
2958  
2959 Pinty B., Janssens-Maenhout, G., Dowell, M., Zunker, H., Brunhes, T., Ciais, P., Dee, D., Denier van der Gon, H.,  
2960 Dolman, H., Drinkwater, M., Engelen, R., Heimann, M., Holmlund, K., Husband, R., Kentarchos, A., Meijer, Y.,

2961 Palmer, P., and Scholze, M.: An Operational Anthropogenic CO<sub>2</sub> Emissions Monitoring & Verification Support  
2962 capacity - Baseline Requirements, Model Components and Functional Architecture, European Commission Joint  
2963 Research Centre, EUR 28736 EN, doi: 10.2760/39384, 2017.

2964

2965 Pisso, I., Sollum, E., Grythe, H., Kristiansen, N. I., Cassiani, M., Eckhardt, S., Arnold, D., Morton, D., Thompson, R.  
2966 L., Groot Zwaaftink, C. D., Evangeliou, N., Sodemann, H., Haimberger, L., Henne, S., Brunner, D., Burkhardt, J. F.,  
2967 Fouilloux, A., Brioude, J., Philipp, A., Seibert, P., and Stohl, A.: The Lagrangian particle dispersion model  
2968 FLEXPART version 10.4, *Geosci. Model Dev.*, 12, 4955–4997, <https://doi.org/10.5194/gmd-12-4955-2019>, 2019.

2969

2970 Polcher, J., McAvaney, B., Viterbo, P., Gaertner, M.-A., Hahmann, A., Mahfouf, J.-F., Noilhan, J., Phillips, T.,  
2971 Pitman, A.J., Schlosser, C.A., Schulz, J.-P., Timbal, B., Verseghy D., and Xue, Y.: A proposal for a general interface  
2972 between land-surface schemes and general circulation models, *Global and Planetary Change*, 19, 263-278,  
2973 [https://doi.org/10.1016/S0921-8181\(98\)00052-6](https://doi.org/10.1016/S0921-8181(98)00052-6), 1998.

2974

2975 Pongratz, J., Reick, C. H., Houghton, R. A., and House, J. I.: Terminology as a key uncertainty in net land use and  
2976 land cover change carbon flux estimates, *Earth Syst. Dynam.*, 5, 177–195, <https://doi.org/10.5194/esd-5-177-2014>,  
2977 2014.

2978

2979 Pongratz, J., Schwingshackl, C., Bultan, S., Obermeier, W., Havermann, F., and Guo, S.: Land Use Effects on Climate:  
2980 Current State, Recent Progress, and Emerging Topics. *Curr Clim Change Rep*, 7, 99–120,  
2981 <https://doi.org/10.1007/s40641-021-00178-y>, 2021.

2982

2983 Pongratz, J., Reick, C., Raddatz, T., and Claussen, M.: A reconstruction of global agricultural areas and land cover  
2984 for the last millennium, *Global Biogeochemical Cycles*, 22, <https://doi.org/10.1029/2007GB003153>, 2008.

2985

2986 Prentice, I. C., Liang, X., Medlyn, B. E., and Wang, Y.-P.: Reliable, robust and realistic: the three R's of next-  
2987 generation land-surface modelling, *Atmos. Chem. Phys.*, 15, 5987–6005, <https://doi.org/10.5194/acp-15-5987-2015>,  
2988 2015.

2989

2990 Ramankutty, N., and Foley, J. A.: Estimating historical changes in global land cover: Croplands from 1700 to 1992,  
2991 *Global biogeochemical cycles*, 13, 997-1027, <https://doi.org/10.1029/1999GB900046>, 1999.

2992

2993 Raymond, P. A., Hartmann, J., Lauerwald, R., Sobek, S., McDonald, C., Hoover, M., and Guth, P. : Global carbon  
2994 dioxide emissions from inland waters, *Nature*, 503, 355–359, <https://doi.org/10.1038/nature12760>, 2013.  
2995  
2996 RECAP2: <https://www.globalcarbonproject.org/Reccap/index.htm>, last access: 22 November 2022.  
2997  
2998 Regnier, P., Friedlingstein, P., Ciais, P., Mackenzie, F. T., Gruber, N., Janssens, I. A., Laruelle, G. G., Lauerwald, R.,  
2999 Luysaert, S., Andersson, A. J., Arndt, S., Arnosti, C., Borges, A. V., Dale, A. W., Gallego-Sala, A., Godd ris, Y.,  
3000 Goossens, N., Hartmann, J., Heinze, C., Ilyina, T., Joos, F., LaRowe, D. E., Leifeld, J., Meysman, F. J. R., Munhoven,  
3001 G., Raymond, P. A., Spahni, R., Suntharalingam, P., and Thullner, M.: Anthropogenic perturbation of the carbon  
3002 fluxes from land to ocean, *Nature Geosci*, 6, 597–607, <https://doi.org/10.1038/ngeo1830>, 2013.  
3003  
3004 Reichstein, M., Bahn, M., Ciais, P., Frank, D., Mahecha, M. D., Seneviratne, S. I., Zscheischler, J., Beer, C.,  
3005 Buchmann, N., Frank, D. C., Papale, D., Rammig, A., Smith, P., Thonicke, K., van der Velde, M., Vicca, S., Walz,  
3006 A., and Wattenbach, M.: Climate extremes and the carbon cycle, *Nature*, 500, 287-95, doi: 10.1038/nature12350,  
3007 2013.  
3008  
3009 Resplandy, L., Keeling, R.F., R denbeck, C. Stephens, B. B., Khatiwala, S., Rodgers, K. B., Long, M. C., Bopp, L.,  
3010 and Tans, P. P.: Revision of global carbon fluxes based on a reassessment of oceanic and riverine carbon transport,  
3011 *Nature Geosci*, 11, 504–509, <https://doi.org/10.1038/s41561-018-0151-3>, 2018.  
3012  
3013 R denbeck, C.: Estimating CO2 sources and sinks from atmospheric mixing ratio measurements using a global  
3014 inversion of atmospheric transport, Tech. Rep. 6, Max Planck Institute for Biogeochemistry, Jena, Germany, 2005.  
3015  
3016 R denbeck, C., Gerbig, C., Trusilova, K., and Heimann, M.: A two-step scheme for high-resolution regional  
3017 atmospheric trace gas inversions based on independent models, *Atmos. Chem. Phys.*, 9, 5331–5342,  
3018 <https://doi.org/10.5194/acp-9-5331-2009>, 2009.  
3019  
3020 R denbeck, C., Bakker, D. C., Metzl, N., Olsen, A., Sabine, C., Cassar, N., Reum, F., Keeling, R. F. and Heimann,  
3021 M.: Interannual sea–air CO2 flux variability from an observation-driven ocean mixed-layer scheme, *Biogeosciences*,  
3022 11, 4599-4613, <https://doi.org/10.5194/bg-11-4599-2014>, 2014.  
3023  
3024 Salln s, O.: A matrix model of the Swedish forest, *Studia Forestalia Suecica*, 183, 1-23,  
3025 <https://pub.epsilon.slu.se/4514/>, 1990.  
3026  
3027 Scarlet, N, Martinov, M, and Dallemand, J.F.: Assessment of the availability of agricultural crop residues in the  
3028 European Union: potential and limitations for bioenergy use, *Waste Manag*, 10, 1889-97, doi:  
3029 10.1016/j.wasman.2010.04.016, 2010.

3030

3031 Schamweber, T., Smiljanic, M., Cruz-García, R., Manthey, M., and Wilmking, M.: Tree growth at the end of the 21st  
3032 century - the extreme years 2018/19 as template for future growth conditions, *Environ. Res. Lett.*, 15, 074022,  
3033 <https://doi.org/10.1088/1748-9326/ab865d>, 2020.

3034

3035 Schelhaas, M.-J., Nabuurs, G.-J., Verkerk, P.J., Hengeveld, G., Packalen, T., Sallnäs, O., Pilli, R., Grassi, G., Forsell,  
3036 N., Frank, S., Gusti, M., and Havlik, P.: Forest Resource Projection Tools at the European Level. In: Barreiro, S.,  
3037 Schelhaas, M.-J., McRoberts, R.E., Kändler, G. (Eds.), *Forest Inventory-based Projection Systems for Wood and*  
3038 *Biomass Availability*, Springer International Publishing, Cham, pp. 49-68, 2017.

3039

3040 Schuldt, K. N., Jacobson, A. R., Aalto, T., Andrews, A., Bakwin, P., Bergamaschi, P., Biermann, T., Biraud, S. C.,  
3041 Chen, H., Colomb, A., Conil, S., Cristofanelli, P., De Mazière, M., De Wekker, S., Delmotte, M., Dlugokencky, E.,  
3042 Emmenegger, L., Fischer, M. L., Hatakka, J., Heliasz, M., Hermanssen, O., Holst, J., Jaffe, D., Karion, A., Kazan, V.,  
3043 Keronen, P., Kominkova, K., Kubistin, D., Laurent, O., Laurila, T., Lee, J., Lehner, I., Leuenberger, M., Lindauer,  
3044 M., Lopez, M., Mammarella, I., Manca, G., Marek, M. V., McKain, K., Miller, J. B., Miller, C. E., Myhre, C. L.,  
3045 Mölder, M., Müller-Williams, J., Piacentino, S., Pichon, J. M., Plass-Duelmer, C., Ramonet, M., Scheeren, B.,  
3046 Schumacher, M., Sha, M. K., Sloop, C. D., Smith, P., Steinbacher, M., Sweeney, C., Tans, P., Thoning, K., Trisolino,  
3047 P., Tørseth, K., Viner, B., Vitkova, G., di Sarra, A. G.: Multi-laboratory compilation of atmospheric carbon dioxide  
3048 data for the period 2020-2021; obspack\_co2\_1\_NRT\_v6.1\_2021-02-02; NOAA Earth System Research Laboratory,  
3049 Global Monitoring Laboratory [data set], <http://doi.org/10.25925/20210108>, 2021a.

3050

3051 Schuldt, K. N., Mund, J., Lujikx, I. T., Aalto, T., Abshire, J. B., Aikin, K., Andrews, A., Aoki, S., Apadula, F., Baier,  
3052 B., Bakwin, P., Bartyzel, J., Bentz, G., Bergamaschi, P., Beyersdorf, A., Biermann, T., Biraud, S. C., Boenisch, H.,  
3053 Bowling, D., Brailsford, G., Chen, G., Chen, H., Chmura, L., Clark, S., Climadat, S., Colomb, A., Commane, R.,  
3054 Conil, S., Cox, A., Cristofanelli, P., Cuevas, E., Curcoll, R., Daube, B., Davis, K., De Mazière, M., De Wekker, S.,  
3055 Coletta, J. D., Delmotte, M., DiGangi, J. P., Dlugokencky, E., Elkins, J. W., Emmenegger, L., Fang, S., Fischer, M.  
3056 L., Forster, G., Frumau, A., Galkowski, M., Gatti, L. V., Gehrlein, T., Gerbig, C., Gheusi, F., Gloor, E., Gomez-  
3057 Trueba, V., Goto, D., Griffis, T., Hammer, S., Hanson, C., Haszpra, L., Hatakka, J., Heimann, M., Heliasz, M., Hensen,  
3058 A., Hermanssen, O., Hintsa, E., Holst, J., Ivakhov, V., Jaffe, D., Joubert, W., Karion, A., Kawa, S. R., Kazan, V.,  
3059 Keeling, R., Keronen, P., Kolari, P., Kominkova, K., Kort, E., Kozlova, E., Krummel, P., Kubistin, D., Labuschagne,  
3060 C., Lam, D. H., Langenfelds, R., Laurent, O., Laurila, T., Lauvaux, T., Lavric, J., Law, B., Lee, O. S., Lee, J., Lehner,  
3061 I., Leppert, R., Leuenberger, M., Levin, I., Levula, J., Lin, J., Lindauer, M., Loh, Z., Lopez, M., Machida, T.,  
3062 Mammarella, I., Manca, G., Manning, A., Manning, A., Marek, M. V., Martin, M. Y., Matsueda, H., McKain, K.,  
3063 Meijer, H., Meinhardt, F., Merchant, L., Mihalopoulos, N., Miles, N., Miller, C. E., Miller, J. B., Mitchell, L.,  
3064 Montzka, S., Moore, F., Morgan, E., Morgui, J.-A., Morimoto, S., Munger, B., Munro, D., Myhre, C. L., Mölder, M.,  
3065 Müller-Williams, J., Necki, J., Newman, S., Nichol, S., Niwa, Y., O'Doherty, S., Obersteiner, F., Paplawsky, B.,  
3066 Peischl, J., Peltola, O., Piacentino, S., Pichon, J. M., Piper, S., Plass-Duelmer, C., Ramonet, M., Ramos, R., Reyes-

3067 Sanchez, E., Richardson, S., Riris, H., Rivas, P. P., Ryerson, T., Saito, K., Sargent, M., Sasakawa, M., Say, D.,  
3068 Scheeren, B., Schuck, T., Schumacher, M., Seifert, T., Sha, M. K., Shepson, P., Shook, M., Sloop, C. D., Smith, P.,  
3069 Steinbacher, M., Stephens, B., Sweeney, C., Tans, P., Thoning, K., Timas, H., Torn, M., Trisolino, P., Turnbull, J.,  
3070 Tørseth, K., Vermeulen, A., Viner, B., Vitkova, G., Walker, S., Watson, A., Wofsy, S., Worsley, J., Worthy, D., Young,  
3071 D., Zaehle, S., Zahn, A., Zimnoch, M., di Sarra, A. G., van Dinter, D., van den Bulk, P.: (2021): Multi-laboratory  
3072 compilation of atmospheric carbon dioxide data for the period 1957-2020;  
3073 obspack\_co2\_1\_GLOBALVIEWplus\_v7.0\_2021-08-18; NOAA Earth System Research Laboratory, Global  
3074 Monitoring Laboratory [data set], <http://doi.org/10.25925/20210801>, 2021b.

3075

3076 Seidl, R., Schelhaas, M. J., Rammer, W. and Verkerk, P. J.: Increasing forest disturbances in Europe and their impact  
3077 on carbon storage, *Nature Clim Change*, 4, 806–810, <https://doi.org/10.1038/nclimate2318>, 2014.

3078

3079 Silva, J. P., Toland, J., Jones, W., Eldrige, J., Thorpe, E., O'Hara, E.: LIFE and Europe's grasslands: Restoring a  
3080 forgotten habitat, report by the European Commission,  
3081 <https://ec.europa.eu/environment/archives/life/publications/lifepublications/lifefocus/documents/grassland.pdf>, (last  
3082 access: 10 November 2022), 2008.

3083

3084 Simmonds, P., Palmer, P. I., Rigby, M., McCulloch, A., O'Doherty, S. G., and Manning, A. J.: Tracers for evaluating  
3085 computational models of atmospheric transport and dispersion at regional to global scales, *Atm. Env.*, 246, 118074,  
3086 doi:10.1016/j.atmosenv.2020.118074, 2021.

3087

3088 Simpson, D., Benedictow, A., Berge, H., Bergström, R., Emberson, L. D., Fagerli, H., Flechard, C. R., Hayman, G.  
3089 D., Gauss, M., Jonson, J. E., Jenkin, M. E., Nyíri, A., Richter, C., Semeena, V. S., Tsyro, S., Tuovinen, J.-P.,  
3090 Valdebenito, Á., and Wind, P.: The EMEP MSC-W chemical transport model – technical description, *Atmos. Chem.*  
3091 *Phys.*, 12, 7825-7865, doi:10.5194/acp-12-7825-2012, 2012.

3092

3093 Simpson, D., Bergström, R., Imhof, H., and Wind, P.: Updates to the emep/msc-w model, 2016-2017. In  
3094 Transboundary particulate matter, photo-oxidants, acidifying and eutrophying components. EMEP Status Report  
3095 1/2017. The Norwegian Meteorological Institute, Oslo, Norway, 2017.

3096

3097 Simpson, D., Bergström, R., Tsyro, S., and Wind, P.: Updates to the EMEP MSC-W model, 2018- 2019. In  
3098 Transboundary particulate matter, photo-oxidants, acidifying and eutrophying components. EMEP Status Report  
3099 1/2019. The Norwegian Meteorological Institute, Oslo, Norway, 2019.

3100

3101 Simpson, D., Gonzalez Fernandez, I. A., Segers, A., Tsyro, S., Valdebenito, A., and Wind, P.: Updates to the EMEP  
3102 MSC-W model, 2021-2022. In Transboundary particulate matter, photo-oxidants, acidifying and eutrophying  
3103 components. EMEP Status Report 1/2022. The Norwegian Meteorological Institute, Oslo, Norway, 2022.



3104  
3105 De Smet, P. A. M., and Hettelingh, J.-P.: Intercomparison of Current European Land Use/Land Cover Databases,  
3106 Status Report 2001 Coordination Center for Effects, RIVM Report 259101010, Bilthoven, Netherlands, pp. 41-52,  
3107 2001.  
3108  
3109 Smith, J. U., Bradbury, N. J., and Addiscott, T.M.: SUNDIAL: A PC-based system for simulating nitrogen dynamics  
3110 in arable land, *Agron J*, 88, 38-43, <https://doi.org/10.2134/agronj1996.00021962008800010008x>, 1996.  
3111  
3112 Smith, J. U., Gottschalk, P., Bellarby, J., Chapman, S., Lilly, A., Towers, W., Bell, J., Coleman, K., Nayak, D. R.,  
3113 Richards, M. I., Hillier, J., Flynn, H. C., Wattenbach, M., Aitkenhead, M., Yeluripurti, J. B., Farmer, J., Milne, R.,  
3114 Thomson, A., Evans, C., Whitmore, A. P., Falloon, P. and Smith, P.: Estimating changes in national soil carbon stocks  
3115 using ECOSSE – a new model that includes upland organic soils. Part I. Model description and uncertainty in national  
3116 scale simulations of Scotland, *Climate Research*, 45, 179-192, doi: 10.3354/cr00899, 2010a.  
3117  
3118 Smith, J. U., Gottschalk, P., Bellarby, J., Chapman, S., Lilly, A., Towers, W., Bell, J., Coleman, K., Nayak, D. R.,  
3119 Richards, M. I., Hillier, J., Flynn, H. C., Wattenbach, M., Aitkenhead, M., Yeluripurti, J. B., Farmer, J., Milne, R.,  
3120 Thomson, A., Evans, C., Whitmore, A.P., Falloon, P. and Smith, P.: Estimating changes in national soil carbon stocks  
3121 using ECOSSE – a new model that includes upland organic soils. Part II Application in Scotland, *Climate Research*,  
3122 45, 193-205, doi: 10.3354/cr00902, 2010b.  
3123  
3124 Smith, B., Wärlind, D., Arneth, A., Hickler, T., Leadley, P., Siltberg, J., and Zaehle, S.: Implications of incorporating  
3125 N cycling and N limitations on primary production in an individual-based dynamic vegetation model, *Biogeosciences*,  
3126 11, 2027–2054, <https://doi.org/10.5194/bg-11-2027-2014>, 2014.  
3127  
3128 SNO-IFA, ICOS-CAL-FCL: SNO-IFA ATC Atmosphere Release SNO-IFA-L2-2022.1 of L2 Greenhouse Gas Mole  
3129 Fractions of CO<sub>2</sub>, CH<sub>4</sub>. [Dataset]. Aeris. <https://doi.org/10.25326/410>, 2023.  
3130  
3131 Solazzo, E., Crippa, M., Guizzardi, D., Muntean, M., Choulga, M., and Janssens-Maenhout, G.: Uncertainties in the  
3132 Emissions Database for Global Atmospheric Research (EDGAR) emission inventory of greenhouse gases, *Atmos.*  
3133 *Chem. Phys.*, 21, 5655–5683, <https://doi.org/10.5194/acp-21-5655-2021>, 2021.  
3134  
3135 Thompson, R. L., Broquet, G., Gerbig, C., Koch, T., Lang, M., Monteil, G., Munassar, S., Nickless, A., Scholze, M.,  
3136 Ramonet, M., Karstens, U., van Schaik, E., Wu, Z. and Rödenbeck, C.: Changes in net ecosystem exchange over  
3137 Europe during the 2018 drought based on atmospheric observations, *Phil. Trans. R. Soc. B*, 375, 20190512,  
3138 <http://dx.doi.org/10.1098/rstb.2019.0512>, 2020.  
3139

3140 Toretì, A., Belward, A., Perez-Dominguez, I., Naumann, G., Luterbacher, J., Cronie, O., Lorenzo Seguini, L.,  
3141 Manfron, G., Lopez-Lozano, R., Baruth, B., van den Berg, M., Dentener, F., Ceglar, A., Chatzopoulos, T., and  
3142 Zampieri, M.: The exceptional 2018 European water seesaw calls for action on adaptation, *Earth's Future*, 7, 652–663,  
3143 <https://doi.org/10.1029/2019EF001170>, 2019.

3144

3145 Tubiello, F. N., Conchedda, G., Wanner, N., Federici, S., Rossi, S., and Grassi, G.: Carbon emissions and removals  
3146 from forests: new estimates, 1990–2020, *Earth Syst. Sci. Data*, 13, 1681–1691, [https://doi.org/10.5194/essd-13-1681-](https://doi.org/10.5194/essd-13-1681-2021)  
3147 2021, 2021.

3148

3149 UK NIR: UK Greenhouse Gas Inventory, 1990 to 2020, Annual Report for Submission under the Framework  
3150 Convention on Climate Change, 978-0-9933975-8-5, 2022.

3151

3152 UNFCCC: Kyoto Climate Change Decision, available at: [https://unfccc.int/process-and-meetings/conferences/past-](https://unfccc.int/process-and-meetings/conferences/past-conferences/kyoto-climate-change-conference-december-1997/decisions-kyoto-climate-change-conference-december-1997)  
3153 [conferences/kyoto-climate-change-conference-december-1997/decisions-kyoto-climate-change-conference-](https://unfccc.int/process-and-meetings/conferences/past-conferences/kyoto-climate-change-conference-december-1997/decisions-kyoto-climate-change-conference-december-1997)  
3154 [december-1997](https://unfccc.int/process-and-meetings/conferences/past-conferences/kyoto-climate-change-conference-december-1997/decisions-kyoto-climate-change-conference-december-1997), (last access: 5 October 2020), 1997.

3155

3156 UNFCCC: Decision 24/CP.19 Revision of the UNFCCC reporting guidelines on annual inventories for Parties  
3157 included in Annex I to the Convention, FCCC/CP/2013/10/Add.3, 2014.

3158

3159 UNFCCC: NGHGI 2021 NIR reports: National Inventory Submissions 2021, available at: [https://unfccc.int/ghg-](https://unfccc.int/ghg-inventories-annex-i-parties/2021)  
3160 [inventories-annex-i-parties/2021](https://unfccc.int/ghg-inventories-annex-i-parties/2021), (last access: 01 January 2022), 2022a.

3161

3162 UNFCCC: NGHGI 2021 CRFs, available at: <https://unfccc.int/ghg-inventories-annex-i-parties/2021>, (last access 01  
3163 March 2022), 2022b.

3164

3165 VERIFY: <http://verify.lsce.ipsl.fr/>, last access: 21 November 2022.

3166

3167 VERIFY Synthesis Plots: <http://webportals.ipsl.jussieu.fr/VERIFY/FactSheets/>, last access: 21 November 2022.

3168

3169 van der Laan-Luijkx, I. T., van der Velde, I. R., van der Veen, E., Tsuruta, A., Stanislawski, K., Babenhauserheide,  
3170 A., Zhang, H. F., Liu, Y., He, W., Chen, H., Masarie, K. A., Krol, M. C., and Peters, W.: The CarbonTracker Data  
3171 Assimilation Shell (CTDAS) v1.0: implementation and global carbon balance 2001–2015, *Geosci. Model Dev.*, 10,  
3172 2785–2800, <https://doi.org/10.5194/gmd-10-2785-2017>, 2017.

3173

3174 Verkerk, P. J., Schelhaas, M.-J., Immonen, V., Hengeveld, G., Kiljunen, J., Lindner, M., Nabuurs, G.-J., Suominen,  
3175 T., and Zudin, S.: Manual for the European Forest Information Scenario model (EFISCEN 4.1), EFI Technical Report  
3176 99, European Forest Institute, 49 pp., 2016.

3177

3178 Viovy, N.: Interannuality and CO<sub>2</sub> sensitivity of the SECHIBA-BGC coupled SVAT-BGC model, *Physics and*  
3179 *Chemistry of The Earth*, 21, 489-497, [https://doi.org/10.1016/S0079-1946\(97\)81147-0](https://doi.org/10.1016/S0079-1946(97)81147-0), 1996.

3180

3181 Vizzarri, M., Pilli, R., Korosuo, A., Blujdea, V. N. B., Rossi, S., Fiorese, G., Abad-Vinas, R., Colditz, R. R., and  
3182 Grassi, G.: Setting the forest reference levels in the European Union: overview and challenges, *Carbon Balance*  
3183 *Manage*, 16, 23, <https://doi.org/10.1186/s13021-021-00185-4>, 2021.

3184

3185 Wang, Y.-P., and Leuning, R.: A two-leaf model for canopy conductance, photosynthesis and partitioning of available  
3186 energy I: Model description and comparison with a multi-layered model, *Agricultural and Forest Meteorology*, 91,  
3187 89-111, [https://doi.org/10.1016/S0168-1923\(98\)00061-6](https://doi.org/10.1016/S0168-1923(98)00061-6), 1998.

3188

3189 Wang, Y. P., Law, R. M., and Pak, B.: A global model of carbon, nitrogen and phosphorus cycles for the terrestrial  
3190 biosphere, *Biogeosciences*, 7, 2261–2282, <https://doi.org/10.5194/bg-7-2261-2010>, 2010.

3191

3192 Wanninkhof, R.: Relationship between wind speed and gas exchange over the ocean revisited: Gas exchange and wind  
3193 speed over the ocean, *Limnol. Oceanogr.-Meth.*, 12, 351–362, <https://doi.org/10.4319/lom.2014.12.351>, 2014.

3194

3195 Williams, J. R.: The Erosion-Productivity Impact Calculator (EPIC) Model: A Case History, *Philos. Trans. R. Soc. B*  
3196 *Biol. Sci.* 329, 421–428, <https://doi.org/10.1098/rstb.1990.0184>, 1990.

3197

3198 Winkler, K., Fuchs, R., Rounsevell, M. D. A., and Herold, M.: HILDA+ Global Land Use Change between 1960 and  
3199 2019. PANGAEA, <https://doi.org/10.1594/PANGAEA.921846>, 2020.

3200

3201 Winkler, K., Fuchs, R., Rounsevell, M. and Herold, M.: Global land use changes are four times greater than previously  
3202 estimated, *Nat Commun*, 12, 2501, <https://doi.org/10.1038/s41467-021-22702-2>, 2021.

3203

3204 WMO: United in Science Report, available at: [https://public.wmo.int/en/our-mandate/climate/wmo-statement-state-](https://public.wmo.int/en/our-mandate/climate/wmo-statement-state-of-global-climate)  
3205 [of-global-climate](https://public.wmo.int/en/our-mandate/climate/wmo-statement-state-of-global-climate), (last access: January 2022), 2021.

3206

3207 Yvon-Durocher, G., Caffrey, J., Cescatti, A., Dossena, M., del Giorgio, P., Gasol, J. M., Montoya, J. M., Pumpanen,  
3208 J., Staehr, P. A., Trimmer, M., Woodward, G., and Allen, A. P.: Reconciling the temperature dependence of respiration  
3209 across timescales and ecosystem types, *Nature*, 487, 472–476, <https://doi.org/10.1038/nature11205>, 2012.

3210

3211 Zhang, J., Balkovič, J., Azevedo, L.B., Skalský, R., Bouwman, A.F., Xu, G., Wang, J., Xu, M., and Yu, C.: Analyzing  
3212 and modelling the effect of long-term fertilizer management on crop yield and soil organic carbon in China. *Sci, Total*  
3213 *Environ*, 627, 361-372. <https://doi.org/10.1016/j.scitotenv.2018.01.090>, 2018.

3214

3215 Zhang, B., Tian, H., Lu, C., Dangal, S. R. S., Yang, J., and Pan, S.: Global manure nitrogen production and application  
3216 in cropland during 1860–2014: a 5 arcmin gridded global dataset for Earth system modeling, *Earth Syst. Sci. Data*, 9,  
3217 667–678, <https://doi.org/10.5194/essd-9-667-2017>, 2017.

3218

3219 Zscheischler, J., Mahecha, M. D., Avitabile, V., Calle, L., Carvalhais, N., Ciais, P., Gans, F., Gruber, N., Hartmann,  
3220 J., Herold, M., Ichii, K., Jung, M., Landschützer, P., Laruelle, G. G., Lauerwald, R., Papale, D., Peylin, P., Poulter,  
3221 B., Ray, D., Regnier, P., Rödenbeck, C., Roman-Cuesta, R. M., Schwalm, C., Tramontana, G., Tyukavina, A.,  
3222 Valentini, R., van der Werf, G., West, T. O., Wolf, J. E., and Reichstein, M.: Reviews and syntheses: An empirical  
3223 spatiotemporal description of the global surface–atmosphere carbon fluxes: opportunities and data limitations,  
3224 *Biogeosciences*, 14, 3685–3703, <https://doi.org/10.5194/bg-14-3685-2017>, 2017.

3225